2006-03-27

Development of Nanocomposite Polymer Electrolyte Membranes for Higher Temperature PEM Fuel Cells

Nikhil H. Jalani
Worcester Polytechnic Institute

Development of Nanocomposite Polymer Electrolyte Membranes for Higher Temperature PEM Fuel Cells

By

Nikhil H. Jalani

A Dissertation

Submitted to the Faculty of

WORCESTER POLYTECHNIC INSTITUTE

In partial fulfillment of the requirement for the

Degree of Doctor of Philosophy

In

Chemical Engineering

By

_____

March 2006

APPROVED:

_____

Professor Ravindra Datta, Advisor

_____

Professor Nikolaos K. Kazantzis

_____

Professor John C. MacDonald

_____

Professor David DiBiasio, Dept. Head

Extended Abstract

Proton exchange membrane (PEM) fuel cells are one of the most promising clean energy technologies under development. The major advantages include electrical efficiencies of up to 60 %, high energy densities (relative to batteries), and low emissions. However, the main obstacles to commercialization of PEM fuel cells are largely related to the limitations of the proton conducting materials, typically solid polymer electrolytes such as Nafion. These membranes are expensive, mechanically unfavorable at higher temperatures, and conduct protons only in the presence of water, which limits the fuel cell operating temperature to about 80 ^{o}C. This in turn, results in low fuel cell performance due to slow electrode kinetics and virtually no CO tolerance. The potential operation of PEM fuel cells at high temperature (above 100 ^{o}C) can provide many advantages such as improved kinetics at the surface of electrode, which is especially important in methanol and CO-containing reformate feeds, and efficient heat rejection and water managements. Another issue above 100 ^{o}C is the reduction of electrochemical surface area of the electrodes due to shrinkage of electrolyte (Nafion phase) within the catalyst layers.

The present research work is thus focused on the development of nanocomposite proton exchange membranes (NCPEMs) which are chemically and mechanically more stable at higher temperatures and electrodes which can result into better fuel cell performance. These are composite materials with inorganic acidic nanoparticles incorporated within a host polymer electrolyte membrane such as Nafion. The target operating fuel cell temperature in this work is above 100 ^{o}C with relative humidity around 30 to 40 %. To achieve these targets, both theoretical and experimental investigations were undertaken to systematically develop these NCPEMs. Various experimental techniques namely, TEOM (Tapered Element Oscillating Microbalance), Impedance Spectroscopy, MEA (membrane electrode assembly) testing, Ion Exchange Capacity, Scanning Electron Microscope (SEM), Optical Electronic Holography (OEH), Thermal Gravimetric Analysis (TGA), and Dynamic Mechanical Analysis (DMA) were employed to characterize the NCPEMs. The application of each of these techniques and its operating principle is explained in this thesis. A special focus is given to TEOM technique as it accurately measures the amount of water sorbed in the nanocomposite membrane, a critical parameter for membrane

development described in Chapters 5 and 6. Another novel technique used in this study is OEH for measuring mechanical properties of Nafion.

Chapter 1 provides an introduction to fuel cells and polymer electrolyte membranes along with the motivation for working on higher temperature operation of PEM fuel cells. In each subsequent chapter, which is each an individually published journal paper, a brief literature review is provided additionally focused on the theme of research covered in that chapter. Chapter 1 also discusses other strategies for solving the issues in higher temperature operation of fuel cells.

The development of Nafion-MO_2 (M = Zr, Si, Ti) nanocomposite membranes *via* sol gel chemistry with the goals to increase the water retention and proton conductivity at higher temperatures and lower relative humidities (120 ^oC, 40 % RHs) as well as to improve the thermo-mechanical properties is described in Chapters 2-4, as guided by a theoretical framework and characterization by the various experimental techniques.

Chapter 2 describes in detail our systematic approach to develop NCPEMs. Chapter 3 provides the thermodynamic model used to describe sorption in proton-exchange membranes (PEMs), which can predict the complete isotherm as well as provide a plausible explanation for the long unresolved phenomenon termed Schroeder's paradox, namely the difference between the amounts sorbed from a liquid solvent versus from its saturated vapor. A comprehensive proton transport model is provided to describe proton diffusion in Nafion/(ZrO_2/SO_4^{2-}) nanocomposite membranes. The conductivity of the *in situ* sol-gel prepared Nafion/(ZrO_2/SO_4^{2-}) nanocomposite membranes is accurately predicted by the model as a function of relative humidity (RH) without any fitted parameters. This transport model developed offers a theoretical framework for understanding the proton transfer in nanocomposite membranes and is an insightful guide in systematically developing high proton-conducting nanocomposite.

Experimental investigation of NCPEMs described in Chapters 2 and 4 shows that at 90 ^oC and 120 ^oC, all Nafion-MO_2 sol-gel composites exhibited higher water sorption than the Nafion membrane. However, at 90 ^oC and 120 ^oC and 40 % RH, Nafion-ZrO_2 sol-gel nanocomposite exhibited 10 % increase in conductivity over Nafion. This is attributed to an increase in the acidity of zirconia based sol gel membranes shown by a measured decrease in its equivalent weight in comparison to other nanocomposite membranes based on Ti and

Si. In addition, the TGA and DMA analyses showed improvement in degradation and glass transition temperature for nanocomposite membranes over Nafion.

Chapter 5 and 6 explains the detailed working of the novel TEOM technique and its application to study the effect of equivalent weight (960 -1200), temperature (30- 90 ^{o}C), various cationic forms (H^+, Li^+, Na^+, K^+ and Cs^+), sorbates (water, methanol, ethanol, and propanol), and inorganic additives on the sorption behavior of Nafion membrane. This study was performed to understand the fundamentals of solvent sorption as a function of membrane properties. The results provide insights into the swelling behavior of ion-exchange membranes, and, thus, are useful in evaluating and designing alternate proton-exchange membranes for fuel cell applications. Similarly, optoelectronic holography (OEH) was developed and applied for the first time to determine modulus of elasticity of membranes as a function of RH and temperature (Chapter 7). These two novel experimental characterization techniques developed in this study provide the foundation for developing higher temperature fuel cell membranes and electrodes, since they provide understanding of the effect of the rendered modifications on its thermomechanical properties.

Finally, commercially available high temperature PBI (polybenzimidazole)-H_3PO_4 (phosphoric acid) gel membrane fuel cell was investigated in the temperature range of 160-180 ^{o}C (Chapter 8). This system exhibited very good and stable performance in this temperature range. A complete electrochemical characterization using impedance spectroscopy and steady state performance was done to evaluate this technology.

Chapter 9 provides conclusions along with some recommended potential research directions based on this study. Detailed experimental procedures for synthesizing and characterizing sol-gel NCPEMs is provided in Appendices A and B. Appendix C provides a listing of publications and conference presentations resulting from this doctoral research work.

Acknowledgements

I would like to thank my advisor, Professor Ravindra Datta, for his guidance and support during the course of my doctoral work at Worcester Polytechnic Institute. It has been my life-time opportunity to pursue my career under his leadership and vision. I am highly impressed by his knowledge and approach to solve problems, his penchant for reading and learning, and his persistence as a research scholar. He has immense patience both in teaching and while solving any problem in research. I also had tremendous personal and professional growth under his leadership. I especially enjoyed the maximum independence I got during my research which gave me the opportunity to become an independent thinker. I would like to thank my research committee members Professor Kazantzis and Professor McDonald for their continuous support and encouragement which improved my thesis substantially.

I would like to thank the faculty and administrative staff of Chemical Engineering Department at WPI for their support and help during last five years. I also want to thank Giacomo Ferraro and Douglas White in Mechanical lab to troubleshoot various technical problems while designing fuel cell test station.

I would also like to thank all of my friends and colleagues at WPI for their kind help and all the fun I had.

I want to thank my parents for their support throughout my life. My life is indebted to them for their support and efforts for providing me with the best possible life and education. I dedicate all of my success to them. I also want to thank my brothers Navneet and Avinash and my wife Pooja for their love, support and encouragement.

Finally, I would like to thank WPI for giving me the opportunity to pursue Ph.D. in Chemical Engineering Department and the world class education facilities which helped me in accomplishing my professional goals. Many thanks to W.L. Gore and Plug Power for partial support of research.

Table of Contents

Extensive Abstract I

Acknowledgement V

List of Figures IX

List of Tables XV

List of Symbols XVI

Chapter 1 Higher temperature operation of Proton Exchange Membrane (PEM) fuel cells: Motivation and Literature Review

1.1 Fuel Cell Background 1
1.2 Introduction to Fuel Cells 2
1.3 Proton Exchange Membrane (PEM) Fuel Cell 4
1.4 Proton Exchange Membranes 10
1.5 Electrodes 20
1.6 Gas Diffusion Layer 20
1.7 Membrane Electrode Assembly (MEA) 23
1.8 Flow Field/Collector Plate 25
1.9 Motivation for Higher Temperature Operation 26
1.10 Design Goals for PEMs 28
1.11 Possible Approaches for Developing PEMs 30
1.12 Alternate PEMs 31
1.13 Research Direction 35
1.14 References 41

Chapter 2 Systematic Approach to Design Higher Temperature Nanocomposite Proton Exchange Membranes (NCPEMs)

2.1 Introduction 50
2.2 Literature Review 51
2.3 Systematic Design of NanoComposite PEMs 57
2.4 Experimental 63
2.5 NanoComposite Membrane Characterization 65
2.6 Results and Discussion 69
2.7 Conclusions 83
2.8 References 86

Chapter 3 Thermodynamics of Water Sorption and Proton Transport in the Understanding and Design of Nanocomposite PEMs

3.1 Introduction 90
3.2 Sorption in Nafion 92

3.3 Theoretical PEM Design for Improved Sorption 95
3.4 Experiments 96
3.5 Transport of Protons 97
3.6 Diffusion of Protons in NCPEMs 102
3.7 Theoretical Predictions 106
3.8 Conclusions 120
3.9 References 121

Chapter 4 Synthesis and Characterization of Nafion - MO_2 (M = Zr, Si, Ti) Nanocomposite Membranes for Higher Temperature PEM Fuel Cells

4.1 Introduction 123
4.2 Experimental 126
4.3 Results and Discussion 130
4.4 Conclusions 142
4.5 References 146

Chapter 5 TEOM: A Novel Technique for Investigating Sorption in Proton-Exchange Membranes

5.1 Introduction 148
5.2 Description of TEOM 150
5.3 Experimental 152
5.4 Results and Discussion 157
5.5 Conclusions 165
5.6 References 169

Chapter 6 The effect of Equivalent Weight, Temperature, Cationic Forms, Sorbates, and Nanoinorganic Additives on the Sorption Behavior of Nafion

6.1 Introduction 173
6.2 Experimental 176
6.3 Results and Discussion 182
6.4 Conclusions 195
6.5 References 197

Chapter 7 Optomechanical Characterization of Proton Exchange Membrane Fuel Cells

7.1 Introduction 202
7.2 Water Sorption Model 204
7.3 Chemical Equilibrium 209
7.4 Uncertainty Analysis of Sorption Model 210
7.5 Optoelectronic Holography 212

7.6 OEH Microscope Set up 212
7.7 Determination of Young's Modulus 215
7.8 Experimental Results 215
7.9 Conclusions and Future Work 217

Chapter 8 High Temperature Phosphoric Acid-PBI Gel Membrane Fuel Cells: Performance Analysis and Impedance Signatures

8.1 Introduction 224
8.2 Experimental 226
8.3 Results and Discussion 231
8.4 Conclusions 246
8.5 References 250

Chapter 9 Conclusions and Recommendations for Future Work

9.1 Conclusions 252
9.2 Future Recommendations 255
9.3 Strategies for Alternate PEMs 255
9.4 Strategies for Modifying Nafion 258
9.5 Membrane Stability and Longevity 260
9.6 References 262

Appendix A Methods of Preparation of Nafion and NCPEMs 263

Appendix B Experimental Procedures 268

Appendix C Listings of Journal Publications and Conference Meetings 273

List of Figures

Figure		Page
1.1(a)	A schematic representation of PEM fuel cell for hydrogen.	6
1.1(b)	Fuel cells view as a series of resistances.	8
1.1(c)	Current density (A/cm2) versus voltage (V) plot for a 5 cm^2 fuel cell operated at 80 ^oC with a H_2/O_2 (30/30 psig) feed; humidifier temperatures of 95 and 90 ^oC for anode and cathode, respectively; E-TEK double-sided electrodes with platinum catalyst (On Vulcan XC-72) loading = 0.4mg Pt/cm^2 and Nafion loading = 0.7 mg/cm^2, and with a Nafion 115 membrane.	9
1.2	Structural formula of the Nafion polymer.	11
1.3	Models Proposed for the interactions between polymer and water in Nafion Membrane.	14
1.4	Simple structural conceptualization of cross-linked polyelectrolyte and clustered ionomeric system with anionic side chain.	15
1.5	Qualitative Picture of Transport in Nafion.	18
1.6	Equilibrium sorption of water on Nafion as a function of water vapor activity	19
1.7	Electrode cross section with carbon black	21
1.8(a)	MEA preparation methods.	23
1.8(b)	Structure of MEA with backing layers.	24
1.9	Bipolar plate materials	25
1.10(a)	Desired membrane conductivity for commercialization.	29
1.10(b)	Desired membrane cost for commercialization.	29
1.11	Classification of membrane materials.	32
2.1	Schematic of structure of (a) Proton-Exchange Membranes (PEMs) and (b) Polymer-Acid Complexes (PACs).	54
2.2	A “dusty-fluid model” depiction of a PEM describing proton conductivity through the Nafion polymer matrix and the superacidic dopant. The framework treats the Nafion matrix as large dust particles through which the current carrying ions must traverse.	60
2.3	The solvent loading vs. activity of water vapor for Nafion (EW=1100) membrane (triangle: ref. 20, square: ref. 21, circle: ref. 44, and star: this	61

work).The design objective is to increase the solvent loading of Nafion. The composite will adsorb more water at fixed RH vs. unmodified Nafion resulting in higher conductivity at low RH.

2.4 SEM images of membranes synthesized by both the *in situ* and doping methods. (a) Nafion ZrO_2 doped membrane. (b) The Nafion ZrO_2 sol-gel PEM is homogeneous and transparent demonstrating no phase separation. 62

2.5 The surface area normalized water uptake of the powder at 120^{o}C vs. RH. The most promising candidates are the ZrO_2 and the SO_4/ZrO_2 samples. 72

2.6 The water uptake of composite membranes and Nafion 112 at 120 ^{o}C vs. RH. The Nafion ZrO_2 sol-gel PEM demonstrates the highest water uptake. 73

2.7 XRD pattern for composite membranes and Nafion. 74

2.8 The conductivity of the PEMs at 10 % RH and 40 % RH at 90 ^{o}C. The Nafion ZrO_2 sol-gel PEM shows the highest conductivity of the samples. 75

2.9 The conductivity of the PEMs at 10 % and 40 % RH at 120 ^{o}C. The Nafion ZrO_2 sol-gel PEM shows the highest conductivity of the samples. 76

2.10 The conductivity of loaded composites PEMs at 90 ^{o}C vs. RH. The optimum conductivity is observed with the 10 wt % PEM. 77

2.11 The conductivity of loaded composite PEMs at 120 ^{o}C. The optimum conductivity is observed with the 10 wt % PEM. 79

2.12 The cell performance of Nafion 112 MEA with conditions as noted on Figure. Operated with 1.5 atm Air /H_2, humidifiers set at 80^{o}C. The exception was when the cell was at 130 ^{o}C, 3 atm. O_2 and the humidifiers set at 130 ^{o}C. 80

2.13 The cell performance of Nafion 112 MEA vs. Nafion ZrO_2 sol-gel composite MEA. Air and H_2 at 2.0 and 1.3 times stoichiometry flows respectively, P = 1.0 atm., $T_{\text{HUMIDIFI ER}}$= 80^{o}C, T_{CELL} = 110 ^{o}C. 81

3.1 Schematic of sorption in pore of Nafion. 111

3.2 Schematics of sorption in pore of Nafion (a) bound free water molecules, and (b) vapor-liquid interface within a pore. 112

3.3 The solvent loading vs. activity of water vapor for Nafion (EW=1100). 113

3.4 The predicted solvent loading with the changes of the dissociation constant. 114

3.5	The predicted solvent loading with the changes of Young's modulus.	115
3.6	A simplified picture of structure and proton transfer in Nafion in fully hydrated state (a) and electrical analog of the proton transport in Nafion (b).	116
3.7	Proton conductivity of Nafion at 25° C and 90 °C.	117
3.8	Proton conductivity of Nafion-ZrO_2 (3 %) sol gel nanocomposite membrane at 25 °C and 90 °C.	118
3.9	Structure of Sulphated ZrO_2.	119
4.1	Water uptake vs. activity of water vapor for Nanocomposite Nafion/ MO_2 and Nafion membrane at 90 °C.	132
4.2	Water uptake vs. activity of water vapor for Nanocomposite Nafion/ MO_2 and Nafion membrane at 120 °C.	133
4.3	Conductivity vs. activity of water vapor for Nanocomposite Nafion/ MO_2 and Nafion membrane at 90 °C.	137
4.4	Conductivity vs. activity of water vapor for Nanocomposite Nafion/ MO_2 and Nafion membrane at 120 °C.	138
4.5	TGA data for Nanocomposite Nafion/ MO_2 and Nafion membranes.	139
4.6	DMA data for Nanocomposite Nafion/ MO_2 and Nafion membranes.	140
4.7	The cell performance of Nafion 112 MEA vs. Nafion -MO_2 sol-gel composite MEA. Oxygen and H_2 at 2.0 and 1.3 times stoichiometry flows respectively, P = 1.0 atm., $T_{HUMIDIFIER}$= 80 °C, T_{CELL} = 80 °C.	143
4.8	The cell performance of Nafion 112 MEA vs. Nafion -MO_2 sol-gel composite MEA. Oxygen and H_2 at 2.0 and 1.3 times stoichiometry flows respectively, P = 1.0 atm., $T_{HUMIDIFIER}$= 80 °C, T_{CELL} = 110 °C.	144
4.9	The cell performance of Nafion 112 MEA vs. Nafion -ZrO_2 sol-gel composite MEA. Oxygen and H_2 at 2.0 and 1.3 times stoichiometry flows respectively, P = 1.0 atm., $T_{HUMIDIFIER}$= 80-90° C, T_{CELL} = 135 °C.	145
5.1	Simplified flow diagram of the TEOM test bed and optics. The flow of inlet gas is shown by large arrows.	154
5.2	Experimental setup for sorption-desorption isotherms.	155
5.3	Real-time mass change data obtained from TEOM. The plateau represents equilibrium for given vapor activity conditions.	158

5.4	Water uptake vs. activity of water vapor for 1100 EW Nafion membrane at 30 ^{o}C (triangle: ref. 10, square: ref. 34, diamond: ref. 30, circle: ref. 13 and dark circle: this work).	160
5.5	Effect of temperature on water uptake vs. activity of water vapor for Nafion membrane.	161
5.6	The experimental variation of Young's modulus vs. activity of water vapor for Nafion membrane (circle: 30 ^{o}C, square: 90 ^{o}C).	162
5.7	Water and Methanol uptake vs. activity of solvent vapor for Nafion membrane at 30 ^{o}C (circle: methanol, triangle: water).	163
5.8	Sorption-Desorption characteristic for water and methanol vs. activity of solvent vapor for Nafion membrane at 30 ^{o}C (circle: methanol, triangle: water).	166
5.9	Effect of pretreatment procedures on water uptake vs. activity of water vapor for Nafion membrane at 30 ^{o}C.	167
5.10	Effect of pretreatment procedures on water uptake vs. activity of water vapor for Nafion membrane at 90 ^{o}C.	168
6.1	Structural details of Nafion membrane.	178
6.2	Effect of EW on water uptake (g/g Nafion) for different water activity conditions at 30 ^{o}C (triangle: EW=960, circle: EW=1100, and square: EW=1200).	182
6.3	Effect of EW on water uptake (λ) for different water activity conditions at 30 ^{o}C (triangle: EW=960, circle: EW=1100, and square: EW=1200).	183
6.4	Effect of EW on water uptake for different water activity conditions at 90 ^{o}C (triangle: EW=960, circle: EW=1100, and square: EW=1200).	184
6.5	Effect of temperature on water uptake vs. activity of water vapor for Nafion membrane.	186
6.6	Effect of various cationic forms on water uptake vs. activity of water vapor for Nafion membrane at 30 ^{o}C.	188
6.7	Effect of various cationic forms on methanol uptake vs. activity of methanol vapor for Nafion membrane at 30 ^{o}C.	189
6.8	Effect of various cationic forms on ethanol uptake vs. activity of ethanol	190

vapor for Nafion membrane at 30 ^{o}C.

6.9 Effect of various cationic forms on propanol uptake vs. activity of propanol vapor for Nafion membrane at 30 ^{o}C. 191

6.10 Water uptake vs. activity of water vapor for Nanocomposite Nafion/ MO_2 and Nafion membrane at 90 ^{o}C. 196

7.1 Detailed Schematic of hydrogen based proton-exchange membrane fuel cell. 205

7.2 Schematic of the internal pore contacting with the elastic membrane. 206

7.3 Uncertainty due to various parameters at (a) 30 ^{o}C and (b) 90 ^{o}C. The symbol represents % uncertainty for the parameters in Equation. 16 [square: E, triangle: η, star: a_i, circle: λ^C]. 213

7.4 OEH setup to determine resonating frequencies of Nafion sample. 214

7.5 Preliminary experimental results for E of Nafion membrane [circle: 30 ^{o}C, square: 90 ^{o}C]. 218

7.6 Experimental results for E of Nafion 117 membrane as a function of temperature and water activity. 219

7.7 Effect of membrane thickness on E of Nafion membrane as a function of water activity at 30 ^{o}C. 220

7.8 Experimental results for E of Nafion 117+ 10 % PTFE membrane as a function of temperature and water activity. 221

7.9 Experimental results for E of Nafion 117+ 10 % PTFE vs Nafion- SiO_2 membrane as a function of temperature and water activity. 222

8.1(a) EIS instrumentation schematic. 229

8.1(b) Correlation between different parts of a EIS spectrum and limiting processes. 230

8.2(a) Polarization curves at different temperatures with air as oxidant. 233

8.2(b) IR corrected polarization curves at different temperatures using air (160-180 ^{o}C). 234

8.3 Hydrogen pumping in comparison with high frequency intercepts at 160 ^{o}C. 235

8.4 Low frequency intercept as a function of current at different temperatures using oxygen as an oxidant. 236

8.5	Effect of fuel inlet dew point temperatures on the performance curves at 160 ^{o}C.	237
8.6	Effect of cathode stoichs on the performance curves at 160 ^{o}C.	239
8.7	Low frequency intercept as a function of current density at 160 and 180 ^{o}C.	240
8.8	Polarization curves at different temperatures with oxygen as oxidant (160-180 ^{o}C) compared with Nafion.	241
8.9	Effect of oxygen concentration on polarization curves at 160 ^{o}C and 180 ^{o}C.	242
8.10	Oxygen gain measurements at 160 ^{o}C and 180 ^{o}C.	243
8.11	Cathode potential at two concentrations of oxygen as a function of low Frequency intercept at 160 ^{o}C.	247
8.12	EIS spectrum when fuel stoichs are lowered to close to 100 % utilization at 0.3 A/cm^2.	248
8.13	EIS spectrum as cell is electrically shorted with 40 milli-ohm resistor.	249

List of Tables

1.1	Types of Fuel Cells.	2
1.2	Various cation exchange membranes.	10
1.3	Properties of Nafion membrane.	12
1.4	Various anode catalyst materials.	22
1.5	Hydrocarbon membranes.	33
1.6	Summary of membrane materials.	38
1.7	Summary of nanocomposite polymer membranes.	39
1.8	Conductivity summary of solid acid conductors.	40
2.1	The partial molar volume, experimental and predicted EW of the Nafion 112, and composite membranes at 25 ^{o}C.	71
2.2	The ECSA of a Nafion 112 MEA at different fuel cell temperatures, when the temperature of the humidifers remains constant at 80 ^{o}C.	85
3.1	Parameter values employed in the model for the sorption of water in Nafion.	107
3.2	Parameter values employed in the model for proton conductivity in Nafion at room temperature.	108
3.3	Data for water sorption in Nafion and Nafion/(ZrO_2/SO_4^{2-}) nanocomposite membranes.	109
3.4	Parameter values employed in the model at room temperature.	110
4.1	EW of Nanocomposites.	134
6.1	Water hydration number, hydration energies, and radius of cations.	192
9.1	Potential high temperature PEMs.	256

List of Symbols

a_i activity of water vapor, or RH

$a_{i.M}^F$ activity of water in fluid phase in membrane

C_{H^+} concentration of protons in the pore bulk, mol/cm^3

$C_{H^+}^{\alpha}$ concentration of protons participating in the diffusion mechanism α, mol/cm^3

$C_{H^+}^{\Sigma}$ concentration of protons participating in surface diffusion, mol/cm^3

$C_{H^+}^{E}$ concentration of protons participating in *en masse* diffusion, mol/cm^3

d_{ij} distance between the centers of the spheres i and j when collision occurs, nm

d_{H^+M} distance between the centers of hydronium ion and matrix of membrane when collision occurs, nm

d_{H^+W} distance between the centers of hydronium ion and water when the collision occurs, nm

$D_{H^+}^{\alpha}$ diffusion coefficient of protons for the diffusion mechanism α, cm^2/s

$D_{H^+}^{E}$ diffusion coefficient of protons for the *en masse* mechanism, cm^2/s

$D_{H^+}^{G}$ diffusion coefficient of protons for the Grotthuss diffusion mechanism, cm^2/s

$D_{H^+,PEM}^{\Sigma}$ diffusion coefficient of protons for the surface diffusion mechanism, cm^2/s

$D_{H^+,FA}^{\Sigma}$ diffusion coefficient of protons via acid group, cm^2/s

$D_{H^+}^{M}$ Stefan-Maxwell diffusion coefficient of protons and polymer matrix, cm^2/s

$D_{H^+}^{W}$ Stefan-Maxwell diffusion coefficient of protons and water, cm^2/s

E modulus of elasticity, Mpa

EW equivalent weight of membrane, e/equiv.

G shear modulus of polymer, MPa

$\Delta G_{\Sigma}^{e,0}$ effective Gibbs free energy of activation for surface diffusion of PEM, J/K

$\Delta G_{\Sigma,FA}^{e,0}$ effective Gibbs free energy of activation for surface diffusion of additives, J/K

h Planck constant, 6.626 x 10^{-34} J-sec

k_B Boltzmann constant, 1.38 x 10^{-23} J/K

K_i equilibrium constants for proton dissociation in membrane, dimensionless

l mean step distance between steps, nm

l_Σ mean step distance for surface diffusion, nm

l_G mean step distance for Grotthuss diffusion, nm

l_E mean step distance for en masse diffusion, nm

m_i molecular mass of *i*, g

m_j molecular mass of *j*, g

m_{ij}^* reduced molecular mass of *i* and *j*, g

m_{H+M}^* reduced molar mass of hydronium ion and membrane, g

m_{H+W}^* reduced molar mass of water and membrane, g

p jump steps starting from proton adjacent to the fixed anion, dimensionless

q_{e^-} electrostatic electrons charge, 1.602 x 10^{-19} C

T_θ torque on the dipole at an orientation angle θ, J

$T_{\max}$ maximum torque, J

r the ratio of partial molar volume of membrane to that of water, dimensionless

$r_{M/W}$ the ratio of partial molar volume of membrane to that of water, dimensionless

$r_{SA/W}$ the ratio of partial molar volume of solid acid to that of water, dimensionless

r_p pore radius, nm

R_f effective radius of fixed anion groups, nm

R_i radius of a component *i* (*i* = hydronium ion), nm

R_w radius of a water molecule, nm

S specific surface area, m^2cm^3

T temperature, K

$\overline{V}_M$ molar volume of membrane, cm^3/mol

$\overline{V}_{H_2O}$ molar volume of water, cm^3/mol

$\overline{V}_{H_3O^+}$ molar volume of hydronium ion, cm^3/mol

x_w mole fraction of water in the membrane phase, dimensionless

x_{PEM}^{Σ} fraction of acid group from PEM, dimensionless

x_{FA}^{Σ} fraction of acid group from additives, dimensionless

z_{H^+} charge number of ion, dimensionless

Greek

δ distance between the proton in hydronium ion and proton accepting water molecule, nm

δ_d concentration dependent Stefan-Maxwell diffusion ratio, dimensionless

ε_i porosity of the membrane, dimensionless

ε_0 permittivity of free space, 8.854×10^{-12} $C^2/J/m$

ε_r relative permittivity of the medium, dimensionless

$\varepsilon_{r(M)}$ relative permittivity of the membrane, dimensionless

$\varepsilon_{r(SA)}$ relative permittivity of the solid acid, dimensionless

ζ_{rot} rotational friction, J-sec

θ orientation angle, dimensionless

θ_I initial angle between diffusing proton and adjacent water molecule, dimensionless

θ_F final angle diffusing proton and an adjacent water molecule, dimensionless

θ_j fraction of acid sites with *j* bound water molecules, dimensionless

κ dimensionality constant of random-walk, dimensionless

κ_E dimensionality constant of en masse diffusion, dimensionless

κ_G dimensionality constant of Grotthuss diffusion, dimensionless

κ_Σ dimensionality constant of surface diffusion, dimensionless

λ_i the moles of water sorbed per acid site, dimensionless

$\lambda_{i,m}$ monolayer coverage being bound, dimensionless

λ_i^C chemical bound water within the pore, dimensionless

λ_i^F free water within the pore, dimensionless

μ_w dipole moment of liquid water, C-m

Π_S swelling pressure, MPa

Π_M pressure due to stretching of polymer matrix, MPa

Π_σ pressure exerted by curved vapor-liquid interface, MPa

ν_0 thermal frequency, 1/sec

ν equilibrium steps in chemical adsorbed water, dimensionless

σ_p proton conductivity in a pore of membrane, S/cm

$\sigma_{H^+}^{\Sigma}$ proton conductivity in the surface of membrane, S/cm

$\sigma_{H^+}^{G}$ proton conductivity by Grotthuss diffusion in the membrane, S/cm

$\sigma_{H^+}^{E}$ proton conductivity by *en masse* diffusion in the membrane, S/cm

τ the tortuosity factor, dimensionless

τ_C characteristic time constant, dimensionless

τ_D mean time between successive jump, ps

τ_D^E mean time between successive jumps of *en masse* diffusion, ps

τ_D^G mean time between successive jumps of Grotthuss diffusion, ps

τ_D^{Σ} mean time between successive jumps of surface diffusion, ps

ω_θ angular velocity, radian/sec

χ fitted polymer-solvent interaction parameter, dimensionless

Chapter 1
Higher Temperature Operation of Proton Exchange Membrane (PEM) Fuel Cells: Motivation and Literature Review

1.1 Fuel Cell Background

Proton exchange membrane (PEM) fuel cells are one of the most promising clean energy technologies currently under development [1-12]. The major advantages include: current prototype efficiency of up to 60 %, high energy densities (relative to batteries) and the ability to operate on clean fuels while emitting no pollutants. Despite these benefits, penetration of PEM fuel cells technology into the market place is being limited by cost and reliability issues. An immense worldwide effort to develop both catalyst and membrane and study long term behavior of fuel cells has so far met moderate success. As a result, it is widely acknowledged that the goal of large scale fuel cell market penetration in areas including transport has moved from 2010 to 2015, and that there are still many technical and market issues to overcome. These challenges include: choosing the appropriate fuel source and infrastructure, industry regulation, safety and public acceptance.

Research into fuel cells has grown exponentially over the last 15 years [1-12]. In the case of the polymer fuel cell, the major breakthroughs in technology that have allowed significant improvement in the overall performance of the PEM fuel cells have been the modification of Nafion by Du Pont. In fact, Nafion is the benchmark by which all new materials are compared. A significant number of these modified derivatives of Nafion and other polymers (e.g. sulfonated polyetherketones or SPEK) are appearing in a wide range of the latest fuel cell prototypes. The development of PEM fuel cells is largely tracked by the history of the membranes. Because fuel cells of various types were known prior to PEM technologies, the catalysts, fuels, and oxidants used in PEM fuel cells were reasonably well-established materials. The first PEM systems served as the power plants for the Gemini space missions in the early 1960s. The cells were short-lived because of the oxidative degradation of the membranes (a copolymer of sulfonated polystyrene and divinylbenzene). In the late 1960s, DuPont introduced the fluorocarbon, cation exchange

polymer, Nafion. The history and current development of PEM fuel cells is linked to advantages and disadvantages of Nafion under different operating conditions.

1.2 Introduction to Fuel Cells

A fuel cell is defined as an electrochemical device in which the chemical energy of a *fuel* is converted *directly* into electrical energy. The *fuel* is typically an alcohol or a hydrocarbon or a substance derivable from it, e.g., hydrogen, which can be supplied continuously. Excluded are fuels such as atomic fuel, i.e., uranium, and metals such as zinc or sodium, the latter being used in batteries. The term *directly* implies that the device has an anode at which the fuel is electrocatalytically oxidized with the production of electrons and a cathode at which the oxygen is reduced.

The most common types of fuel cells, characterized by the electrolyte are listed in Table 1.1:

Fuel Cell Type	**Proton Exchange Membrane (PEMFC)**	**Direct Methanol (DMFC)**	**Alkaline (AFC)**	**Phosphoric Acid (PAFC)**	**Molten Carbonate (MCFC)**	**Solid Oxide (SOFC)**
Mobile Ion	H^+	H^+	OH^-	H^+	CO_3^{2-}	O^{2-}
Operating Temperature (°C)	50 – 100	30-80°C	50 – 200	~ 220	~ 650	600 - 1000
Power Density (kW/m^2)	3.8 – 2.6	2.5-1.5	0.7 – 8.1	0.8 – 1.9	0.1 – 1.5	1.5 – 2.6
Reforming	external	external	external	external	external or internal	external or internal
Electrical 1st Law Efficiency (%)	40 – 55 (stack)	40 - 55	45 – 60 (stack)	40 – 50 (stack) 41(system)	50 – 60 (system)	50 – 65 (stack) 45 – 50 (system)
Start-up Time	sec – min	sec – min	min	hours	hours	hours

Table 1.1 Types of Fuel Cells [1]

In general, fuel cells offer many advantages over conventional energy conversion devices [3]. One of the major factors that have influenced the development of fuel cells is the concern from environmental consequence point of view. Less pollution for the betterment of human life has become a matter of great concern. In this present scenario fuel cells help to reduce our dependence on fossils fuels and diminishes poisonous and toxic emissions in to the atmosphere, since fuel cells have more electrical efficiencies compared to heat engines. The main by-product of PEM fuel cell reaction is water, thus completely eliminating locally all emissions. As mentioned above, fuel cells have many characteristics that make them a possible alternative to conventional energy conversion systems [3]:

• ***Efficiency:*** Because they convert chemical energy directly into electrical energy, fuel cell efficiencies are not limited by the Carnot limit. Therefore, they are potentially far more efficient than internal combustion engines. Efficiencies of present fuel cell plants are in the range of 50 to 60 %, and hybrid fuel cell/gas reheat turbine cycles have demonstrated efficiencies greater than 70 %. In addition, the efficiency is nearly independent of the electric load down to a small fraction of full load. This makes fuel cells very suitable for applications such as vehicles, where good efficiency is desired even far from peak power (full load).

• ***Low emissions****:* When pure hydrogen is used directly as a fuel, only water is created and no pollutant is rejected. However, the processing of hydrocarbon fuels into hydrogen can result in a smaller output of NO_x, SO_x, CO, and an amount of CO_2 which is significantly lower when compared, for example, to classical internal combustion engines, due to higher overall efficiency.

• ***Cogeneration capability:*** The exothermic chemical and electrochemical reactions produce usable heat.

• ***Scalability****:* Fuel cells can be configured to suit a wide range of sizes for applications, ranging from a few watts to megawatts. Thus, fuel cells are expected to serve as a power source for portable electronic and computers as well as vehicles and small or large power plants.

• ***Fuel flexibility:*** Fuel cells can be operated using commonly available fuels such as natural gas, methanol, and various complex hydrocarbons.

• ***Reliability and low maintenance:*** The absence of moving parts reduces the maintenance requirements and minimizes system down-time.

• ***Quiet operation:*** By virtue of absence of moving parts, the operation is quite and there is no noise pollution.

1.3 Proton Exchange Membrane (PEM) Fuel Cell

Proton exchange membrane (PEM) fuel cell can be divided into hydrogen fuel cell or direct methanol fuel cell, depending on the fuel used. The hydrogen fuel cell uses H_2 gas as a fuel and provides excellent fuel cell performance.

The half cell reactions for the hydrogen PEM fuel cell are as follows:

Anode: $H_2 \leftrightarrows 2H^+ + 2e^-$ $\Delta G^0 = 0.00$

Cathode: $\frac{1}{2} O_2 + 2H^+ + 2e^- \leftrightarrows H_2O$ $\Delta G^0 = -237$ kJ/mol

Overall: $H_2 + \frac{1}{2} O_2 = H_2O$ $\Delta G^0 = -237$ kJ/mol

The Gibbs free energy change of a chemical reaction is very well correlated to the cell voltage as:

$$\Delta G = -nFV_0$$

where n is the number of electrons involved in the reaction, F is the Faraday constant, and V_0 is the cell voltage for thermodynamic equilibrium in the absence of a current flow i.e., open circuit conditions at equilibrium.

Hence, the equilibrium cell voltage V_0 at 25 ^{o}C is calculated for hydrogen fuel cell as:

$$V_0 = \frac{-\Delta G}{nF} = 1.23 \text{ V}$$

This equilibrium cell voltage is the difference of the equilibrium electrode potentials of the cathode and the anode.

The main components of PEM fuel cell are:

1. Electrodes : Anode and Cathode
2. Polymer Electrolyte Membrane (PEM)
3. Gas Diffusion Layer (GDL)

4. Collector Graphite Plates

A schematic diagram of fuel cell is shown in Figure 1.1(a). At the interface between the anode catalyst, which is typically Pt based, and the electrolyte, fuels are converted into protons (H^+) and electrons (e^-). The protons travel through a PEM, which prohibits electrons, to the cathode side. This is the unique property of PEM that it allows only protons to diffuse, hence avoid shorting of cell. The electrons (e^-) are thus forced to travel through an external wire and deliver part of their energy to a 'load' on their way to the cathode. At the cathode, the transferred protons and the energy depleted electron combine with oxygen to produce water. Theoretically, any substance capable of chemical oxidation that can be supplied continuously can be used as a fuel at the anode of the fuel cell. Similarly, the oxidant can be any fluid that can be reduced at a sufficient rate. However, cost, availability, and reactivity are the key issues in their selection. The hydrogen fuel cell uses H_2 gas as the fuel and provides very high fuel cell performance and efficiency for pure hydrogen, while direct methanol fuel cell uses liquid methanol as a fuel that provides relatively low performance and efficiency, but precludes the use of a reformer to produce hydrogen.

Gaseous oxygen or air is the most common choice for the oxidant because it is readily and economically available. The electrochemical reaction takes place at the surface of the electrodes that are attached to a carbon paper or carbon cloth, called the gas diffusion layer (GDL). The carbon is conductive and porous that allows the flow of gases and electrons through it. The catalyst particles are properly dispersed in ionomeric material which aids in proton conduction. The membrane in a PEM cell is typically a solid electrolyte called Nafion, a perfluorosulfonic acid polymer made by Dupont. This membrane allows protons to travel through but inhibits the electrons from passing through it. The proton transfers through the membrane by virtue of the electric field created across the membrane. The typical performance of the fuel cell is shown in the form of current density versus voltage plots. This provides the steady state performance of given fuel cell system for the purpose of design, optimization, and development.

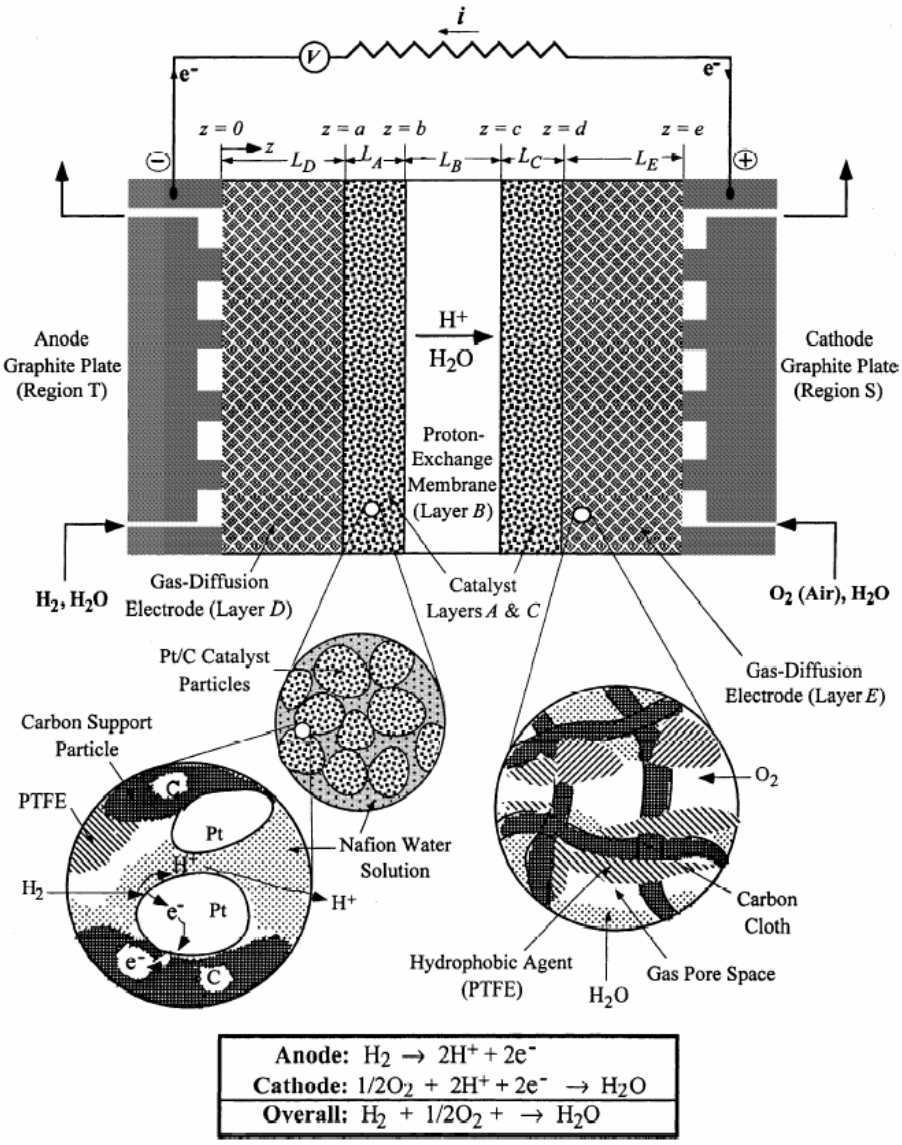

Figure 1.1(a) A schematic representation of PEM fuel cell for hydrogen [13].

PEMFC Theory

The reaction kinetics on the anode and cathodes are typically described in terms of the Butler-Volmer equation [13]

$$i = i_0\left[\exp(\alpha_A F\eta / RT) - \exp(-\alpha_C F\eta / RT)\right] \tag{1.1}$$

where i_0 is the exchange current density, α_A and α_C is the transfer coefficients for the anodic and cathodic reaction, respectively, and η is the overpotential to derive the reaction. The fuel cell can be viewed as it has a number of resistances as shown in Figure 1.1(b). Then, based on Ohm's law, the voltage-current relationship can be written as

$$V = V_0 - iR_A - iR_M - iR_C - iR_I \tag{1.2}$$

where specific anode resistance is a combination of diffusion and kinetic resistance.

In the so called "reversible" fuel cell, there are no irreversibilities (losses), and thus the cell voltage $V = V_0$ regardless of current "*i*" drawn. In reality, however, the available voltage drops due to the various diffusions, kinetic and ohmic resistances as

$$V = V_0 - |\eta_A| - |\eta_M| - |\eta_C| - |\eta_I| \tag{1.3}$$

where V_0 is the equilibrium open circuit potential, η_A, η_C, η_M and η_I represent the overpotential due to anode, membrane, cathode and interfaces, respectively. These overpotentials can be obtained as

$$\eta_A = \frac{RT}{\alpha_A F}\sinh^{-1}\left\{\frac{1}{2}\left[\frac{i_A / i_{A,0}}{1 - i_A / i_{A,L}}\right]\right\} = \eta_{D,A} + \eta_{K.A} \tag{1.4}$$

where i_A is the current density at anode, $i_{A,0}$ is the exchange current density at anode, $i_{A,L}$ is the limiting current density at anode, $\eta_{D,A}$ is the overpotential due to the diffusion of hydrogen at anode, and $\eta_{K,A}$ is the overpotential due to the kinetics at anode surface.

Similarly, the cathode overpotential is

$$-\eta_C = \frac{RT}{\alpha_C F}\sinh^{-1}\left\{\frac{1}{2}\left[\frac{i_C / i_{C,0}}{1 - i_C / i_{C,L}}\right]\right\} = \eta_{D,C} + \eta_{K.C} \tag{1.5}$$

The above two expressions between current density and potential loss are non-linear, unlike Ohm's Law.

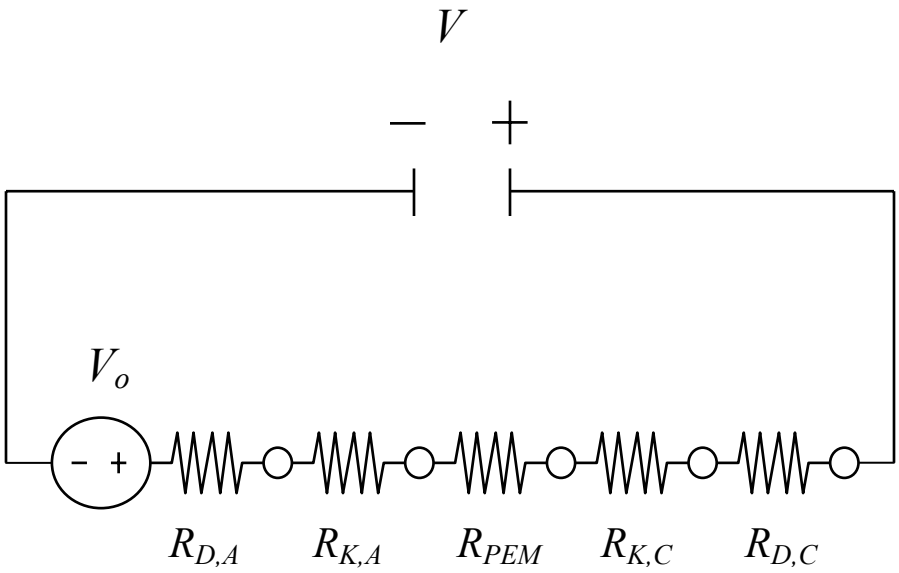

Figure 1.1(b) Fuel cells view as a series of resistances [13].

For PEM, however, Ohm's law is applicable

$$i = -\sigma_B \frac{d\Phi_B}{dz} \tag{1.6}$$

Integrating this over the membrane thickness for constant *i* provide

$$\eta_M = i\left(\frac{L_B}{\sigma_B}\right) \tag{1.7}$$

where L_B and σ_B are the thickness and the conductivity of PEM. Thus, the current-voltage relation can be written with $i_A = i_C = i$,

$$V = V_0 - \frac{RT}{\alpha_A F}\sinh^{-1}\left\{\frac{1}{2}\left[\frac{i\ /i_{A,0}}{1-i\ /i_{A,L}}\right]\right\} - \frac{RT}{\alpha_C F}\sinh^{-1}\left\{\frac{1}{2}\left[\frac{i\ /i_{C,0}}{1-i\ /i_{C,L}}\right]\right\} - i\left(\frac{L_B}{\sigma_B}\right) - iR_I \tag{1.8}$$

Figure 1.1(c) shows the prediction of voltage versus current density using Eq. 1.8 for fuel cell operating at 80 ^oC in H_2 / O_2 saturated environment. The predictions compare very well with the experiment data [13].

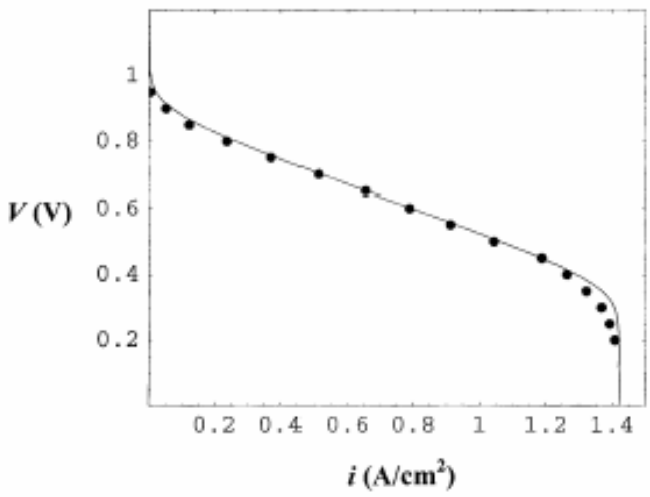

Figure 1.1(c) Current density (A/cm2) versus voltage (V) plot for a 5 cm^2 fuel cell operated at 80 ^oC with a H_2/O_2 (30/30 psig) feed; humidifier temperatures of 95 and 90 ^oC for anode and cathode, respectively; E-TEK double-sided electrodes with platinum catalyst (On Vulcan XC-72) loading = 0.4mg Pt/cm^2 and Nafion loading = 0.7 mg/cm^2, and with a Nafion 115 membrane.

1.4 PFSA Proton Exchange Membranes

As early as in 1940s, the research scientists were already involved in developing organic ion exchange membranes [14-16]. These new ion containing polymers were termed as *ionomers.* It was believed that these ionomeric polymers would possess better properties as compared to conventional polymers like nylon or polyester, as they involved the interaction between polymer and ions. Typical applications of these ionomers were visualized as thermoplastics, coatings, fuel cell membranes, ion exchange membranes etc. One of the most important breakthroughs in the field of ionomers is the development of fluorocarbon based ionomers. It essentially consists of a linear perfluorinated backbone with side chains that are terminated with ionic groups. Commercially available ionomer of this sort are Nafion membrane (DuPont), the Dow membrane (Dow Chemicals, USA), Flemion (Asahi Glass Co, Japan) and Aciplex-S (Asahi Chemical Industry Company). The typical thickness of the Nafion membrane for Fuel cell applications is generally between 50 and 175 microns. Table 1.2 summarizes various cation exchange membranes.

Properties of commercial cation-exchange membranes

Membrane	Membrane type	IEC (mequiv./g)	Thickness (mm)	Gel water (%)	Conductivity (S/cm) at 30 °C and 100% RH
Asahi Chemical Industry Company Ltd., Chiyoda-ku, Tokyo, Japan					
K 101	Sulfonated polyarylene	1.4	0.24	24	0.0114
Asahi Glass Company Ltd., Chiyoda-ku, Tokyo, Japan					
CMV	Sulfonated polyarylene	2.4	0.15	25	0.0051
DMV	Sulfonated polyarylene	–	0.15	–	0.0071
Flemion	Perfluorinated	–	0.15	–	–
Ionac Chemical Company, Sybron Corporation, USA					
MC 3470	–	1.5	0.6	35	0.0075
MC 3142	–	1.1	0.8	–	0.0114
Ionics Inc., Watertown, MA 02172, USA					
61AZL386	–	2.3	0.5	46	0.0081
61AZL389	–	2.6	1.2	48	–
61CZL386	–	2.7	0.6	40	0.0067
Du Pont Company, Wilmington, DE 19898, USA					
N 117	Perfluorinated	0.9	0.2	16	0.0133
N 901	Perfluorinated	1.1	0.4	5	0.01053
Pall RAI Inc., Hauppauge, NY 11788, USA					
R-1010	Perfluorinated	1.2	0.1	20	0.0333

Table 1.2 Various cation exchange membranes [14-16]

Nafion is widely used for PEM fuel cell applications. This polymer is based on a polytetrafluoroethylene (PTFE) backbone and has perfluorovinyl ether pendant side chains, with the sulphonate groups at the end [16]. This type of membrane was found to have exceptional stability and possesses properties that could be used in many areas. Thus, it has been extensively used in the chloro-alkali industry as it has good ion selectivity, chemical resistance and ionic conductivity. As far back as 1966, the General Electric Company used Nafion membranes in proton exchange fuel cells. At that time, the fuel cell was used to supply power in space projects by NASA. Although the PEMFC was environmentally friendly it was not considered as a technology reaching the common man. More recently, however, the need for cleaner and pollution free power sources has drawn tremendous attention to the fuel cells.

It is evident from a literature review that Nafion is the leading candidate for PEM fuel cell, though other membranes mentioned have been investigated. In addition to fuel cell applications, Nafion has been widely used in metal ion recovery, as a super acid catalyst in organic reactions and different electrochemical devices.

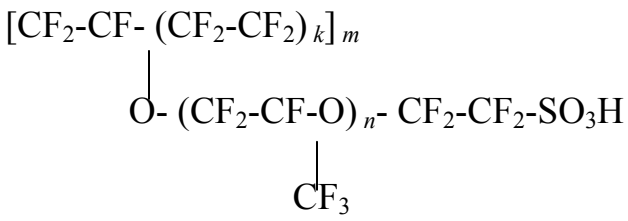

Figure 1.2 Structural formula of the Nafion polymer

The chemical structure of Nafion is shown in the Figure 1.2 and its properties are provided in Table 1.3. Generally for the Nafion 117 membrane $n = 1$, $k = 6.5$ and $100<m<1000$. The numeral 117 attached to the Nafion stands for 1100 g equivalent weight of polymer per equivalent of sulphonate group and a thickness of 0.007 inches. There are other Nafion membranes with different equivalent weights and different thickness designed for other applications (Table 1.3).

Property	Typical Value
Water Uptake, % water [a]	35
Tensile Modulus, Mpa 50% RH, 23^{0}C water soaked, 100^{0}C	 249 64
Tensile Strength, max, Mpa 50% RH, 23^{0}C water soaked, 100^{0}C	 43[b], 32[c] 25[b], 24[c]
Density, g/cm^3	2.0
Conductivity, S/cm (80^{o}C)[a]	0.10

a = Water uptake from dry membrane soaked in water at 100^{0}C for 1 hour.

b = Measured in machine direction

c = Measured in transverse direction

Membrane Type	Typical Thickness(μm) (At 23 ^{0}C, 50% Relative Humidity)	Basis Weight (g/m^2)
NE-112	51	100
NE-1135	89	190
N-115	127	250
N-117	183	360

Table 1.3 Properties of Nafion Membranes [14-16]

An important thing to understand about Nafion is the interaction between the ionic groups and the polymer backbone. From the various studies made, the following models have been proposed:

1) Gierke's *et al* Cluster – Network Model

Model was described by Gierke *et al*. who proposed that Nafion has a microstructure which consisting of a cluster network where the polymer ions and the absorbed water exist in spherical domains [17]. They are separated from the PTFE matrix. The three dimensional structure is composed of 10 ^{o}A wide channels that interconnect spherical clusters creating a matrix of inverted micelles. The size of the spherical domains grows in size from 25 ^{o}A to 40 ^{o}A, as the water absorbed increases. Figure 1.3(a).

2) Yeager and Steck's Model

The model proposed by Yeager and Sheck and it basically depicts three different regions within the polymer membrane [18]. These regions determine the transport properties in the membrane. The regions are: fluorocarbon phase, interfacial region and ionic clusters. Figure 1.3(b) shows the model pictorially.

The FC is the region consisting of the polymer backbone, i.e. for Nafion the PTFE backbone. The IF region is where there is a combination of side chains, water and sulphonate groups. The IC region is where most of the water absorbed remains.

3) Yeo and Eisenberg's Model

Eisenberg developed a theory of ionomer structure which explains the formation of ionic clusters in organic polymer [19]. Nafion is an example of clustered polyelectrolyte. Figure 1.4 shows the formation of such a polyelectrolyte. The existence of ionic clustering in perfluorinated sulphonate ionomer was reported by Yeo and Eisenberg in 1975 and many experimental evidence such as spectroscopic data, swelling behavior and transport properties support its existence.

4) Mauritz *et al*. Model

In 1978 Mauritz, Hopfinger and Hora suggested structural organization of Nafion membrane under different physiochemical conditions [20]. It considers the balance between the elastic deformation of polymer matrix and various molecular interactions that exist in the polymer.

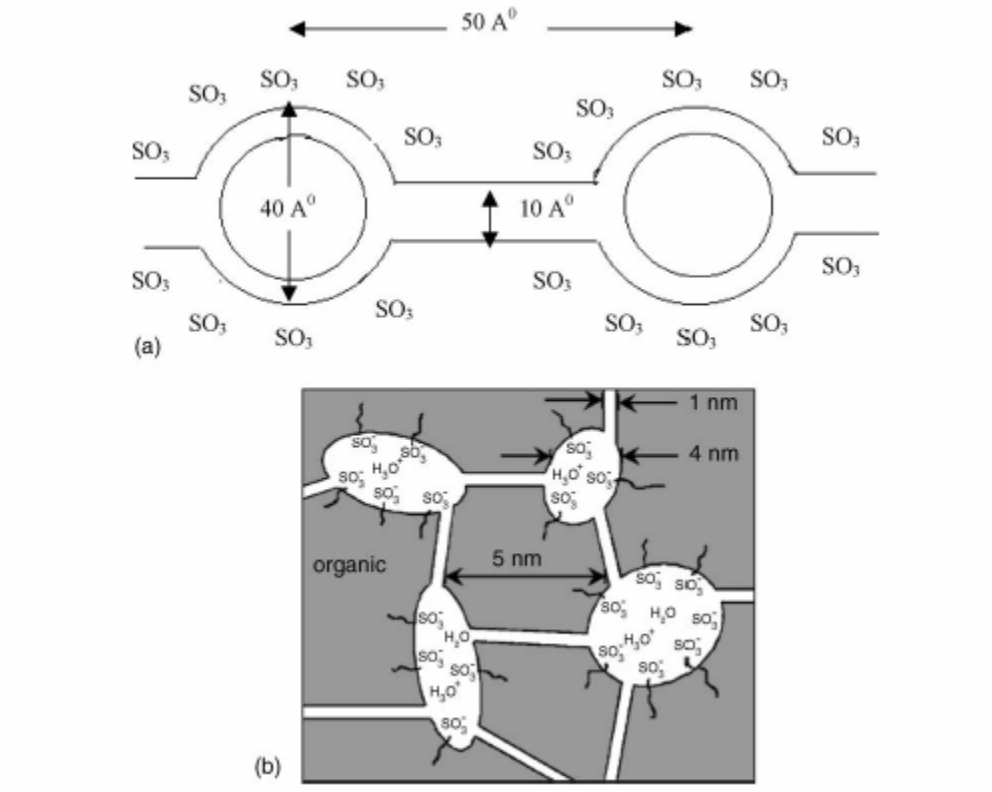

Figure 1.3 Models Proposed for the interactions between polymer and water in Nafion membrane [17-18].

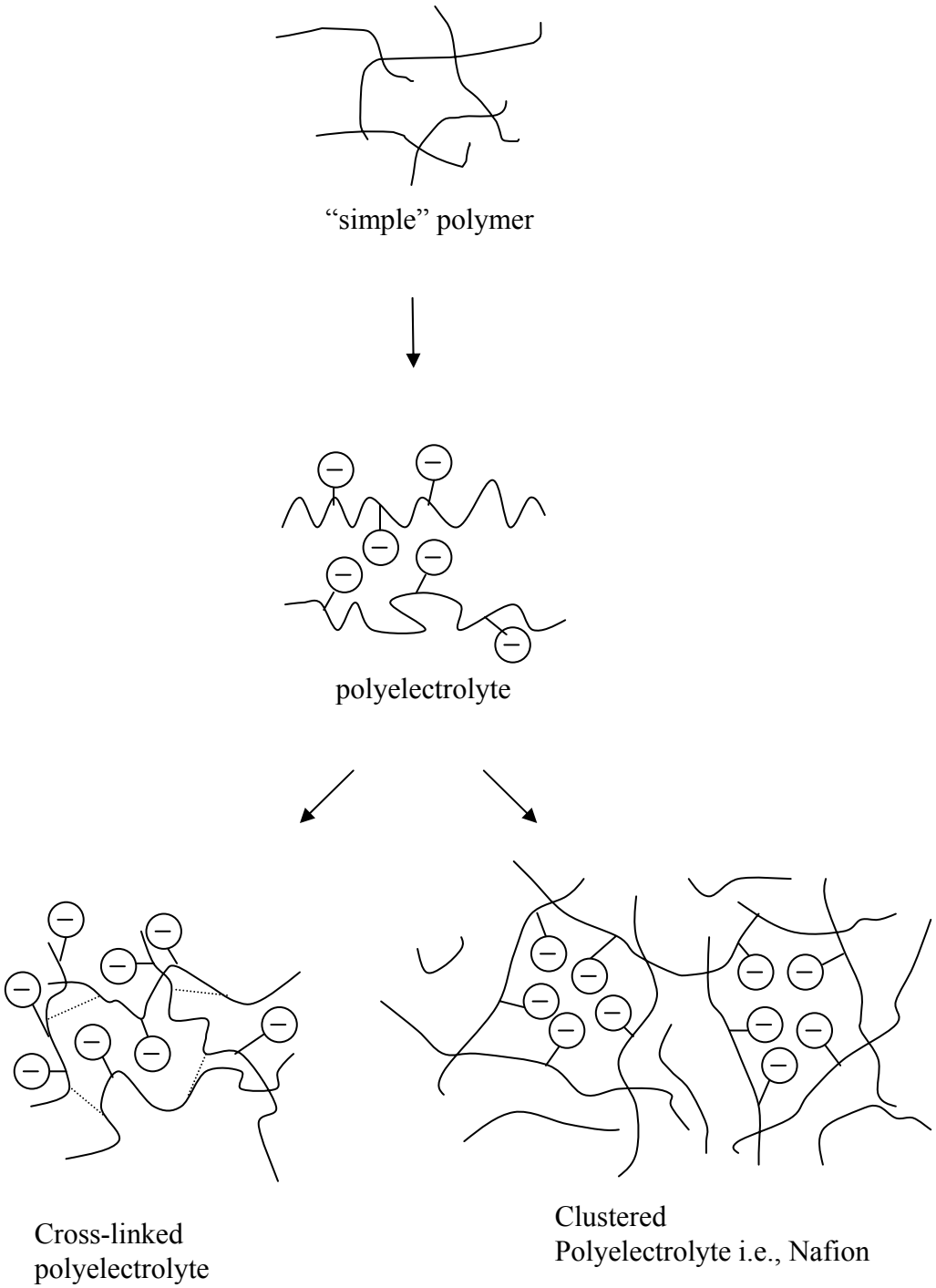

Figure 1.4 Simple structural conceptualization of cross-linked polyelectrolyte and clustered ionomeric system with anionic side chain [19].

Nafion membranes are produced by forming the sulfonyl fluoride polymer into sheets and then hydrolyzing to the sulfonate [2]. Once the sulfonate is formed, the membranes swell in various organic solvents, but the material is extremely insoluble. Based on the insolubility and inertness of fluorocarbons, Nafion is normally thought to be a very stable and robust material. Under pressure and temperature, the sulfonate polymer can be suspended in mixed solvents; these suspensions are used to modify electrodes and are often used in the formation of membrane electrode assemblies of PEM fuel cells to control wetting.

The transfer of protons in solid electrolyte polymer is also widely studied [21-30]. In the case of Nafion the proton transport depends mainly on the water content of the membrane [21]. Although the precise mechanism by which proton transfer in solvated form in Nafion is not completely know, a qualitative picture was shown by Zawodzinski *et al*. in Figure 1.5 [25]. Basically it is assumed that the state of water in Nafion membrane is not fixed. Some of the water is tightly bound to the SO_3^- is called chemically bound water. These are less hydrogen bonded than in the bulk water because of the less water-water contacts. The bulk water is described as physically bound water. Away from the pore surface, in the central region of the pore, the water is present as bulk water [24].

The transfer of proton near pore surface, i.e., within 3-4 Å, which is roughly the thickness of water molecule, would take place through the tightly bound water molecules along the array of SO_3^- group because of the cooperative electrostatic attraction of SO_3^- group and the large distance between them (6-12 Å) [23]. On the other hand, the transfer of proton in the center of the pore would follow the transfer in bulk water. The transfer of protons through surface water can be characterized by higher activation energy and lower proton transfer. The surface density of SO_3^- group and the pore structure/size would determine the contributions of proton transfer from the surface and bulk water. As the membrane becomes saturated, the size of pore increases and this will increase the bulk-like portion of water, leading bulk-like transfer that gives high rate of proton transfer in the middle of pores. Thus, the overall rate of proton transfer increases with pore radius until it reaches saturation where the average diameters of pores are 4-6 nm.

In an earlier study done [25, 29], the two types of membranes were proposed namely: “E- form” membranes which were swollen and expanded in the high temperature

water and the "S-form" membranes which were shrunken in vacuum at high temperatures. The normal membranes were termed as "N-membranes". It is found that the E-form membrane becomes rubbery and viscous when the temperature is increased. Hence there is a tendency to absorb more water. But when dried in vacuum, the ionic clusters shrink and there is less water uptake [25, 29]. The state of membrane is critical as it affects the amount of water adsorbed within the pores of membrane. I have explained the effect of few treatment in Chapter 5.

The vapor phase absorption is typically less well studied as compared to liquid phase absorption. It is already very well explained in the literature about the famous Schroeder Paradox. Schroeder found that polymeric materials absorb less water from vapor phase as compared to liquid phase. This is known as the famous Schroeder's Paradox [23].

Figure 1.6 shows the water sorption data for Nafion membrane at 30 ^{o}C. The vapor sorption isotherm can be broadly divided into two main regions [25]:

1. The low vapor activity region, i.e. from 10 to 60 % relative humidity (RH). In this region there is relatively gradual increase in the water uptake by the membranes. The enthalpy of sorption is about 12.5 Kcal/mol which is greater than the enthalpy of water liquefaction. This region corresponds to uptake of water of solvation by the ions in the membranes.
2. The higher activity region, i.e. 70 to 100% RH. In this region there is a steep increase in the water uptake with water activity and the enthalpy of sorption is as low as 5 Kcal/mol which is lower than the enthalpy of water liquefaction. This region corresponds to water which fills the pores and swells the polymer. Also the lower values of enthalpy clearly indicate the weaker water-ion interaction. This may be due to endothermic deformation of the polymer matrix on swelling. There is also a decrease in the degree of hydrogen bonding in the polymer matrix as compared to state of pure liquid water. The swelling of the membrane at higher water vapor activities is driven mainly by increase in entropy of mixing.

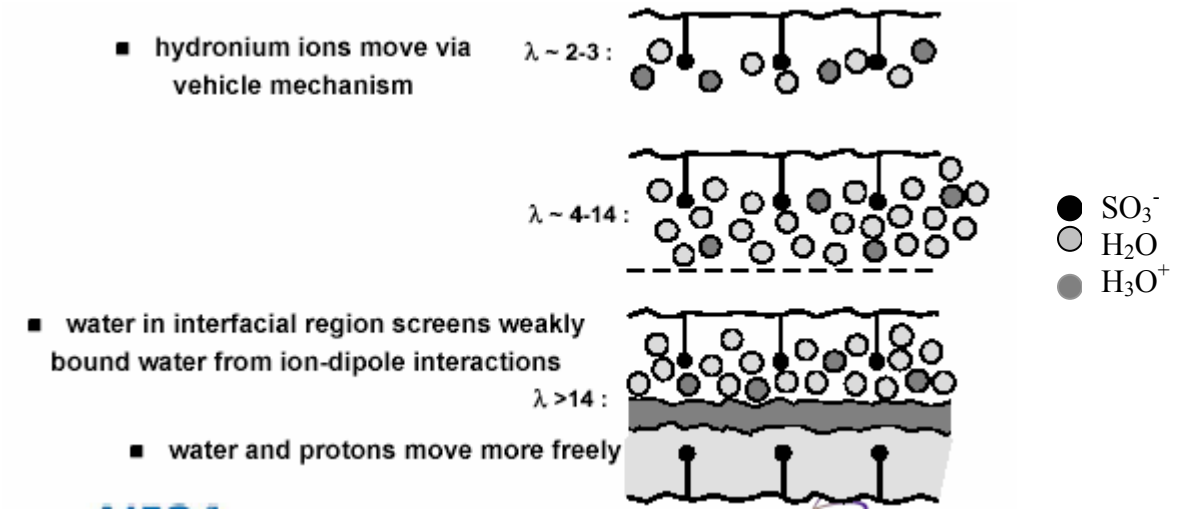

Figure 1.5 Qualitative Picture of Transport in Nafion [25]

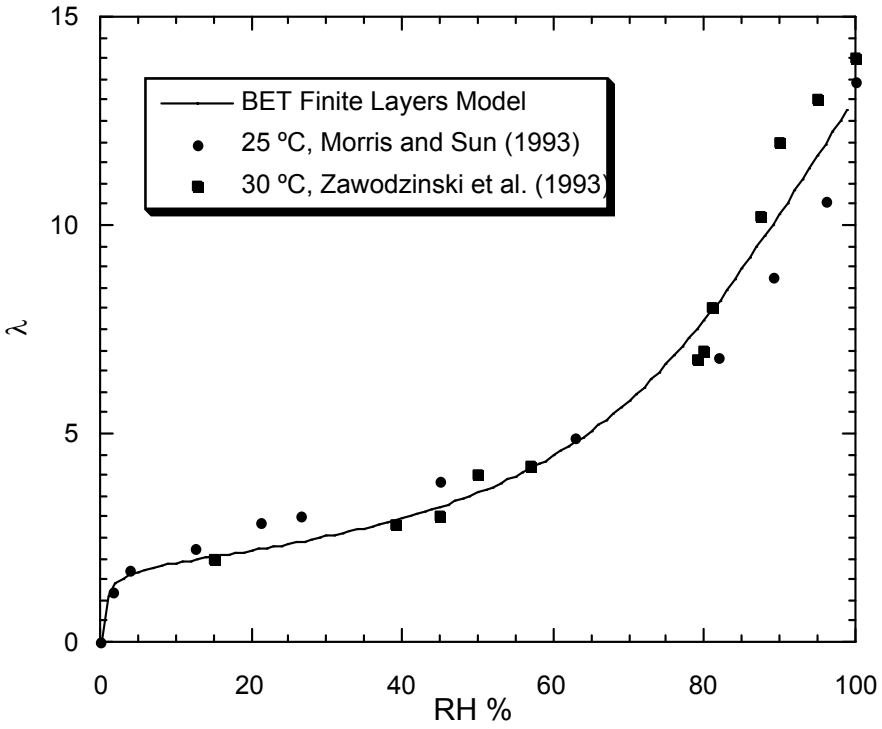

Figure 1.6 Equilibrium sorption of water on Nafion as a function of water vapor activity [25].

1.5 Electrodes

The electrodes consist of nanosized platinum (3-5 nm) supported on carbon particles (30 microns) and mixed with proton conducting ionomeric material. On the top of each electrode layer is a 100-300 μm thick gas diffusion backing layer made from carbon cloth or porous carbon paper. Figure 1.7 shows the typical cross section of electrode with the carbon black. Enormous amount of research has been done to develop high performing catalyst for fuel cells. In PEM fuel cells, the type of fuel used dictates the appropriate type of catalyst needed. Within this context, tolerance to carbon monoxide (CO) is an important issue, particularly when hydrogen is formed from fuel reforming. It has been shown that PEM fuel cell performance drops with a CO concentration of only several parts per million. This is due to the strong chemisorption force of CO onto the catalyst. Table 1.4 shows various catalysts developed to improve fuel cell performance and also CO tolerance [31-40].

1.6 Gas Diffusion Layer (GDL)

The GDLs, one next to the anode and the other next to the cathode, are usually made of a porous carbon paper or carbon cloth, typically 100–300 μ thick [35]. The porous nature of the GDL material ensures effective diffusion of each reactant gas to the catalyst on the membrane/electrode assembly. The structure allows the gas to spread out as it diffuses so that the gas will be in uniform contact with the entire surface area of the catalyzed membrane. The GDL also assists in water management during the operation of the fuel cell. A GDL that allows the appropriate amount of water vapor to reach the membrane/electrode assembly keeps the membrane humidified and improves the efficiency of the cell. The GDL allows the liquid water produced at the cathode to leave the cell so it does not flood. The GDL is typically wet-proofed to ensure that at least some, and hopefully most, of the pores in the carbon cloth or paper do not become clogged with water, which would prevent the rapid gas diffusion necessary for a good rate of reaction to occur at the electrodes. PTFE is the wet-proofing agent used for carbon-based PEM GDLs by fuel cell community. The amount of PTFE determines the porosity and water content of GDL.

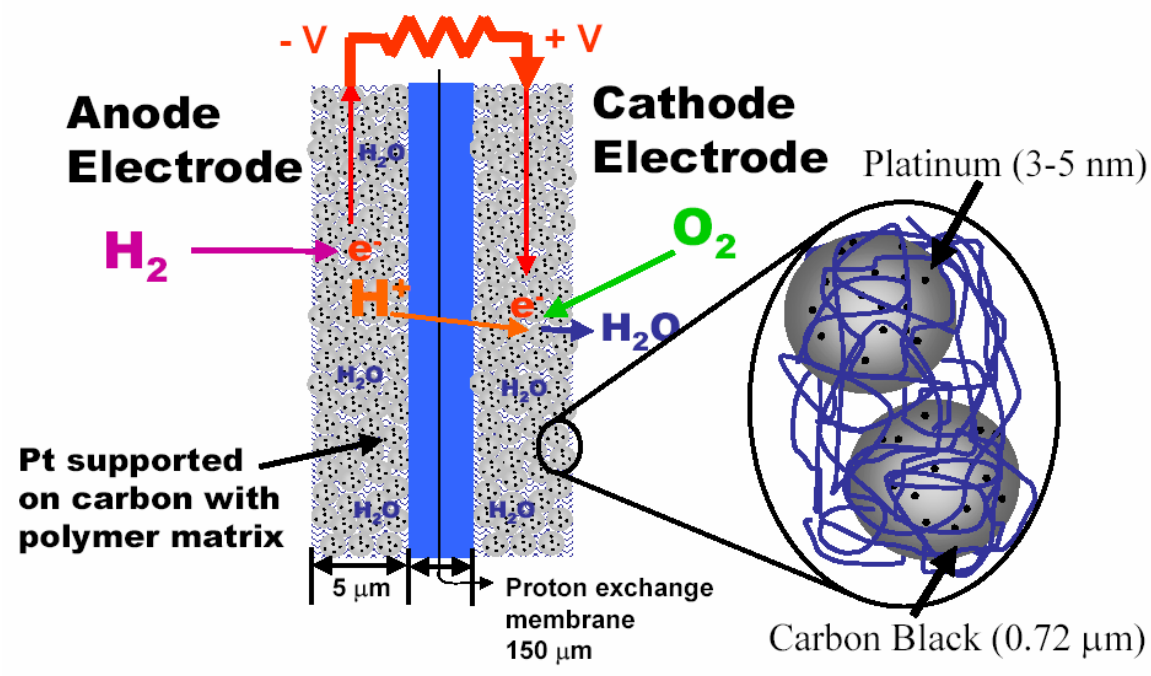

Figure 1.7 Electrode cross section with carbon black [40].

	Single metal catalyst	Binary catalyst	Ternary catalyst
Pt/C	X		
Pt-Co/C		X	
Pt-Cr/C		X	
Pt-Fe/C		X	
Pt-Ir/C		X	
Pt-Mn/C		X	
Pt-Mo/C		X	
Pt-Ni/C		X	
Pt-Pd/C		X	
Pt-Rh/C		X	
Pt-Ru/C		X	
Pt-V/C		X	
Au-Pd/C		X	
Pt-Ru-Al_4			X
Pt-Ru-Mo/C			X
Pt-Ru-Cr/C			X
Pt-Ru-Ir/C			X
Pt-Ru-Mn/C			X
Pt-Ru-Co			X
Pt-Ru-Nb/C			X
Pt-Ru-Ni/C			X
Pt-Ru-Pd/C			X
Pt-Ru-Rh/C			X
Pt-Ru-W/C			X
Pt-Ru-Zr/C			X
Pt-Re-(MgH_2)			X

Table 1.4 Various anode catalyst materials [31-40].

1.7 Membrane Electrode Assembly (MEA)

The combination of the anode:membrane:cathode is called the membrane electrode assembly (MEA). Figure 1.8(a) shows two different modes to prepare MEA depending on whether catalyst is applied directly to the membrane or to the GDL [39, 41-43]. The original MEA was made in 1965 for GEMINI space program and used 4mg of platinum per square centimeter of membrane area. Figure 1.8(b) shows a typical MEA in fuel cell. The thickness of MEA depends on type of membrane and how much platinum is used in each electrode. Typical thickness of MEA could be about 200 μm or 0.2 mm. The electrodes now use less than 0.4 mg Pt/ cm^2 MEA.

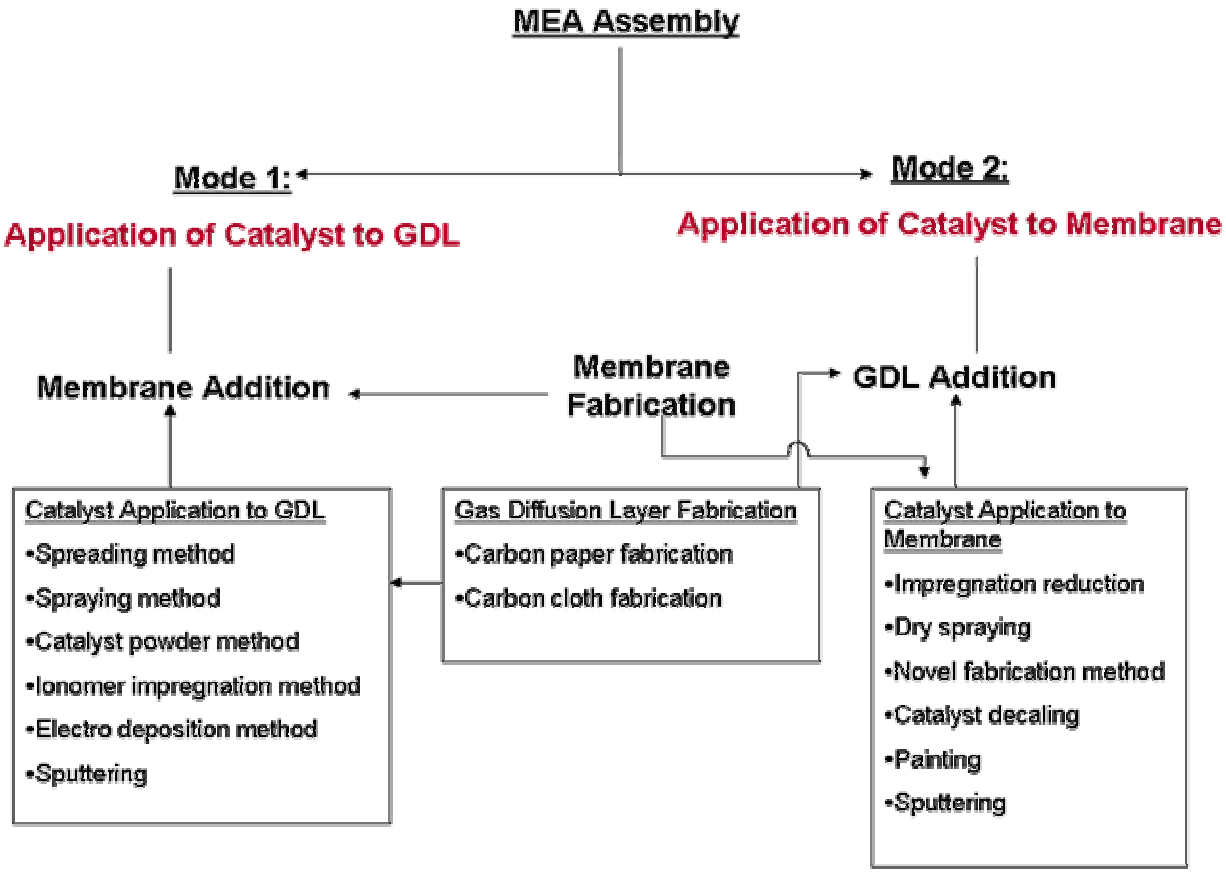

Figure 1.8(a) MEA preparation methods [41-43]

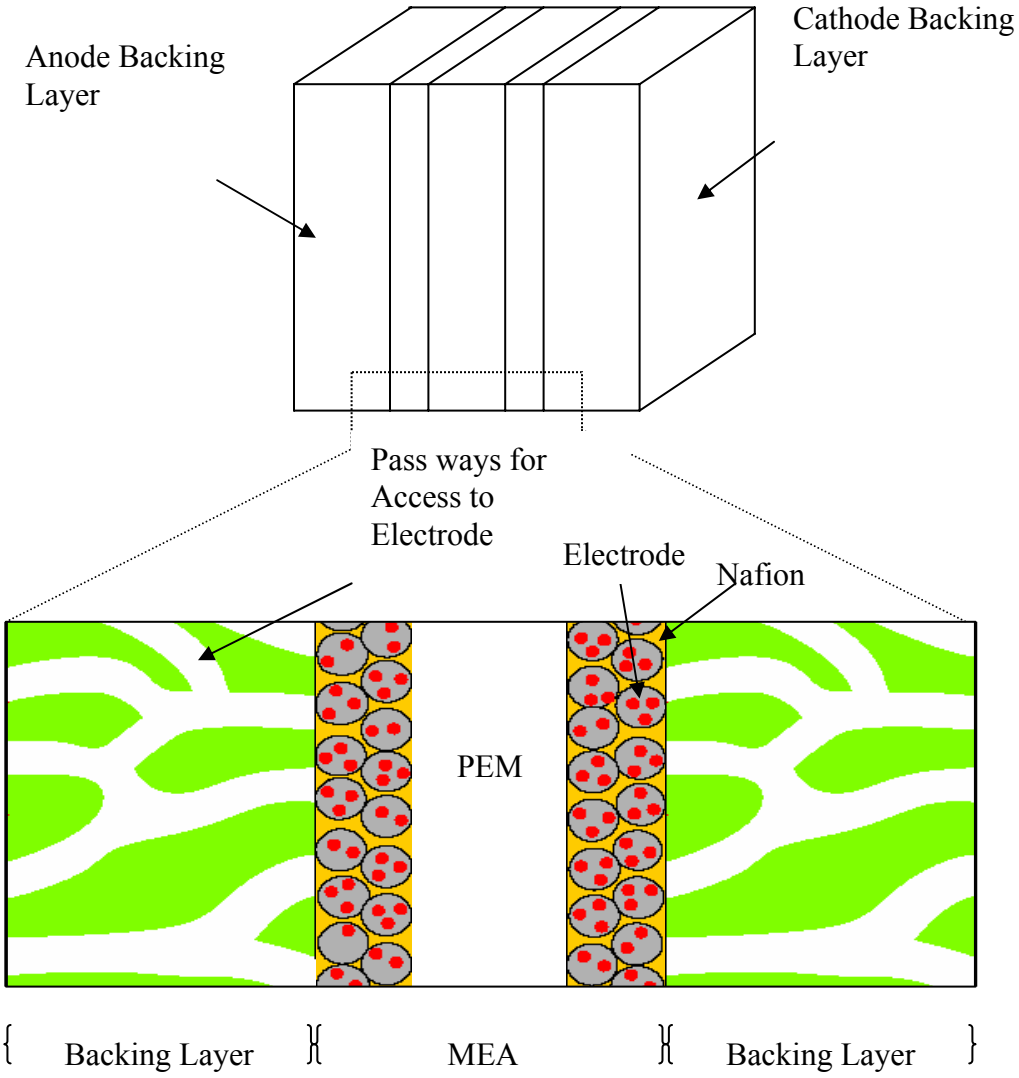

Figure 1.8(b) Structure of MEA with backing layers.

1.8 Flow Field/ Current Collector

The final element on the outer side of the unit cell is the current collector plate which also typically contains a machined gas flow field. These two functions of current collector and gas flow field may be fulfilled, in principle, by two separate components but, in most of the cells and stacks tested to date the flow field is machined in the current collector plate using a range of geometries, e.g., a single serpentine channel, parallel channel flow and series-parallel combinations. The flow-field geometry is quite significant in fulfilling the requirements of effective and uniform gas and water supply and effective liquid water removal from the cathode. The current collector plate becomes the bipolar plate in a PEFC stack. It should, therefore, exhibit high electronic conductivity and be impermeable to oxygen and hydrogen gases. Both carbon and metals like stainless steel or titanium have been considered as potential materials. Also these are non corrosive in nature for fuel cell operations. Finally, by adding a load containing circuit, the PEM fuel cell is complete. Figure 1.9 lists different materials for bipolar plates under consideration [44-48].

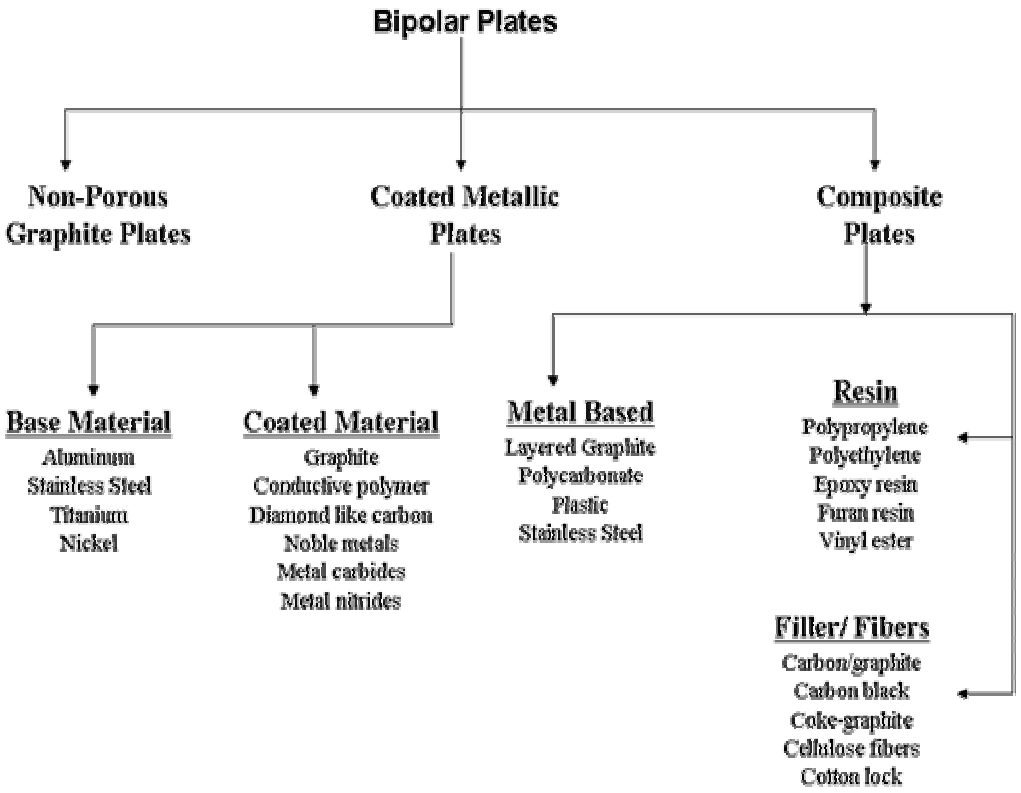

Figure 1.9 Bipolar plate materials

1.9 Motivation for Higher Temperature Operation of PEM Fuel Cells

Nafion and other perfluorinated PEMs have been widely used because of their excellent proton conductivity and electrochemical stability due to the PTFE backbone. However, they are expensive, not as durable as desirable especially under cycling voltage, humidity, and freezing and thawing conditions, unstable at temperatures over 100º C, and effectively conduct protons only when they imbibe sufficient water, which limits operating temperatures of PEM fuel cells to around 80º C. On the other hand, fuel cell temperature above 100º C is a highly desirable goal. As the operation of fuel cells at higher temperature increases electrochemical kinetics, improves CO tolerance, facilitates heat rejection, and reduces the problems associated with water management, there have been extensive research efforts to find alternatives membranes that are stable at higher temperature. In fact, a desirable PEM must not only be highly proton conductive under hot and dry conditions, it should be thin for low resistance and high protonic conductivity, compliant to make a good contact with electrodes but rigid enough to provide support to the membrane electrode assembly (MEA), thermally and dimensionally stable, impervious to gaseous or liquid fuels, as well as to electrons, with a low electro-osmotic drag, and mechanically strong enough to last several years. This is a tall order indeed, and it is small wonder that success at finding alternates to Nafion has been limited despite a very large-scale research effort.

The following are the advantages for operating the PEM fuel cell at high temperatures (i.e. above 100 ^{o}C) [12, 49-60]:

(i) CO catalyst poisoning: Carbon monoxide concentrations in excess of about 10 ppm at low temperatures poison the electro-catalyst. This tolerance increases with the increase in the operating fuel cell temperature above about 100 ^{o}C. This has further been reinforced by Yang *et al*. [49] who completed a theoretical thermodynamic analysis demonstrating how the CO coverage of the surface of the catalyst is reduced as a function of increasing temperature.

(ii) Heat management: Operating at higher temperatures has the advantage of creating a greater driving force for more efficient cooling. This is particularly important for transport

applications to reduce balance of plant equipment (e.g. radiators). Furthermore, high grade exhaust heat can be integrated into fuel processing stages.

(iii) Prohibitive technology costs: The cost of fabrication of current polymers is prohibitive, mainly as a result of the necessity to use fluorine. Combining manufacturing issues with the potential savings from a reduction in electro-catalyst loading forms a very strong economical driving force to develop fuel cells that operate at high temperatures.

(iv) Humidification and water management: The pressurization needed to reach temperatures beyond 130 ^{o}C and maintain high humidities would likely out-weigh any efficiency gains of going beyond this temperature. Membranes that are capable of operating at reduced humidities would not require pressurization. In addition, it is less likely that they will be affected by the significant water management problems of polymer membranes.

(v) Increased rates of reaction and diffusion: As the temperature increases the reaction and interlayer diffusion rates increase. Additionally, the reduction of liquid water molecules will increase the exposed surface area of the catalysts and improve the ability of the reactants to diffuse into the reaction layer.

For these reasons, it is desirable to move hydrogen PEMFC technology toward high temperature operation for certain applications. Current polymer membranes are not capable of operating at high temperatures for two reasons: degradation at temperatures above 100–120 ^{o}C as a result of the low glass transition temperature and because proton conduction is dependant on the hydration levels in membranes. The main solutions to this problem have been to substitute the present polymer membranes with composite polymer membranes or use solid acid membranes. Unfortunately, the available alternative PEMs compromise performance and longetivity. Thus, there is world wide effort currently underway to find suitable alternatives to Nafion that might allow higher temperature operation and cost benefit.

1.10 Design Goals for PEMs

The following are thus the goals for the development of membrane materials for higher temperature operations [12]:

1. A good performance at a temperature of 120 ºC without the need to pressurize, i.e., at a relative humidity (RH) ≤ 40%. At this temperature, about 50 ppm CO can be tolerated without air bleed. At higher temperatures (≥ 160 ºC), the stability of carbon support becomes an issue along with a reduction in the Nernst potential. Thus, 120 ºC appears to be optimal.
2. A conductivity of around σ = 0.1 S/cm under these conditions (Figure 1.10(a)).
3. A hydrogen-oxygen gas permeability that is no more than that in current PFSA membranes (≤ $1x10^{-12}$ (mol cm)/(cm^2 s kPa)).
4. A limited swelling in water (≤ 100% water uptake when boiled in water).
5. A low water electro-osmotic drag in the membrane.
6. A functional component that does not leach out in liquid water.
7. Mechanical properties that are better than Nafion, although the specific criteria are not yet defined because of lack of understanding of stresses in operating fuel cells.
8. A chemical stability similar or superior to Nafion, i.e., a durability of around 40,000 h (≤ 1 μV/h) for stationary power and around 10,000 h (≤ 10 μV/h).
9. A cost which would eventually allow an MEA cost target ≤ $10/kW at 500,000 stacks/y for automotive application (Figure 1.10(b)).

This is, however, particularly challenging task because of the desired performance characteristics. The targets listed above are very aggressive targets that are not likely to be achieved without a better fundamental theoretical and experimental understanding of the functioning of current polymer electrolytes that can provide the necessary insights to allow the deliberate design of improved or new PEMs. This research work is thus focused on developing better understanding of the various physicochemical phenomena and developing high temperature nanocomposite membrane based on the guidelines of the model.

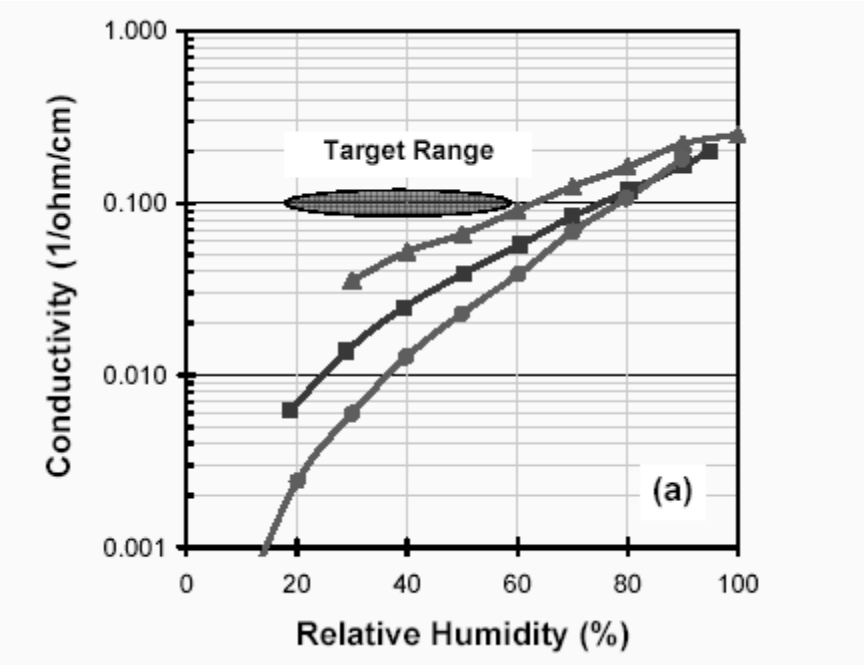

Figure 1.10(a) Desired conductivity for commercialization [12]

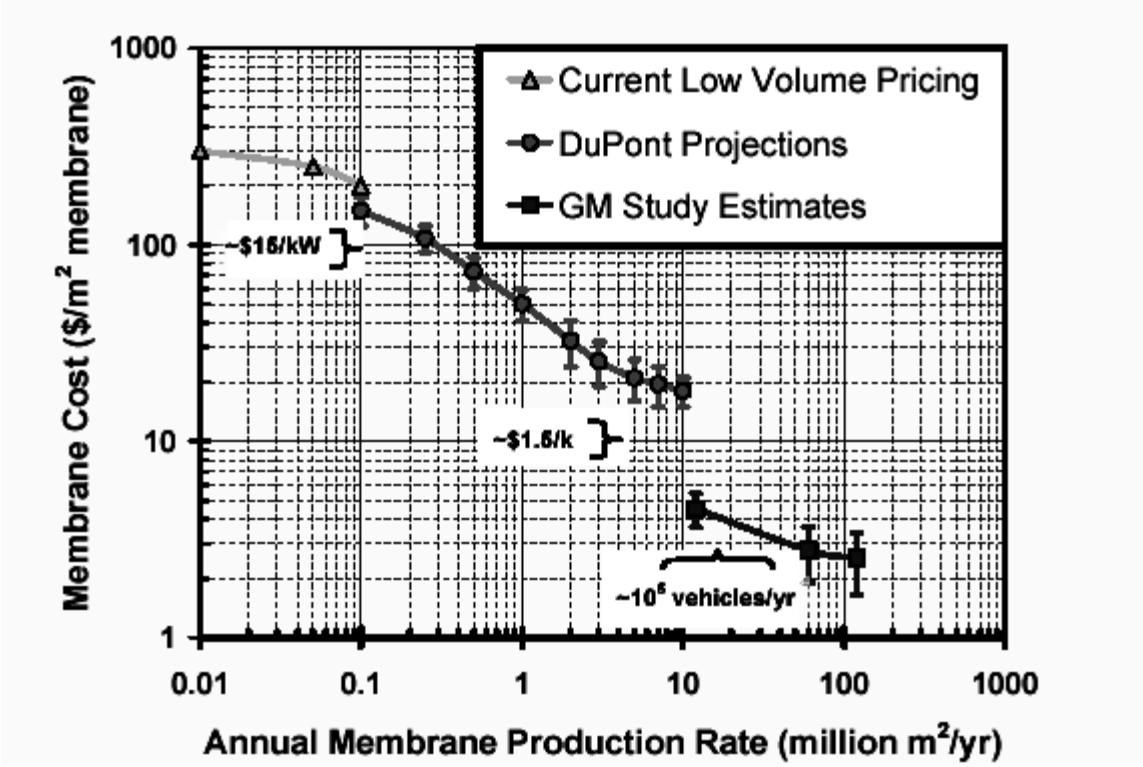

Figure 1.10(b) Desired membrane cost for commercialization [12]

1.11 Possible Approaches for Developing Higher Temperature Membranes

1.11.1 Modification of Existing Polymer Membrane

Most commonly, a hydrophilic inorganic additive is added to retain water at higher temperatures and to increase acidity as proposed by Malhotra and Datta (1997) [51]. This hydrophilic, acidic, inorganic material may be incorporated into the perfluorinated membrane to increase the binding energy of water and the number and strength of acid sites. The efficacy of this procedure has been demonstrated by the case of heteropolyacids in Nafion by Malhotra and Datta (1997). The underlying basis of the approach is: the acid may increase proton conductivity by additional acidity and increased solvent (water) uptake. Examples of other subsequent inorganic additives are: sulphated zirconia, zirconium phosphate, heteropolyacids and silica gel. Though this concept seems promising, the success so far seems limited and the interaction between the inorganic phase and proton conductor is not sufficiently understood. Further the stability of the material in the polymer host is uncertain. Certain material (e.g. heteropolyacids) dissolve in the water produced in the fuel cell and also leach out.

1.11.2 Use of Non Aqueous Solvent

Another approach that has been tried is replacement of the water with a non-volatile, non aqueous solvent that serves the same function as water. Two salient examples of such 'water replacements' are phosphoric acid and imidazole. The rationale is that other liquid solvents can perform the function of water in proton conduction but with improved physical characteristics (i.e. low volatility). In order for other solvent to serve as a replacement of water, it should have the ability to act as Bronsted base to solubilize the protons, and have high dielectric constant and low volatility. Unfortunately these solvents are typically soluble in the water produced and can eventually leach out.

1.11.3 Use of Solid State Protonic Conductor

A good solid proton conductor evidently requires mobile protons. Thus, inorganic proton conductors without a liquid phase, while conceptually very attractive, require temperatures in excess of 800 ^{o}C to provide adequate conductivities via a proton hopping mechanism owing to the high activation energy. At lower temperatures, a liquid-phase for

proton conduction is essential, either as a molten or a solvated acid. When a solvent other than water is used, the challenge of complete immobilization of the liquid must be first addressed to ensure stable performance over extended periods. When water is the solvent, the challenge is to retain water within the membrane under hot and dry conditions owing to its high volatility. As compared to the first two approaches which relied on an acidic polymeric membrane such as Nafion and a liquid solvent for proton transport, this approach is based on a solid state material that conducts protons in the absence of a solvent. Solid oxide conductors have been employed for many years in high temperature fuel cells. Cesium hydrogen sulfate, a low temperature solid state conductor, was immobilized in a porous support and incorporated in fuel cell [49].

1.11.4 Use of Skin Layer

From the nature, it is observed that all biological materials including fruits, vegetables, and cellular materials retain water even under dry conditions. This is attributed to the presence of hydrophobic skin layer that helps in retaining water. Using the similar strategy it may be possible to develop a hydrophobic layer on the Nafion membrane so that is does not lose water. This hydrophobic layer can be teflon based which can be coated on the membrane before assembling the membrane electrodes assembly.

1.12 Alternate PEMs

There have been numerous candidates developed for higher temperature operation of fuel cells, both by modifying Nafion membranes and also by developing completely new system of membrane [49-88]. Figure 1.11 summarizes various types of membrane materials studied. A thorough literature review is also provided in Chapter 2, but two main types of polymer membranes have dominated research efforts: sulfonated aromatic polymers (e.g. sulfonated polyetherketone, SPEEK and polyetherketone, SPEK) and perfluorosulfonic acid membranes such as Nafion which have been the industry benchmark. These membranes both exhibit phase separated domains consisting of an extremely hydrophobic backbone which gives morphological stability and extremely hydrophilic functional groups. These functional groups aggregate to form hydrophilic nano-domains which act as water reservoirs.

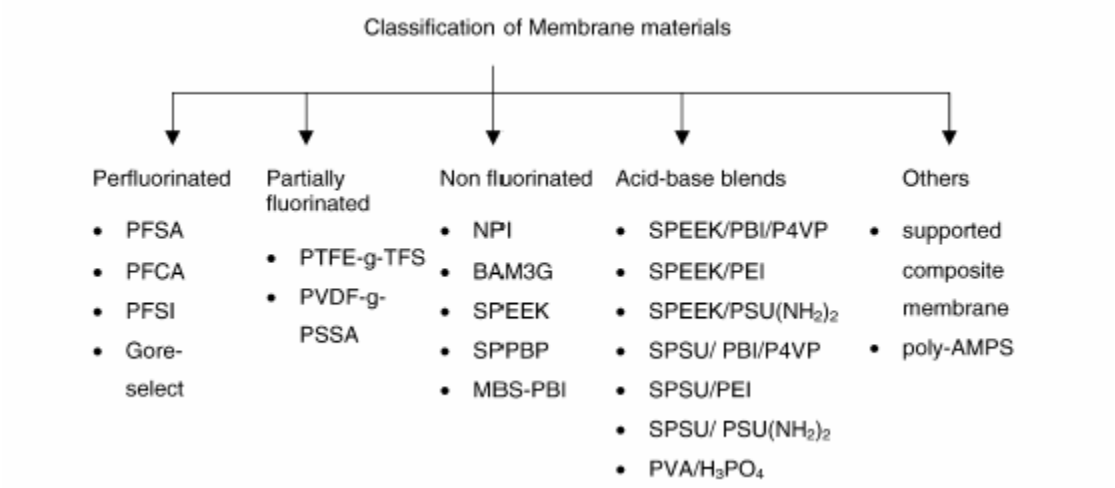

Figure 1.11 Classification of membrane materials [53].

But the conductivity of sulfonated aromatic polymers is also heavily dependant on the degree of sulfonation. At reduced levels of sulfonation the aromatic polymers have lower water contents and reduced conductivity of 10^{-2} S cm^{-1} which is not acceptable for use in fuel cell membranes. However, if the degree of sulfonation is increased to improve conductivity, the mechanical properties of the membrane deteriorate. One proposed solution is to produce nanocomposite membranes with controlled mechanical, physical and chemical properties.

Hydrocarbon Membranes

Hydrocarbon membranes provide some definite advantages over PFSA membranes. They are less expensive, commercially available and their structure permits the introduction of polar sites as pendant groups in order to increase the water uptake. Among these 15 membranes showed potential for replacing Nafion membranes. Table 1.5 summarizes information on synthesis of these 15 candidates [89-94].

Membrane type	Design methodology
Gore-Select membrane (f)	Ultra-thin integral composite consisting of a base material preferably made of expanded PTFE that supports an ion exchange material such as perfluorinated sulfonic acid resin, perfluorinated carboxylic acid resin, PVA, divinyl benzene (DVB), etc.
Perfluorocarboxylic acid (f)	Copolymer of tetrafluoroethylene (TFE) and perfluorovinyl ether (PFVE).
Bis(perfluoroalkylsulfonyl) Imide (f)	Copolymerization of sodium 3,6-dioxa-4-trifluoro methyl perfluorooctyl trifluoromethyl with TFE.
α,β,β-Trifluorostyrene grafted membrane (pf)	Grafting of α,β,β-trifluorostyrene and PTFE/ethylene copolymers
Styrene grafted and sulfonated poly(vinylidene fluoride) membranes [PVDF-G-PSSA] (pf)	Pre-irradiation grafting of styrene onto a matrix of PVDF after electron beam irradiation. The proton conductivity can be increased by crosslinking with DVB.
BAM3G membrane (Ballard advance material of third generation membrane) (nf)	Polymerization of α,β,β-trifluorostyrene, includes monomers selected from a group of substituted α,β,β-trifluorostyrene
Membrane of base-doped with S-polybenzimidazoles (PBI) (nf composites)	Introduction of organic and inorganic bronsted bases to sulfonated PBI
Crosslinked/non-crosslinked (SPEEK) (nf)	Direct sulfonation of PEEK in conc. sulfuric acid medium yields high proton conductivity along with thermal stability
Imidazole doped sulfonated polyetherketone (SPEK) (nf)	Complexation with imidazoles to obtain high proton conductivities
Methylbenzenesulfonated PBI/methylbenzenesulfonate poly(*p*-phenylene terephthal amide) membranes (nf)	These alkylsulfonated aromatic polymer electrolyte posses very good thermal stability and proton conductivity when compared to PFSA membranes, even above 80 °C
Sulfonated napthalenic polyimide membrane (nf)	Based on sulfonated aromatic diamines and dihydrides. Its performance is similar to PFSA
Sulfonated poly(4-phenoxybenzoyl-1,4-phenylene) (SPPBP) (nf)	Derived from poly(*p*-phenylene) and structurally similar to PEEK. Direct sulfonation results in a proton conductive polymer.

Membrane type	Design methodology
Supported composite membrane (other)	Made of ion conducting polymer and poly-*p*-phenylene benzobisoxazole (PBO) substrate.
Poly(2-acrylamido-2-methylpropanesulfonic acid) (other)	Made from polymerization of AMPS monomer. AMPS monomer is made from acrylonitrile, isobutylene and sulfuric acid.

f = fluorinated, nf = nonfluorinated, pf = partially fluorinated

Table 1.5 Hydrocarbon membranes [89-94]

1.13 Research Direction

It is important to understand that high temperature operation is being prevented by three main barriers [12]:

1. Loss of hydration of the PEM and instantaneous increase in membrane resistance,
2. Membrane degradation of the polymer above 120 ^{o}C; and
3. Lack of intermediate proton conductors in the range of 100–400 ^{o}C with a unique proton 'solvating' species supporting conduction in the regime.

The factor that has the highest influence on conductivity of proton conducting polymers is the degree of hydration. Hence to understand the design parameters for high temperature PEMs, it is important to have a fundamental understanding of water and proton transport mechanisms. As discussed earlier the hydration is dependent on the phase separation of the hydrophilic and hydrophobic domains. The effect of hydration in Nafion at constant temperature is significant. The conductivity of Nafion membranes quoted in literature often very widely depends on the system, pretreatment, and equilibrium parameters used. At 100 % relative humidity (RH) the conductivity is generally about 0.1 S cm^{-1} and drops by several orders of magnitude as the humidity is decreased. As a result, generally one or both of the streams for the perfluorinated sulfonic acid polymers and sulfonated aromatic polymers (e.g. Nafion and SPEK) must be hydrated to keep the membranes swollen so that the ionic inclusions are bridged. Consequently, understanding transport within PEM membranes is partly a matter of understanding the conduction through water [95-99].

Transport in water is generally a result of protonic defects and occurs through the breaking and reformation of bonds. This is caused because the protonic defect weakens the intermolecular interactions which cause large variations in bond length combined with rapid breaking and forming of bonds. In a PEM, the hydrated environment, often acidic, acts as a solvent for the diffusion of the hydronium and dimer ions which are formed.

With the migration of protons through the membrane comes other associated design issues. Firstly the transport of the defect pulls other water molecules through the membrane. This is known as electro-osmotic drag and is caused in part by the size of the molecule and by the molecular attractions between molecules. Secondly, another

competing force to proton conduction is back diffusion from the cathode, this occurs because of the driving forces formed as the water is removed from the anode due to the electro-osmotic drag. Integrated systems balancing these processes by using product water to maintain hydration are still underdevelopment.

The design parameters that affect PEM performance are thus the nature of polymer backbone, the nature of the side chain, the nature and strength of the acid group, the equivalent weight, the degree of cross-linking, and thermo-mechanical properties of the membranes. In order to understand the effects of these parameters and to obtain better insight into the design parameters of the membrane, a model should be developed that simulates the transport of protons through a Nafion membrane at different temperatures and RHs (relative humidity). The challenge when designing PEM membranes is also to synthesize a microstructure capable of facilitating the aforementioned proton transport while meeting the other design hurdles.

These barriers directly affect the research direction for developing higher temperature membranes which is focused on:

1. Modification of existing polymer membranes with composites to increase water retention and possibly contribute to conduction (limited by glass transition temperature);

2. Novel non-polymer based solid proton conductors that have reduced or no dependence on hydration (often called solid acid proton conductors).

Greatest promise for solid acids has been demonstrated by zirconium, titanium and cesium phosphates. The thermodynamic limitation of high temperature use of water dependant PEMs has been discussed earlier by Yang *et al*. [49]. The addition of the organic phases in composite membranes which interacts strongly with the water can reduce the chemical potential of the liquid water. This in turn reduces the differential in the chemical potential between the liquid and vapor phase reducing the water loss from the membrane at a given relative humidity. Thus any modifications to the membrane that can reduce the chemical potential of the liquid phase would be advantageous. Unfortunately however, above 100 ^{o}C the gains realized by reducing the chemical potential by addition of an organic phase are limited as a result of the low water vapour pressure.

The use of microporous membranes also has to be considered in terms of the potential effect on the vapour–liquid equilibrium. It is well established that the thermodynamic assumptions that hold for large volumes cannot be directly applied to micro and nano-domains that are a feature of microporous membranes. Capillary forces and diffusion should be given considerations to understand the effect of nano domains on membrane properties. Ultimately the best way of testing the limitations of these membranes is to study them in prototype MEAs and fuel cells.

There are many other significant issues that will need to be resolved before solid acid membranes are used in PEM fuel cells. These issues include standard operating considerations such as mechanical strength and durability, cyclability, synthesis and integration in addition to design issues including catalyst compatibility and scale up (or down). Finally, it is important to recognize potentially that the greatest barrier faced will be startup and shut down operation, as typically the cells low temperature and high temperature conductivity mechanisms vary greatly.

A summary of high temperature proton conductors in hydrated, semi-hydrated and anhydrous conditions are presented in Table 1.6 and Table 1.7 [30-88]. A summary of different solid acid conductors and their conductivities is shown in Table 1.8.

Polymer System	Producer/ Developer	Classification	Temperature Range(°C)	Conductivity Scm^{-1} (°C)	Durability (hours)	Suitability
Nafion® EW 1100	DuPont, USA	Hydrated	25-80 H_2 PEM 25-140 DMFC*	~$2x10^{-1}$ (80)	60,000	Low
Composite Silica/recast Nafion®	CNR-TAE- Institute Transformation and Storage of Energy, Italy	Hydrated	25-80 H_2 PEM 25-140 DMFC*	1x10-1	1000 (100mV loss)	Low/Med
BMITf doped Nafion®	DuPont, USA	Anhydrous	180	0.1(180)	Not Determined	Med/High
Phosphoric Acid Doped PBI	Case Western Reserve University, USA	Anhydrous	130-230	$3.5x10^{-2}$ (190)	Not Determined	Med/High
Substituted PPO	Polymer Research Institute, NY State University, USA	Hydrated	100-150**	$<1x10^{-1}$	Not Determined	Low
Sulfonated PEEK	ICI Victrex, UK	Hydrated	25-130***	N/A	N/A	High
Sulfonated PEEK	Fuma-Tech, Germany	Hydrated	25-130***	N/A	N/A	High
Sulfonated PEEK	Axiva, Germany	Hydrated	25-130***	$6x10^{-2}$ (25)	4000	High
Sulfonated Poly(arylether sulfone)	CNR-TAE- Institute Transformation and Storage of Energy, Italy	Hydrated	25-160	$4x10^{-2}$ (80)	Not Determined	Med
Sulfonated Poly(4-phenoxybenzoyl-1,4-phenylene)	Maxdem Inc, USA	Hydrated	50-130	$9x10^{-2}$ (80)	200	High
Imidazole doped poly-Polly(ether ketone)	Max Plank Institute FKF, Germany	Anhydrous	200 max.	$2x10^{-2}$ (200)	N/A	Med/High
S-PEEK/PBI blends	University of Stuttgart, Germany	Hydrated	25-130***	N/a	N/A	Med/High

* - only at high pressures (4 Bar Abs.)
** - reported to be under development
*** - predicted temperature range

Table 1.6 Summary of membrane materials [53].

Membrane System	Comments on high temperature operation
Nafion/ZrP	Conductivity similar to Nafion, improved MEA and fuel crossover
Nafion/silica	Conductivity similar to Nafion, improved fuel crossover
Nafion/HPA	Good improvements in conductivity over Nafion counteracted by leaching
Nafion/mordenite	Very small conductivity improvements at high temperatures only
Nafion/imidazole	Very good conductivity results however imidazole poisoned Pt catalyst
SPEEK/ZrP	No appreciable improvement over SPEEK
SPEEK/ZrO_2	$\leq$ 1 Order of magnitude reduction in methanol permeability and conductivity
SPEEK/silica	Reduction in H_2O permeability without a significant decrease in conductivity
SPEEK/ZrP /ZrO_2	Large reduction in methanol permeability without a large conductivity sacrifice
SPEEK/BPO_4	Reasonable conductivity compared to Nafion composites at 100–140 ^oC

Table 1.7 Summary of nanocomposite polymer membranes [49-53].

Compound	Comments on high temperature operation
Zirconium phosphate (ZrP)	Reasonable conductivity in all temperature ranges compared to Nafion
Sulfonated ZrP	Very significant increases in conductivity compared to ZrP
Milled ZrP	Small increases in proton conductivity compared to ZrP
Pillared ZrP	Large increase in conductivity compared to ZrP; stability questionable
Sulfonated TiP	Higher conductivities than comparable zirconium materials
Cesium phosphate	Good conductivity above 140 ^{o}C; requires further development
Cesium sulfate	Good conductivity above 140 ^{o}C; questionable stability
Sol–gel P_2O_5–TiO_2–SiO_2	Conductivity of ca 10^{-3} S cm^{-1}; low stability
ZrO_2	Slightly improved conductivity compared to ZrP
Sulfonated ZrO_2	Conductivity of ca 0.05 S cm^{-1} from 60 to 100 ^{o}C at saturated conditions
Fullerenes	Promising results for dry conductivity up to 200 ^{o}C
Fumed silica/ZrP	Hydration dependant conductivities ca. one order of magnitude below Nafion

Table 1.8 Conductivity summaries of solid acid conductors [49-53].

1.14 References

1. K. D. Kreuer, In Handbook of Fuel Cell Fundamentals, Technology, and Applications; Vielstich *et al*., Eds.; John Wiley: Chichester, UK, 2003; Vol. 3, Part 3, Chapter 33, 420.
2. Doyle, M.; Rajendran, G. In Handbook of Fuel Cell Fundamentals, Technology, and Applications; Vielstich *et al*., Eds.; John Wiley: Chichester, UK, 2003; Vol. 3, Part 3, Chapter 30,351
3. F. Babir and T. Gomez, Efficiency and economics of proton exchange membrane fuel cells, *Int. J. Hyd. Energy* **21** (1996), 891.
4. Fuel Cell Industry Review, May 2003
5. T.D. Gierke and W.Y. Hsu In: A. Eisenberg and H.L. Yeager, Editors, *Perfluorinated Ionomer Membranes, ACS Symposium Series No. 180*, American Chemical Society, Washington, DC (1982), 283.
6. S. Motupally, A.J. Becker and J.W. Weidner, Diffusion of water in Nafion 115 membranes, *J. Electrochem. Soc.* **147** (2000) (9), 3171–3177.
7. M. Rikukawa and K. Sanui, Proton-conducting polymer electrolyte membranes based on hydrocarbon polymers, *Prog. Polym. Sci.* **25** (2000), 1463–1502.
8. T.E. Springer, T.A. Zawodzinski and S. Gottesfeld, Polymer electrolyte fuel cell model, *J. Electrochem. Soc.* **138** (1991), 2334–2344.
9. EG&G Services, Fuel Cell Handbook, 5th ed., Parsons Inc., October, 2000.
10. S. Gottesfeld and T. Zawodzinski, Polymer electrolyte fuel cell, *Adv. Electrochem. Sci. Eng.* **5** (1997), pp. 195–381.
11. DOE Report Basic Research Needs for the Hydrogen Economy. Report of the Basic Energy Sciences Workshop on Hydrogen Production, Storage and Use, May 13-15, 2003, http://www.sc.doe.gov/bes/hydrogen.pdf.
12. Mathias, M. F.; Makharia, R.; Gasteiger, H. A.; Conley, J. J.; Fuller, T. J.; Gittleman, C. J.; Kocha, S. S.; Miller, D. P.; Mittelsteadt, C. K.; Xie, T.; Yan, S. G.; Yu, P. T. Interface 2005, 14 (3), 24
13. T. Thampan, S. Malhotra and R. Datta, PEM fuel cell as a membrane reactor, *Catalysis Today* **67** (2001, 15-32.

14. W.G. Grot, Discovery and development of Nafion perfluorinated membranes, *Chem. Ind.* **19** (1985), 647.
15. J. Roziere and D.J. Jones, *Ann. Rev. Mater. Sci.* **33** (2003), 503.
16. Kerres, State of art of membrane development, *J. Membr. Sci.* **185** (2001),1.
17. T.D. Gierke and W.Y. Hsu In: A. Eisenberg and H.L. Yeager, Editors, *Perfluorinated Ionomer Membranes, ACS Symposium Series No. 180*, American Chemical Society, Washington, DC (1982), 283.
18. A. Steck, in: O. Savadago, P.R. Roberge, T.N. Veziroglu, Proceedings of the First International Symposium on New Materials for Fuel Cell Systems, Montreal, July 9–13, 1995, 74.
19. S.C. Yeo and A. Eisenberg, *J. Appl. Poly. Sci.* **21 (1997),** 875.
20. K. A. Mauritz, C. J. Hora and A. J. Hopfinger , *Prep. Am. Chem. Soc. Div. Polym. Chem.* **19** (1978) 324.
21. M. Bae, I. Honma, M. Murata, T. Yamamoto, M. Rikukawa and N. Ogata, Properties of selected sulfonated polymers as proton-conducting electrolytes for polymer electrolyte fuel cells, *Solid State Ionics* **147** (2002), 89–194.
22. Gebel, P. Aldebert and M. Pineri, Swelling study of perfluorinated ionomer membrane, *Polymer* **34** (1993), 333.
23. P. Choi, N. H. Jalani and R. Datta, Thermodynamics and Proton Transport in Nafion II. Proton diffusion Mechanisms and Conductivity, *J. Electrochem. Soc.,* **152(3)** (2005), E123-130.
24. P. Choi, N. H. Jalani and R. Datta, "Thermodynamics and Proton Transport in Nafion I. Membrane Swelling, Sorption, and Ion-Exchange Equilibrium, *J. Electrochem. Soc.*, **152(3)** (2005) E84-89.
25. T. Zadowzinski, J. Davey, J. Valerio and S. Gottesfeld, The water content dependence of electro-osmotic drag in proton conducting polymer electrolytes, *Electrochim. Acta* **40** (1995), 297–302.
26. M. Cappadonia, J.W. Erning, S.M.S. Niaki and U. Stimming, Conductance of Nafion 117 membranes as a function of temperature and water content, *Solid State Ionics* **77** (1995), 65–69.

27. P. Sridhar, R. Perumal, N. Rajalakshmi, M. Raja and K.S. Dhatatreyan, Humidification studies on polymer electrolyte membrane fuel cell, *J. Power Sources* **101** (2001), 72–78.
28. H. Miyake, M. Matsuyama, K. Ashida and K. Watanabe, Permeation, diffusion, and solution of hydrogen isotopes, methane, and inert gases in/through tetrafluoroethylene and polyethylene, *J. Vacuum Sci. Technol.* **1** (1983) (3),1447–1451.
29. T. Zadowzinski, J. Davey, J. Valerio and S. Gottesfeld, The water content dependence of electro-osmotic drag in proton conducting polymer electrolytes, *Electrochim. Acta* **40** (1995), 297–302.
30. J.S. Wainright, J.J. Fontanella, M.C. Wintersgill, R.F. Savinell and M. Litt, High pressure electrical conductivity studies of acid doped polybenzimidazole, *Electrochim. Acta* **43** (1998), 289–1294.
31. M. Iwase, S. Kawatsu, Optimized CO tolerant electrocatalysts for polymer electrolyte fuel cells, in: Proceedings of the First International Symposium on Proton Conducting Membrane Fuel Cells, vol. 1, 1995,12–18.
32. R.J. Bellows, E. Marucchi-Soos, R.P. Reynolds, Proposed Mechanism of CO mitigation in PEMFC's, using dilute H_2O_2 in the anode humidifier, in: Proceedings of the Second International Symposium on the Proton Conducting Membrane Fuel Cells, vol. 2, 1998, 21–126.
33. D. Bevers, N. Wagner and M. Bradke , Innovative production procedure for low cost PEFC electrodes and electrode membrane structures. *Int. J. Hydrogen Energy* **23** (1998), 57–63.
34. S. Cha and W. Lee , Performance of proton exchange membrane fuel cell electrodes prepared by direct deposition of ultra thin platinum on the membrane surface. *J. Electrochem. Soc.* **146** (1999), 4055–4060.
35. T. Ralph, G. Hards and J. Keating , Low cost electrodes for proton exchange membrane fuel cells. *J. Electrochem. Soc.* **144** (1997), 3845–3857.
36. E. Taylor, E. Anderson and N. Vilambi , Preparation of high platinum untilization gas diffusion electrode for proton exchange membrane fuel cells. *J. Electrochem. Soc.* **139** (1992), L45–L46.

37. P.N. Ross, N.M. Markovic, T.J. Schmidt, V. Stamenkovic, New Electrocatalysts for Fuel Cells, Transportation Fuel Cell Power System, 2000 Annual Progress Report, 2000, 15–118.
38. E. Ticianelli, C. Derouin, S. Srinivasan and A. Redondo , Methods to advance technology of proton exchange membrane fuel cells. *J. Electrochem. Soc.* **135** (1998), 2209–2214.
39. P. Fedkiw and W. Her , An impregnation reduction method to prepare electrodes on Nafion SPE. *J. Electrochem. Soc.* **136** (1989), 899–900.
40. S. Gottesfeld and M. Wilson , High performance catalyzed membrane of ultra-low Pt loading for polymer electrolyte fuel cells. *J. Electrochem. Soc.* **139** (1992), L28–30.
41. S. Gottesfeld and M. Wilson , Thin film catalyst layers for polymer electrolyte fuel cell electrodes. *J. Appl. Electrochem.* **22** (1992), 1–7.
42. G. Faubert, R. Cote, J.P. Dodelet, A new method to prepare non-noble metal based catalysts for the reduction of oxygen in polymer electrolyte fuel cells, in: Proceedings of the Second International Symposium on the Proton Conducting Membrane Fuel Cells, vol. 2, 1998, 31–38.
43. S. Foster, P. Mitchell, R. Mortimer, in: Proceedings of the Fuel Cell—Program and Abstracts on the Development of a Novel Electrode Fabrication Technique For Use In Solid Polymer Fuel Cells, 1994, 442–443.
44. J. Allen, in: Proceedings of the Fuel Cell—Program and Abstracts on the Bipolar Separator and Current Collector Design and Manufacture, 1994, 424–427.
45. A. Woodman, E. Anderson, K. Jayne, M. Kimble, Physical Science Inc. Home Page, 1999, Development of corrosion-resistant coatings for fuel cell bipolar plates, at World Wide Web: http://www.psicorp.com/publications/subject_Fuel_Cells.shtml.
46. H. Wolf and M. Willert-Porada, Electrically conductive LCP–carbon composite with low carbon content for bipolar plate application in polymer electrolyte membrane fuel cell, *J. Power Sources* **153** (2006), 41-46.
47. F. Mahlendorf, O. Niemzig, C. Kreuz, Low-Cost Bipolar Plates for PEM Fuel Cells, 2000 Fuel Cell Seminar, Portland, Oregon, 2000, 38–140.

48. A. Heinzel, H. Kraus, C. Kreuz, F. Mahlendorf, O. Niemzig, Low-Cost Composite Bipolar Plates for PEM Fuel Cells, 2002 Fuel Cell Seminar, Palm Springs, CA, 2002, 153–156.
49. C. Yang, P. Costamagna, S. Srinivasan, J. Benziger and A. B. Bocarsly, Approaches and technical challenges to high temperature operation of proton exchange membrane fuel cells, *J. Power Sources* **103** (2001), 1-9.
50. A. S. Arico, V. Baglio, A. Di Blasi, and P. Cretio, P. L. Antonucci and V. Antonucci, Influence of the acid–base characteristics of inorganic fillers on the high temperature performance of composite membranes in direct methanol fuel cells, *Solid State Ionics*, **161**(2003), 251.
51. S. Malhotra and R. Datta, Membrane-supported nonvolatile acidic electrolytes allow higher temperature operation of proton-exchange membrane fuel cells, *J. Electrochem. Soc.* **144(2)** (1997), L23-L26.
52. P. Jannasch, Recent developments in high-temperature proton conducting polymer electrolyte membranes, *Curr. Opin. Colloid Interf. Sci.* **8** (2003), 96–102.
53. V. Mehta and J.S. Cooper, Review and analysis of PEM fuel cell design and manufacturing, *J. Power Sources* **113** (2005), 32–55.
54. M. Rikukawa and K. Sanui, Proton conducting polymer electrolyte membranes based on hydrocarbon polymers, *Prog. Polym. Sci.* **25** (2000), 1463–1502.
55. H. Miyake, M. Matsuyama, K. Ashida and K. Watanabe, Permeation, diffusion, and solution of hydrogen isotopes, methane, and inert gases in/through tetrafluoroethylene and polyethylene, *J. Vacuum Sci. Technol.* **1** (1983) (3), 447–1451.
56. Heitner-Wirguin, C. Recent advances in perfluorinated ionomer membranes: structure, properties and applications. J. Membr. Sci. **120 (1)** (1996), 1-33.
57. Savadogo, O. Emerging membranes for electrochemical systems: part II. high temperature composite membranes for polymer electrolyte fuel cell (PEFC) applications. J. Power Sources **127 (1-2)** (2004), 135-161.
58. Li Q.; He, R.; Jensen, J. O.; Bjerrum, N. J. PBI-based polymer membranes for high temperature fuel cells – preparation, characterization and fuel cell demonstration. Fuel Cells 4 **(3)** (2004)**,** 147-159.

59. Alberti, G.; Casciola, M. Composite membranes for medium-temperature PEM fuel cells. Annu. Rev. Mater. Res. **33 (2003),** 129-154.
60. Mauritz, K. A.; Moore, R. B. State of understanding of Nafion. Chem. Rev. **104(10)** (2004), 4535-4585.
61. N. Ogata, M. Rikukawa, Sulfonated polymers for solid polymer electrolytes, US Patent 5,403,675 (April 1995).
62. B. Baradie, J.P. Dodelet and P. Guay, Hybrid Nafion®-inorganic membrane with potential applications for polymer electrolyte fuel cells, *J. Electroanal. Chem.* **489** (1998), 209–214.
63. S. Wasmus, A. Valeriu, G.D. Mateescu, D.A. Tryk and R.F. Savinell, Characterization of H_3PO_4-equlibriated Nafion 117 membranes using ^{1}H and ^{31}P NMR spectroscopy, *J. Membr. Sci.* **185** (2000), 78–85.
64. B. Tazi, O. Savadago, New cation exchange membranes based on Nafion, Silicotungstic acid and thiophene, J. New Mater. Electrochem. Syst., in press (cf. JMS 185 (2001) 3–27).
65. B. Smitha, S. Sridhar and A.A. Khan, Polyelectrolyte complexes of chitosan and poly(acrylic acid) for fuel cell applications, *Macromolecules* **37** (2004), 2233–2239.
66. N. Carretta, V. Tricoli and F. Picchioni, Ionomeric membranes based on partially sulfonated poly(styrene): synthesis, proton conduction and methanol permeation, *J. Membr. Sci.* **166** (2000), 189–197.
67. H. Bashir, A. Linares and J.L. Acosta, Heterogeneous sulfonation of blend systems based on hydrogenated poly butadiene-styrene block copolymer. Electrical and structural characterization, *Solid State Ionics* **139** (2001), 189–197.
68. F. Buchi, B. Gupta, O. Haas and G. Scherer, Study of radiation grafted FEP-g-polystyrene membranes as polymer electrolytes in fuel cells, *Electrochim. Acta* **40** (1995),345–353.
69. Stefan Haufe and Ulrich Stimming, Proton conducting membranes based on electrolyte filled microporous matrices, *J. Membr. Sci.* **185** (2001), 95–103.
70. Q. Guo, P.N. Pintauro, H. Tang and S. O'Connor, Sulfonated and cross-linked polyphosphazene based polymer electrolyte membranes, *J. Membr. Sci.* **154** (1999), 175–181.

71. E. Vallejo, G. Pourcelly, C. Gavach, R. Mercier and M. Pineri, Sulfonated polyimide as proton conductor exchange membranes, physicochemical properties and separating H+/Mz+ by electrodialysis comparison with perfluorosulfonic membranes, *J. Membr. Sci.* **160** (1999), 127–137.
72. F. Wang, M. Hickner, Y.S. Kim, T.A. Zawodzinski and J.E. McGrath, Direct polymerization of sulfonated poly(arylene ether sulfone) random (statistical) copolymers: candidates for new proton exchange membranes, *J. Membr. Sci.* **197** (2002), 231–242.
73. Li, J. Zhang and Y Wang, sulfonated poly(ether ether ketone) membranes for direct methanol fuel cell, *J. Membr. Sci.* **226** (2003), 159.
74. Y.A. Elabd, E. Napadensky, J.M. Sloan, D.M. Crawford and C.W. walker, Triblock copolymer ionomer membranes. Part I. Methanol and proton transport, *J. Membr. Sci.* **217** (2003) (1–2), 227–242.
75. A. Taeger, C. Vogel, D. Lehmann, D. Jehnichen, H. Komber, J. Meier-Haack, N.A. Ochoa, S.P. Nunes and K. Peinmann, Ion Exchange membranes derived from sulfonated polyimides, *React. Funct. Polym.* **57** (2003), 77.
76. M. Kang, Y. Chio, I. Choi, T. Yoon and S. Moon, Electrochemical characterization of sulfoanted poly(arylene ether sulfone) (S-PES) cation exchange membranes, *J. Membr. Sci.* **216** (2003), 39.
77. X. Guo, J. Fang, T. Watari, K. Tanaka, H. Kita and K. Okamoto, Novel sulfonated polyimides as polyelectrolytes for fuel cell application. 2. Synthesis and proton conductivity of polyimides from 9,9-bis (4-aminophenyl)fluorene-2,7-disulfonic acid, *Macromolecules* **35** (2002), 6707–6713.
78. C. Genies, R. Mercier, B. Sillion, N. Cornet, G. Gebel and M. Pineri, Soluble sulfonated naphthalenic polyimides as materials for proton exchange membranes, *Polymer* **42** (2001), 359–373.
79. S. Besse, P. Capron and O. Diat *et al.*, Sulfonated polyimides for fuel cell electrode membrane assemblies (EMA), *J. New Mater. Electrochem. Syst.* **5** (2002), 109–112.
80. J.A. Asensio, S. Borros and Romero Gomez, Proton conducting polymers based on benzimidazole and sulfonated benzimidazoles, *J. Polym. Sci. Part A: Polym. Chem.* **40** (2002),3703–3710.

81. J.M. Bae, I. Honma, M. Murata, T. Yamamoto, M. Rikukawa and N. Ogata, Properties of selected sulfonated polymers as proton-conducting electrolytes for polymer electrolyte fuel cells, *Solid State Ionics* **147** (2002), 189–194.
82. L. Qinfeng, H.A. Hjirker and N.J. Bjerrum, Phosphoric acid doped polybenzimidazole membranes, *J. Appl. Electrochem.* **31** (2001),773–779.
83. J.J. Wang, R.F. Savinell, J. Wainright, M. Litt and H. Yu., A H_2/O_2 fuel cell using acid doped polybenzimidazole as polymer electrolyte, *Electrochim. Acta* **41** (1996), 193–197.
84. J.C. Lassegues, J. Grondin, M. Hernandez and B. Maree, Proton conducting polymer blends and hybrid organic inorganic materials, *Solid State Ionics* **145** (2001), 37–45.
85. C. Hasiotis, V. Deimede and C. Kontoyannis, New polymer electrolytes based on blends of sulfonated polysulfones with polybenzimidazole, *Electrochim. Acta* **46** (2001), 2401–2406.
86. J. Kerres, W. Zhang and W. Cui, New sulfonated engineering polymers via the metalation route.2. Sulfinated-sulfonated poly(ethersulfone) PSU Udel® and its crosslinking, *J. Polym. Sci. A: Polym. Chem.* **36** (1998), 1441–1448.
87. W. Priedel, M. Baldauf, U. Gebhardt, J. Kerres and A. Ullrich, New ionomer membranes and their FC applications. 2. H_2 fuel cell and DMFC application, *Extended Abstracts of Third International Symposium New Materials for Electrochemical Systems* Montreal, Canada, 4-8 July (1999), 233–234.
88. M.A. Vargas, R.A. Vargas and B.-E. Mellander, New proton conducting membranes based on PVAL/$H_3PO_2 \cdot H_2O$, *Electrochim. Acta* **44** (1999),4227–4232.
89. H. Miyake, The design and development of Flemion® membranes, Modern Chlor-Alkali Technology 5 (1980) 59–67.
90. S. Heitala, M. Paronen, S. Holmberg, J. Nasman, J. Juhanoja, M. Karjalainen, R. Serimaa, M. Tivola, T. Lehtinen, K. Parovuori, G. Sundholm, H. Ericson, B. Mattsson, L. Torell and F. Sundholm, Phase Separation and crystallinity in proton conducting membranes of styrene grafted and sulfonated poly(vinylidene fluoride), *J. Polym. Sci.* **37** (1999),1741–1753.

91. J. Wei, C. Stone, A.Steck, Trifluorostyrene and substituted trifluorostyrene copolymeric compositions and Ion-Exchange membranes formed therefrom, US Patent 5,422,411 (June 1995).
92. J.S. Wainright, J.J. Fontanella, M.C. Wintersgill, R.F. Savinell and M. Litt, High pressure electrical conductivity studies of acid doped polybenzimidazole, *Electrochim. Acta* **43** (1998), 1289–1294.
93. F. Helmer-Metzman, F. Osan, A. Schneller, H. Ritter, K. Ledjeff, R. Nolte, R. Thorwirth, Polymer electrolyte membrane, and process for the production thereof, US Patent 5,438,082 (August 1995).
94. K.D. Kreuer, On the development of proton conducting membranes for fuel cell applications, *J. Membr. Sci.* **185** (2001), 13.
95. T. Susai, M. Kaneko, K. Nakatoa, T. Isono, A. Hamada and Y. Miyake, Optimization of proton exchange membranes and the humidifying conditions to improve cell performance for polymer electrolyte membranes, *Int. J. Hyd. Energy* **26** (2001), 631–637.
96. T. Okada, G. Xie, O. Gorseth, S. Kjelstrup, N. Nakamura and T. Arimura, Effect of water uptake and relative humidity on Nafion, *Electrochem. Acta* **43** (1998), 3741–3747.
97. H.G. Haubold, T. Vad, H. Jungbluth and P. Hiller, Nano structure of Nafion: a SAXS study, *Electrochim. Acta* **46** (2001), 559–1563.
98. P.J. James, T.J. McMaster, J.M. Newton and M.J. Miles, In situ rehydration of perfluorosulfonate ion-exchange membrane studied by AFM, *Polymer* **41** (2000), 4223–4231.
99. T. Sakari, H. Takenaka, N. Wakabayashi, Y. Kawami and K. Tori, Gas permeation properties of SPE membranes, *J. Electrochem. Soc.* **132** (1985),1328.

Chapter 2

Systematic Approach to Design Higher Temperature Nanocomposite PEMs

In this chapter, the design of higher temperature nanocomposite proton-exchange membranes (PEMs) with adequate performance under low relative humidity (RH) is discussed based on experimental and theoretical considerations. The approach is based on enhancing the acidity and water sorption of a conventional polymer electrolyte membrane by incorporating in it a solid acidic inorganic material. A systematic investigation of the nanocomposite Nafion/inorganic additive PEMs based on characterization of water uptake, ion-exchange capacity (IEC), conductivity, and fuel cell polarization is presented. The effects of particle size, chemical treatment, additive loading and alternate processing methodologies are investigated. The most promising candidate investigated thus far is the nano-structured ZrO_2/Nafion PEM exhibiting an increase of ~10 % in IEC, and ~ 40 % increase in water sorbed and ~5 % enhancement in conductivity vs. unmodified Nafion® 112 at 120°C and 40 % RH. This appears to be an attractive candidate for incorporation into a membrane-electrode assembly for improved performance under these hot and dry conditions. This chapter was published in J. Electrochemical Society, 152(2) A316-325 (2005) with co authorship of Dr. Tony Thampan and Dr. Pyoungho Choi.

2.1 Introduction

It is fair to say that the commercialization and large-scale deployment of polymer electrolyte membrane (PEM) fuel cells is currently hamstrung by the limitations imposed by the available polymer electrolyte membranes. For instance, Nafion, one of the oldest but still one of the best available PEMs, limits the operating temperature of PEM fuel cells to 80°C on the one hand, thus requiring pure hydrogen as the fuel and consequently imposing severe constraints on reformers, while on the other hand it is still far too expensive, making fuel cells economically unattractive. Unfortunately, the available alternative PEMs

compromise performance and longetivity. Thus, there is world wide effort currently underway to find suitable alternatives to Nafion that might allow higher temperature operation and cost benefit.

This is, however, particularly challenging task because of the desired performance characteristics. Thus, a good polymer electrolyte membrane must be thin for low resistance, compliant to make a good contact with electrodes but rigid enough to provide support to the membrane electrode assembly (MEA), thermally and dimensionally stable, impervious to gaseous or liquid fuels as well as electrons, must be durable, and should be able to provide excellent proton conductivity rivaling liquid electrolytes (~0.1 S/cm) under hot and dry conditions.

A good proton conductor evidently requires mobile protons. Thus, inorganic proton conductors[1-3] without a liquid phase, while conceptually very attractive, require temperatures in excess of 800 ^{o}C to provide adequate conductivities via a proton hopping mechanism owing to the high activation energy. At lower temperatures, a liquid-phase for proton conduction is essential, either as a molten or a solvated acid. When a solvent other than water is used, the challenge of complete immobilization of the liquid must be first addressed to ensure stable performance over extended periods. When water is the solvent, the challenge is to retain water within the membrane under hot and dry conditions owing to its high volatility.

An alternate approach, first proposed by Malhotra and Datta [4], is to incorporate inorganic acidic materials within the conventional polymer electrolytes such as Nafion in order to improve water retention while simultaneously increasing the number of available acid sites. This approach shows promise for developing PEMs that function adequately at temperatures above 120^{o}C under low relative humidity (RH) conditions, and has consequently become a very active area of research. This paper is concerned with a systematic investigation of the issues related to the design and development of such nanocomposite membranes.

2.2 Literature Review

A brief literature review of the available ingredients (polymer electrolyte and inorganic additives) for designing nanocomposite PEMs is provided below. The available

polymer electrolyte membranes may be subdivided into two categories: 1) *proton-exchange membranes* (PEMs) , e.g., Nafion, in which the acid anion is covalently attached to the polymer backbone so that only the proton is mobile requiring a solvent such as water, and 2) *polymer-acid complexes* (PACs) , e.g., PBI/H_3PO_4, in which the acid is simply complexed with a basic membrane so that both the proton and the anion are mobile, i.e., the transference number of protons is less than unity. While a solvent such as water is not essential for conduction in PACs, it aids by further ionizing the acid, but unfortunately can also cause leaching of the acid from the membrane, a serious limitation for long-term stability.

2.2.1 Proton Exchange Membranes (PEMs)

Fig. 2.1(a) shows a schematic of the major components of a proton-exchange membrane, namely the polymer backbone, chemical cross-links, side chains, and the pendant acid group. The right combination of these elements confers the desirable properties listed above. The backbone polymers are: i) fluorinated, and ii) hydrocarbon polymers. The common acid groups covalently bound are either: i) sulfonic acid (-SO_3H), ii) carboxylic acid (-COOH), iii) phosphonic acid (-PO_3H_2), and iv) sulfonyl imide (-$SO_3NHSO_2CF_3$). The backbone along with any cross-links confers appropriate thermo-mechanical properties, inertness, and extent of swelling, while the number (equivalent weight, *EW*) and strength (*pK*) of acid groups confers the electrolyte properties.

The perfluorinated PEMs are the most commercially advanced membranes owing primarily to their chemical inertness [5-8]. Thus, Nafion has demonstrated fuel cell lifetimes of over 60,000 hours at 80^oC [9], although higher temperature lifetime studies have not yet been reported. The PTFE backbone enhances the chemical and mechanical properties of the PEM albeit at the cost of limited water sorption due to its hydrophobicity. Other perfluorinated membranes include the Dow membrane which has a shorter side chain than Nafion but otherwise has similar structural and morphological properties. Both Aciplex-S and Flemion, available from Asahi Chemical and Asahi Glass Company, respectively, have long side chain perfluorosulfonated membranes with performance similar to Nafion. Perfluorinated PEMs have been developed by modification of the acid group [11-13]. Thus, DesMarteau [12, 14] replaced the sulfonic acid group (-SO_3H) in

Nafion with a sulfonyl imide group ($-SO_2NHSO_2CF_3$), which results in an increase in the water uptake while Kotov *et al*. [13] developed membranes with a phosphonic acid group that has the potential for higher thermal stability. Other perfluorinated PEMs include Gore-select [15] which uses a PTFE matrix embedded in the perfluorinated PEM to provide mechanical strength, thus allowing membrane thickness to be reduced to below $20\mu m$. These membranes possess conductivity up to 0.01- 0.1 S/cm depending on RH.

Partially fluorinated PEMs such as the sulfonated trifluorostyrene membranes have also been developed [16]. Ballard Power Systems has developed BAM3G [17], a family of PEMs with equivalent weights 375 to 920, by incorporating α, β, β-trifluorostyrene monomer and a series of substituted- α, β, β-trifluorostyrene comonomers. These membranes are less expensive than Nafion and have demonstrated good stability (>15,000 hours).

The alternate hydrocarbon backbone based polymers not only provide the potential for high temperature performance at low RH, but also promise a cost advantage [18-19]. The early research with hydrocarbon PEMs was abandoned due to their short life spans. However, the new generation of polymers designed for higher temperature and corrosion resistance include sulfonated poly (oxy-1, 4-phenyleneoxy-1, 4-phenylenecarbonyl-1, 4-pheneylene) or polyether ether ketone (PEEK), poly (4-benzoyl-1, 4-phenylene) (PPBP), sulfonated poly (phenylene sulfide), alkylsulfonated polybenzimidazol (AS-PBI) and sulfoarylated PBI. Others include polyphosphazene (PP), polyether sulfones, polyphenylene oxide (PPO), and poly (phenyl quinoaniline) (PPQ), polyimide, and styrene/ethylene-butadiene / styrene copolymer. McGrath and coworkers have presented promising MEA results utilizing poly (arylene ether sulfone) PEMs [20-21].

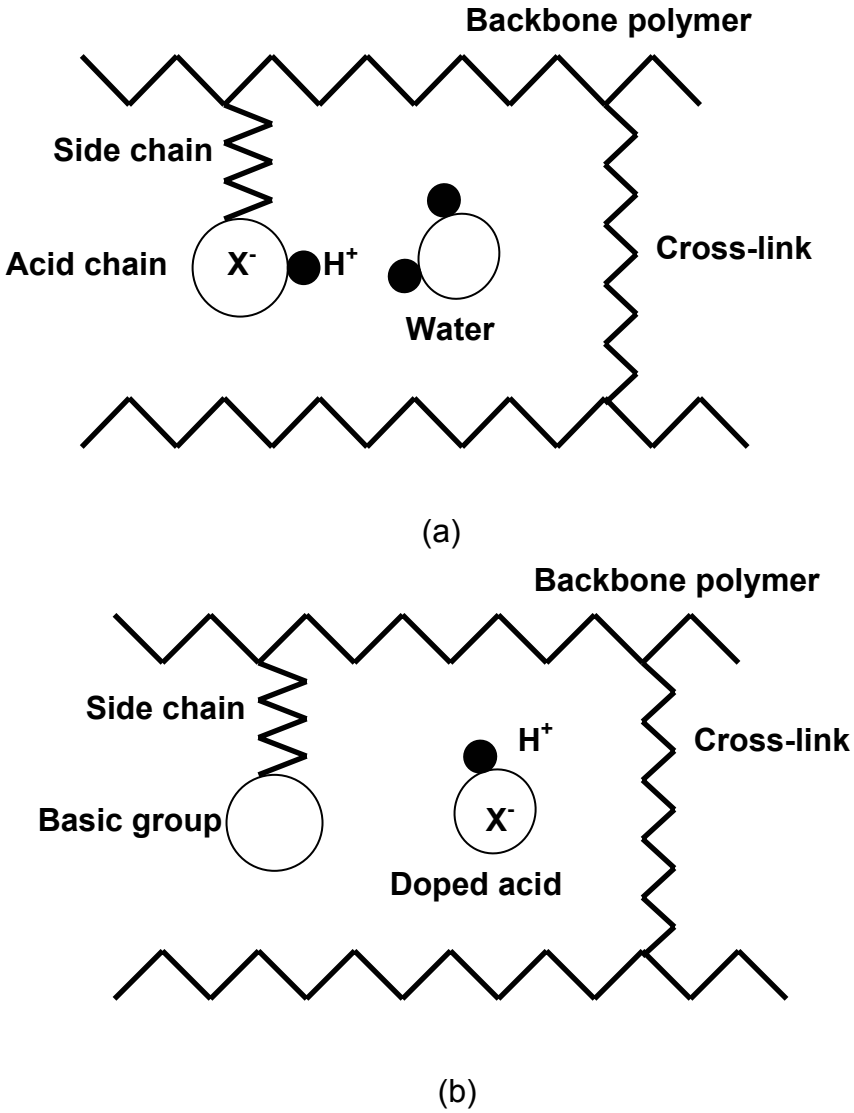

Figure 2.1 Schematic of structure of (a) Proton-Exchange Membranes (PEMs) and (b)Polymer-Acid Complexes (PACs).

2.2.2 Polymer-Acid Complexes (PACs)

Fig. 2.1(b) shows a schematic of the basic elements of a PAC including the backbone, cross-links, basic sites and the doped acid electrolyte. PACs are distinct from PEMs in that the acid is not covalently bound to the polymer but is retained with the help of basic sites within the polymer. Thus, both anion and protons are mobile. A recent example of PAC that has generated considerable interest is the H_3PO_4/PBI membrane. PBI is basic (pKa ~ 5.5) and forms a complex with H_3PO_4. The conductivity depends upon doping level. For 5 mol H_3PO_4/PBI unit, $\sigma > 10^{-4}$ S/cm at 25 ^oC and $\sigma > 3x10^{-2}$ S/cm at 190 ^oC are achieved. However, long term stability of these needs to be carefully investigated. Other examples of PACs include poly (ethyleneimine) (PEI), poly (vinylpyrrolidone) (PVP), and poly (acrylamide) (PAAM). The acids commonly used for doping are H_3PO_4, H_2SO_4, HCl, and $HClO_4$. Until the longetivity issues are clear, PACs are not considered suitable for developing nanocomposite polymer electrolytes.

2.2.3 PEMs with Solvents of Lower Volatility

The solvent, e.g., water or methanol in the PEM works as a Bronsted base by solvating the protons of the pendant acid. A possible approach, therefore for increasing the operating temperature of the PEM at low relative humidity is to replace water with a lower volatile solvent. Thus, Savinell *et al*. [23] utilized H_3PO_4 doped Nafion and were able to attain high conductivity at elevated temperatures. However, H_3PO_4 is corrosive and would eventually leach out with the liquid water produced. Similarly Doyle *et al*. [24] demonstrated that Nafion imbibed with ionic liquids such as the molten salt 1-butyl, 3-methyl imidazolium triflate (BMITf) provides good conductivity at high temperatures. Unfortunately, the challenge of complete immobilization of the ionic liquid must first be addressed to ensure stable cell performance over extended periods.

2.2.4 Nanocomposite Proton Exchange Membranes (NCPEMs)

Malhotra and Datta first proposed the incorporation of inorganic solid acids in the conventional polymeric ion-exchange membranes such as Nafion with the objective of serving the dual functions of improving water retention as well as providing additional

acidic sites. Thus, they doped Nafion membranes with heteropolyacids, e.g., phosphotungstic acid (PTA), and were able to show high cell performance at low RH and elevated temperature (120 ^{o}C). The improved performance was ascribed to the presence of PTA that provides high proton concentrations and improved water retention. Unfortunately, due to high water solubility, the PTA [25] eventually leaches out from the PEM. Recently, Fenton *et al.* have shown that Nafion-PTA membranes can be stabilized by heat treatment and the leaching of PTA can be reduced [26-27].

To decrease the humidification requirements of PEMs, Watanabe *et al*. [28-30] modified Nafion PEMs by the incorporation of nano-sized particles of SiO_2, TiO_2, Pt, Pt-SiO_2 and Pt-TiO_2. These modified PEMs showed a much higher water uptake. When operated at 80^{o}C under low humidification PEMFC, the modified PEMs showed lower resistance than Nafion. This improvement was attributed to the suppression of H_2 cross over by *in situ* Pt and to the subsequent sorption of the water produced on the incorporated oxides.

Based on the above two pioneering studies, there is now a great deal of effort along the lines of development of organic-inorganic nanocomposite membranes [31-34]. Thus, Adjemian *et al*. [35-36] introduced nanosized SiO_2 into Nafion pores [37] and tested various thickness and EW membranes. The benefit of these nanocomposite membranes appears to be stable operation versus conventional Nafion at a cell temperature of 130^{o}C due to high rigidity, both tested under fully humidified conditions. The investigators note that the unmodified PEMs showed thermal degradation, while the SiO_2 modified PEMs did not show such damage. Costamagna *et al*. [31] incorporated zirconium phosphate into a Nafion 115 membrane and the results obtained are similar. Zaidi *et al*. [39] embedded heteropolyacids to different extents in sulfonated polyether ether ketone (S-PEEK). The highest performing nanocomposite was a tungstophosphoric acid doped, 80 % sulfonated PEEK PEM. It showed conductivity similar to that of Nafion.

2.2.5 Inorganic Acidic Additives

Although there exist numerous liquid superacids, (e.g. mixtures of HSO_3F and SbF_5, with Hammett acidity (H_0) = -20), which could enhance conductivity, they are unsuitable for fuel cell applications as it is a challenge to immobolize them within the

PEM. Thus, solid acids are of the primary interest as additives. The heteropolyacids (HPA) are an example of a class worth investigating as they demonstrate high acidity and hydrophilicity. These properties could be exploited if HPAs could be anchored within the polymer matrix, e.g., using cesium salts of HPAs.

The sulfated metal oxides, such as TiO_2, ZrO_2, and Fe_2O_3, have become subjects of intensive catalytic studies because these strong superacids are thermally more stable than other solid superacids [40]. Currently, sulfated Zirconia (SO_4^{2-}/ZrO_2) is the strongest superacid among all known solids ($H_0 < -16$) [41]. It retains the sulfonic acid groups, responsible for proton conduction, until about 500^oC. As SO_4^{2-}/ZrO_2 exhibits the highest acidity of all the solid superacids [42], the additives selected in the study are based on zirconia.

2.3 Systematic Design of NanoComposite PEMs

It is evident from the literature that NCPEMs are promising for higher temperatures above 120 ^oC. However, the investigations done so far have not been systematic. Thus, a more systematic approach to the design of CPEMs is discussed here. As a start, let us first review the reasons for improvement of CPEMs:

1) Higher water retention in the CPEMs: The presence of a hygroscopic additive binds a larger amount of water in the membrane, increasing the membrane water content at a given RH.
2) Greater number of acid sites: This increases the concentration of mobile protons.
3) Lower gas cross over: The presence of nanoparticles in the membrane pores reduces the permeability of gas through the membrane. The cross over current measured with the modified membrane is an order of magnitude lower than that of the unmodified PEMs.
4) Improved thermo-mechanical properties: There are indications that the T_g and Young's Modulus of the polymer are improved by incorporation of inorganic additives.
5) Improved electrode performance: Due to the increased water retention in the modified PEM, an extended reaction zone maybe available, resulting in better electrode performance at high temperatures.

The reasoning above is, however, qualitative [43]. In order to better appreciate some of the key factors involved in the design of a high temperature nanocomposite Nafion based PEM, it is beneficial to consider this within a framework of a quantitative model of the conductivity. Such a model is readily obtained by an extension of our previous work on simulation of the transport of protons through a Nafion membrane at different temperatures and RHs [44]. This transport model is based on the dusty- fluid model (DFM) [45], where the obstruction presented by the polymer matrix to proton diffusion is viewed as an additional frictional interaction with large immobile "dust" or gel particles. Within this framework, the inorganic additive is simply viewed (Fig. 2.2) as an additional dust species immobilized within the polymer matrix.

The final form that describes the proton conductivity of a nanocomposite PEM is

$$\sigma = (\varepsilon - \varepsilon_0)^q \left(\frac{\lambda_{H^+}}{1 + \delta_{AH} + \delta_{ZH}} \right) \left(c_{AH,0} \alpha_{AH} + c_{ZH,0} \alpha_{ZH} \right) \qquad (2.1)$$

with $\delta_{AH} = D_{12}/D_{1M}$ and $\delta_{ZH} = D_{12}/D_{1Z}$. Here D_{12}, D_{1M} and D_{1Z} are the diffusion coefficients for (H_3O^+)/solvent (H_2O), H_3O^+/PEM matrix and H_3O^+/additive particle, respectively. In Eq. 1, ε and ε_0 are the volume fraction of water in the membrane and the percolation threshold, respectively, where ε is a function of the water uptake (λ_{H_2O})

$$\varepsilon = \frac{\lambda_{H_2O}}{\frac{\overline{V}_M}{\overline{V}_{H_2O}} + \lambda_{H_2O}} \qquad (2.2)$$

where $\overline{V}_M$ is the effective partial molar volume of the PEM and is calculated as:

$$\overline{V}_M = \overline{V}_{PEM}(1 - \omega_Z) + \overline{V}_Z \omega_Z \qquad (2.3)$$

where the partial molar volume of the additive, $\overline{V}_Z = d_Z / (6 c^*_{ZH_0})$, where $c^*_{ZH_0}$ is the surface acid site density of additive (mol/cm^2) and d_Z is the additive particle size. Also ω_Z is the mass fraction of the additive in the nanocomposite PEM. ε_0 is defined in a similar manner, being based on the water uptake at monolayer coverage [44-45]. The Bruggeman, or critical, exponent q=1.5, and λ_{H^+} is the equivalent conductance of a proton in water. The solvent uptake in the transport model can be predicted by either the finite layer BET isotherm of Thampan *et al*. or by the more sophisticated approach recently developed by

Choi and Datta [46]. Thus at low RH, the water uptake of the PEM is low and the resulting low ε results in poor conductivity. The water uptake and the conductivity rise sharply above ~70 % RH.

The concentration of acid sites available within the PEM is the sum of the pendant acid sites $c_{AH,0}$ in the polymer plus the additive acid sites, $c_{ZH,0}$. Of course, these sites only contribute to the conductivity when the protons are dissociated in the presence of water or other solvent. The extent of dissociation depends upon the level of hydration and the strength of the acid groups, and is denoted as α_{AH} and α_{ZH} for the polymer and the additive, respectively.

Thus, within the framework of this simple model for the design of nanocomposite PEMs, the objective of increased PEM conductivity at lower RH and higher temperature may be achieved by the presence of hygroscopic acidic additives, since:

1. The presence of a hydrophilic additive increases the water uptake ε or λ_{H_2O} of the PEM at a given RH, as shown schematically in Figure 2.3. In other words, the equilibrium content of water in the membrane is shifted to higher values at a given vapor activity, because of greater number of acid sites and since water is bound more strongly. However, the Young's modulus *E* of the polymer also increases with the additive, which counters the increased hydrophilicity and hence also affects swelling. The presence of the acid sites on the surface of nanoparticles increases the total number of acid sites available within the PEM as shown in Fig. 2.2, effectively reducing $\overline{V}_M$ (Eq. 3). This enhances the conductivity because the number of charge carriers available increases correspondingly (Eq. 1).
2. The number of additional acid sites is proportional to the specific surface area of inorganic particles, $S_Z = 6/(\rho_Z d_Z)$ (cm^2/g), where d_Z is the additive particle size and ρ_z is its density. Thus, smaller particles are better for a given loading.
3. There is an optimum amount of additive loading ω_Z in the PEM. This is so since the diffusional resistance represented by δ_{ZH} would increase with loading as more nanoparticles occupy the pore volume. Also from Eq. 3 we understand that $\overline{V}_M$ would first decrease and then increase depending on $\overline{V}_Z$.

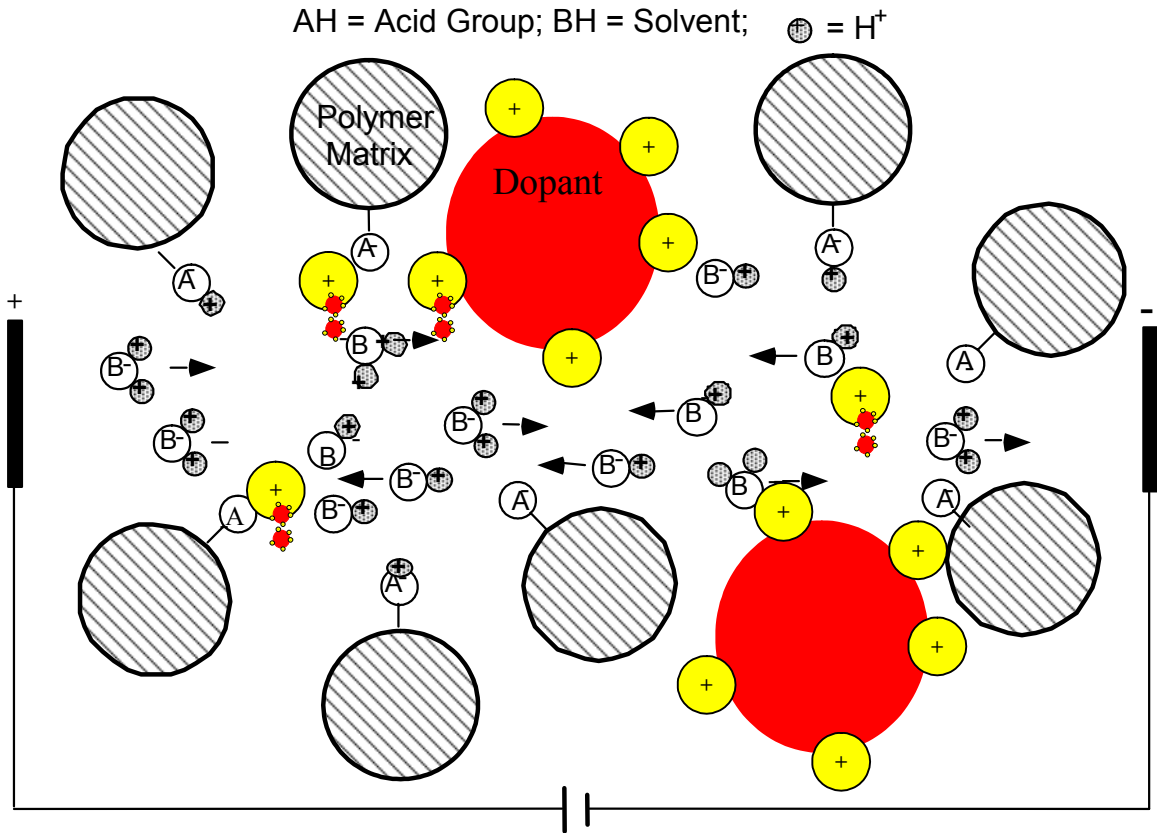

Figure 2.2 A "dusty-fluid model" depiction of PEM describing proton conductivity through the Nafion polymer matrix and the superacidic dopant. The framework treats the Nafion matrix as large dust particles through which the current carrying ions must traverse.

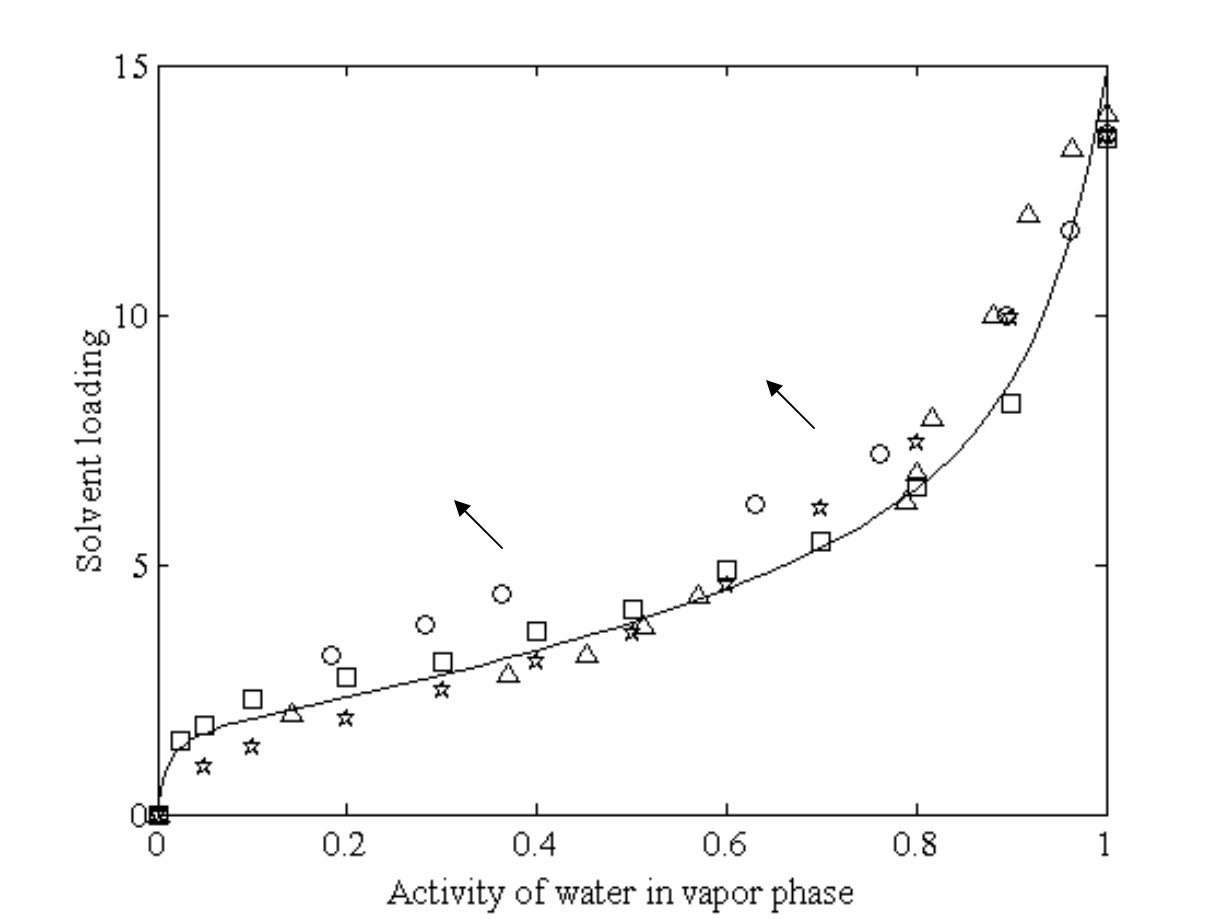

Figure 2.3 The solvent loading vs. activity of water vapor for Nafion (EW=1100) membrane (triangle: ref. 20, square: ref. 21, circle: ref. 44, and star: this work).The design objective is to increase the solvent loading of Nafion. The nanocomposite will adsorb more water at fixed RH vs. unmodified Nafion resulting in higher conductivity at low RH.

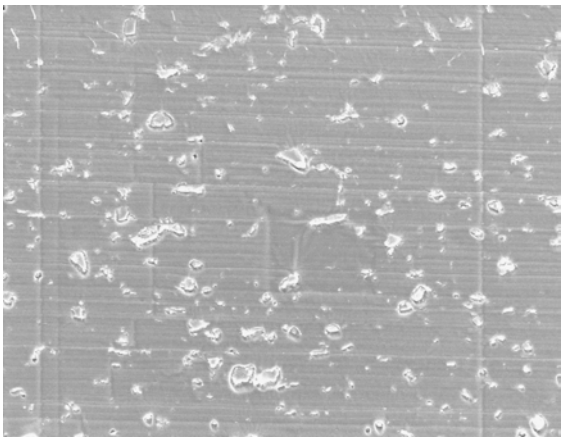

(a)

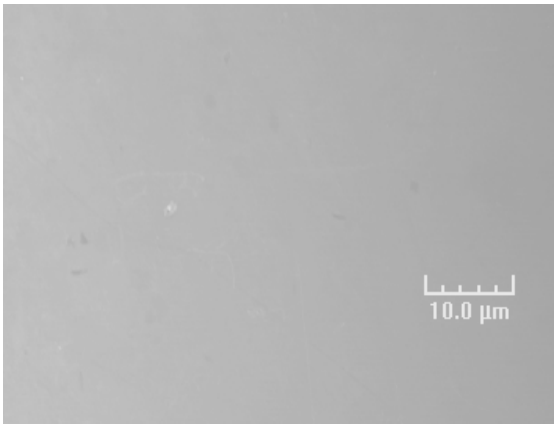

(b)

Figure 2.4 SEM images of membranes synthesized by both the *in situ* and doping methods. (a) Nafion ZrO_2 doped membrane. (b) The Nafion ZrO_2 sol-gel PEM is homogeneous and transparent demonstrating no phase separation.

Additionally, the additive must be selected in a way (a) such that it can be immobilized within the polymer matrix, (b) which is compatible with the electro-catalyst, and (c) which can maintain/increase the thermo-mechanical properties of the polymer at higher temperature. Thus materials that may leach out or poison the membrane or electro-catalyst are not useful. Another factor affecting performance is that since the acid dissociation constants decline with temperature, the degree of dissociation and hence the number of charge carriers decline at higher temperatures. It must also be noted that the particle size of the additive particles ('dust') is crucial both because they form an additional diffusional barrier to the transport of protons (Eq. 1), and because the number of surface acid sites depend upon the particle surface area.

2.4 Experimental

The experimental methods involved additive synthesis, nanocomposite membrane fabrication, and additive and PEM characterization via water uptake and *ex situ* conductivity measurements.

NanoComposite PEM Synthesis

NanoComposite membranes were fabricated by two alternate methods:

1. Mixing Nafion gel and inorganic particles followed by membrane casting, and
2. *In situ* nanoparticles synthesis via sol gel processing in precast or commercial Nafion membranes.

The first procedure was utilized so that the literature protocol of producing sulfated zirconia (requiring calcination at 600 ^{o}C) could be followed for producing the particles first. However, this procedure resulted in relatively large particles (in the μm range). The second procedure was followed to produce nanoparticles *in situ* using the precast Nafion as a template. However, particles formed by this procedure were evidently not amenable to the high temperature sulfation procedure. Appendix A lists all the procedures to synthesize these membranes.

Zirconia Particle Preparation - The SO_4^{2-}/ZrO_2 particles were synthesized based on Arata's work on metal oxides [47]. Thus, ZrOH powder (MEI Chemicals, Flemington, NJ)

was stirred in 0.5 M H_2SO_4 for 15 minutes at room temperature. The acid was decanted and the remaining powder dried at 100^oC overnight. The dried powder was then calcined in air at 600^oC for 2 hours and the resulting particles were crushed with a mortar and pestle. These particles are denoted here as "SO_4/ZrO_2".

Particles were also prepared from a colloidal solution of 20 wt % ZrO_2/Acetic Acid (Nyacol Nano. Technologies, Ashland MA). The solution was evaporated and the ZrO_2 precipitate was obtained. This precipitate is denoted as "ZrO_2". The precipitate was heated in 6 M H_2SO_4, in an order to sulfate the ZrO_2, then dried at 120^oC for 2 hours and finally calcined in air at 600^oC for an additional 2 hours. The resulting particles were crushed with a mortar and pestle, and are denoted as "ZrO_2 (A)". Additionally, a sample of the ZrO_2 (A) was pulverized with a Jet Mill (Laboratory Jet Mill, Clifton NJ) to obtain a reduction in the particle size. This sample is denoted in the following as "ZrO_2 (AP)".

Cast Nanocomposite Membranes- Based on experimental procedures described in the literature, the protocol described below was developed to produce uniform and reproducible cast PEMs [48]. To obtain the desired weight loading of additive Ω_Z in the PEM, selected additive particles were dispersed in a 23 wt % Nafion/ethanol solution with a magnetic stirrer. After stirring for 8 hours, the solution was cast as a PEM on a glass dish utilizing a doctor blade. The cast membrane was placed in a convection oven at 100 ^oC for 15 minutes, which was sufficient to produce a solid membrane. The PEM was removed from the glass dish with DI water, dried and then annealed in a Teflon sleeve at 170^oC at 10 tons for 15 minutes in a mechanical press (Carver Model C, Wabash IN). This processing step was necessary to produce pliant, insoluble PEMs with mechanical properties similar to those of commercially available Nafion films. The resulting cast PEM had a thickness of around 50 μm.

Sol-gel ZrO_2/Nafion Nanocomposite PEMs - The alternate method of preparation of a ZrO_2 nanocomposite PEM was via *in situ* sol-gel synthesis based on methods developed by Mauritz's and coworkers for the synthesis of asymmetric ZrO_2/Nafion nanocomposites [49]. In this procedure, the host PEM serves as a template that directs the morphology and particle size of the oxide in the PEM matrix, resulting in nano-sized particles [50]. As

received Nafion membranes (Sigma-Aldrich Corp., St. Louis MO) were boiled in 3 wt % H_2O_2 for 1 hour and then rinsed in water. They were then immersed in 50 % vol. HNO_3/H_2O and heated for 6 hours, rinsed in water, and then heated in 50 % vol. H_2SO_4/H_2O for an additional 6 hours. The membranes were finally boiled in water for 1 hour and then rinsed and washed in water several times to ensure complete removal of any residual acid.

The purified membranes were then placed in a vacuum oven and heat treated at 110 ^oC for 12 hours. Thereafter, the membranes were boiled in H_2O for 1 hour and subsequently dried at 50^oC for 4 hours. The membranes were then immersed in 10:1 ethanol/H_2O solution for an additional hour. The ethanol/H_2O mixture served to further swell the pores of the PEM to maximize the absorption of the precursor solution. The membrane was removed and immersed into a 20:1 (v/v) ethanol: zirconium tert butoxide solution for 10 minutes and then rinsed in ethanol in order to remove surface ZrO_2. The membranes were then removed and heated at 110 ^oC in vacuum for 24 hours to complete the condensation reactions. This nanocomposite PEM is denoted here as "Nafion ZrO_2 sol-gel".

The membranes synthesized by this method are completely transparent and homogenous as compared to membranes prepared by the casting method which were cloudy due to the much larger particles. Figure 2.4 shows SEM (Amray Model 1610 Turbo SEM) images for both the membranes. The membrane prepared using the casting method had larger zirconia particles with size ranging in 5-15 μm. On the other hand, the sol gel membranes showed no X-ray scattering. Also the surface of sol gel membranes did not show any deposition of oxides which confirms that the zirconia is present within the pores of Nafion membrane. This provides evidence that these membranes have nano-sized zirconia particles within the pores of the membrane.

2.5 NanoComposite Membrane Characterization

Water Uptake Measurements - To measure the water uptake of the nanocomposite PEMs, a Tapered Element Oscillating Microbalance (TEOM Series 1500 PMA Reaction Kinetics Analyzer, Rupprecht & Patashnick Co. Inc. Albany NY) was utilized [51]. The sample mass change in TEOM is measured as the frequency change in the tapered element

oscillation. The instrument has a sensitivity of 1 μg and a temperature range of up to 700°C. The RH was controlled by mixing metered flows of a wet (saturated with H_2O) and a dry helium stream. Calibration was done with a RH meter (FH A646-R, ALMEMO, Ahlborn, Munich, Germany). The membrane was cut into thin strips (1.5 mm by 1.5 mm) and packed carefully along with quartz wool into the oscillating glass chamber of the TEOM to avoid rattling. The water uptake was measured for all samples at 25 °C and 90°C from 0 % to 90 % RH, and at 120 °C from 0 % RH to 40 % RH. After the sample was loaded, it was exposed to the helium gas with the desired RH, and the real-time mass change was observed to determine when the equilibrium amount of water had been adsorbed onto the membrane.

Ion-Exchange Capacity Measurements - A 0.2 g sample of the nanocomposite PEM was exchanged with NH_4^+ by immersing the sample in 1 M ammonium acetate for 24 hours and then in ammonium chloride for an additional hour [52, Appendix A]. The PEM was then washed with DI water to remove any excess NH_4^+ ions. To ensure that all excess NH_4^+ had been removed, a drop of 1 M silver nitrate was added to the wash. If NH_4^+ ions were present, a white precipitate would form. The PEM was then stored in 50 ml DI water. Adding 2 ml of 5 M NaOH solution to the sample, caused the subsequent exchange of NH_4^+ with Na^+. Utilizing a calibrated ammonia electrode (Model 95-12 ORION, Boston MA), the amount of NH_4^+ released could be accurately quantified thus providing a measure of the ion-exchange capacity.

Ex Situ Conductivity Testing - A nanocomposite membrane sample was sandwiched between two electrodes each on either side to measure the conductivity, similar to the procedure reported in literature and then placed in humidity controlled chamber [53-55]. The humidity of the chamber was monitored utilizing a dewpoint/temperature probe (HMP 238, Vaisala, Woburn, MA). An air stream was saturated with water by bubbling through a humidifier. This wet stream was heat-traced to the chamber to avoid condensation. The chamber and the humidifier were both heated to 90°C and 120°C, respectively, to obtain the desired partial pressure of water. The conductivity of the PEM was measured at 90 °C in the RH range from 10 % to 90 %, while at 120 °C the RH range was from 10 % to 40 % to simulate dry conditions. These conditions are the same as those utilized for the water

uptake measurements. The conductivity measurements were made with a perturbation voltage of 10 mV in the frequency range 0.01 Hz to 10^6 Hz using a Solartron SI 1260 FRA (Solartron, Hampshire, U.K.). Both real and imaginary components of the impedance were measured and the real *z*-axis intercept was closely approximated to provide an estimate of the membrane resistance, and hence, conductivity.

MEA Testing - The electrodes utilized are commercially available from E-TEK (Somerset, NJ). The type selected was the single-sided ELAT® gas-diffusion electrode (20 % Pt-on-C, 0.35~0.4 mg Pt/cm^2). The active layer of electrode was brushed with 5 % Nafion® solution (0.6 ~0.8 mg/cm^2 MEA). This electrode was placed on either side of the PEM and the resulting membrane-electrode assembly (MEA) placed in a hot press. The temperature of the hot press was then raised to 130 ^{o}C and a pressure of 272 atm applied for 120 s. The MEA thus prepared was mounted in a 5 cm^2 fuel cell test fixture, obtained from Fuel Cell Technologies (Los Alamos, NM). The cell was fed with humidified H_2 and O_2 or air supplied at pressure 1 to 3 atm utilizing electronic mass flow controllers (MKS Model No. 1179A22CS1BV-S, Andover, MA) and was controlled by the electronic load (Series 890B Fuel Cell Test System, Scribner Associates Inc. Southern Pines, NC). Utilizing software (Fuel Cell Test Software Version 2.0, Scribner Associates, Inc.), the mass flow rate of the feed gas was programmed to stoichiometry dependent flow rates. The load has an inbuilt feature of measuring *in situ* MEA ohmic resistance utilizing the current interruption method.

The pressure of the reactant gases was monitored using pressure gauges (Matheson, Model No. 63-5612). Back pressure regulators (Tescom Model No. 44-2300) were used at the outlet of both the anode and the cathode to control the gas pressure. Humidification of the cell was accomplished by bubbling the feeds through stainless steel cylinders containing DI water and equipped with a sight glass. Heating tape was wrapped around the feed lines to prevent any condensation in the lines, and water traps were added after the exit gas stream to facilitate removal of water. The temperature of the humidifiers as well as that of the fuel cell was controlled using individual temperature controllers (Omega CN9100A).

The following MEA test protocol was utilized [54]. The startup procedure involved bringing the humidifier temperature up to a set value of 80 ^{o}C, then increasing the fuel cell to 70^{o}C and operating with 1 atm H_2 and air at current controlled mass flow rates, being 1.3 times anode stoichiometric flow for H_2 and 2.0 times cathode stoichiometric flow for air. The load was cycled for additional 6 hours and then a constant voltage polarization curve was taken. Thereupon, another 12 hours of break-in period was utilized and then a final polarization curve was obtained as follows. The voltage was set at 0.6 V set for 10 minutes then data was taken every 6 seconds for 3 minutes. The voltage was held for 3 minutes, before the first data point was collected, and then data were collected every 6 seconds for 3 minutes at each voltage set-point. This continued for the following voltage sequence, 0.55 V, 0.5 V, 0.45 V, 0.4 V, 0.6 V, 1(for 1 minute), 0.65 V, 0.7 V, 0.75 V, 0.8 V, 0.85 V, and 0.6 V.

The electrochemical surface area (ECSA) and crossover were measured utilizing the potentiostat. Potentiostats often allow the choice of 2, 3, or 4 terminal connections to the cell depending on the particular application to measure the ECSA and cross-over current. The two terminal connections are usually used when it is difficult to position the reference electrodes inside the cell itself. Although there is a reference electrode machined in the test fixture, it is assumed that the H_2 anode behaves as a reference electrode. The ECSA is a measure of the surface area of Pt that takes part in the reaction and was measured in the following manner:

1. The cathode was purged with N_2 and the anode with H_2, both set at 50 sccm and 1 atm.
2. After the OCV is < 0.14 V, the ECSA was measured by utilizing the 1287 potentiostat (Solartron, Hampshire, U.K.). The counter electrode (CE) and reference electrode 1 (RE 1) were connected to the anode, while the working electrode (WE) and the reference electrode 2 (RE2) were connected to the cathode.
3. To measure the ECSA of the MEA, the potential was swept from 0.0 V to 0.6 V for 4 cycles at 100 mV/s, while the cross- over is measured at 0.0 V to 1.0 V at 2 mV/s for 3 cycles.
4. The total charge between 0.0 V and 0.6 V was integrated and after correcting for the double layer (assuming it is the baseline), the total charge produced by the

reaction was calculated. The ECSA was calculated by assuming a stoichiometry of 1 e^- / Pt. Site [55]. The crossover is simply the plateau in current observed.

The pressure of the cell was next increased to 1.5 atm for both the H_2 and air feeds, and a polarization curve was obtained again. The temperatures of the fuel cell and the humidifiers were then increased to 80°C. After utilizing the break-in protocol for 2 hours, to ensure steady-state performance has been reached, a polarization curve was obtained. Finally, the ECSA and crossover current were measured again.

In a similar fashion, the polarization curves and ECSA were measured at increasingly higher temperatures. The temperatures of the humidifiers were maintained at 80°C and the cell temperature was returned to 70°C at the end of the experiment. Thus, the sequential temperature test protocol was: (a) Cell = 70°C, Hum. = 80°C, Beginning of Life (BOL), (b) Cell = 90°C, Hum. = 80°C, (c) Cell = 100°C, Hum. = 80°C, (d) Cell = 110°C, Hum. = 80°C, (e) Cell = 120°C, Hum. = 80°C (f) Cell = 130°C, Hum = 130°C, P = 3 atm O_2, and (g) Cell = 70°C, Hum. = 80°C, End of Life (EOL).

2.6 Results and Discussion

Water Uptake Measurements- Fig. 2.5 shows the area specific water uptake at 120°C of all the additive powders utilized in this study. Among the additives investigated the most promising appears to be the ZrO_2 (sample with no acid treatment). Fig. 2.6 shows the water uptake of the nanocomposite membranes measured at 120°C. All the nanocomposites show an enhanced water uptake at 120°C when compared to Nafion. The Nafion ZrO_2 sol-gel nanocomposite shows the highest water uptake of all the samples tested and is around 40 % higher than Nafion 112 at 40% RH. The 5 wt % SO_4/ZrO_2 and the 5 wt % ZrO_2 both show water uptake that is 20 % higher than the Nafion 112 sample at 40 % RH. Thus, the behavior of the nanocomposite PEMs reflects the trend due to the effect of size of inorganics particles. The Nafion ZrO_2 sol-gel nanocomposite has the smallest particle size as compared to other membranes and hence, has the highest water uptake of all the nanocomposites. Further, the benefit of inorganic additives in PEMs is evident at higher temperatures and low RHs.

Ion-Exchange Capacity - Table 1 lists the experimental EW and partial molar volumes along with the predicted EW using Eq. 3 for the nanocomposite membranes. The additive acid site concentration c^*_{ZH0} was estimated using data for 5 % ZrO_2 (A) EW and assuming an average $10\mu m$ particle size as 7.77×10^{17} molecules/cm^2. Assuming c^*_{ZH0} constant for all the nanocomposite membranes, the partial molar volume of other nanocomposite membrane was calculated and is listed in Table 1. The corresponding EW can be thus obtained by multiplying $\overline{V}_M$ with the measured membrane density. The EW obtained from Eq. 3 and experimentally are in good agreement. Thus, it is evident that for nano sized particles, the EW is low, implying higher acidity. Also it is observed that an increase in particle size increases the $\overline{V}_M$ which causes a decrease in the acidity of the membrane. The Nafion ZrO_2 sol-gel nanocomposite has the highest number of acid sites available of the membranes investigated due to the larger surface area of the nano sized particles. Based on gravimetric and preliminary ash analysis, the loading of particles in the Nafion ZrO_2 sol-gel nanocomposite is around 3 to 4 wt %. The incorporation of zirconium oxide in Nafion using sol gel method increased the effective acid site concentrations in the membrane also resulting in higher water uptake.

The X-ray diffraction (Model Rigaku Geigerflex X-ray Diffractometer) analysis for the nanocomposite membranes compared to Nafion shown in Fig. 2.7 was done at room temperature. The 10 wt % SO_4^{2-}/ZrO_2 showed some extra peaks as compared to Nafion corresponding to ZrO_2. However, the Nafion ZrO_2 sol-gel showed a pattern essentially identical to Nafion due to the low loading and the nanosized ZrO_2. Hence a future goal is to increase the loading of ZrO_2 in the membrane by varying the synthesis procedure during sol gel process.

It is evident that for the membrane to be more acidic, the equivalent weight ought to decrease. However, lowering EW implies that the membrane would swell more due to high water sorption. However, the mechanical strength of the membrane is also related to the additive loading. Thus, an optimum amount of inorganic additive is indicated. Polymeric membranes with EW below 900 show low mechanical strength and are not suitable for fuel cell applications. Hence an objective is to design membrane having EW

around 900 for best fuel cell performance with the highest water uptake and proton conductivity.

Samples	Partial Molar Volume $\overline{V}_M$ (cm^3/mol)	EW (g/mol. H^+) (Experimental)	EW (g/mol. H^+) (From Eq. 3)
Nafion® 112	537	1106	1106
Nafion ZrO_2 Sol-gel.	515	1016	1030
5% ZrO_2 (A)	517	1084	1084
10% ZrO_2 (A)	528	1121	1109
20% ZrO_2 (A)	545	1159	1146

Table 2.1 The partial molar volume, experimental and predicted EW of the Nafion 112, and nanocomposite membranes at 25°C.

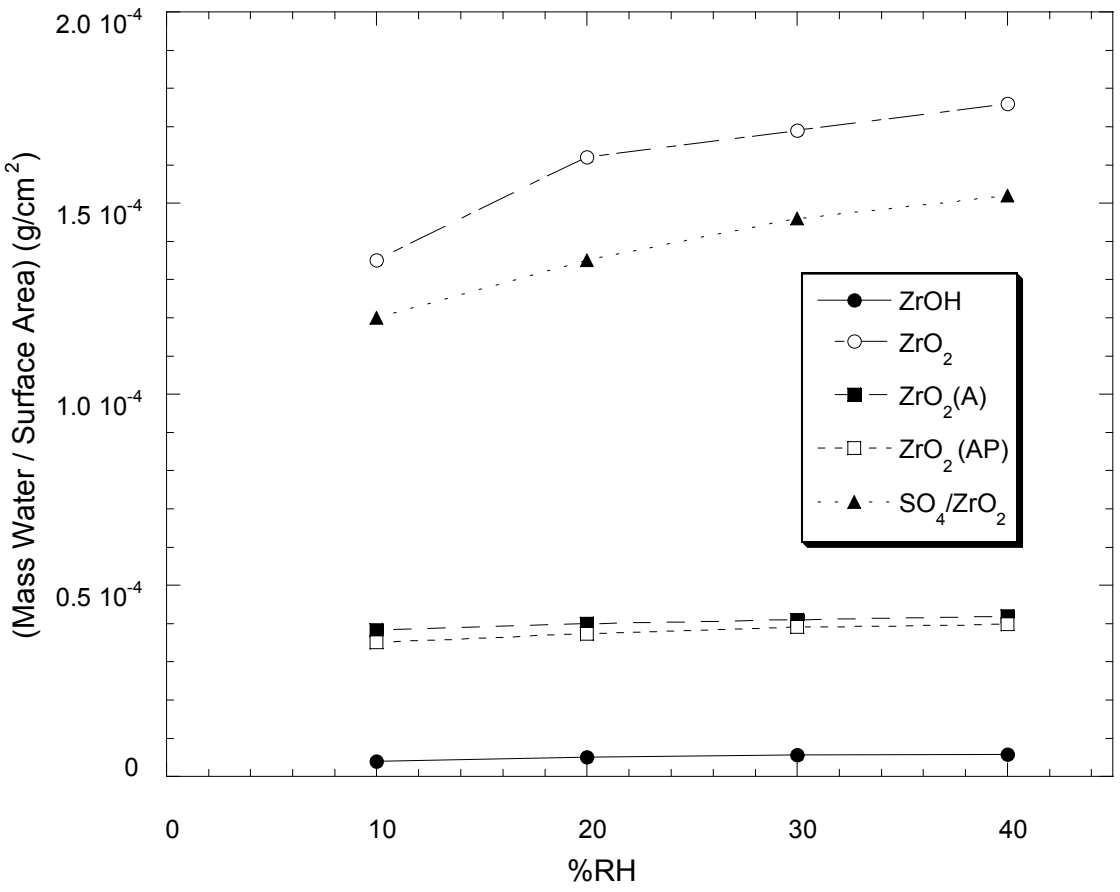

Figure 2.5 The surface area normalized water uptake of the powder at 120°C vs. RH. The most promising candidates are the ZrO_2 and the SO_4/ZrO_2 samples.

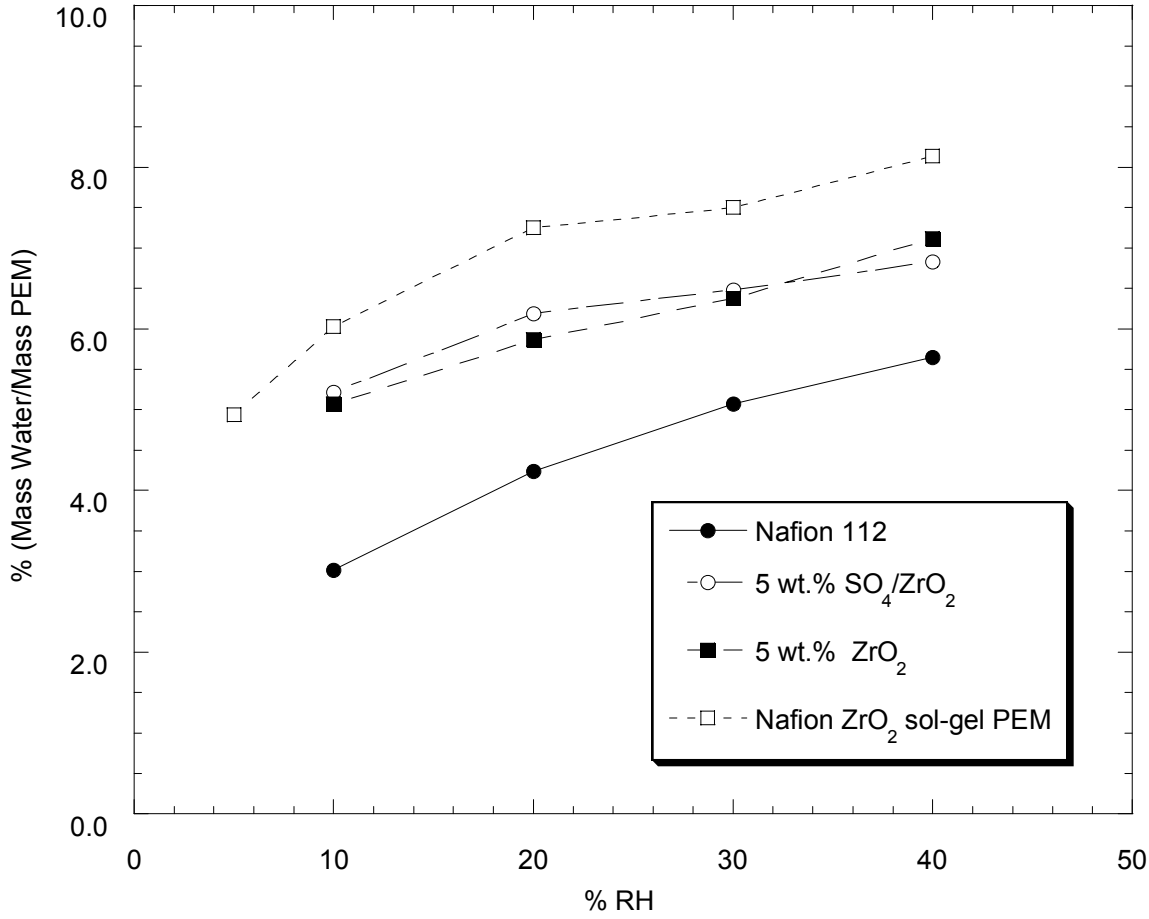

Figure 2.6 The water uptake of nanocomposite membranes and Nafion 112 at 120°C vs. RH. The Nafion ZrO_2 sol-gel PEM demonstrates the highest water uptake.

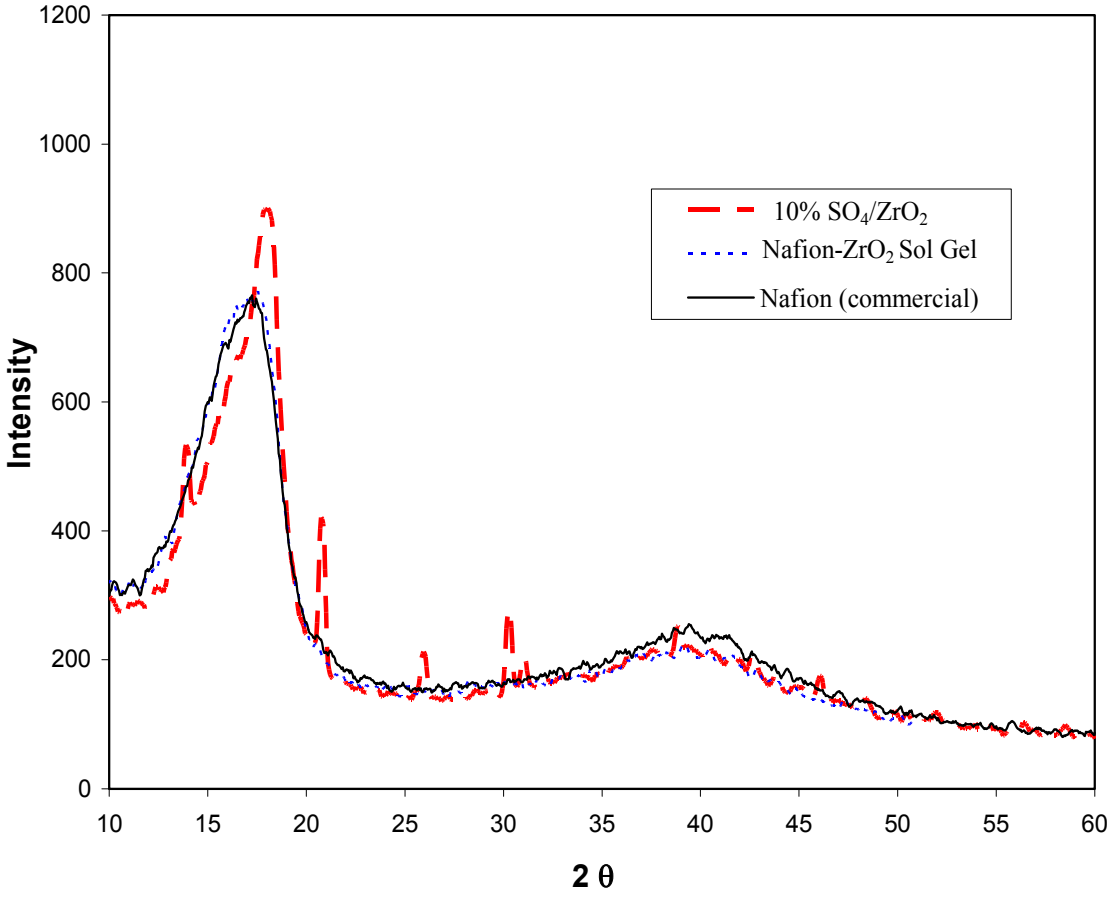

Figure 2.7 XRD pattern for nanocomposite membranes and Nafion.

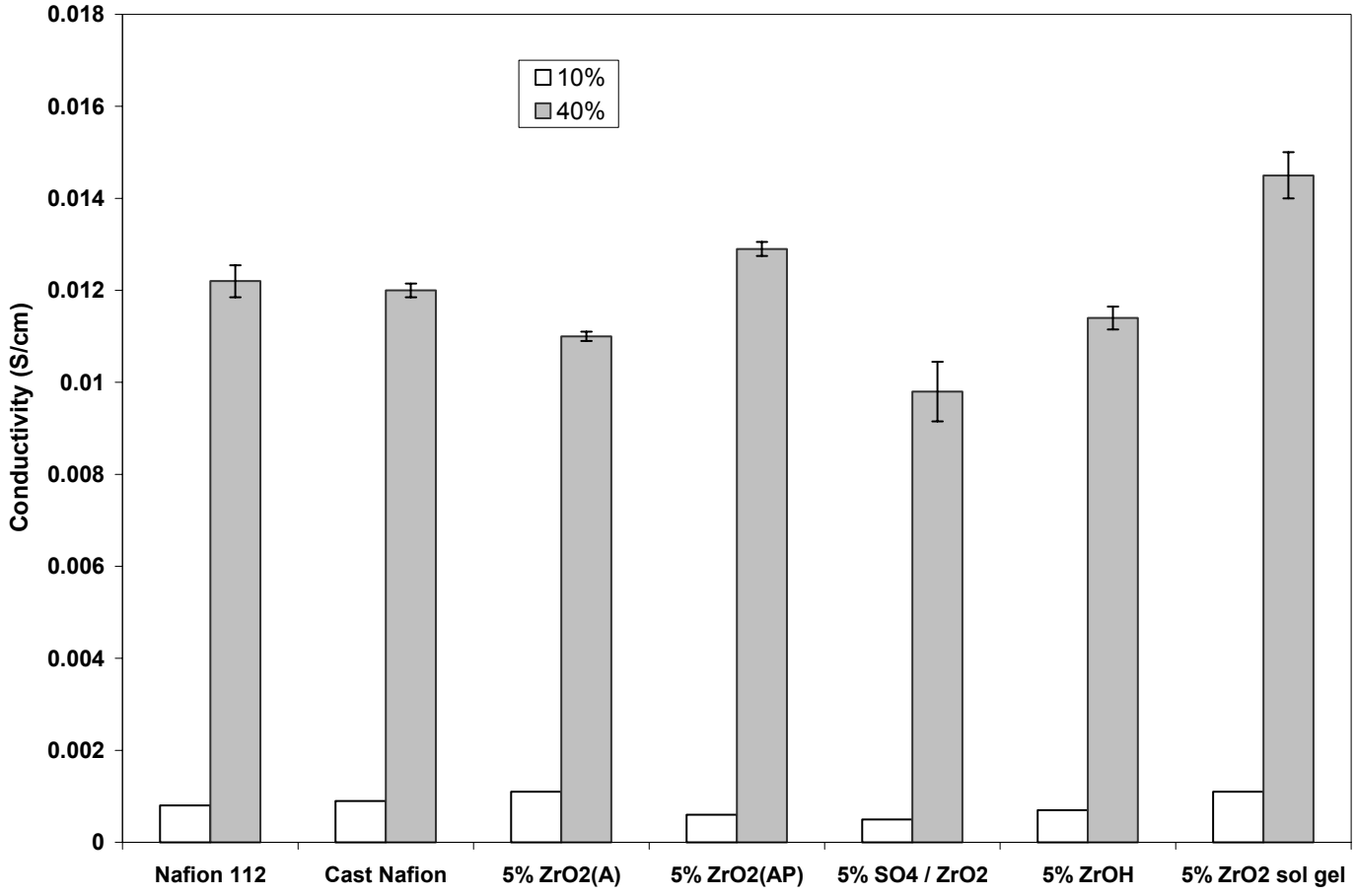

Figure 2.8 The conductivity of the PEMs at 10 % RH and 40 % RH at 90°C. The Nafion ZrO_2 sol-gel PEM shows the highest conductivity of the samples.

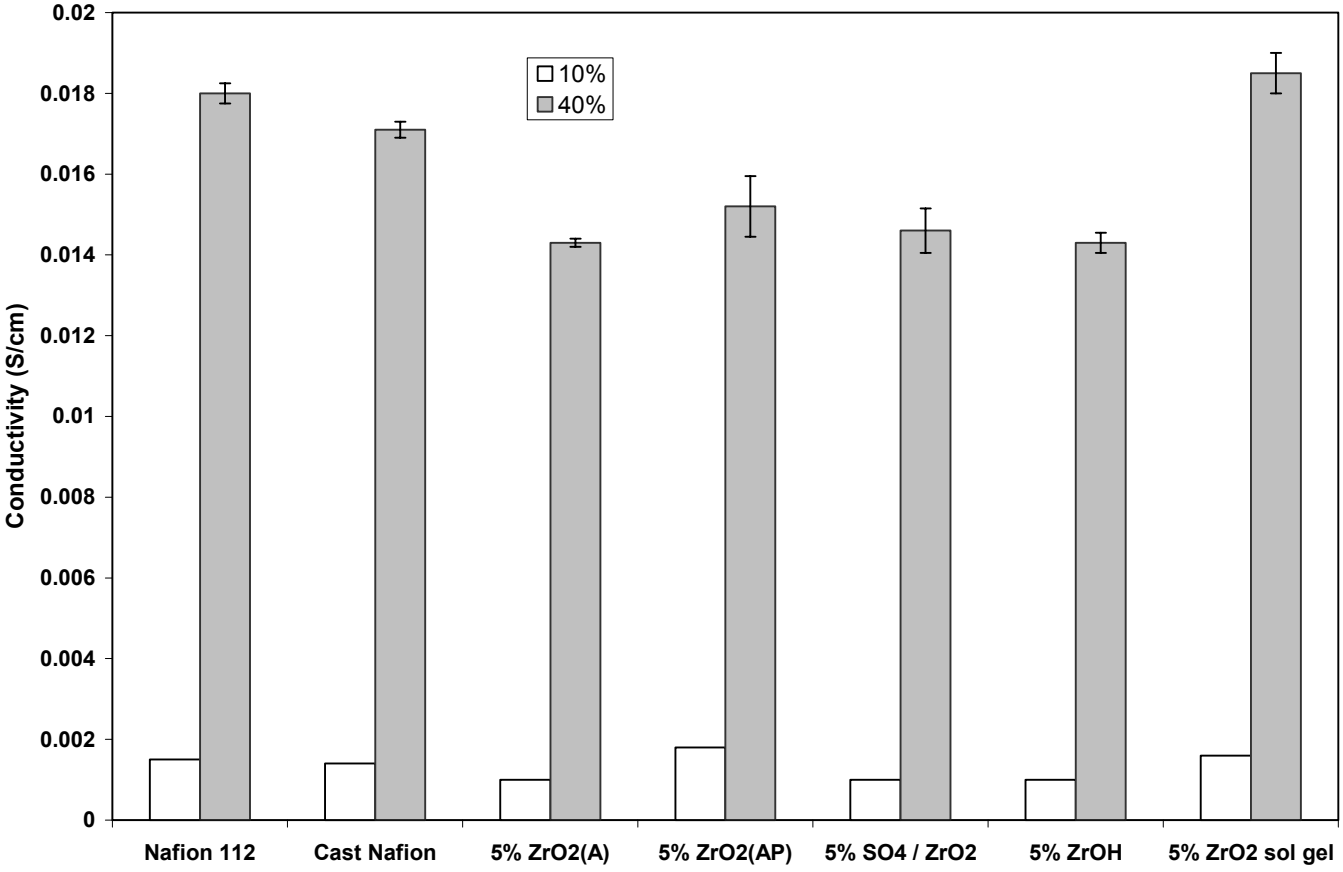

Figure 2.9 The conductivity of the PEMs at 10 % and 40 % RH at 120°C. The Nafion ZrO_2 sol-gel PEM shows the highest conductivity of the samples.

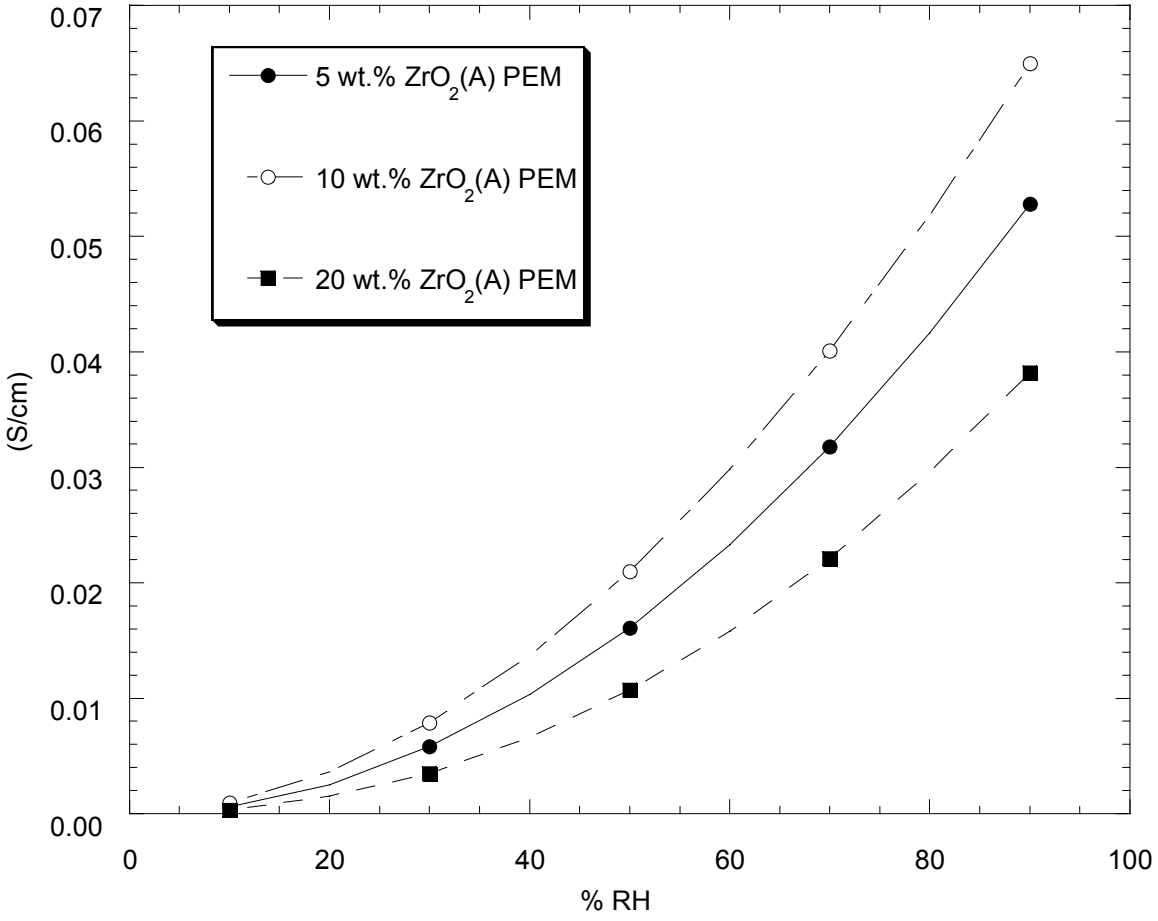

Figure 2.10 The conductivity of loaded nanocomposites PEMs at 90°C vs. RH. The optimum conductivity is observed with the 10 wt % PEM.

Conductivity Measurements - Fig. 2.10 shows the measured conductivity of the commercial Nafion 112, solvent cast Nafion, and the solvent cast and the sol gel nanocomposite PEMs measured at 10 % RH and 40 % RH at a temperature of 90^{o}C. The Nafion ZrO_2 sol-gel nanocomposite has the highest conductivity among all nanocomposites. Fig. 2.11 presents the conductivity of the nanocomposite PEMs measured at 120 ^{o}C. The conductivities for Nafion and other nanocomposite membranes were reproduced and the error bars are shown for each nanocomposite. In general the conductivities at 120^{o}C are higher than 90 ^{o}C. The conductivity exhibited by the Nafion ZrO_2 sol-gel nanocomposite is about 4-5 % higher than Nafion 112 at 40 % RH. All the other nanocomposites have conductivity smaller than that of Nafion despite a higher water uptake.

The increase in the conductivity of the Nafion ZrO_2 sol-gel nanocomposite than that of Nafion is the combined result of the enhanced water uptake as well as acidity. Also the membrane structure influences the overall conductivity of the membrane. Our concomitant efforts to develop proton transport model for both Nafion and CPEMs shows that tortuosity of the membranes affects the water sorption properties which in turn impacts the conductivity. Although the other nanocomposites show an enhanced water uptake at 120^{o}C, the acidity (Table 2.1) as well as conductivity of these PEMs is less than that of Nafion. It is thus noteworthy that an enhancement in the water sorption properties of the PEM does not necessarily translate directly into an enhanced conductivity.

To study the effect of the additive loading, the conductivity of 5 %, 10 % and 20 % ZrO_2 nanocomposites versus RH is shown in Figs. 2.10 and 2.11 at 90^{o}C and 120^{o}C, respectively. It is observed that the optimum conductivity in both cases is with the 10 % ZrO_2 PEM. An increase in conductivity is observed when the loading is increased from 5 % to 10 %, while a dramatic decline is observed when the loading is increased to further 20 %. Although the water uptake of the nanocomposites increases monotonically with loading of the additive, the IEC measurements show that an increase in the loading causes EW to increase (Table 2.1) and thereby reducing the acid strength of the nanocomposite membrane. Hence, enhanced water sorption with lower EW of the nanocomposite membrane and optimum loading will result into highest conductivity.

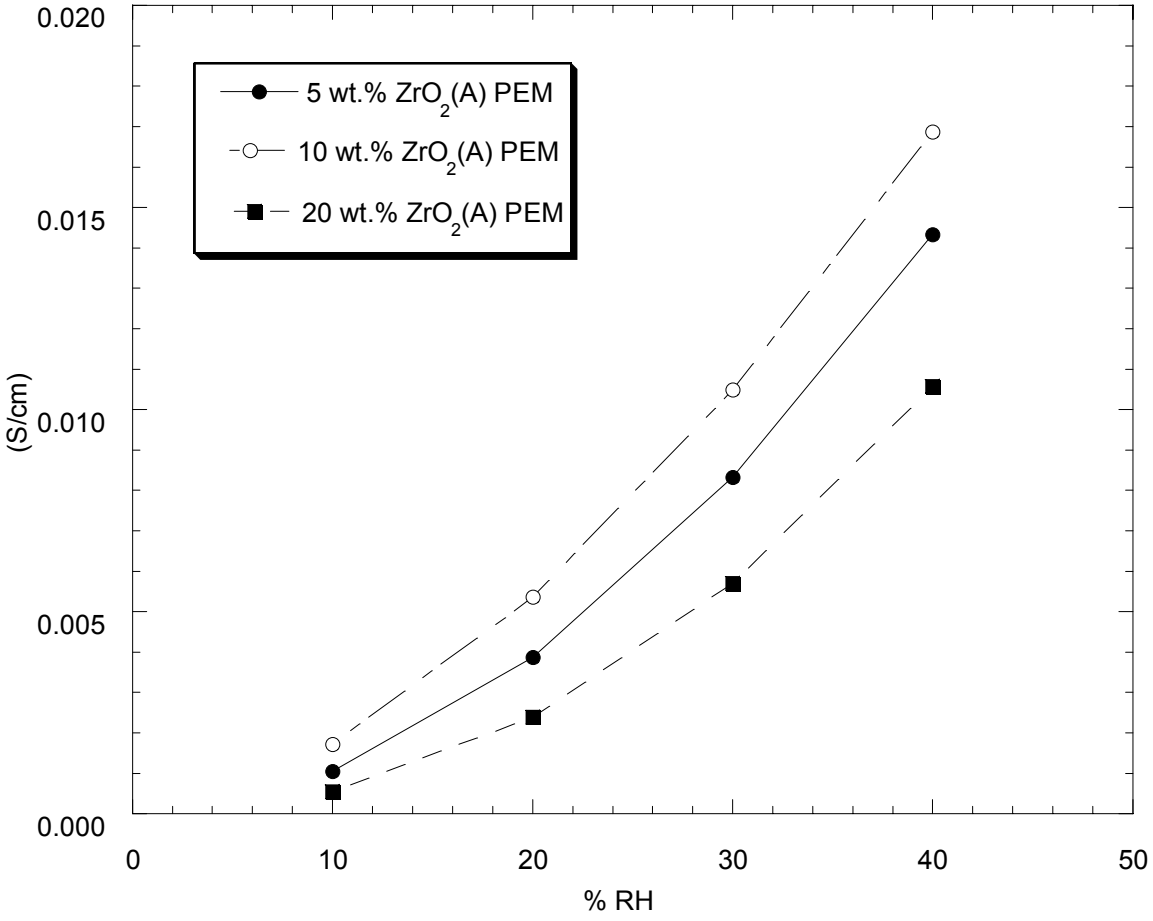

Figure 2.11 The conductivity of loaded nanocomposite PEMs at 120 ^{o}C. The optimum conductivity is observed with the 10 wt % PEM.

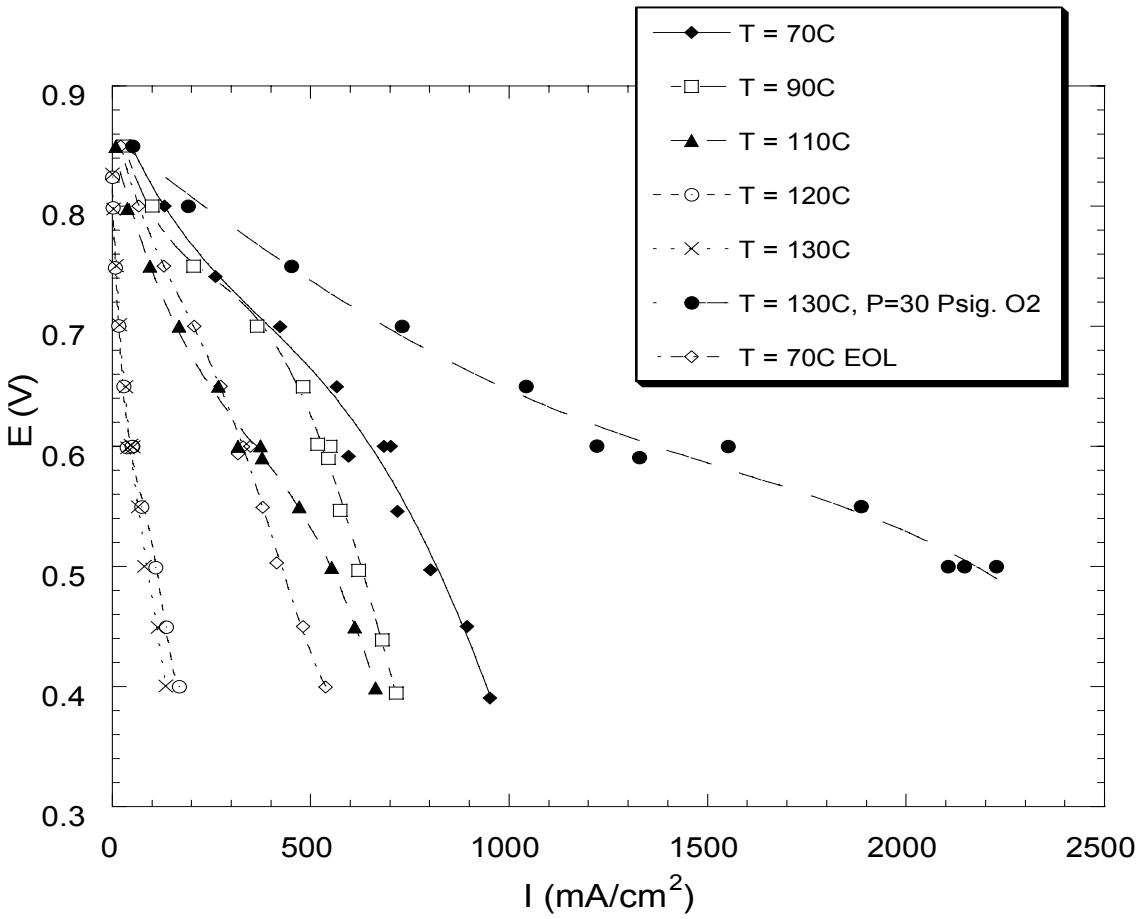

Figure 2.11 The cell performance of Nafion 112 MEA with conditions as noted on figure. Operated with 1.5 atm Air /H_2, humidifiers set at 80 ^oC. The exception was when the cell was at 130 ^oC, 3 atm. O_2 and the humidifiers set at 130^oC.

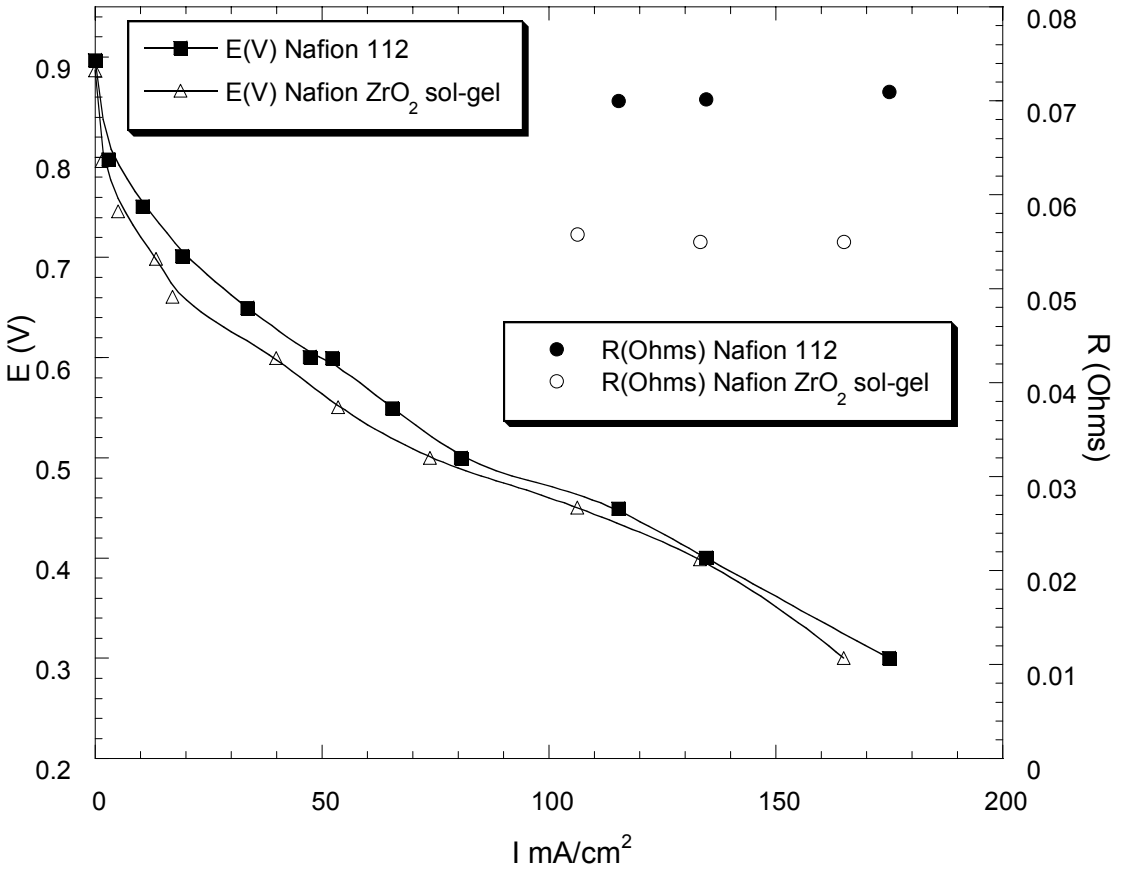

Figure 2.12 The cell performance of Nafion 112 MEA vs. Nafion ZrO_2 sol-gel nanocomposite MEA. Air and H_2 at 2.0 and 1.3 times stoichiometry flows respectively, P = 1.0 atm., $T_{\text{HUMIDIFI ER}}$= 80 ^{o}C, T_{CELL} = 110 ^{o}C.

MEA Performance - Fig. 2.12 shows the fuel cell performance obtained with a Nafion 112 MEA that was tested at 70°C, 90°C, 100°C, 110°C, 120°C, 130°C and then returned to 70°C, following the test protocol described above. The performance drops with increasing temperature and a reduction in RH. To distinguish between the membrane resistance and the kinetics, the electrochemical surface area measurements were also made and are shown in Table 2.2. As the temperature increases, the ECSA decreases due to ionomer shrinkage within the catalyst layer indicating a reduced active area, thus countering the increased rate of reaction at higher temperatures. For instance, when the temperature is increased from 90 °C to 120 °C, the ECSA declines to one-third its value at 90 °C. Kanamura *et al.* investigated the Nafion/Pt interface with *in situ* spectroscopic techniques (FTIR, AFM and surface potential measurements). The interface was observed to have a dynamic nature, in the dry state the interface is very small while in the humidified state the interface was greatly extended. Additionally, the conductivity of the Nafion ionomer present within the catalyst layer will also drop at higher temperatures and low RH. Thus, the performance of the fuel cell is limited at lower RH at higher temperatures both due to the increased transport resistance in the PEM layer as well as due to the decrease in ECSA in the catalyst layer.

From Fig. 2.12 it is also observed that there is a decline in the performance not only as the cell temperature increases (and concomitantly as the RH decreases), but also between BOL and EOL polarization, of about 300 mA/cm^2 at 0.6 V. It is also noted that the ECSA measurements at 70°C BOL and 70°C EOL are 40.8 mC/cm^2 and 29.2 mC/cm^2 respectively, while the cell resistance measurements are 20.3 mΩ and 21.5 mΩ at 70°C BOL and 70°C EOL respectively. Thus, the performance loss is mainly a result of kinetic overpotential, as the ohmic PEM resistance measured at the BOL and EOL is similar. The crossover current measurements demonstrated low current (0.5 mA/cm^2) generated by H_2 crossover at high temperature (120°C). The excellent performance at 130°C under fully humidified conditions (Humidifiers at 130°C, P= 3 atm) shows no degradation over several hours.

Finally, a MEA was fabricated with a Nafion/ZrO_2 sol-gel nanocomposite membrane and tested under dry hot conditions (T_{cell} = 110°C, $T_{Humidifier}$= 80°C). The resulting performance is shown in Fig. 2.13 along with Nafion 112 for comparison.

Although no performance improvement was observed, it is noted that the *in situ* MEA ohmic measurements show improvement of conductivity of the nanocomposite versus Nafion 112, under these conditions. However, it is clear that the reduction of ECSA in the catalyst layer under dry conditions (Table 2.2) must also be addressed before improved performance can be obtained. It is noteworthy that literature contains few results of improved MEA performance despite improved *ex situ* conductivity reported for some nanocomposite membranes.

Based on our earlier fuel cell model simulations, an order of magnitude drop in conductivity from 0.05 S/cm at 80^{o}C to 0.005 S/cm at 120^{o}C with Nafion 112 under dry conditions is the cause of the poor cell performance. The most promising nanocomposite, Nafion/ZrO_2 sol-gel nanocomposite on the other hand, demonstrates enhanced conductivity and water sorption compared to Nafion 112. An important outcome from utilizing the sol gel approach is that the nanocomposite membranes synthesized were homogenous. This implies that this approach can be used to synthesize homogeneous membranes with inorganics exhibiting higher acidity and better properties than Nafion. Therefore, it is evident that we need to further increase the conductivity of the nanocomposite PEMs for a substantial improvement in MEA performance at higher temperatures and low RH. Additionally, at lower RH and higher temperatures, the shrinkage and dehydration of the ionomer in the catalyst layer must also be addressed.

2.7 Conclusions

Based on a systematic approach, the synthesis and *ex situ* and *in situ* performance of nanocomposite PEMs for higher temperature/lower RH operation have been investigated. The promising potential of the sol-gel nanocomposite PEMs has been demonstrated with improved hydration as well as conductivity at higher temperature and lower RH conditions. Although greater conductivity improvement is necessary to obtain high performance at higher temperatures/lower RH, the increase in rates of reactions, improved CO tolerance and water management may provide useful power densities even with a smaller enhancement, provided that the shrinking of ECSA under dry conditions can be first addressed. Thus, the incorporation of the zirconia additives in the catalyst layer to minimize electrode overpotential, and the long-term evaluation of these MEAs by fuel cell

testing is being undertaken. In summary, significant progress has been made in the understanding and design of nanocomposite PEMs, and it is expected that continued development following a systematic approach will eventually result in high performance nanocomposite PEMs.

Nafion 112	**ECSA (mC/cm^2)**
70^oC (BOL)	40.8
90^oC	43.8
110^oC	21
120^oC	15
70^oC (EOL)	29.2

Table 2.2 The ECSA of a Nafion 112 MEA at different fuel cell temperatures, when the temperature of the humidifers remains constant at 80 ^oC.

2.8 References

1. P. Murugaraj, K. D. Kreuer, T. He, T. Schober, and J. Maier, *Solid State Ionics*, **98**, 1 (1997).
2. T. Norby, *Solid State Ionics*, **125**, 1 (1999).
3. P. Colomban, *Proton Conductors*, Cambridge University Press, Cambridge (1992).
4. S. Malhotra and R. Datta, *J. Electrochem. Soc.*, **144,** L23 (1997).
5. A. Eisenberg and J. S. Kim, *Introduction to Ionomers*, John Wiley & Sons, New York (1998).
6. S. C. Yeo and A. Eisenberg, *J. App. Polym Sci*., **21**, 875 (1977).
7. R. M. Ikeda, *Polymer Preprints*, ACS, Div. of Poly. Chem., Amer. Chem. Soc., **19 (2)**, 215 (1978).
8. H. L. Yeager and A. Steck, *J. Electrochem. Soc.*, **128**, 1880 (1981).
9. A. Steck, Proceedings of the First International Symposium on New Materials for Fuel Cell Systems, (Eds. O. Savagodo, P. R. Roberge, and T. N. Veziroglu), Montreal, Canada, July 9-13, 74 (1995).
10. D. S. Watkins, Abstracts 33rd Int. Power Sources Symp., *The Electrochemical Society*, Pennington, NJ, 782 (1988).
11. M. Hogarth and X. Glipa, High Temperature Membranes For Solid Polymer Fuel Cells ETSU F/02/00189/REP DTI/Pub URN 01/893 (2001).
12. D. D. DesMarteau, *J. Fluorine Chem*., **72**, 203 (1995).
13. S. V. Kotov, S. D. Pederesen, W. Z-M Qui, and D. J. Burton, *J. Fluorine Chem*., **82**, 13 (1997).
14. S. C. Savett, J. R. Atkins, C. R. Sides, J. L. Harris, B. H. Thomas, S. E. Creager, W. T. Pennington, and D. D. DesMarteau, *J. Electrochem. Soc.,* **149**(12), A1527 (2002).
15. W. Liu, K. Ruth, and G. Rusch, *J. New Mat. Electrochemical Syst.*, **4**, 227(2001).
16. R. B. Hogdon, *J. Polymer Sci.*, **6**, 171 (1968).
17. A. E. Steck and C. Stone*, Proceedings of the 2nd International Symposium on New Materials for Fuel Cell and Modern Battery Systems*, (Eds. O. Savagodo, P. R. Roberge, and T. N. Veziroglu) Montreal, Canada, July 6-10, 792 (1997).
18. M. Rikukawa and K. Sanui, *Prog. Polym. Sci.*, **25**, 1463 (2000).

19. O. Savagodo, *J. New Mater. Electrochem. Syst.*, **1**, 66 (1998).

20. J. E. McGrath, *Proton Exchange Membrane Nanocomposites for Fuel Cells*, Advances in Materials for Proton Exchange Membrane Fuel Cell Systems, ACS, Pacific Grove, CA (2003) Feb. 23-27.

21. F. Wang, M. Hickner, Y. S. Kim, T. A. Zawodzinski, and J. E. McGrath, *J. Membr. Sci.*, **197**, 231 (2002).

22. R. F. Savinell, J. S. Wainright, and M. Litt, *Proton Conducting Membrane Fuel Cells II,*(Eds. S. Gottesfeld and T. F. Fuller), PV 98-27, ECS, Pennington, NJ 81 (1999).

23. R. Savinell, E. Yeager, D. Tryk, U. Landau, J. Wainright, D. Weng, K. Lux, M. Litt, and C. Rogers*, J. Electrochem. Soc.,* **141**, L46 (1994).

24. M. Doyle, S. K. Choi, and G. Proulex, *J. Electrochem. Soc.,* **147**, 34 (2000).

25. S. Chandra, *Superionic Solids and Solid Electrolytes Recent Trends*, (Eds. A. L. Laskar and S. Chandra), Material Science Series, Academic Press, Inc 190 (1989).

26. P. Costamagna, C. Yang, A. B. Bocarsly, and S. Srinivasan, *Electrochimica Acta.*, **47,** 1023 (2002).

27. V. Ramani, H. R. Kunz, and J. M. Fenton, *J. Membr. Sci*., **232**, 31 (2004).

28. M. Watanabe, H. Uchida, Y. Seki, M. Emori, and P. Stonehart, *J. Electrochem. Soc.,* **143**(12), 3847 (1996).

29. M. Watanabe, H. Uchida, Y. Seki, and M. Emori, *J. Phys. Chem. B,* **102,** 3129 (1998).

30. H. Uchida, Y. Ueno, H. Hagihara, and M. Watanabe, *J. Electrochem. Soc.,* **150**(1), A57 (2003).

31. C. Yang, P. Costamagna, S. Srinivasan, J. Benziger, and A. B. Bocarsly, *J. Power Sources,* **103**, 1 (2001).

32. Y. Si, J. M. Fenton, and H. R. Kunz, *Preparation of MEAs for PEM Fuel Cells Operating At Above 100*°C, 199th ECS, Washington DC 2001, March 25-29.

33. Y. I. Park, J. D. Kim, and M. Nagai, *J. Mat. Sci. Letts.*, **19,** 1621 (2000).

34. M. A. Harmer and Q. Sun, *U.S. Patent 6,515,190*, (2003).

35. K. T. Adjemian, S. J. Lee, S. Srinivasan, J. Benziger, and A. B. Bocarsly, *J. Electrochem. Soc.,* **149**(3), A256 (2002).

36. K. T. Adjemian, S. Srinivasan, J. Benziger and A. B. Bocarsly, *J. Power Sources ,* **109**, 356 (2002).

37. K. A. Mauritz, I. D. Stefanithis, S. V. Davis, R. W. Scheez, R. K. Pope, G. L. Wilkes, and H. H. Huang, *J. Appl. Polym. Sci.,* **55**, 181 (1995).

38. W. G. Grot and G. Rajendran, *U.S. Patent 5,919,583*, (1999).

39. S. M. J. Zaidi, S. D. Mikhailenko, G. P. Robertson, M. D. Guiver, and S. Kaliaguine, *J. Membr. Sci.*, **173**, 17 (2000).

40. F. Lonyi, J. Valyon, J. Engelhardt, and F. Mizukami, *J. Catal.,***60**, 279 (1996).

41. M. Misono and T. Okuhara, *CHEMTECH*, **23**, (Nov 1993) & M. Misono, T. Okuhara and N. Mizuno, *Succesful Design of Catalysts*, (Ed. T Inui), p. 267, Elsevier, Amsterdam (1988).

42. G. A. Olah, G. K. Surya Prakash, and J. Sommer, *Superacids*, Wiley, New York (1985).

43. K. Kanamura, H. Morikawa, and T. Umegaki, *J. Electrochem. Soc.*, **150**(2), A193 (2003).

44. T. Thampan, S. Malhotra, H. Tang, and R. Datta, *J. Electrochem. Soc.*, **147**(1), 3242 (2000).

45. E. A. Mason and A. P. Malinauskas, *Gas Transport in Porous Media: The Dusty Gas Model,* p. 142, Elsevier Amsterdam (1983).

46. P. Choi and R. Datta, *J. Electrochem. Soc.,* 1**50** (12), E601 (2003).

47. K. Arata, *Applied Catalysis A: General,* **146**, 3 (1996).

48. R. B. Moore and C. R. Martin, *Anal. Chem.*, **58**, 2570 (1986).

49. W. Apichatachutapan, R. B. Moore, and K. A. Mauritz, *J. Appl. Polym. Sci.,* **62**, 417 (1996).

50. P. Liu, J. Bandara, Y. Lin, D. Elgin, L. F. Allard, and Y. P. Sun, *Langmuir*, **18**(26), 10398 (2002).

51. J. E. Resoke and M. A. Barteu, *J. Phys. Chem. B*, **101,** 1113 (1997).

52. E. Busenberg and C. V. Clemency, *Clays and Clay Materials,* **21**, 213 (1973).

53. W. B. Johnson and L. Wen, *High Temperature Materials Symposium in Honor of the 65th Birthday of Professor Wayne L. Worrell*, (Ed. S. C. Singhal), PV 2002-5, p. 132, The Electrochemical Society Proceedings, Pennington, NJ (2002).

54. B. Bahar, C. Cavalca, S. Cleghorn, J. Kolde, D. Lane, M. Murthy, and G. Rusch, *J. New Mater. Electrochem. Syst.*, **2**(3), 179 (1999).

55. T. J. Schmidt, H. A. Gasteiger, G. D. Stäb, P. M. Urban, D. M. Kolb, and R. J. Behm, *J. Electrochem*. *Soc*., **145**(7), 2354 (1998).

Chapter 3

Thermodynamics of Water Sorption and Proton Transport in the Understanding and Design of Nanocomposite PEMs

A phenomenological theory, largely devoid of fitted parameters, is provided for water sorption and proton transport in polymer electrolyte membranes (PEMs) as well as in polymer-inorganic nanocomposite membranes (NCPEMs) that serves to not only rationalize the sorption and conductivity behavior of conventional PEMs such as Nafion, but also provides a framework for rational design of improved PEMs and NCPEMs. The thermodynamic model based on the influence of osmotic pressure on the activity of free water within the membrane pores not only predicts the entire sorption isotherm, but also provides a plausible explanation for the so-called Schroeder's paradox, namely the difference in amounts sorbed from liquid versus saturated vapor. The transport model incorporates the various mechanisms of proton transport, namely, surface hopping, Grotthuss diffusion, and *en masse*, or vehicle diffusion. In particular, it provides a predictive expression for Grotthuss diffusion, which turns out to be the dominant mechanism for proton transport in Nafion. Since the design of alternate PEMs suitable for effective proton transport under hot and dry conditions is a key current technological goal, the rational design of NCPEMs for this purpose is considered here in detail, based on an extension of the transport model to account for the effect of the inclusion of functional additives in NCPEMs. The results also point to the reason that Nafion is an excellent PEM, namely the hydrophobic nature of its backbone that induces water away from surface into pore bulk where most of the proton diffusion occurs. This chapter is co-authored with Dr. Pyoungho Choi and is under review in J. Polymer Science: Part B: Polymer Physics.

3.1 Introduction

Extensive research efforts are being made worldwide to find new proton conducting materials for proton-exchange membrane (PEM) fuel cell applications because the main obstacles to commercialization of PEM fuel cells are mostly related to the proton

conducting materials, typically solid polymer electrolytes such as perfluorosulfonic acid membranes [1-3] They are expensive, mechanically unfavorable at high temperature, and conductive only when soaked in water, which limits fuel cell operating temperature to 100°C, which in turn results in low fuel cell performance due to low electrode kinetics and less CO tolerance. The operation of fuel cells at high temperature provides many advantages [4-5] such as improved kinetics at the surface of electrode, which is especially important in methanol and CO-containing reformate feeds, fast transport of protons across PEM, efficient heat and water managements, and also opening a new possibility of integrating fuel cells with methanol reformer, which can result in compact fuel cell systems. Thus, the development of stable membranes at high temperature is an active area of research in fuel cells.

The so-called "higher temperature membranes" can be developed via the modification of polymer (host membrane) with hygroscopic oxides such as SiO_2 and TiO_2 to increase water uptake, or inorganic solid acids such as ZrO_2/SO_4^{2-} to increase the water uptake as well as the concentration of acid sites, or inorganic proton conductor such as heteropoly acids to further enhance proton conductivity using the inorganic-assisted proton transport together with the high water uptake and high acid concentrations in the membrane. Some examples of polymer/inorganic nanocomposite membranes are Nafion/SiO_2, Nafion/Al_2O_3, Nafion/TiO_2, Nafion/ZrO_2, Nafion/ZrP, Nafion/PTA, Nafion/HPA, SPEK/ZrO_2, SPEEK/ZrP, SPEK/(ZrO_2/PTA), and PBI/(SiWA+SiO_2),[6-17] etc. These membranes can be prepared by casting a bulk mixture of powder or colloidal state of inorganics with a polymer solution, or *in-situ* formation in a polymer membrane. The size and dispersion of solid particles are of special importance in both methods. The *in-situ* method is based on sol-gel reactions in the membrane and the formations of nanometer sized particles in host membrane are claimed. These sol-gel prepared nanocomposite membranes are Nafion/ZrO_2, Nafion/SiO_2, and Nafion/TiO_2 [18-20] etc. The nanocomposite membranes show a much higher water uptake, reduced methanol crossover, improved mechanical and thermal stabilities at high temperature, and improved fuel cell performance [8,11,21] although the reason for the performance enhancement was not elucidated and the long-term stability of these membranes is still in question. In spite of their substantial increase in the amount of water uptake and better fuel cell performance at high temperature compared

with unmodified membrane, the improved proton conductivity of the nanocomposite membranes has not been yet proven and is a subject of current debate. For example, Miyake *et al*.[6] reported that conductivities of sol-gel prepared Nafion/SiO_2 nanocomposite membranes were 0.185 S/cm, 0.16 S/cm, and 0.112 S/cm for 4-5%, 10-12 %, and 16-17 % loadings of SiO_2, respectively, while that of Nafion was 0.21 S/cm at the same condition of 120°C and 78 % relative humidity environments. On the other hand, Arico *et al*.[7] reported higher proton conductivity of inorganic acid doped-nanocomposite membranes such as Nafion/SiO_2, Nafion/(PWA+SiO_2), and Nafion/ZrO_2 over all the temperature ranges of experiment.

Major issues in nanocomposite-PEMs are the compatibility of PEM with the solid acids, interaction between the inorganic elements with the polymer backbone and its acid sites, uniform dispersion, and the effect of the inorganics on water sorption, including the fraction of bound versus free water, and on proton transport. The size, propensity for water uptake, the acid site density, and acid strength are the key properties of the functional additives that affect the proton conductivity of composite-PEMs. The amount and distribution (or dispersion) of the functional additives should be optimized to achieve highest proton conductivity of composite-PEMs as well as highest mechanical/thermal stability.

The discussion above is, however, qualitative. It is clearly necessary to understand at a more basic level the effect of the properties and parameters on the water sorption and transport of protons in nanocomposite-PEMs. In this paper, we focus on the rational design of nanocomposite PEMs based on a more fundamental understanding of the effect of its sorptive, mechanical, and transport properties. In order to accomplish this, however, it is necessary to first develop a comprehensive theoretical framework for sorption and transport in conventional PEMs such as Nafion, which has so far been lacking in the literature despite two or more decades of intensive investigation into its structure and properties.

3.2 Sorption in Nafion

Here the water sorption in Nafion is described [22]. As water is gradually sorbed, it initially aids in the dissociation of the acid functional groups followed by a solvation of

the formed hydronium ions (Figure 3.1). It is, thus, assumed in the model that the solvent molecules per acid site, λ_i, are of two types, i.e., those that strongly (or, chemically) interact with the acid sites, λ_i^C, i.e., molecules in the immediate hydration sheath, and those that are free, λ_i^F. An alternate way of classifying these molecules is freezing (free) versus nonfreezing (bound) water molecules. Figure 3.2a shows the free water and bound water molecules. Thus, the total number of solvent molecules per acid site [22]

$$\lambda_i = \lambda_i^C + \lambda_i^F \tag{3.1}$$

For equilibrium between the membrane (*M*) and the fluid phases, the chemical potential of solvent *i* is equal, i.e., $\mu_{i,M}^F = \mu_i$. With the assumption that the chemical potential of *i* within the membrane $\mu_{i,M}^F$ is also influenced by the swelling pressure Π_S within the membrane exerted due to the stretching of the polymer chains as a result of solvent ingress, this provides

$$\ln \frac{a_{i,M}^F}{a_i} = -\left(\frac{\overline{V}_i}{RT}\right)\Pi_S \tag{3.2}$$

where a_i is the activity, or RH, of the solvent in the fluid phase outside the membrane. When the sorption is from vapor, the swelling includes pressure terms due to stretching of polymer matrix Π_M as well as Π_σ, i.e.,

$$\Pi_S = \Pi_M + \Pi_\sigma \tag{3.3}$$

where the pressure exerted by the curved vapor-liquid interface in a pore of radius r_p (Figure 3.2b) is given by the equation of Young and Laplace [22]

$$\Pi_\sigma = -\frac{2\sigma\cos\theta}{r_p} \tag{3.4}$$

where σ is vapor-liquid surface tension, θ is the contact angle, and the pore radius

$$r_p = 2\,\varepsilon_i / S \tag{3.5}$$

where S is specific surface area (m^2/cm^3). Further, ε_i is solvent pore volume fraction

$$\varepsilon_i = \lambda_i / (\lambda_i + r) \tag{3.6}$$

where r is the ratio of partial molar volume of polymer membrane, $r = \overline{V}_M / \overline{V}_i$.

For membrane pressure Π_M, Freger's model for microscopically phase-separated swollen polymers is adopted [23]

$$\Pi_M = (2G/3)(\Phi_M{}^{1/3} - \Phi_M{}^{7/3}) \tag{3.7}$$

where Φ_M is the volume fraction of polymer, $\Phi_M = r/(\lambda_i + r)$, and G is the shear modulus of polymer, related to Young's modulus of elasticity by

$$E = 2(1+\upsilon)G \tag{3.8}$$

where υ is Poisson's ratio, assumed here as 0.5.

The activity of free solvent in the membrane phase $a_{i,M}^F$ is assumed to be given by the statistical mechanical Flory-Huggins theory derived on the basis of a quasi-crystalline lattice [22]

$$\ln a_{i,M}^F = \ln \varepsilon_i^F + (1-1/r)(1-\varepsilon_i^F) + \chi(1-\varepsilon_i^F)^2 \tag{3.9}$$

where ε_i^F is solvent pore volume fraction of the free solvent, $\varepsilon_i^F = \lambda_i^F/(\lambda_i^F + r)$, and χ is the Flory-Huggins polymer-solvent interaction parameter. The first two terms on the right hand side of Eq. 3.9 represent the configurational (entropic) contributions, while the third represents (enthalpic) interaction contribution to mixing. The interaction parameter χ depends upon nature of the polymer backbone and the solvent, and is usually fitted. Alternately, this may be estimated from molecular modeling.

The number of strongly bound solvent molecules per acid site, λ_i^C, result from the condition of chemical equilibrium, $\Sigma \nu_{\rho i}\mu_i = 0$, finally resulting in[34]

$$\lambda_i^C = \lambda_{i,m}\left(\frac{K_1 a_i}{1-a_i}\right)\left\{\frac{1-(v+1)(a_i)^v + v(a_i)^{v+1}}{1+(K_1-1)a_i - K_1(a_i)^{v+1}}\right\} \tag{3.10}$$

where v is the number of equilibrium steps, and K_1 is the equilibrium constant of the first step (acid dissociation constant).

Combining the above relations, thus, sorption of water in Nafion can be calculated by the following implicit expression for λ_i versus fluid phase activity a_i

$$\ln\left(\frac{\lambda_i-\lambda_i^C}{\lambda_i+r}\right)+\left(1-\frac{1}{r}\right)\left(\frac{\lambda_i^C+r}{\lambda_i+r}\right)+\chi\left(\frac{\lambda_i^C+r}{\lambda_i+r}\right)^2-\ln a_i=$$
$$-\frac{\overline{V}_i}{RT}\left\{\left[\frac{2}{3}G\left[\left(\frac{r}{\lambda_i+r}\right)^{1/3}-\left(\frac{r}{\lambda_i+r}\right)^{7/3}\right]-S\sigma\cos\theta\left(1+\frac{r}{\lambda_i}\right)\right]\right\} \quad (3.11)$$

where λ_i^C in terms of activity a_i is provided by Eq. 3.10.

The model above provides a very good fit to the available experimental data from the literature as shown in Figure 3.3, with the Flory-Huggins parameter χ as the only fitted parameter. Table 3.1 lists parameters values employed in the model. The interaction parameter varies with the free water in Nafion and be fitted using $\chi = -44.5(\varepsilon_i^F)^3 + 42.5(\varepsilon_i^F)^2 - 13.1(\varepsilon_i^F) + 2.2$, reflecting that the free water molecules face different environments in polymer matrix with increasing water imbibitions in Nafion.

The Young's modulus of H^+-Nafion used in the model was measured utilizing the OEH technique described below and fitted using $E = E_0 \exp(-2.1753\varepsilon_i)$. Based on Π_σ (Eq. 3.4), the model also explains "Schroeder's paradox,"i.e., $\lambda_{i,L}^{sat}$ = 22 for sorption from liquid water, while $\lambda_{i,V}^{sat}$ = 14 for saturated vapor, both with a_i = 1.

3.3 Theoretical PEM Design for Improved Sorption

The above approach will be further developed to provide a theoretical framework for rational PEM design, e.g., by investigating the effect of the model variables K_1 (acid strength), EW (as described in the model by the ratio *r*), χ (the interaction energy between polymer and water), and *E* (membrane elasticity) on water uptake. Thus, the water uptake is predicted to increase, as expected, for polymers having low E_0. However, more water uptake, although desirable for low RH operation, does not necessarily bode well for the membrane, as it can compromise both the mechanical strength of the membrane and the conductivity.

In order to demonstrate the use of the sorption model described above for design purposes, the effects of the polymer variables K_1 (acid strength) and E (membrane elasticity) on the amounts of water uptake are analyzed as shown in Figures 3.4 and 3.5,

respectively. As the dissociation constant increases, *i.e.*, as *pK* decreases, the water uptake increases initially and reaches $\lambda_i = 13.9$ at $K_1 = 10^2$ and then no further increase in water uptake is predicted. Thus, there appears to be a limit to the acid strength of acid sites, beyond which the water uptake is not affected by it. The effect of Young's modulus of the polymer in the dry state E_0 on the water uptake varies with the polymer type and the temperature. As shown in Figure 3.5, the water uptake increases as expected for polymers having low E_0. However, this must be balanced by other considerations such as mechanical durability and strength of a membrane in an operating fuel cell. In summary, the water uptake of PEMs increases with the activity of the functional group (K_1) up to certain extent, low Young's modulus of polymer elasticity (E), and low equivalent weight (*EW*) of polymer. Although high water uptake is desirable for high proton conductivity in general, too high a water uptake could lead to an overly swollen state and eventual destruction of the membrane. Therefore, an optimal level of water uptake is needed to maintain the stability of the membrane.

3.4 Experiments

Membrane preparation – A Nafion/(ZrO_2/SO_4^{2-}) nanocomposite membrane was prepared via *in-situ* sol-gel synthesis developed by Watanabe *et al*.[9] Nafion 112 serves as a template that directs the morphology and particle size of the oxide in the PEM matrix. As received Nafion was purified by boiling in pure water at 60-70 °C for 30 minutes, treated in 3 wt. % H_2O_2 solution at 60-70 °C for 30 minutes, and washed with deionized water at 60-70 °C for 30 minutes. It was then converted to Na^+ form by heating in 1 M NaOH solution at 60 °C for 30 minutes and washed with deionized water. The Na^+ form of Nafion was soaked in Zr (OCH $(CH_3)_2)_4$ ZrP/2-propanol solution at 25 °C for 24 hours. The membrane was then removed, blotted, and placed 2-propanol/H_2O solution for 2 hours at 80°C. After the hydrolysis and condensation reactions, the membrane was removed and vacuum dried thoroughly at 25 °C for 24 hours and then at 110 °C for 2 hours. The membrane is boiled in 1 M H_2SO_4 solution at 60 °C for 1 hour to sulfate the ZrO_2 nanoparticles and rinsed in water.

Water uptake and proton conductivity measurements – The experimental details of water uptake and proton conductivity are provided elsewhere [10].

3.5 Transport of Protons

Diffusion of Protons in Nafion

Here, a comprehensive phenomenological framework for proton transport in PEMs, which accurately describes conductivity at various hydration levels in Nafion by incorporating water uptake and the various proton transport mechanisms is described. Figure 3.6 shows the various proton transport mechanisms along with an electrical analog. These include: 1) proton hopping along pore surface, i.e., surface diffusion, in an interfacial zone of roughly 3-5 Å for which the dielectric constant is substantially lower than that in the bulk, 2) Grotthuss diffusion (or structural diffusion) in pore bulk, as well as 3) ordinary *en masse* diffusion (or vehicular mechanism) of hydronium ions. In the vehicular mechanism, proton rides along with the diffusing H_2O (or vehicle) as H_3O^+. In fact, it also takes along strongly bound water molecules in the first hydration shell, i.e., electroosmotic drag. On the other hand, in Grotthuss mechanism, the proton simply hops from one solvent to the adjacent one, without *en masse* diffusion or electroosmosis [23].

Thus, the proton conductivity in a pore, σ_p, can be written as $\sigma_p = \sigma_{H^+}^{\Sigma} + \sigma_{H^+}^{G} + \sigma_{H^+}^{E}$, which, respectively, are the contributions from the surface, Grotthuss, and *en masse* transport mechanisms. In turn, σ can be written in terms of diffusion coefficients using the Nernst-Einstein relation $\sigma_{H^+}^{\alpha} = (F^2/RT) D_{H^+}^{\alpha} C_{H^+}^{\alpha}$. Thus, overall proton conductivity in PEM

$$\sigma_{H^+} = \frac{\varepsilon_i}{\tau}\left[\frac{F^2}{RT}\left(D_{H^+}^{\Sigma} C_{H^+}^{\Sigma} + D_{H^+}^{G} C_{H^+} + D_{H^+}^{E} C_{H^+}\right)\right] \tag{3.12}$$

along with

$$\frac{1}{D_{H^+}^{E}} = \frac{x_w}{D_{H^+}^{W}}\left(1 + \frac{1-x_w}{x_w}\frac{D_{H^+}^{W}}{D_{H^+}^{M}}\right) \approx \frac{1+\delta}{D_{H^+}^{W}} \tag{3.13}$$

where x_w is the mole fraction of water in the membrane phase, and δ is the ratio of diffusion (or frictional) coefficients of hydronium ion with water, $D_{H^+}^{M}$ and that with the

polymer matrix, $D_{H^+}^{W}$. Therefore, the measured proton conductivity of nanocomposite-PEMs is the result of weighted average of the surface and bulk diffusion coefficients ($D_{H^+}^{\Sigma}$, $D_{H^+}^{G}$, and $D_{H^+}^{E}$) and the concentrations $C_{H^+}^{\Sigma}$ and C_{H^+} of protons participating in surface and bulk diffusion, respectively, along with the nanostructure (ε_i and τ) of PEM.

The tortuosity factor τ, of course, varies with the water content ε_i in Nafion. While there are several alternate models for the tortuosity factor, here we adopt Preger's model already used in Nafion

$$\tau = \frac{2(1-\varepsilon_i) + 2\varepsilon_i \ln \varepsilon_i - 0.5\varepsilon_i (\ln \varepsilon_i)^2}{\varepsilon_i (1-\varepsilon_i) + \varepsilon_i^2 \ln \varepsilon_i} \tag{3.14}$$

The diffusion coefficients in Eq. (3.9) are obtained based on a random walk statistical mechanical framework that connects the molecular details of proton transfer to the diffusion coefficients

$$D_{H^+}^{\alpha} = \frac{l_\alpha^2}{\kappa \tau_D^{\alpha}} \tag{3.15}$$

where κ is dependent upon the dimensionality of random-walk (κ = 2, 4, or 6 for a one-, two-, or three-dimensional walk, respectively), l_α is the mean step distance, and τ_D^{α} is the mean time between successive steps.

Surface Diffusion

For the two dimensional surface diffusion, κ_Σ = 4, and the hopping time τ_D^{Σ} can be written as

$$\tau_D^{\Sigma} = \frac{h}{k_B T} \exp\left(\frac{\Delta G_{\Sigma}^{e,0}}{k_B T}\right) \tag{3.16}$$

where h is the Planck constant and k_B is the Boltzmann constant. Based on the further assumption that the Coulombic interaction energy between the negatively charged fixed sulfonic ion and the positively charged hydronium ion represents the main energy barrier $\Delta G_{\Sigma}^{e,0}$

$$\Delta G_{\Sigma}^{e,0} \approx \frac{(q_{e^-})^2}{4\pi\varepsilon_0\varepsilon_r}\left[\frac{l_{\Sigma}}{(R_f + R_i + l_{\Sigma})(R_f + R_i)}\right] \tag{3.17}$$

where q_{e^-} is the electrostatic charge of an electron (1.602 x 10^{-19} C), R_f is the effective radius of fixed anion groups, R_i is the radius of the hydronium ion, l_{Σ} is the mean step distance for surface diffusion, ε_0 is the permittivity of free space, and ε_r is the relative permittivity of the medium in the surface diffusion region. Thus, the surface diffusion coefficient becomes [23]

$$D_{H^+}^{\Sigma} = \frac{k_B T}{h}\frac{l_{\Sigma}^2}{4}\exp\left[-\frac{(q_{e^-})^2}{4\pi\varepsilon_0\varepsilon_r k_B T}\left\{\frac{l_{\Sigma}}{(R_f + R_i + l_{\Sigma})(R_f + R_i)}\right\}\right] \tag{3.18}$$

Grotthuss Diffusion

The Grotthuss mechanism involves two sequential steps, namely, rotation of a water molecule due to the electric field of the adjacent hydronium ion into a receptive orientation, followed by the transfer of proton to the water molecule, via quantum mechanical tunneling from the hydronium ion. Assuming the rate of rotation of the water molecule, as determined by the hydrodynamic Stokes equation for rotation, to be the rate-determining step and using $\kappa_G = 6$ in Eq. (3.15)

$$D_{H^+}^{G} = \frac{l_G^2 \mu_w (z_{H^+} q_{e^-})}{192\pi^2 \eta(\varepsilon_r\varepsilon_0) R^3 \delta^2} \Bigg/ \left[\ln\left\{\frac{\tan(\theta_I/2)}{\tan(\theta_F/2)}\right\}\right] \tag{3.19}$$

where z_{H^+} is the charge number of a proton, μ_w is the dipole moment of water, δ is the distance between the proton in hydronium ion and proton accepting water molecule of radius R_w, l_G is the hopping distance, η is water viscosity, ε_r is dielectric constant, and θ_I is initial and θ_F the final angle of rotating water molecule. Although Eq. 3.19 is derived based on a simplified molecular hydrodynamics rather than very detail molecular dynamics, it contains the essence of the Grotthuss mechanism and explains abnormal conductivity of protons quite well.

En Masse Diffusion

The diffusion coefficient of hydronium ion through water D_{H+}^{W} is approximated as the self-diffusion coefficient of water, which has been reported as 2.1-2.3 x 10^{-5} cm^2/s at room temperature, or may be obtained by Stokes-Einstein equation, assuming the hydronium ion as a diffusing entity in a continuum of water

$$D_{H^+}^{W} = \frac{k_B T}{6\pi\eta R_i} \tag{3.20}$$

where η is the viscosity of the medium and R_i is the hydrodynamic radius of hydronium ion. As the concept of hydrodynamic radius is rather not clear in the Stokes-Einstein equation, the self-diffusion coefficient of water corresponds the effective water radius R_i = 0.108 nm, smaller than the geometric radius of water molecule R_{H_2O} = 0.143-0.144. The *en masse* diffusion coefficient can also be obtained by subtracting Grotthuss diffusion coefficient from the proton diffusion coefficient in aqueous solution known as 9.31 x 10^{-5} cm^2/s at room temperature.

The Diffusion Coefficient Ratio δ

The parameter δ is estimated as follows

$$\delta = \frac{1}{\lambda_i}\frac{D_{H^+}^{W}}{D_{H^+}^{M}} \approx \frac{\sqrt{2}}{\lambda_i}(r)^{2/3} \tag{3.21}$$

where r is the ratio of partial molar volume of Nafion to that of water. Thus, the ratio δ depends upon the EW and water content in Nafion, λ_i.

We now have predictive relations for all the parameters in Eq. 12, except for $C_{H^+}^{\Sigma}$ and C_{H^+}, which are discussed below.

Distribution of Protons between Surface and Bulk Regions

Some of the dissociated protons remain close to the anion surface sites and participate in surface diffusion, whereas others with a higher degree of hydration breakaway into the pore bulk and participate in bulk diffusion comprising of Grotthuss and

en masse mechanisms. It is assumed that dissociated acid sites with up to two water molecules remain close to the surface and designated as surface water, while those with more than two water molecules move away from the surface into the pore bulk. This is based on the hypothesis that sulfonic acid groups are sufficiently strong acids so that ion pairs $SO_3^- H_3O^+$ or $SO_3^- H_5O_2^+$ are formed. With this assumption the concentration of surface protons [23]

$$C_{H^+}^{\Sigma} = \frac{1}{\lambda_i \overline{V}_i} \frac{K_1 a_i (1-a_i)(1+K_2 a_i)}{(1-a_i)(1+K_1 a_i) + K_1 K_2 a_i^2 (1-a_i^{\nu-1})} \tag{3.22}$$

where K_1 and K_2 are the equilibrium constants for the first and second hydration steps, and the concentration of bulk protons

$$C_{H^+} = \frac{1}{\lambda_i \overline{V}_i} \frac{K_1 K_2 a_i^3 (1-a_i^{\nu-2})}{(1-a_i)(1+K_1 a_i) + K_1 K_2 a_i^2 (1-a_i^{\nu-1})} \tag{3.23}$$

Figure 3.7 shows the conductivity data of Nafion (EW=1100) at room temperature as a function of activity of water vapor along with the model predictions. The parameters used in this prediction are presented in Table 3.2. It is noteworthy that these predictions involve no fitted parameters. Further, it is clear that the Grotthuss diffusion is the dominant mechanism.

Theoretical PEM Design

Now that a theoretical framework exists for sorption and proton transport, we can use it to investigate the effect of various design parameters. As an example, the effect of EW is examined by comparing the proton conductivity predicted by the model with experiments for Nafion of EW in the range of 800-1200 immersed in liquid water. The model estimates the proton conductivity very well over the range of EW. The maximum conductivity of Nafion predicted by the model is in between EW of 900 and 1000, which is also obtained in experimental measurements. For EW less than 900, the proton conductivity decreases because the dilution effect of protons at very low EW overwhelms the increase due to increase of water volume fraction and the corresponding decrease in tortuosity.

In summary, the proton conductivity depends on the porosity ε_i, i.e., the volume fraction of sorbed water, tortuosity τ, proton concentrations in the surface region $C_{H^+}^{\Sigma}$ and in the bulk C_{H^+}, diffusion coefficients for the surface $D_{H^+}^{\Sigma}$, Grotthuss $D_{H^+}^{G}$, and the *en masse* mechanisms $D_{H^+}^{W}$, as well as the ratio δ. These also indicates, thus, the basic design variables that need to be optimized for developing alternative high proton-conducting polymers for fuel cell applications. In general, it is desirable to have PEMs that can sorb more water at a given water vapor activity, but only up to a certain point, when dilution effect on the proton concentration becomes significant. For a given PEM system, the membrane pores becomes larger and less tortuous when it sorbs large amounts of water, which in turn increase the conductivity of protons in the membranes. The distribution of protons between the surface $C_{H^+}^{\Sigma}$ and the pore bulk C_{H^+} is also important and depends upon the acid strength of the functional groups as well as the nature of polymer backbone. Since the Grotthuss diffusion in the pore bulk is the major contributor to the total conductivity, the formation of a high fraction of bulk hydronium ions is needed for the fast transfer of protons through the membrane. This may explain one of the reasons for the success of Nafion of which hydrophobic backbone facilitates the formation of bulk, rather than surface water. However, too high a water uptake in a PEM leads to a dilution of proton concentration and even membrane failure in an operating fuel cell. Especially for direct methanol fuel cell application, high water uptake and swelling is not desirable due to the methanol crossover problem.

3.6 Diffusion of Protons in NCPEMs

The proton transport model described above may be modified to incorporate the effect of the inorganic additives present within the pores of Nafion membrane [25]. Thus, Eq. (3.12) still applies but with modified values of the diffusion coefficients ($D_{H^+}^{\Sigma}$, $D_{H^+}^{G}$, and $D_{H^+}^{E}$) and the concentrations $C_{H^+}^{\Sigma}$ and C_{H^+}. The key effect of these nanoparticles is to provide additional surface functional sites for the adsorption of water, thus enhancing sorbed water as well as the overall surface diffusion. The enhancement of bulk diffusion (Grotthuss and *en masse*) would, however, depend upon whether the fraction of bulk water

and the bulk proton concentrations are increased as a result of the inorganic additives. However, the nanoparticles also provide an additional obstruction to the bulk diffusion mechanisms. Therefore, an increase in the acidity of the NCPEM and in the amount of water sorbed may not necessarily translate into an enhancement of proton conductivity.

Surface Diffusion

The surface diffusion coefficient of protons in a nanocomposite-PEM is written as

$$\frac{1}{D_{H+}^{\Sigma}} = \frac{x_{PEM}^{\Sigma}}{D_{H+,PEM}^{\Sigma}} + \frac{x_{FA}^{\Sigma}}{D_{H+,FA}^{\Sigma}} \tag{3.24}$$

where $D_{H+,PEM}^{\Sigma}$ and $D_{H+,FA}^{\Sigma}$ are the two surface diffusion coefficients of protons via acid groups of PEM, and via acid groups of functional additives (FA), respectively, and x_{PEM}^{Σ} and x_{FA}^{Σ} are the fractions of the acid groups from PEM and functional additives, respectively. The fraction of acid groups can be written in terms of the molar ratio, i.e., $x_{PEM}^{\Sigma} = 1/(1+q)$ and $x_{FA}^{\Sigma} = q/(1+q)$, where q = moles of acid sites of FA/moles of acid site of PEM. The molar ratio of acid sites for *w* gram of functional additives per gram of PEM can be written as

$$q = \frac{6w}{d_P \rho_P} EW_{PEM} C_{H+,FA}^{*} \tag{3.25}$$

where d_p is particle diameter, ρ_p is particle density and $C_{H+,FA}^{*}$ [mol/m^2] is the effective surface site density of acid groups from the functional additive, and EW_{PEM} is the equivalent weight of the PEM. The use of the Einstein-Smoluchowski relation, thus, provides

$$D_{H+}^{\Sigma} = \frac{1+\left(\frac{6w}{d_p\rho_p} EW_{PEM}\right) C_{H+,FA}^{*}}{4} \left(\frac{k_B T}{h}\right) \left[\frac{l_{\Sigma,PEM}^2 \exp\left(\frac{-\Delta G_{\Sigma,PEM}^{e,0}}{k_B T}\right)}{1 + C_{H+,FA}^{*}\left(\frac{6w}{d_p\rho_p} EW_{PEM}\right)\left(\frac{l_{\Sigma,PEM}^2}{l_{\Sigma,FA}^2}\right) \exp\left(\frac{-\Delta G_{\Sigma,PEM}^{e,0} + \Delta G_{\Sigma,FA}^{e,0}}{k_B T}\right)} \right]$$

(2)

where $\Delta G^{e,0}_{\Sigma,PEM}$ and $\Delta G^{e,0}_{\Sigma,FA}$ are the effective Gibbs free energy of activation for the surface diffusion around acid groups of PEM and functional additives, respectively, as given by Eq. (3.17).

Grotthuss Diffusion

The Grotthuss diffusion coefficient in NCPEMs, of course, remains the same and may be calculated as described above in the PEMs section.

En Masse Diffusion

The *en masse* diffusion coefficient of hydronium ion in the medium of water, acid groups of PEM, and acid groups of functional additives is

$$\frac{1}{D^{E}_{H+}} = \frac{x_W}{D^{W}_{H+}}\left(1 + \frac{x_{PEM}}{x_W}\frac{D^{W}_{H+}}{D^{PEM}_{H+}} + \frac{x_{FA}}{x_W}\frac{D^{W}_{H+}}{D^{FA}_{H+}}\right) \tag{3.27}$$

as a diffusing hydronium ion also encounters friction in its collisions with the inorganic nanoparticles. Here x_W, x_M, and x_{FA} denote the fraction of water, PEM, and functional additive, respectively, and D^{W}_{H+}, D^{PEM}_{H+}, and D^{FA}_{H+} denote the Stefan-Maxwell diffusion coefficients of hydronium ion and bulk water, hydronium ion and PEM matrix, and hydronium ion and functional additives, respectively.

The fraction of water in the membrane can be written as $x_W = \lambda_W / (\lambda_W + 1)$, where the solvent loading λ_W is given by

$$\lambda_W = \frac{p(1+w)}{MW_W\left(1/EW_{PEM} + \left(6w/d_p\rho_p\right)C^{*}_{H+,FA}\right)} \tag{3.28}$$

where p is the mass of absorbed per mass of dry nanocomposite-PEM and MW_W is the molecular weight of water. As above, using the analogy between Einstein-Smoluchowski relation and the elementary kinetic theory, the ratios between diffusion coefficients can be calculated as[??] $D^{W}_{H+} / D^{PEM}_{H+} \approx \sqrt{2}\left(r_{PEM/W}\right)^{2/3}$ and $D^{W}_{H+} / D^{FA}_{H+} \approx \sqrt{2}\left(r_{FA/W}\right)^{2/3}$, where $r_{PEM/W}$ and $r_{FA/W}$ are the ratio of partial molar volume of

PEM to that of water, and partial molar volume of functional additive to that of water, respectively. Using these in Eq. 3.27 and from $x_{PEM}/x_W = 1/\lambda_W(1+q)$ and $x_{FA}/x_W = q/\lambda_W(1+q)$, the *en masse* diffusion coefficient of hydronium ion becomes

$$D^E_{H^+} = \left\{ \frac{(\lambda_W + 1)\left(1 + \frac{6w}{d_P\rho_P} EW_{PEM} C^*_{H+,FA}\right)}{\lambda_W\left(1 + \frac{6w}{d_P\rho_P} EW_{PEM} C^*_{H+,FA}\right) + \sqrt{2}(r_{PEM/W})^{2/3} + \sqrt{2}(r_{FA/W})^{2/3} \frac{6w}{d_P\rho_P} EW_{PEM} C^*_{H+,FA}} \right\} D^W_{H+} \quad (3.29)$$

where the diffusion coefficient of hydronium ion through water D^W_{H+} is given by Eq. 3.20.

Proton Concentrations in Surface and Bulk Regions

Some protons in a hydrated nanocomposite-PEM remain close to the acid sites and diffuse the medium via surface diffusion, whereas others break away into the pore bulk and diffuse via bulk diffusion mechanism. It is assumed that up to two water molecules adsorbed per acid site remain close to the surface, designated as surface water, while those with more than two water molecules move away from the surface to the pore bulk. The total concentration of acid sites is calculated from $C_{H^+,0} = 1/\lambda_W \overline{V}_W$, and the concentration of surface protons $C^{\Sigma}_{H^+} \approx C_{H^+,0}(\theta_1 + \theta_2)$, where θ_i denotes the fraction of acid sites with i bound water molecule. The total surface concentration is $C^{\Sigma}_{H+} = C^{\Sigma}_{H+,PEM} + C^{\Sigma}_{H+,FA}$ in which the surface concentration can be written as $C^{\Sigma}_{H+,PEM} = f^{\Sigma}_{PEM} C_{H+,0}$ and $C^{\Sigma}_{H+,FA} = f^{\Sigma}_{FA} C_{H+,0}$, where f^{Σ}_{PEM} and f^{Σ}_{FA} represent the surface fraction of protons near PEM and functional additives, respectively, i.e.,

$$f^{\Sigma}_{PEM} = \frac{d_P\rho_P}{\left(d_P\rho_P + 6wEW_{PEM}C^*_{H+,FA}\right)}\left[\frac{K_{1,PEM}a_w(1-a_w)(1+K_{2,PEM}a_w)}{(1-a_w)(1+K_{1,PEM}a_w) + K_{1,M}K_{2,PEM}a_w^2(1-a_w^{\nu-1})}\right] \quad (3.30)$$

and

$$f_{FA}^{\Sigma} = \frac{6wEW_{PEM}C_{H+,0}^{*}}{\left(d_P\rho_P + 6wEW_{PEM}C_{H+,FA}^{*}\right)}\left[\frac{K_{1,FA}a_w\left(1-a_w\right)\left(1+K_{2,FA}a_w\right)}{\left(1-a_w\right)\left(1+K_{1,FA}a_w\right)+K_{1,FA}K_{2,FA}a_w^2\left(1-a_w^{\nu-1}\right)}\right] \quad (3.31)$$

where $\overline{V}_W$ is partial molar volume of water, ν is the number of equilibrium steps with acid groups, K_i is equilibrium steps between water and acid groups, a_w is the activity of water in surroundings. The bulk proton concentration can be approximated as $C_{H+} \approx C_{H+,0} - C_{H+,PEM}^{\Sigma} - C_{H+,FA}^{\Sigma}$. The fraction of surface proton is high at low water content due to strong interaction between proton and surface water but decreases as the water content increases, while the bulk concentration increases monotonically with water content.

Volume Fraction of Water

The volume fraction of water in the nanocomposite-PEM can be obtained from

$$\varepsilon_i = \frac{\lambda_W\left(1/EW_{PEM} + w/MW_{FA}\right)}{\lambda_W\left(1/EW_{PEM} + w/MW_{FA}\right) + r_{PEM/W}/EW_{PEM} + wr_{FA/W}/MW_{FA}} \quad (3.32)$$

where $r_{PEM/W}$ is the ratio of partial molar volume of membrane to that of water, $r_{FA/W}$ is the ratio of partial molar volume of solid acids to that of water.

3.7 Theoretical Predictions

Theoretical predictions for the proton conductivity of Nafion-ZrO_2 sol-gel membrane as a function of activity of water vapor along with experimental results are shown in Figure 3.8 at two different temperatures. Figure 3.9 shows the structure of sulphated ZrO_2. Table 3.3 and 3.4 has parameters used in the model to predict the conductivity for NCPEMs. When compared with the proton conductivity of Nafion shown in Figure 3.7, it is clear that there is noticeable improvement in conductivity. The proton conductivity of Nafion can be improved by about 10-15 % with the incorporation of ZrO_2/SO_4^{2-} if the model parameters such as particle size and particle distributions are carefully controlled during the preparation procedure.

Parameter	Value	Unit	Comments
$\overline{V}_M$	537	cm^3/mol	partial molar volume of Nafion
$\overline{V}_i$	18	cm^3/mol	partial molar volume of water
S	210	m^2/cm^3	specific pore surface area
K_1	1000	dimensionless	the first ionization constant of sulfuric acid
ν	5	dimensionless	the number of chemical equilibrium steps of reaction
$\lambda_{i,m}$	1.8	dimensionless	monolayer coverage being bound
σ	72.1	mN/m	surface tension of water
θ	98	dimensionless	contact angle of saturated water vapor in Nafion
χ	0.9-2.4	dimensionless	fitted polymer-solvent interaction parameter

Table 3.1 Parameter values employed in the model for the sorption of water in Nafion.

Parameter	Value or Eq.	Unit	Comment
$C_{H^+}^{\Sigma}$	Eq. 22	mol/cm^3	concentration of protons at the surface
C_{H^+}	Eq. 23	mol/cm^3	concentration of protons in the pore bulk
τ	Eq. 14	dimensionless	tortuosity of Nafion with water content
$D_{H^+}^{\Sigma}$	1.01 x 10^{-7}	cm^2/s	surface diffusion coefficient of proton
$D_{H^+}^{G}$	7.05 x 10^{-5}	cm^2/s	Grotthuss diffusion coefficient of proton
$D_{H^+}^{W}$	2.26 x 10^{-5}	cm^2/s	*en masse* diffusion coefficient of proton

Table 3.2 Parameter values employed in the model for proton conductivity in Nafion at room temperature.

Activity	Nafion (g water/g dry Nafion)		Nafion/(ZrO_2/SO_4^{2-}) (g water/g dry nanocomposite)	
	25°C	90°C	25°C	90°C
0.1	0.0339	0.0344	0.0351	0.0413
0.2	0.0491	0.0488	0.0498	0.0586
0.3	0.0573	0.0499	0.0510	0.0599
0.4	0.0655	0.0614	0.0626	0.0737
0.5	0.0659	0.0749	0.0764	0.0899
0.6	0.0810	0.0875	0.0893	0.1051
0.7	0.0949	0.1127	0.1150	0.1352
0.8	0.1080	0.1309	0.1343	0.1584
0.9	0.1490	0.1710	0.1743	0.2053
1.0	0.2291	0.2701	0.2754	0.3247

Table 3.3 Data for water sorption in Nafion and Nafion/(ZrO_2/SO_4^{2-}) nanocomposite membranes.

Diff. Coef.	Symbols	Values	Units	Comments
$D_{H^+}^{\Sigma}$	EW_M	1100	g/equiv.	equivalent weight of membrane
	MW_{SA}	219.29	g/mol	molecular weight of solid acid
	w	0.03	dimensionless	weight ratio of solid acid to membrane
	d_p	2	nm	the size of solid acid in the membrane
	ρ_p	5.83	g/cm^3	density of zirconium oxide used
	k_B	1.38×10^{-23}	J/K	Boltzmann constant
	h	6.626×10^{-34}	J·sec	Planck constant
	l_{Σ}	0.255	nm	jump length of surface proton
	$R_{f(M)}$	0.254	nm	radius of acid site of membrane
	$R_{f(SA)}$	0.260	nm	radius of acid site of solid acid
	R_{H2O}	0.143	nm	radius of water molecule
	ε_0	8.854×10^{-12}	$C^2/J \cdot m$	permittivity
	$\varepsilon_{r(M)}$	6	dimensionless	relative permittivity of membrane
	$\varepsilon_{r(SA)}$	6	dimensionless	relative permittivity of solid acid
	q_{e^-}	1.602×10^{-19}	C	electronic charge
$D_{H^+}^{G}$	l_G	0.255	nm	proton jump length in Grotthuss mechanism
	τ_D^G	1.5	ps	proton jump time in Grotthuss mechanism
$D_{H^+}^{E}$	λ_W	Equation 9	dimensionless	mol H_2O/mol nanocomposite membrane
	$r_{M/W}$	29.83	dimensionless	partial molar volume ratio of membrane to water
	$r_{SA/W}$	2.06	dimensionless	partial molar volume ratio of solid acid to water

Table 3.4 Parameter values employed in the model at room temperature.

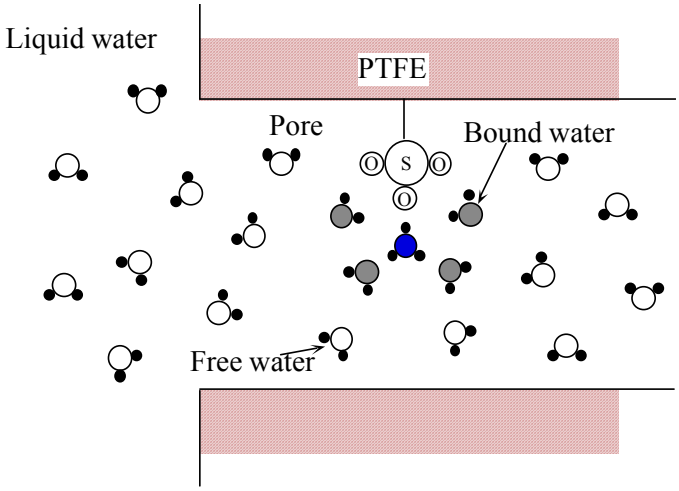

Figure 3.1 Schematic of sorption in pore of Nafion.

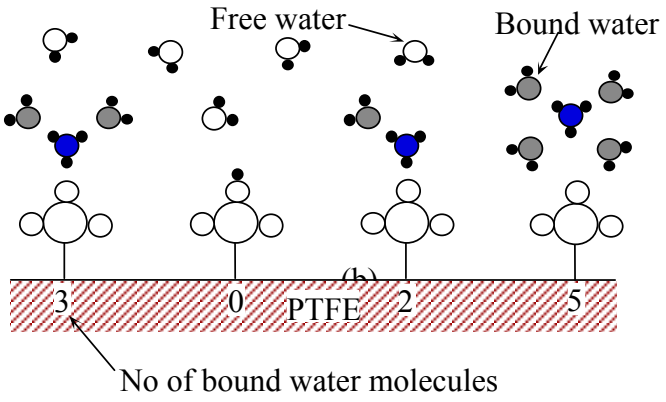

(a)

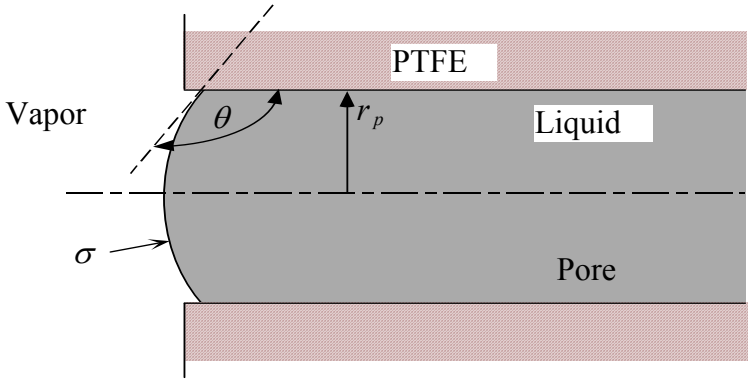

(b)

Figure 3.2 Schematics of sorption in pore of Nafion (a) bound free water molecules, and (b) vapor-liquid interface within a pore.

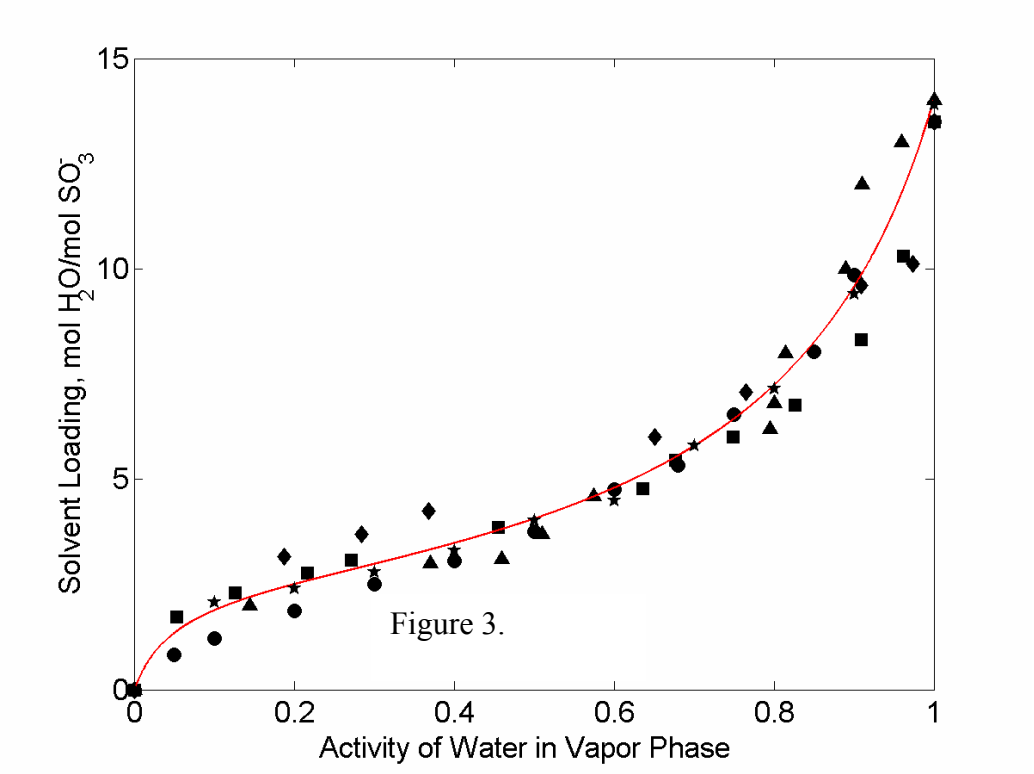

Figure 3.3 The solvent loading vs. activity of water vapor for Nafion (EW=1100).

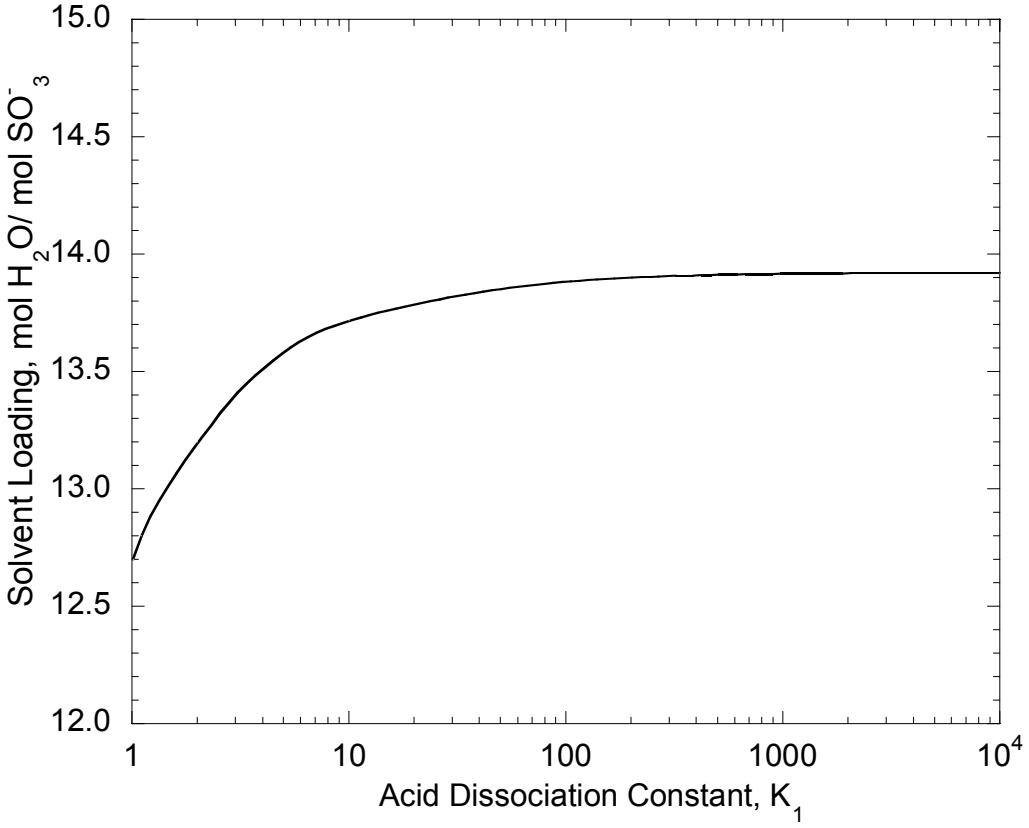

Figure 3.4 The predicted solvent loading with the changes of the dissociation constant.

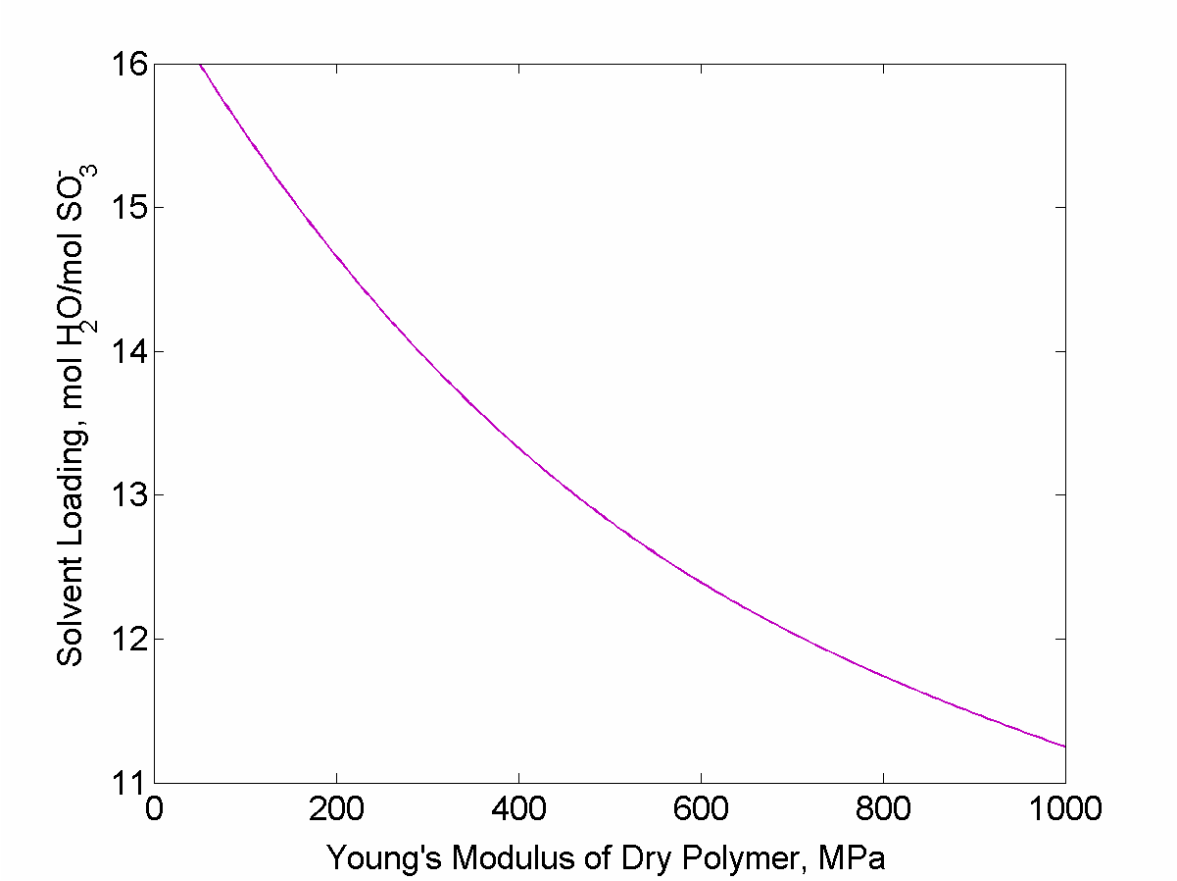

Figure 3.5 The predicted solvent loading with the changes of Young's modulus.

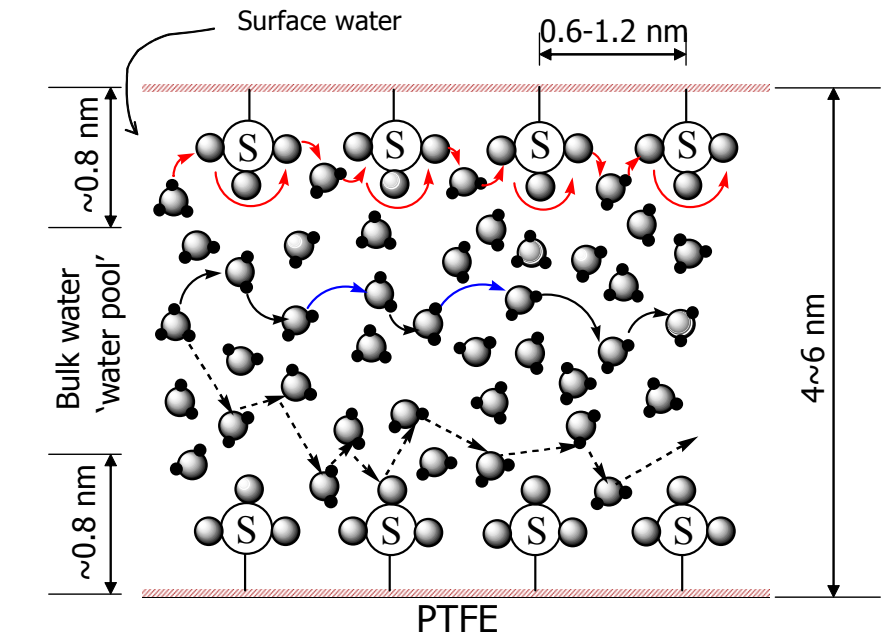

(a)

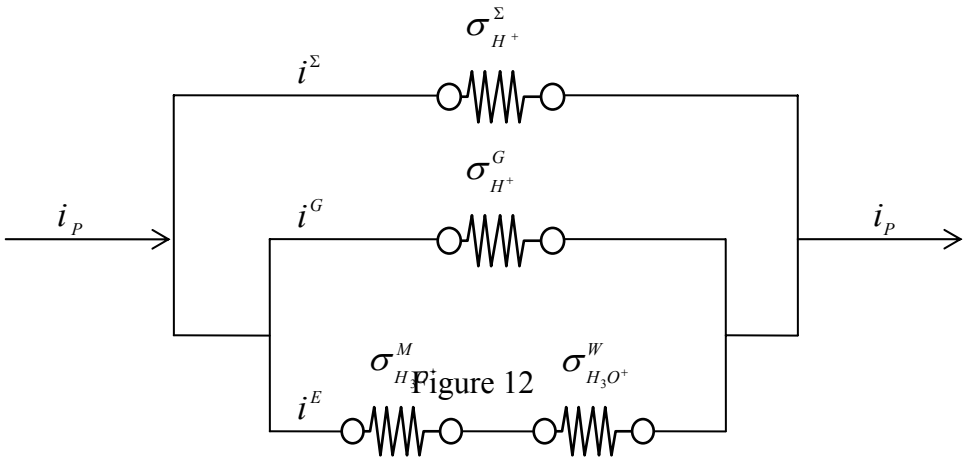

(b)

Figure 3.6 A simplified picture of structure and proton transfer in Nafion in fully hydrated state (a) and electrical analog of the proton transport in Nafion (b).

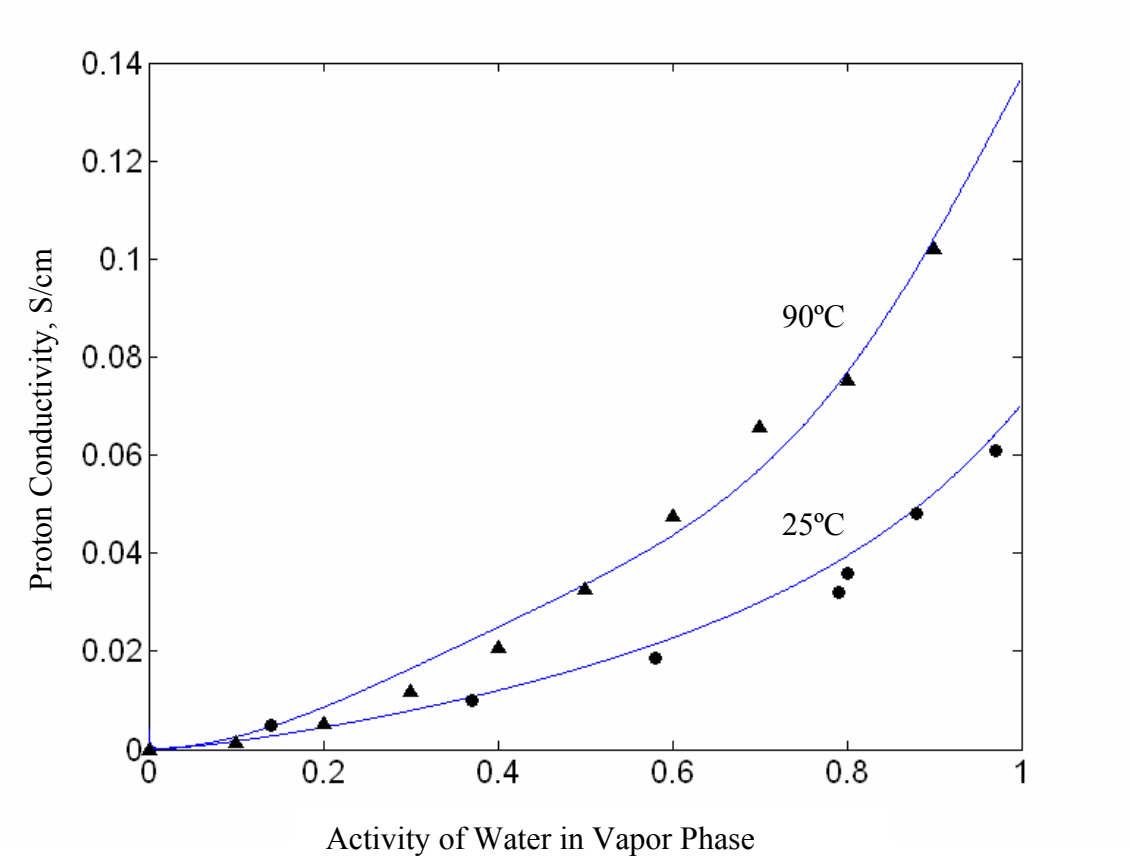

Figure 3.7 Proton conductivity of Nafion at 25° C and 90 °C.

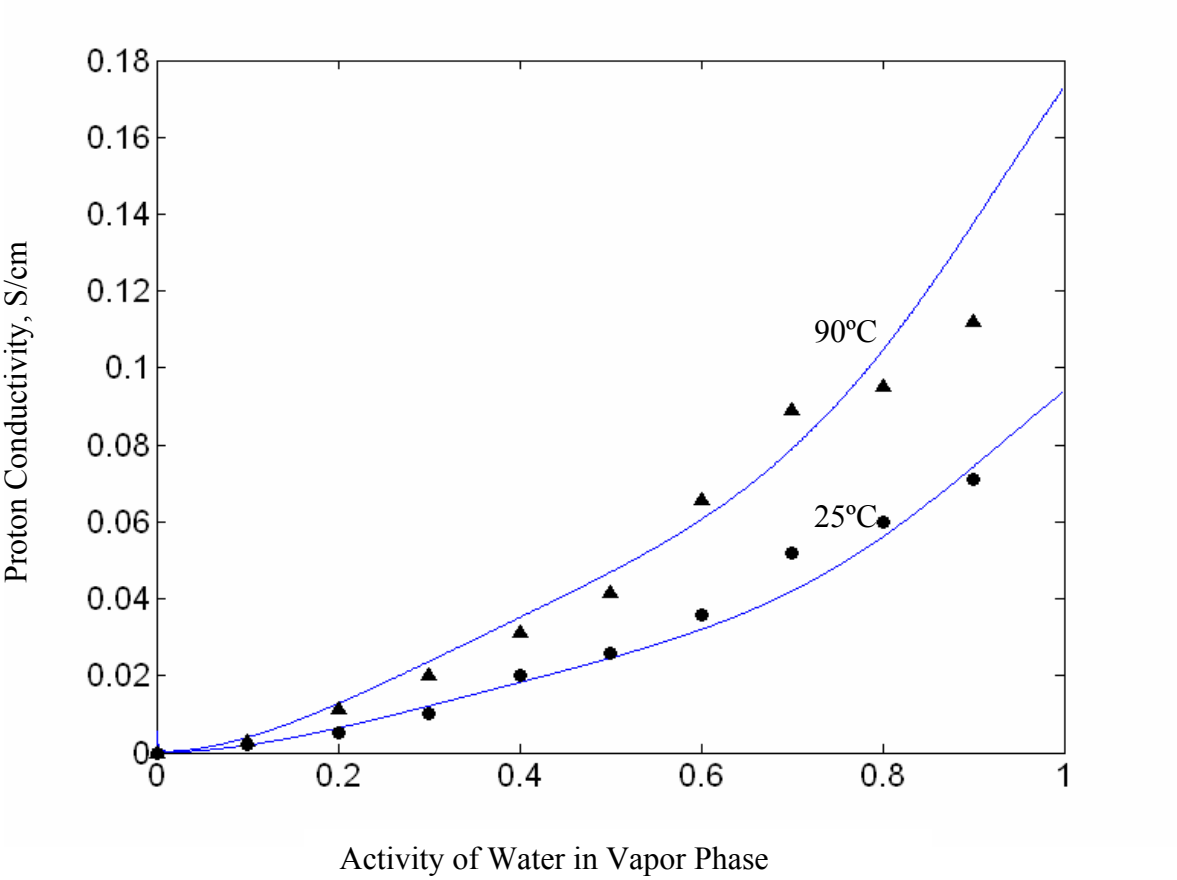

Figure 3.8 Proton conductivity of Nafion-ZrO_2 (3 %) sol gel nanocomposite membrane at 25 ^oC and 90 ^oC.

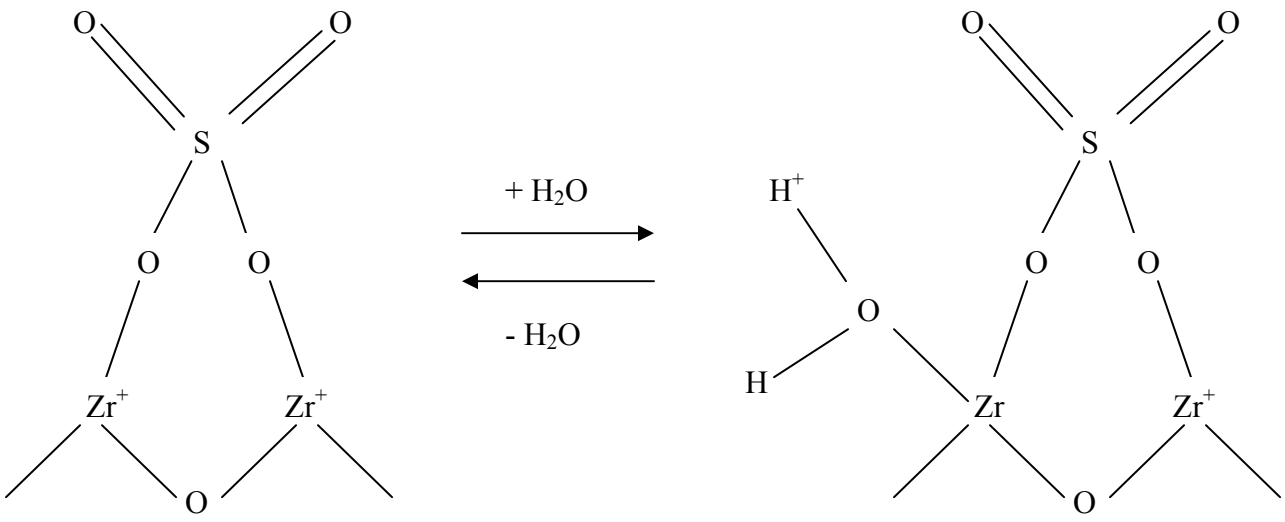

Figure 3.9 Structure of ZrO_2/SO_4^{2-} solid acid.

3.8 Conclusions

A comprehensive proton transport model in Nafion/(ZrO_2/SO_4^{2-}) nanocomposite membrane has been proposed based on the understanding of structural and physicochemical properties of the membranes. The solvent (i.e., water) sorption, the dissociation of protons around the acid sites, and the distribution of protons in the hydrated Nafion/(ZrO_2/SO_4^{2-}) nanocomposites have been taken into consideration prior to the diffusion process. The transport model distinguishes the surface and bulk mechanisms of proton transport in the nanocomposite membrane in which the proton conduction depends on the water content, diffusion coefficients at the surface and bulk regions in the membrane, and concentration and distribution of protons. The surface diffusion of proton, which takes place dominantly under low humidity environments, is slow due to high Coulombic interaction around the acid surface, while the transport of protons in the bulk water is relatively fast and occurs via Grotthuss and *en masse* mechanisms. The sol-gel incorporation of ZrO_2/SO_4^{2-} into Nafion increased the amount of water uptake and provided additional acid sites for proton diffusion, which resulted in higher proton conductivity compared to the host membrane. The transport model developed here offers a theoretical framework for understanding the proton transfer in nanocomposite membranes and should also be helpful in systematically developing high proton-conducting nanocomposite membranes based on the incorporation of inorganic materials into the host membranes.

3.9 References

1. G. Alberti and M. Casciola, *Annu. Rev. Mater. Res.*, **33**, 129 (2003).
2. B. C. H. Steele and A. Heinzel, *Nature*, **414**, 345 (2001).
3. P. Jannasch, *Curr. Opin. Colloid Interf. Sci.* **8,** 96 (2003).
4. Q. Li, R. He, J. O. Jensen, and N. J. Bjerrum, *Chem. Mater.*, **15**, 4896 (2003).
5. C. Yang, P. Costamagna, S. Srinivasan, J. Benziger, and A. B. Bocarsly, *J. Power Sources,* **103**, 1 (2001).
6. N. Miyake, J. S. Wainright, and R. F. Savinell, *J. Electrochem. Soc.*, **148**, A905 (2001).
7. A. S. Arico, V. Baglio, A. Di Blasi, and V. Antonucci, *Electrochem. Comm.*, **5**, 862 (2003).
8. A. S. Arico, V. Baglio, A. Di Blasi, P. Creti, P. L. Antonucci, and V. Antonucci, *Solid State Ionics*, **161**, 251 (2003).
9. H. Uchida, Y. Ueno, H. Hagihara, and M. Watanabe, *J. Electrochem. Soc.*, **150**, A57 (2003).
10. T. M. Thampan, N. H. Jalani, P. Choi, and R. Datta, *J. Electrochem. Soc.*, **152**, A316 (2003).
11. P. Costamagna, C. Yang, A. B. Bocarsly, and S. Srinivasan, *Electrochim. Acta*, **47**, 1023 (2002).
12. S. Malhotra and R. Datta, *J. Electrochem. Soc.*, **144**, L23 (1997).
13. V. Ramani, H. R. Kunz, and J. M. Fenton, *J. Membr. Sci.,* **232**, 31 (2004).
14. S. P. Nunes, B. Ruffmann, E. Rikowski, S. Vetter, and K. Richau, *J. Membr. Sci.*, **203**, 215 (2002).
15. B. Bonnet, D. J. Jones, J. Roziere, L. Tchicaya, G. Alberti, M. Casciola, L. Massinelli, B. Bauer, A. Peraio, and E. Ramunni, *J. New. Mater. Electrochem. Syst.*, **3**, 87 (2000).
16. M. L. Ponce, L. Prado, B. Ruffmann, K. Richau, R. Mohr, and S. P. Nunes, *J. Membr. Sci.*, **217**, 5 (2003).
17. P. Staiti, *Materials Letters*, **47**, 241 (2001).
18. W. Apichatachutapan, R. B. Moore, and K. A. Mauritz, *J. Appl. Polym. Sci.*, **62**, 417 (1996).

19. Q. Deng, R. B. Moore, and K. A. Mauritz, *J. Appl. Polym. Sci.*, **68**, 747 (1998).

20. P. Liu, J. Bandara, Y. Lin, D. Elgin, L. F. Allard, and Y. P. Sun, *Langmuir*, **18**, 10389 (2002).

21. K. T. Adjemian, S. J. Lee, S. Srinivasan, J. Benziger, and A. B. Bocarsly, *J. Electrochem. Soc.*, **149**, A256 (2002).

22. P. Choi, N. H. Jalani, and R. Datta, *J. Electrochem. Soc.*, **152**, E84 (2005).

23. P. Choi, N. H. Jalani, and R. Datta, *J. Electrochem. Soc.*, **152**, E123 (2005).

25. Choi, P.; Jalani, N. H.; Datta, R. J Electrochem Soc, **152**, A1548 (2005).

Chapter 4

Synthesis and Characterization of Nafion - MO_2 (M = Zr, Si, Ti) Nanocomposite Membranes for Higher Temperature PEM Fuel Cells

In this chapter Nafion-MO_2 (M = Zr, Si, Ti) nanocomposite membranes were synthesized with the goal of increasing its the proton conductivity and water retention at higher temperatures and lower relative humidities (120 ^oC, 40 % RHs) as well as to improve the thermo-mechanical properties. The sol gel approach was utilized to incorporate inorganic oxide nanoparticles within the pores of Nafion membrane. The membranes synthesized by this approach were completely transparent and homogenous as compared to membranes prepared by alternate casting methods which are cloudy due to the larger particle size. At 90 ^oC and 120 ^oC, all Nafion- MO_2 sol-gel nanocomposites exhibited higher water sorption than Nafion membrane. However, at 90 ^oC and 120 ^oC, the conductivity was enhanced in only Nafion- ZrO_2 sol-gel nanocomposite with a 10 % enhancement at 40 % RH over Nafion. This can be attributed to the increase in acidity of zirconia based sol gel membranes shown by a decrease in equivalent weight in comparison to other nanocomposites based on Ti and Si. In addition, the TGA and DMA analyses showed improvement in degradation and glass transition temperature for nanocomposite membranes over Nafion. This chapter is published in Electrochimica Acta, 51(3) 553-560 (2005).

4.1 Introduction

In recent years, there have been extensive research efforts in the development of newer proton conducting membranes for higher temperature proton-exchange membrane (PEM) fuel cell [1-2]. Nafion, the conventional proton conducting polymer electrolyte membrane is expensive, mechanically unstable at temperatures above 100 ^oC, and conductive only when soaked in water, which limits fuel cell operating temperatures to 80 ^oC, which in turn results in lower fuel cell performance due to slower electrode kinetics and low CO

tolerance [3]. The operation of fuel cells at higher temperature possesses many systems advantages such as smaller heat exchangers, and easier integration with reformers. Thus, the development of membranes which are mechanically and chemically stable at higher temperatures (above 100 ^{o}C) is an active area of research for producing economical fuel cells.

There efforts to develop these high temperature membranes include modification of the conventional host polymers, e.g., via incorporation of various hygroscopic inorganic nanosized particles or by developing alternate new polymer systems [4-17]. Malhotra and Datta first proposed the incorporation of inorganic solid acids in the conventional polymeric ion-exchange membranes such as Nafion with the objective of serving the dual functions of improving water retention as well as providing additional acidic sites [4]. Thus, they doped Nafion membranes with heteropolyacids, e.g., phosphotungstic acid (PTA), and were able to show high cell performance at lower RH and elevated temperature (120^{o}C). Unfortunately, due to high water solubility, the PTA eventually leaches out from the PEM. Fenton *et al.* have more recently shown that Nafion-PTA membranes can be stabilized by heat treatment and the leaching of PTA can be reduced [5]. Nafion can also be modified by the incorporation of hygroscopic oxides such as SiO_2 and TiO_2 to increase water uptake [6], or inorganic solid acids such as ZrO_2/SO_4^{2-} [18].

Watanabe *et al*. modified Nafion PEMs by the incorporation of nano-sized particles of SiO_2, TiO_2, Pt, Pt-SiO_2 and Pt-TiO_2 to decrease the humidification requirements of PEMs [7].When operated at 80^{o}C under low humidification PEMFC, the modified PEMs showed lower resistance than Nafion. This improvement was attributed to the suppression of H_2 cross over by *in situ* Pt along with the subsequent sorption of the water produced on the incorporated oxides.

Adjemian *et al*. introduced nanosized SiO_2 into Nafion pores and tested various thickness and EW membranes [8]. The benefit of these nanocomposite membranes appears to be in stabler operation versus conventional Nafion at a cell temperature of 130 ^{o}C due to higher rigidity, when both were tested under fully humidified conditions. The investigators note that the unmodified PEMs showed thermal degradation, while the SiO_2 modified PEMs did not show such damage. Costamagna *et al*. incorporated zirconium phosphate into a Nafion 115 membrane and the results obtained were similar [11]. Zaidi *et al*. embedded

heteropolyacids to different extents in sulfonated polyether ether ketone (S-PEEK) [12]. The highest performing nanocomposite was a tungstophosphoric acid doped, 80 % sulfonated PEEK PEM. It showed conductivity similar to that of Nafion. Adjemian *et al* have also synthesized Nafion PEMs containing silicon oxide, as well as zirconium phosphate particles [14]. They found that silicon oxide modified membranes exhibited better robustness and water retention and better performance. Similarly, Staiti *et al*. have also investigated Nafion-silica membranes doped with phosphotungstic acid and silicotungstic acid for direct methanol fuel cell operation at 145 ^{o}C [15]. Tazi and Savadogo have prepared membranes based on Nafion, silicotungstic acid and thiophene [16]. These modified membrane had better water retention and thermomechanical properties. On the other hand, Arico *et al*. reported higher proton conductivity of inorganic acid doped composite membranes such as Nafion /SiO_2, and Nafion / (PWA+SiO_2) over all the temperature range of experiments [17]. Other examples of polymer/inorganic composite membranes include Nafion /Al_2O_3, Nafion /ZrO_2, Nafion /ZrP, Nafion /PTA, Nafion /Zeolite, SPEK/ZrO_2, SPEEK/ZrP, SPEK/(ZrO_2/PTA), and PBI/(SiWA+SiO_2), etc.

Based on this work accomplished on higher temperature membranes, it can be concluded that the approach of synthesizing nanocomposite membranes either by casting a bulk mixture of powder or colloidal state of inorganics with a polymer solution, or *in-situ* formation of inorganic particles utilizing the membrane as template [13], is very promising. The advantage of in-*situ* method is that the particle size can be controlled by the concentration of precursors because the size and dispersion of these solid particles are of utmost importance in final performance of fuel cells. Mostly, the *in-situ* methods are based on sol-gel reactions between the organo metallic compound as the precursor and water within the pores of the membrane. Though these membranes shows better water sorption and proton conduction properties, better mechanical properties with higher fuel cell performance and long term stability are yet to be established.

In our earlier work, we have shown the potential of preparing nanocomposite membranes using sol gel chemistry with improved hydration as well as conductivity at higher temperature and lower RH conditions [18]. In addition, we have developed a theoretical model for proton transport in Nafion and in nanocomposite membranes based on the parallel pore model incorporating various proton transport mechanisms such as surface

proton hopping, Grotthuss diffusion, and traditional *en masse* diffusions [19-20]. This allows an understanding of the contributions from various proton transport mechanism in nanocomposite membranes and the effect of the inorganic additives for designing new PEMs.

In the present work, we synthesized Nafion / ZrO_2, Nafion/ SiO_2 and Nafion/ TiO_2 nanocomposite membranes via *in situ* sol-gel technique and compared with unmodified Nafion in terms of water uptake, proton conductivity at different relative humidity conditions (RHs), fuel cell performance, and ion exchange measurements. These nanocomposite membranes were further characterized using TGA (thermo gravimetric analysis) and DMA (dynamic mechanical analysis) to determine degradation and glass transition temperatures (T_g).

4.2 Experimental

4.2.1 Membrane Preparation

The method of preparation of the ZrO_2, SiO_2 and TiO_2 nanocomposite PEMs was based on the *in situ* sol-gel synthesis methods developed by Mauritz's and coworkers [13]. In this procedure, the host PEM serves as a template that directs the morphology, and particle growth and size of the oxide in the PEM matrix, resulting in nano-sized particles. As received Nafion membranes (Sigma-Aldrich Corp., St. Louis MO) were boiled in 3 wt % H_2O_2 for 1 hour and then rinsed in water. They were then immersed in 1 M NaOH solution and heated for 6 hours to convert the membrane to Na^+ form. This ensures mechanical strength of Nafion membrane for withstanding the subsequent processing steps. Then the membrane was rinsed in DI water at 60 ^oC for 30 minutes [21-22].

The purified Na^+ form membranes were then placed in a vacuum oven and heat treated at 110 ^oC for 12 hours. The membranes were then immersed in 10:1 ethanol/H_2O solution for an hour. The ethanol/H_2O mixture served to further swell the pores of the PEM to maximize the absorption of the precursor solution. The membranes were removed and immersed in 0.5 M 70 wt % Zirconium (IV) propoxide solution (purchased from Aldrich) for 6 hours and then rinsed in acetone in order to remove surface ZrO_2. The membranes were then removed and heated at 110 ^oC in vacuum for 24 hours to complete the

condensation reactions. After this the membranes were boiled in 50 vol % H_2SO_4: H_2O solution for 6 hours for sulfation. This nanocomposite PEM is denoted here as "Nafion-ZrO_2 sol-gel". Using a similar protocol, Titanium (IV) tert-butoxide and Tetraethyl orthosilicate (TEOS) were utilized as the precursors utilized to synthesize "Nafion- TiO_2 sol-gel" and "Nafion- SiO_2 sol-gel" membranes, respectively.

The membranes synthesized by this method were completely transparent and homogenous as compared to membranes prepared by our previous the casting methods [18], which were cloudy due to presence of much larger particles. Figure 2.4 shows scanning electron microscope (Amray Model 1610 Turbo SEM) images for the membranes prepared by both methods. The membrane prepared using the casting method had larger zirconia particles with size ranging in 5-15 μm. On the other hand, the sol gel membranes showed no X-ray scattering. Also the surface of sol gel membranes did not show any deposition of oxides which confirms that the zirconia is present within the pores of Nafion membrane. This provides evidence that these membranes have nano-sized zirconia particles within the pores of the membrane. Similar observations were made for other nanocomposite membranes synthesized using the sol gel method.

4.2.2 Water Uptake Measurements

The tapered element oscillating microbalance (TEOM Series 1500 PMA Reaction Kinetics Analyzer, Rupprecht & Patashnick Co. Inc. Albany NY) was utilized to measure the water uptake of the nanocomposite PEMs as compared to unmodified Nafion membrane [20-21]. The sample mass change in TEOM was measured as the frequency change of the tapered element oscillatory bed as described by us earlier [20]. The RH was controlled by mixing metered flows of a wet (saturated with H_2O) and a dry helium stream.

Calibration was done with a RH meter (FH A646-R, ALMEMO, Ahlborn, Munich, Germany). The membrane was cut into thin strips (1.5 mm by 1.5 mm) and packed carefully along with quartz wool into the oscillating test bed of the TEOM to avoid rattling. The water uptake was measured for all samples at 90 ^{o}C from 0 % to 90 % RH, and at 120 ^{o}C from 0 % RH to 40 % RH. After the sample was loaded, it was exposed to the helium gas having the desired RH, and the real-time mass change was observed to determine when the equilibrium amount of water had been adsorbed onto the membrane. The working principle and data collection procedures are also explained elsewhere [23-24].

4.2.3 Ion-Exchange Capacity Measurements

A 0.2 g sample of the nanocomposite PEM was exchanged with NH_4^+ by immersing the sample in 1 M ammonium acetate for 24 hours and then in ammonium chloride for an additional hour. The PEM was then washed with DI water to remove any excess NH_4^+ ions. To ensure that all excess NH_4^+ had been removed, a drop of 1 M silver nitrate was added to the wash. If NH_4^+ ions were present, a white precipitate would form. The PEM was then stored in 50 ml DI water. Adding 2 ml of 5 M NaOH solution to the sample, caused the subsequent exchange of NH_4^+ with Na^+. Utilizing a calibrated ammonia electrode (Model 95-12 ORION, Boston MA), the amount of NH_4^+ released could be accurately quantified thus providing an accurate measure of the ion-exchange capacity [25].

4.2.4 Ex Situ Conductivity Testing

The conductivity measurements were made with a perturbation voltage of 10 mV in the frequency range 0.01 Hz to 10^6 Hz using a Solartron SI 1260 FRA (Solartron, Hampshire, U.K.). Both real and imaginary components of the impedance were measured and the real *z*-axis intercept was assumed to provide the membrane resistance, and hence, conductivity. A nanocomposite membrane sample was sandwiched between two electrodes each on either side to measure the conductivity, similar to the procedure reported in literature and then placed in humidity controlled chamber [26]. The humidity of the chamber was monitored utilizing a dew point / temperature probe (HMP 238, Vaisala,

Woburn, MA). An air stream was saturated with water by bubbling through a humidifier. This wet stream was heat-traced to the chamber to avoid condensation. The chamber and the humidifier were both heated to 90 ^{o}C and 120 ^{o}C, respectively, to obtain the desired partial pressure of water. The conductivity of the PEM was measured at 90 ^{o}C in the RH range from 10 % to 90 %, while at 120 ^{o}C the RH range was from 10 % to 40 % to simulate dry conditions. These conditions are the same as those utilized for the water uptake measurements.

4.2.5 MEA Testing

The electrodes utilized are commercially available from E-TEK (Somerset, NJ). The type selected was the single-sided ELAT gas-diffusion electrode (20 % Pt-on-C, 0.35~0.4 mg Pt/cm^2). The active layer of electrode was brushed with 5 % Nafion solution (0.6 ~0.8 mg/cm^2 MEA). This electrode was placed on either side of the PEM and the resulting membrane-electrode assembly (MEA) placed in a hot press. The temperature of the hot press was then raised to 130 ^{o}C and a pressure of 272 atm applied for 120 s. The MEA thus prepared was mounted in a 5 cm^2 fuel cell test fixture, obtained from Fuel Cell Technologies (Los Alamos, NM). The cell was fed with humidified H_2 and O_2 supplied at pressure 1 atm utilizing electronic mass flow controllers (MKS Model No. 1179A22CS1BV-S, Andover, MA) and was controlled by the electronic load (Series 890B Fuel Cell Test System, Scribner Associates Inc. Southern Pines, NC). Utilizing software (Fuel Cell Test Software Version 2.0, Scribner Associates, Inc.), the mass flow rate of the feed gas was programmed to stoichiometry dependent flow rates. The load has an inbuilt feature of measuring *in situ* MEA ohmic resistance utilizing the current interruption method. The pressure of the reactant gases was monitored using pressure gauges (Matheson, Model No. 63-5612). The startup procedure involved bringing the humidifier temperature up to a set value of 80 ^{o}C, then increasing the fuel cell to 80 ^{o}C and operating with 1 atm H_2 and O_2 at current controlled mass flow rates. The load was cycled for additional 6 hours and then a constant voltage polarization curve was taken. Thereupon, another 12 hours of break-in period was utilized and then a final polarization curve was obtained as follows. The voltage was set at 0.6 V set for 30 minutes and then data were taken every 6 seconds for 15 minutes. Similar procedure was repeated for other voltage

conditions. After setting the required voltage, data were collected every 6 seconds for 15 minutes at each voltage set-point.

4.2.6 Thermo-mechanical characterization

The morphology of the synthesized nanocomposite membranes was investigated using scanning electron microscope (Amray Model 1610 Turbo SEM).

Thermogravimetry analysis (TGA) of the nanocomposite membranes was accomplished on a TGA TA Instruments 2050 system in a temperature range 25 to 700 ^{o}C at the heating rate of 20 ^{o}C/min. A known mass of sample was placed into the analyzer and was heated at a constant rate so that the entire polymer eventually volatilizes.

Dynamic Mechanical Analysis (DMA) was also employed to determine glass transition temperature for the nanocomposite membranes using Thermal Analysis 2980 DMA in a temperature range 25 to 175 ^{o}C. For viscoelastic materials, like Nafion®, stress consists of elastic and a viscous component. The elastic component or storage modulus, accounts for how the material behaves like an ideal solid and the viscous component or loss modulus, accounts for how the material behaves like an ideal fluid. The phase angle shift between stress and strain is represented by δ, which varies between 0 (100% elastic) and 90 (100% viscous) [29-30]. The glass transition temperature (T_g) of a material can be taken as either the peak of the loss modulus versus temperature curve or the peak of the tan (δ) versus temperature curve. In the present work, *Tg* is obtained from the peak of tan (δ) versus temperature data.

$$\frac{E''}{E'} = \tan(\delta) \tag{4.1}$$

where E' storage modulus (elastic component) and E'' is loss modulus (viscous component) of the material.

4.3. Results and Discussion

4.3.1 Water uptake measurements

Figures 4.1 and 4.2 shows the water uptake measurements for the nanocomposite membranes at 90 and 120 ^{o}C respectively. At both temperatures, all Nafion-MO_2

nanocomposite exhibited better water uptake at a given RH than unmodified Nafion membrane. Nafion-ZrO_2 nanocomposite demonstrated about 33 % and 45 % higher water uptake at 90 and 120 ^oC respectively at water activity of 0.4 as compared to Nafion membrane. Similarly, titania based membranes showed about 20-25 % higher water uptake than Nafion at the temperatures of interest. Silica membrane showed water uptake similar to Nafion at 90 ^oC, and about 15 % higher than Nafion at 120 ^oC. The enhanced water uptake can be attributed to the hydrophilic nature of the acidic inorganic additives within the pores of Nafion membrane and the increased acidity and surface areas of nanoparticles. The basic uptake trend at both temperatures was similar, with water uptake increasing from silica to titania to zirconia nanocomposites. This is in order of increasing acid strength. From the results obtained, it can be concluded that incorporation of nanosized acidic inorganics with higher surface areas, enhances water uptake properties of Nafion membrane, which is a key design objective for high temperature membranes. The advantage of inorganic additives in PEMs is more evident more at higher temperatures and lower RHs. Higher water uptake and enhanced acidity result in greater proton conductivity, which would presumably result into better fuel cell performance under hot and dry conditions. Also, the sorption isotherm shape obtained for nanocomposite membranes were found to be similar to that of Nafion, with lower water uptake at low RHs and then sharp increase in the amounts of water uptake after water activity of 0.6. Hence, the basic mechanism of water sorption must be similar for all nanocomposite membranes. The difference is due to the change in acidity and active surface area of membrane.

4.3.2 Ion exchange capacity

Table 4.1 lists the experimental EW measured for all the nanocomposite membranes. It was observed that Nafion-ZrO_2 sol gel was the most acidic membrane, having the lowest EW of about 1020±10. Hence, as observed from Figures 4.1 and 4.2, this membrane exhibited highest water uptake, as compared to other nanocomposite membranes, which had higher EW as shown in Table 1. Hence, the ion exchange measurements are in agreement with the water uptake results, and also due to the fact the sulfated zirconia is more acidic than other additives.

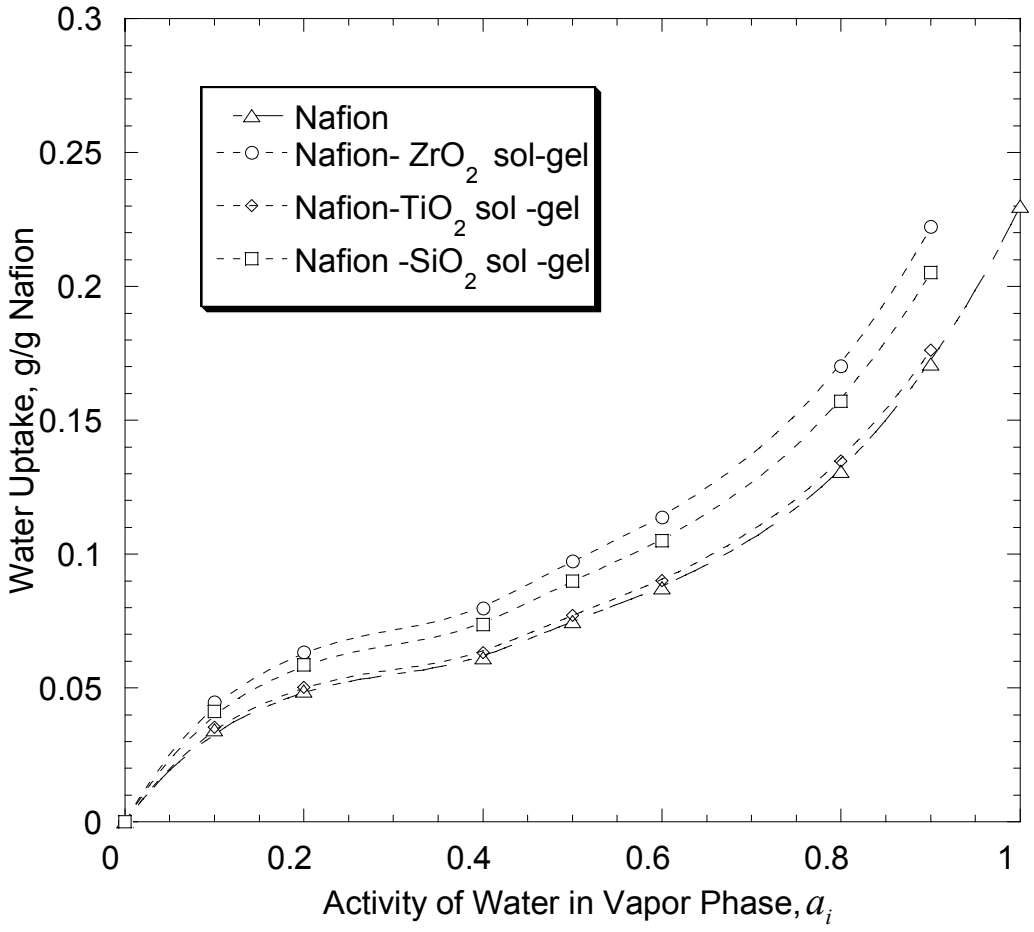

Figure 4.1 Water uptake vs. activity of water vapor for Nanocomposite Nafion/ MO_2 and Nafion membrane at 90 ^{o}C

.

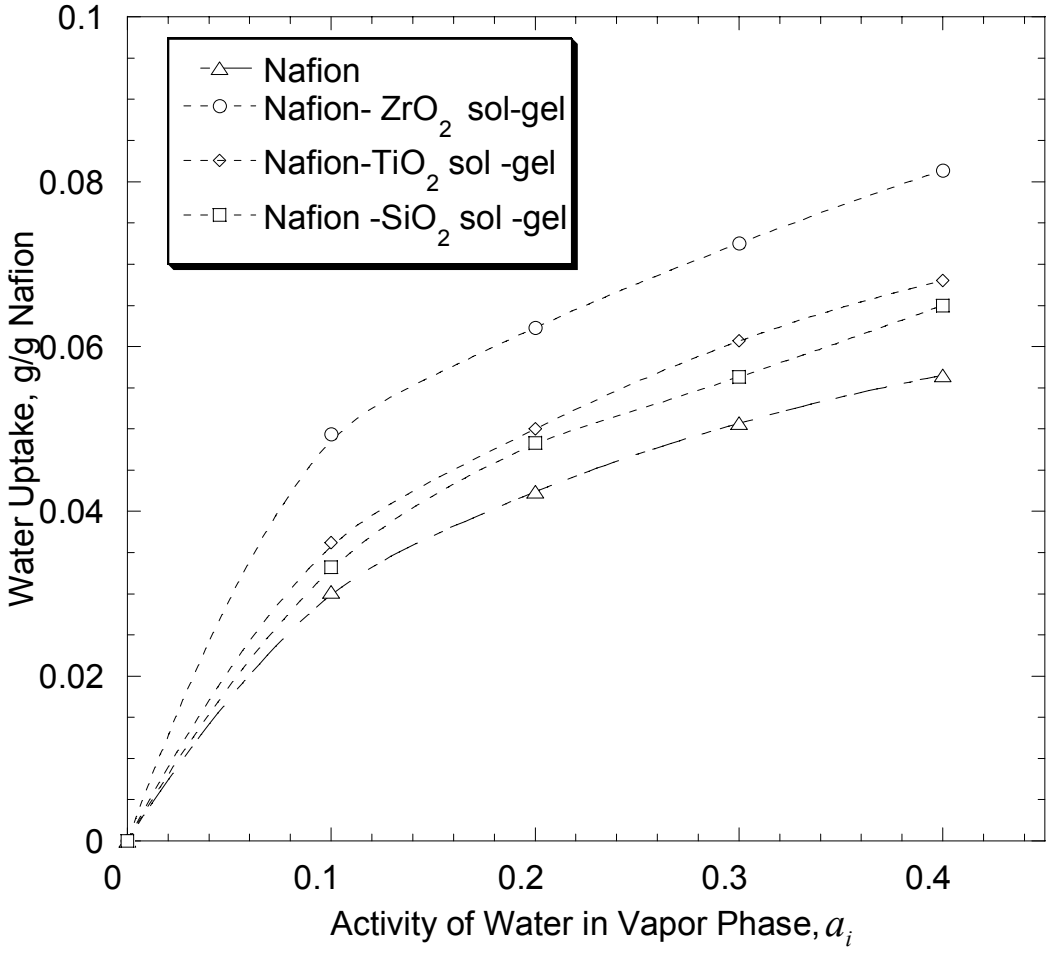

Figure 4.2 Water uptake vs. activity of water vapor for Nanocomposite Nafion/ MO_2 and Nafion membrane at 120 ^{o}C.

Samples	**EW (g/mol. H^+) (Experimental)**
Nafion 112	1100±10
Nafion-ZrO_2 Sol-gel.	1020±10
Nafion-TiO_2 Sol-gel	1090±10
Nafion-SiO_2 Sol-gel	1120±10

Table 4.1 EW of Nanocomposites

4.3.3 Conductivity measurements

Figures 4.3 and 4.4 shows the conductivity measurements for the nanocomposite membranes at 90 and 120 ^{o}C, respectively, as compared to Nafion membrane. At both temperatures, Nafion-ZrO_2 sol gel nanocomposite showed higher conductivity than Nafion for over the complete range of water activity. At 90 ^{o}C, both titania and silica nanocomposites showed somewhat lower conductivity than Nafion, while zirconia membranes had a sharp increase in conductivity at water activity of 0.7. At 120 ^{o}C, Nafion-SiO_2 sol gel nanocomposites exhibited lower conductivity than Nafion, while zirconia membranes showed about 8-10 % higher conductivity.

The increase in the conductivity of Nafion- ZrO_2 sol gel nanocomposites is the combined result of higher water uptake as well as acidity. Although other nanocomposites demonstrated higher water uptake, they showed about similar acidity and lower conductivity than Nafion. Hence, from water uptake, ion exchange capacity and conductivity results, it is evident that higher water uptake does not inevitably result into higher conductivity. As described in our modeling analysis, it is not only the total water uptake, but also the distribution of water between surface and bulk that determines conductivity. Bulk water is much more effective in proton conduction.

4.3.4 Thermo-mechanical Analysis

The TGA thermograms of the nanocomposites are displayed in Fig. 4.5 as compared to Nafion membrane. From the Fig. 4.5, it is observed that all the membranes retain more than 90 % of their weight up to a temperature of about 310 ^{o}C. Above 310 ^{o}C, all the membranes started to decompose and lose weight quite rapidly. This decomposition behavior can be attributed to the loosening of sulfonic acid groups present in the unmodified Nafion membrane [27]. However, it was observed that the temperature at which this decomposition occurs shifts with the nature of inorganic additive within the pores of Nafion membrane. For example, sharp thermal degradation of the unmodified Nafion occurs at about 325 ^{o}C, whereas, for Nafion-ZrO_2, and Nafion-SiO_2 sol gel membranes degradation temperature shifts to about 360 ^{o}C and 470 ^{o}C, respectively. The TiO_2 membranes showed not much improvement in thermal degradation temperature as compared with Nafion. Deng *et al*. also reported an initial increase in the degradation

temperature, when SiO_2 was added into Nafion membrane [28]. We observed similar increment for ZrO_2 nanocomposite membrane. Since the inorganic particles were in nanosized range, the increment in the decomposition temperature could be due to cross-linking of these inorganic additives frameworks in the nanocomposite membranes. A systematic investigation of the TGA behavior of these additives would give more insights for the trends observed.

The DMA thermogram for nanocomposite membranes along with unmodified Nafion membrane is shown Fig. 4.6. For all membranes, T_g was obtained from the peak of tan (δ). It can be seen that the T_g for all the nanocomposite membrane shifts to higher temperatures. From the literature, it is known that above 115 ^oC the network of hydrophilic clusters, made up from the sulfonic groups, is becoming extremely mobile, before the clustered structure finally collapses [29-30]. This can be either due to loss of water under dry and hot conditions, of further uptake of solvents if exposed to saturated solvent/water vapor. This high mobility of the backbone and cluster network is shown by high value of loss tangent for unmodified Nafion membrane, reaching values of 0.62 as shown in Fig. 4.6.

Further, we see that the T_g increases for the nanocomposites, which implies that they are thermo-mechanically more stable than unmodified Nafion membrane. For instance, the T_g for Nafion®-112 membrane was found to be around 110 ^oC, whereas, for Nafion-SiO_2, Nafion-TiO_2 and Nafion-ZrO_2 sol gel membranes temperature shifts to about 118 ^oC, 122 ^oC and 135 ^oC, respectively. The peak loss tangent values decreases from 0.62 for Nafion to 0.52 for Nafion-ZrO_2 sol gel membranes. The membrane thus becomes more elastic in nature and can withstand higher temperatures due to the presence of the inorganic additives within the pores of unmodified Nafion membrane. These results are also in agreement with the TGA thermograms, which show increase in the degradation temperatures for the nanocomposite membranes.

Thus, the results obtained from TGA and DSC shows the improved potential of the nanocomposite membranes for high temperature operations for fuel cells applications.

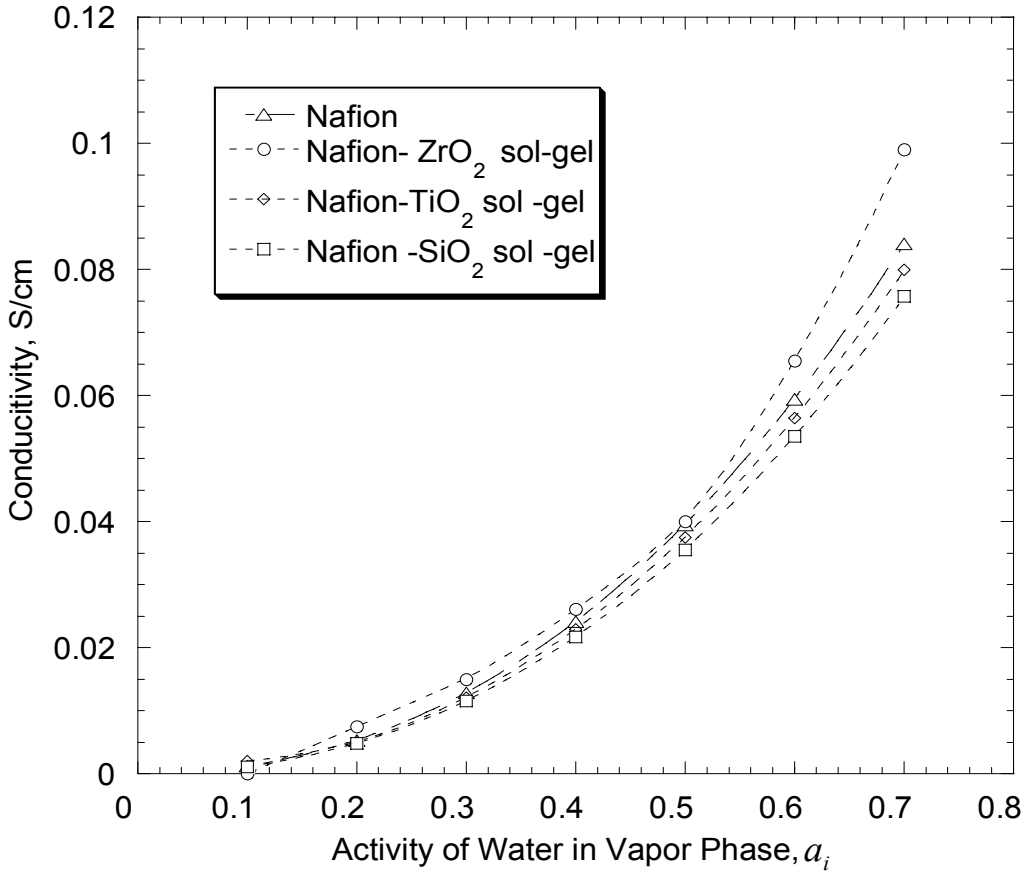

Figure 4.3 Conductivity vs. activity of water vapor for Nanocomposite Nafion/ MO_2 and Nafion membrane at 90 ^oC.

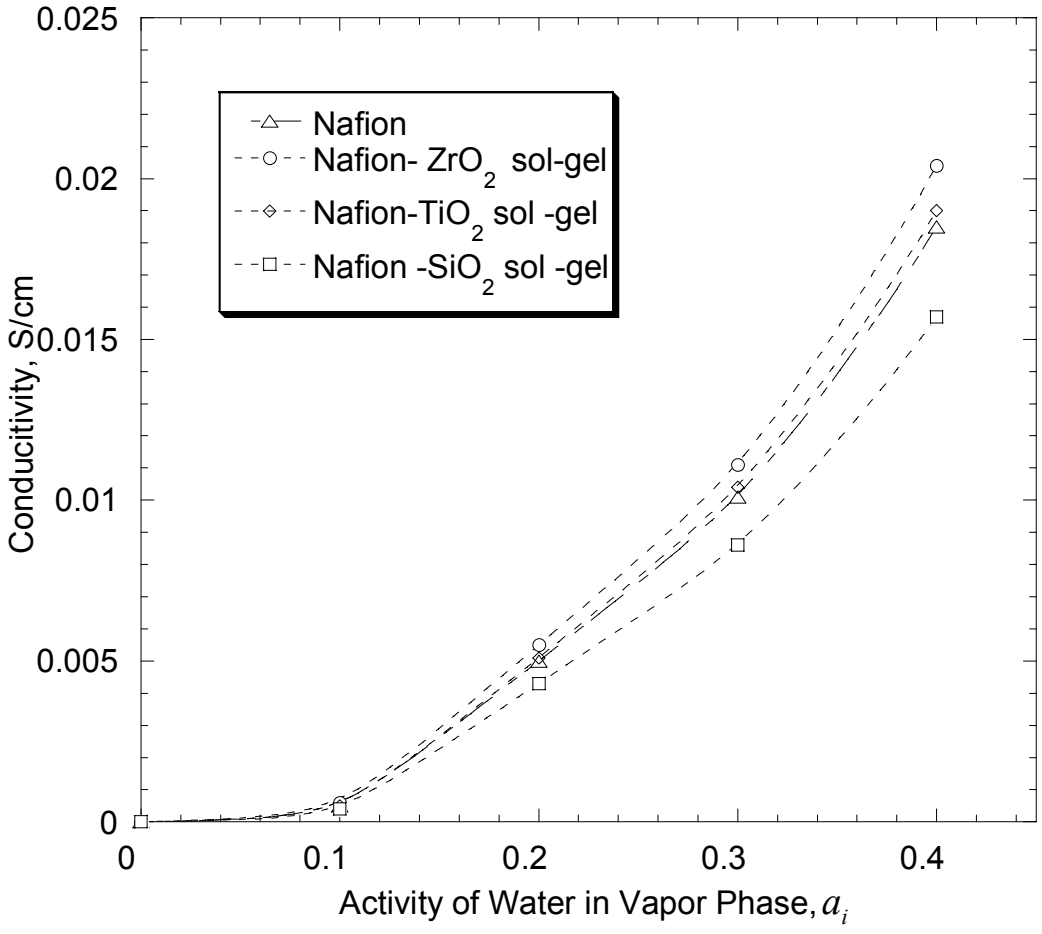

Figure 4.4 Conductivity vs. activity of water vapor for Nanocomposite Nafion/ MO_2 and Nafion membrane at 120 ^oC

.

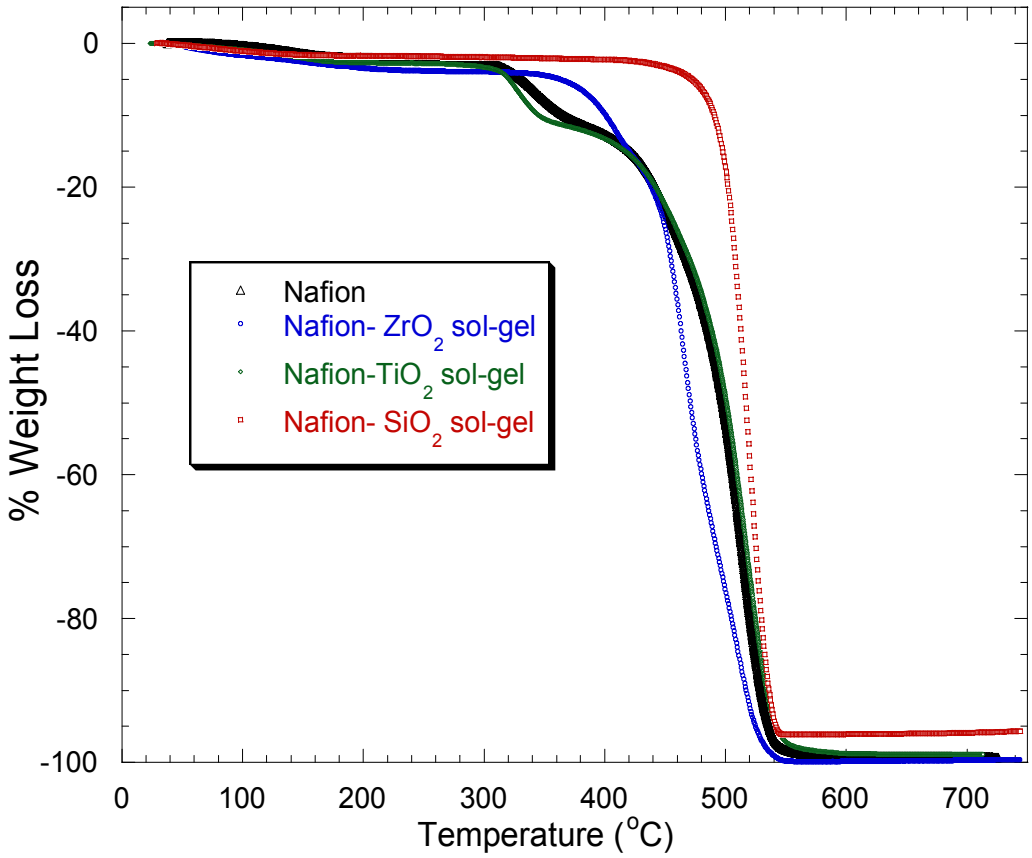

Figure 4.5 TGA data for Nanocomposite Nafion/ MO_2 and Nafion membranes.

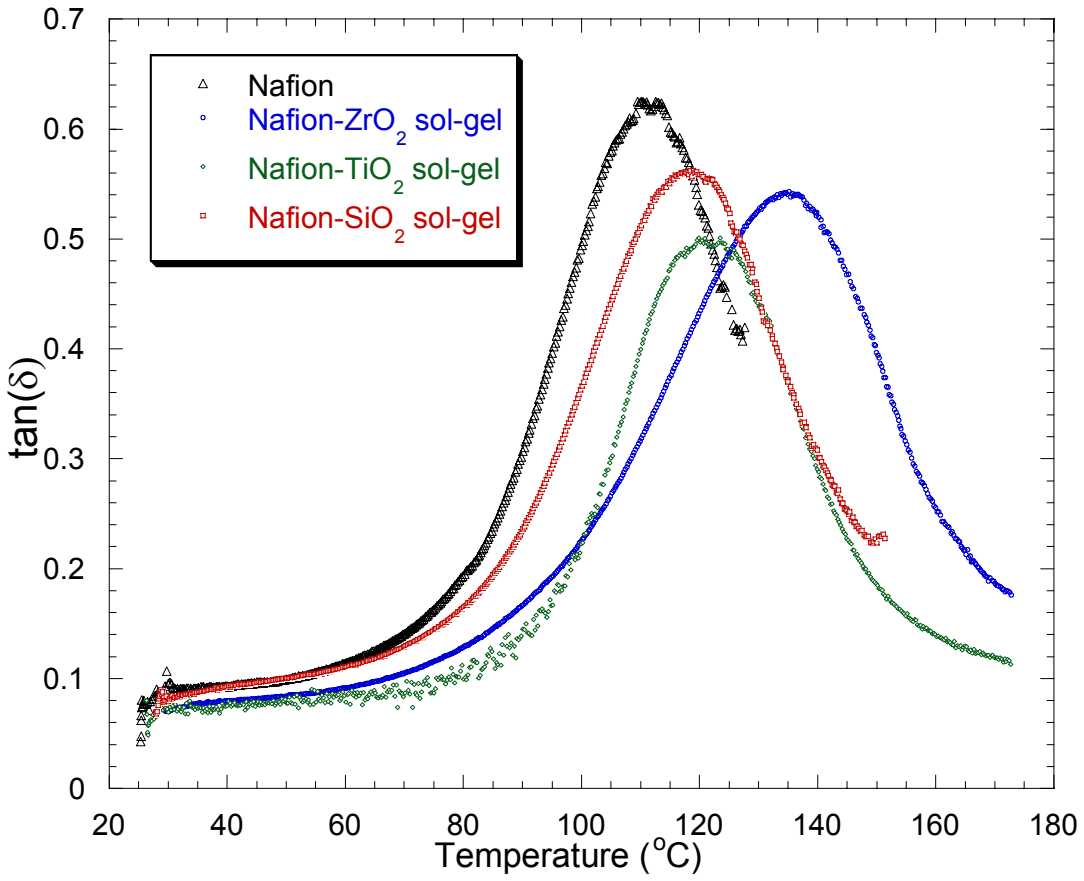

Figure 4.6 DMA data for Nanocomposite Nafion/ MO_2 and Nafion membranes.

4.3.5 MEA measurements

The fuel cell performance of a single cell with all four types of membranes under fully humidified conditions at 80 ^{o}C is shown in Figure 4.7 and under dry conditions (T_{cell}: 110 ^{o}C, $T_{Humidifiers}$: 80 ^{o}C) in Figure 4.8. Figure 4.9 shows the fuel cell performance for Nafion-ZrO_2 nanocomposite membrane at T_{cell}: 135 ^{o}C and $T_{Humidifiers}$: 80 ^{o}C and 90 ^{o}C. Since the conductivity of Nafion-ZrO_2 sol gel nanocomposite was improved because of the combined effect of higher water sorption and lower equivalent weight (EW) as mentioned in Table 4.1. Lower EW implies higher acidity of composite membranes. Since sulfated zirconia is acidic, it causes higher water sorption in the nanocomposites. Our recent modeling paper predicts the conductivity of the *in situ* sol-gel prepared Nafion-ZrO_2 nanocomposite membranes accurately as a function of relative humidity without any fitted parameters. Nafion-ZrO_2 nanocomposite membrane showed higher proton conductivity compared to Nafion at the same temperature and humidity conditions due to the improved water uptake, provision of strong acid sites and higher bulk to surface water ratio, which is critical for higher proton conductivity. Hence, there is an improvement in performance of fuel cell at 80 ^{o}C for Nafion-ZrO_2 sol gel nanocomposite as compared to other membranes. However, Nafion-SiO_2 exhibited subsequently lower performance than Nafion as contrary to results reported in literature. The reason for poor performance for SiO_2 membranes may be attributed to lower conductivity of SiO_2 membrane and higher EW as compared to Nafion membrane. At 110 ^{o}C, both TiO_2 and ZrO_2 membranes have about 30-40 mA/cm^2 higher current at 0.5 V compared to Nafion® membranes, while SiO_2 membranes had similar performance to Nafion®. At 135 ^{o}C, we obtained current densities for ZrO_2 membranes where Nafion membranes fail to perform. These results suggest that there is a potential for improvement in fuel cell performance using sol gel nanocomposites.

Under all the test conditions, the *in situ* conductivity for nanocomposite membranes, measured using current interrupt methods, was higher than that of Nafion. Further, it is possible that the membrane- electrode interface has undergone morphological change under hot and dry conditions. The conventional catalyst layer is still unmodified with nanocomposite membrane, which on modification could considerably further improve the performance. Hence, our future work would focus on optimizing the catalyst structure

including incorporating sol gel nanocomposite within the catalyst layer to increase its conductivity under hot and dry conditions. This would eventually, lead to the development of stable composite membrane electrode assemblies that perform better and are more durable under higher temperatures and lower RH.

4.4 Conclusions

Nanocomposite Nafion/ MO_2 (M = Zr, Si, Ti) membranes were synthesized by *in situ* sol gel method and characterized for high temperature operation of PEM fuel cells. Nafion- ZrO_2 sol gel membranes, especially, demonstrated higher water uptake and conductivity than unmodified Nafion membranes. Also, Nafion-MO_2 (M = Si, Ti) showed good water uptake properties. Further, all the nanocomposites exhibited better thermomechanical properties than Nafion. The degradation temperatures and T_g improved for all nanocomposites. This shows that these membranes are tolerant to high temperature above 120 ^oC, which is a design goal of this work. Thus, both chemical and physical properties were modified by incorporating nanosized inorganic additives having higher acidity and water uptake properties. The membranes synthesized by sol gel methods were very homogenous.

The future work includes testing the long term durability of these nanocomposite membranes. Since Nafion-ZrO_2 membranes exhibited better water sorption and acidity, our future goal is to characterize the electrode catalyst layer by incorporating the sol gel membrane. This might enable us to address the issue of loss of active electrochemical surface area at higher temperatures. The understanding developed could result into stable composite membrane electrode assemblies (CMEAs) for fuel cell commercialization.

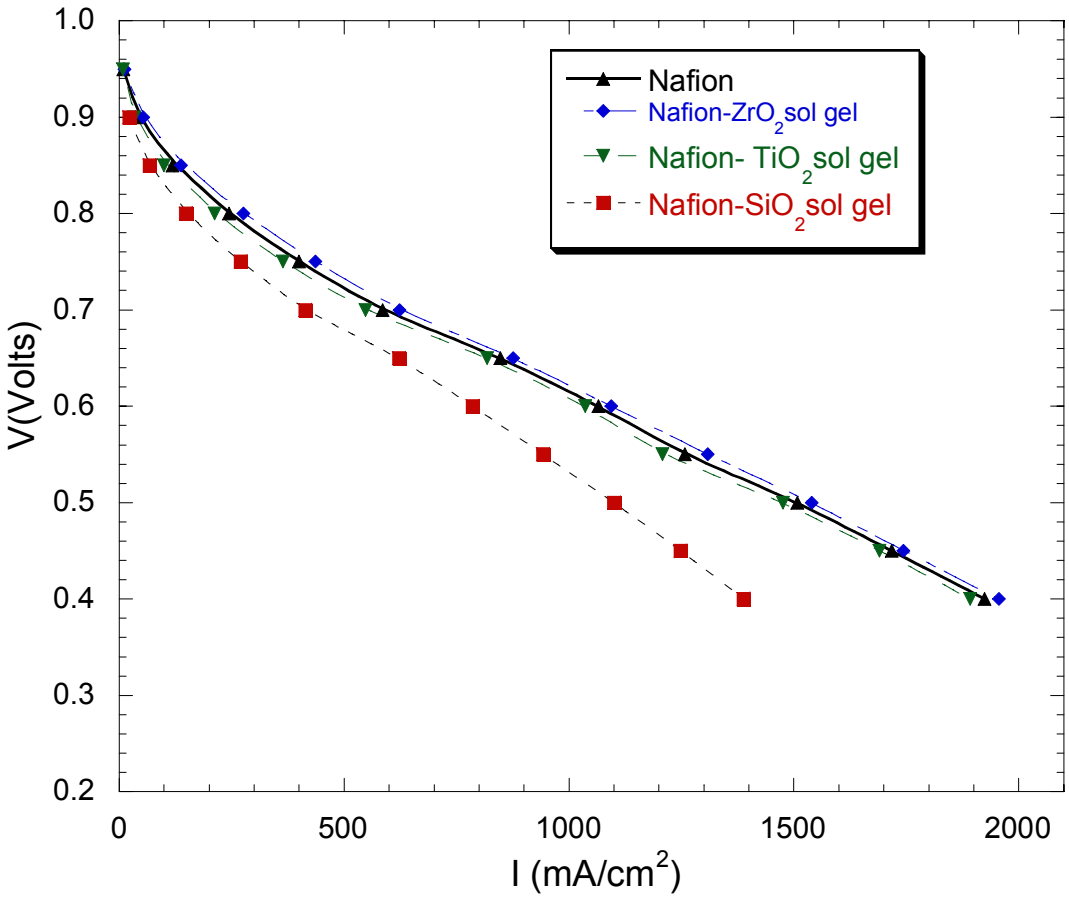

Figure 4.7 The cell performance of Nafion 112 MEA vs. Nafion -MO_2 sol-gel nanocomposite MEA. Oxygen and H_2 at 2.0 and 1.3 times stoichiometry flows respectively, P = 1.0 atm., $T_{HUMIDIFI\ ER}$= 80 ^{o}C, T_{CELL} = 80 ^{o}C.

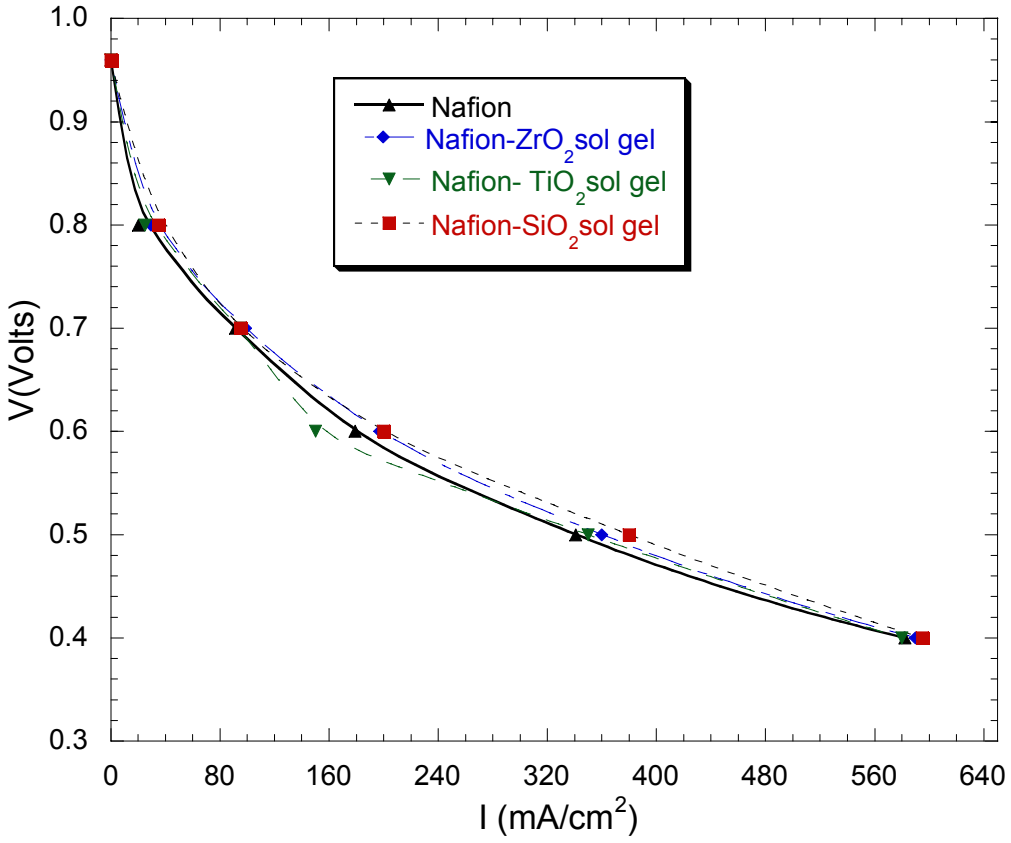

Figure 4.8 The cell performance of Nafion 112 MEA vs. Nafion -MO_2 sol-gel nanocomposite MEA. Oxygen and H_2 at 2.0 and 1.3 times stoichiometry respectively, P = 1.0 atm., $T_{HUMIDIFIER}$= 80 ^{o}C, T_{CELL} = 110 ^{o}C.

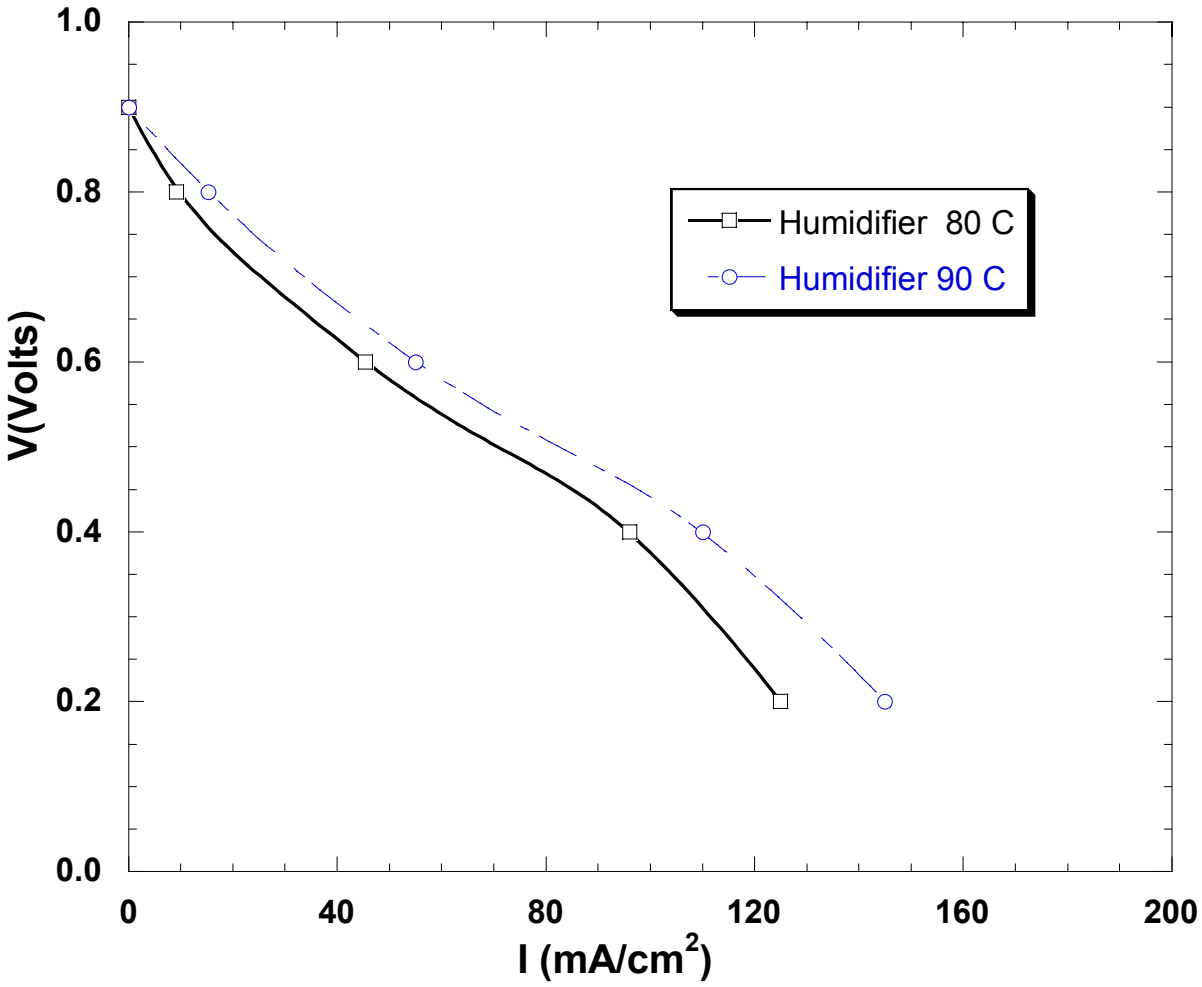

Figure 4.9 The cell performance of Nafion 112 MEA vs. Nafion -MO_2 sol-gel nanocomposite MEA. Oxygen and H_2 at 2.0 and 1.3 times stoichiometry respectively, P = 1.0 atm., $T_{HUMIDIFIER}$= 80 -90^o C, T_{CELL} = 135 ^{o}C.

4.5 References:

[1] K. D. Kreuer, J Membr Sci 185 (2001)29.

[2] A. J. Appleby, F. R. Foulkes, Fuel Cell Handbook, Van Nostrand Reinhold, New York (1989).

[3] T. A. Zawodzinski, J. Davey, J. Valerio, S. Gottesfeld, Electrochim. Acta 40 (1995) 297.

[4] S. Malhotra, R. Datta, J. Electrochem. Soc. 144 (1997) 23.

[5] V. Ramani, H. R. Kunz, J. M. Fenton, J. Membr. Sci. 232 (2004) 31.

[6] M. Watanabe, H. Uchida, Y. Seki, M. Emori, P. Stonehart, J. Electrochem. Soc. 143(12) (1996) 3847.

[7] M. Watanabe, H. Uchida, Y. Seki, M. Emori, J. Phys. Chem. B, **102,** 3129 (1998).

[8] K. T. Adjemian, S. J. Lee, S. Srinivasan, J. Benziger, A. B. Bocarsly, J. Electrochem. Soc.149 (2002) A256.

[9] N. Miyake, J. S. Wainright, R. F. Savinell, J. Electrochem. Soc. 149 (2001) A256.

[10] W. Apichatachutapan, R. B. Moore, K. A. Mauritz, J. Appl. Polym. Sci. 62 (1996) 417.

[11] C. Yang, P. Costamagna, S. Srinivasan, J. Benziger, A. B. Bocarsly, J. Power Sources 103 (2001) 1.

[12] S. M. J. Zaidi, S. D. Mikhailenko, G. P. Robertson, M. D. Guiver, S. Kaliaguine, J. Membr. Sci. 173 (2000) 17.

[13] K. A. Mauritz, I. D. Stefanithis, S. V. Davis, R. W. Scheez, R. K. Pope, G. L. Wilkes, H. H. Huang, J. Appl. Polym. Sci. 55 (1995) 181.

[14] K. T. Adjemian, S. J. Lee, S. Srinivasan, J .Benziger, A. B. Bocarsly, J. Electrochem. Soc. 149 (2002) A256.

[15] P. Staiti, A. S. Arico, V. Baglio, F. Lufrano, E. Passalacqua, V. Antonucci, Solid State Ionics 145 (2001) 101.

[16] O. Savagodo, J. New Mater. Electrochem. Syst. 1 (1998) 66.

[17] A. S. Arico, V. Baglio, A. D. Blasi, V. Antonucci, Electrochem. Comm. 5 (2003) 862 .

[18] T. Thampan, N. Jalani, P. Choi, R. Datta, J. Electrochem. Soc. 152(2) (2005) A316.

[19] P. Choi, N. Jalani, R. Datta, J. Electrochem. Soc. 152(30) (2005) E84.

[20] N. Jalani, P. Choi, R. Datta, J. Membr. Sci. 254(1-2) 31-38 (2005).

[21] N. Jalani, R. Datta, J. Membr. Sci. 264(1-2) 167-175 (2005).

[22] R.B. Moore III, C.R. Martin, Macromolecules 21 (1988) 1334.

[23] E. Voltera, E. C. Zachmanoglou, Dynamics of Vibrations, Columbus, Charles E., Merrill Books, Inc.(1965).

[24] D. Chen, A. Grønvold , H. P. Rebo, K. Moljord , A. Holmen, Applied Catalysis A. General 137 (1996) L1.

[25] E. Busenberg, C. V. Clemency, Clays and Clay Materials 21 (1973) 213.

[26] T. A. Zawodzinski, M. Neemand, L.O. Silerud, S. Gottesfeld, J Phys Chem. 95 (1991) 6040.

[27] T. Kyu, M. Hashiyama, A. Eisenberg, Can. J. Chem. 61(1983) 680.

[28] Q. Deng, C. A. Wilkie, R. B. Moore, K. A. Mauritz, Polymer 39 (1998) 5961.

[29] G. Alberti, M. Casciola, L. Massinelli, B. Bauer, J. Membr. Sci. 185(2001) 73.

[30] S. H. Almeida, Y. Kawano, J. Therm. Anal. Calor. 58(1999) 569.

Chapter 5
TEOM: A Novel Technique for Investigating Sorption in Proton-Exchange Membranes

In this chapter, a new technique, namely, the Tapered Element Oscillating Microbalance (TEOM) is explained to investigate the equilibrium water and methanol vapor phase sorption and desorption in Nafion membrane at different relative humidity (RH) and temperatures. The water sorption was found to increase with temperature from 30^{o} C to 90^{o} C. This is explained by the increase in the flexibility of polymer chains via a decrease in Young's Modulus of membrane with temperature. The effect of various pretreatments, *e.g.*, heating, vacuum treatment, and hot pressing on the water sorption properties is also investigated. It is observed that the water sorption for Nafion membrane depends both on the pretreatment of the membrane and on the temperature of sorption. The desorption isotherm exhibits a hysteresis with respect to sorption for both water and methanol. This hysteresis behavior may be attributed to the relaxation or viscoelastic properties of Nafion membrane. In summary, TEOM appears to be an attractive technique for characterizing sorption-desorption behavior of proton exchange membranes. This chapter is published in J. Membrane Science, 254(1-2) 31-38 (2005).

5.1 Introduction

Recently there has been much interest in polymer electrolyte membrane (PEM) fuel cells. An important factor determining the performance of the PEM fuel cells is the hydration level of the proton-exchange membrane (PEM) [1-3]. A common PEM is Nafion, a polymer consisting of a polytetrafluoroethylene (PTFE) backbone with side-chains culminating in $SO_3^-H^+$ groups. It exhibits excellent chemical, mechanical, and thermal stability along with low gas permeability and high proton conductivity when adequately hydrated. The amount of water sorbed in the membrane is critical as the proton conductivity directly depends upon the water content of the membrane [4-6]. The main factors that affect the extent of water sorption in a PEM are the nature of polymer

backbone, temperature, ion-exchange capacity, pretreatment, as well as the physical state of external water *i.e*., whether it is in liquid or vapor form. Water basically dissociates the acid groups and provides a medium for conduction of protons.

In the operation of a typical PEM fuel cells, the reactant feed gases are prehumidified to provide adequate hydration levels in the membrane. This is supplemented by the water produced at the cathode due to the electrochemical reaction, which also results in a gradient in the activity of water across the membrane causing water to diffuse back from cathode to anode [7]. Further water is transported from anode to cathode along with the protons, *i.e.*, via the electro osmotic drag. Thus, water management is critical to successful working of a PEMFC, which necessitates an understanding of water sorption characteristics of PEMs.

Many investigators have studied the uptake of water in PEMs. Several investigations have been done on the hydration, swelling, and drying under different conditions for Nafion, based on spectroscopic, gravimetric and other methods [7-11]. The adsorption from liquid phase is quicker as compared to that from vapor phase. Further, Nafion adsorbs around 22 water molecules per acid site from liquid water, while it adsorbs around 14 water molecules from saturated vapor [7-8], *i.e*., the so called Schroeder's Paradox recently explained by Choi and Datta [12].

An important variable is the pretreatment of a PEM that affects its water sorption. In an early study, the following nomenclature was used to describe pretreatment of Nafion, namely, "E- form" for a membrane swollen and expanded in high temperature water, and "S-form" for a membrane shrunk in vacuum at high temperatures [13]. The normal membranes were termed "N-form". It was found that the E-form membrane becomes rubbery when the temperature increases, with a tendency to adsorb more water. However, in S-form membranes, the ionic clusters shrink and the water uptake drops. Kawano *et al*. studied the stress-strain characteristics of Nafion membrane for various pretreatments (boiling, soaking in other solvents, heating, etc.) [14]. They observed that the slope of stress-strain *i.e*., Young's Modulus (E) of the membrane, decreased for a membrane boiled in water, making them more pliable for higher water uptake.

The sorption of methanol in Nafion is also of interest in context of the direct methanol fuel cells (DMFC) [15-17]. The two main obstacles that currently limit DMFC

performance are the low activity of methanol electro-oxidation catalysts and the crossover of methanol through the polymer electrolyte membrane. It has been observed that methanol crossover to the cathode not only lowers the fuel utilization but also adversely affects the oxygen kinetics at the cathode, resulting into lower cell performance [18-19].

Consequently, there is a strong motivation to systematically study the water/methanol sorption isotherms for Nafion and other polymer electrolyte membranes. Experiments with the conventional gravimetric methods are slow, providing data of low accuracy. The sorption data are affected by the flow patterns, bypassing, and incomplete contact of the gas with the sample [20]. Further the equipment has limited temperature and pressure range. There is also significant reduction in mass resolution at high temperatures. Here the use of a novel and relatively fast technique, namely the Tapered Element Oscillating Microbalance (TEOM) is described to accurately measure equilibrium water/methanol sorption-desorption isotherms for PEMs. The effects of solvent activity or relative humidity (RH), temperature, and various pretreatment protocols on sorption behavior of Nafion are investigated. Further, the use of this technique in studying sorption behavior of inorganic powder additives is described in our efforts to develop high temperature proton-exchange membranes by improving water retention at elevated temperatures [21-22].

5.2 Description of the TEOM

The tapered element oscillating microbalance (TEOM) Series 1500 Pulse Mass Analyzer (PMA) purchased from Rupprecht & Patashnick Co., Inc., Albany, NY, was utilized to study the equilibrium solvent sorption-desorption behavior for Nafion membranes. This offers a novel means of analyzing real-time mass change of sample in a fixed-bed while the gases pass through the sample. It includes a tapered element oscillating microbalance, which is based on inertial forces rather than gravity, to measure the mass change of sample [23]. The TEOM possess certain advantages over conventional gravimetric techniques in measuring sorption in polymer electrolyte membranes:

1. The steady flow of gas through the sample provides complete contact with the test material.
2. High mass resolution ($1x10^{-6}$ g) and a low standard deviation.

3. The experiments can be performed over a wide range of temperatures (25 ^{o}C to 500 ^{o}C) and pressures (vacuum to 60 atm).
4. The microbalance employs a resonant cantilever to measure changes in inertia rather than weight, hence the data obtained is not influenced by flow patterns of gas streams, buoyancy and other aerodynamic factors.

However, there are some limitations in using TEOM. It cannot be used for volatile or fragile samples, which may alter the natural oscillating frequency of the test bed. Also, liquid phase studies cannot be performed using this technique.

The heart of the TEOM is an oscillating tapered test bed in which the sample is packed. This tube containing the sample vibrates constantly at its natural frequency of oscillation. There is a feedback system which maintains the oscillation of the tapered bed [23]. The frequency is obtained optically with a transmitter and receiver located on the opposite sides of the oscillating test bed. A simplified diagram of the 100 mg (0.1 cc) test bed and optics is shown in Figure 5.1 [24]. The sample was carefully packed between quartz wool in the test TEOM bed.

The motion of TEOM test bed may be approximated as free undamped vibrations of a cantilever in one of the principle planes of the beam [25-26]. The effects of rotatory inertia and of transverse shear deformation are neglected. The equation of motion for beam of uniform cross section is

$$EI\frac{\partial^2 y}{\partial x^2}+\rho A\frac{\partial^2 y}{\partial t^2}=0 \tag{5.1}$$

where E is the Young's Modulus, I is the second moment of area of the cross section, ρ is the density, A is the beam cross sectional area, y is the displacement from the centerline of the beam at any section x and t is the time.

For free undamped vibration, the solution is of the form

$$y(x, t) = Y(x)\sin(\omega t+\alpha) \tag{5.2}$$

where ω is the frequency of vibration, and α is the phase angle.

Substituting this in Eq.1,

$$\frac{d^4Y}{dx^4}-\kappa Y=0 \tag{5.3}$$

where,

$$\kappa = \frac{\rho A \omega^2}{EI} \tag{5.4}$$

The solution for Eq. 5.3 is of the form,

$$Y = B\,exp(\kappa x) \tag{5.5}$$

Now, the frequency of vibration f is defined as $\omega/2\pi$. Thus,

$$f^2 = \frac{\omega^2}{4\pi^2} = \frac{\kappa EI}{\rho A 4\pi^2} = \frac{\kappa_o}{m} \tag{5.6}$$

where $m = \rho A$ is the dynamic mass of the system and κ_o is the effective spring constant for the tapered element. Thus, the change in mass of system Δm for the corresponding change from initial frequency f_o to final frequency f_f is

$$\Delta m = \kappa_o \left(\frac{1}{f_f^2} - \frac{1}{f_o^2}\right) \tag{5.7}$$

Thus, with an increase in the mass, the frequency decreases, and vice versa. In TEOM apparatus, spring constant κ_o depends weakly on temperature. For instance, change in the spring constant for a temperature range of 30 – 250 ^oC corresponds to a mass change of $1x10^{-5}$ g [24]. In the present study the temperature range investigated is 30 – 90 ^oC. Hence, the effect of temperature on the effective spring constant is neglected.

5.3 Experimental Section

5.3.1 TEOM Apparatus

The TEOM experimental set up is shown schematically in Figure 5.2. Helium gas is bubbled through water kept in a bottle (saturator) and is combined with another stream of dry helium gas downstream for obtaining the desired relative humidity. All the gas flows are controlled by means of mass flow controllers (MKS Model No. 1179A22CS1BV-S,

Andover, MA). A preheated bath of ethylene glycol–water (50: 50 by volume) is circulated around saturator to maintain the desired temperature, in the range of 25 ^{o}C to 115 ^{o}C. The temperature of water in the saturator is monitored via a thermocouple connected to a digital multimeter. As shown in Figure 5.2, a purge helium stream is used to avoid condensation at the external surface of the test bed and back flow of exiting gas stream from the test bed.

The real-time dynamic mass change of the sample in the TEOM test bed can be analyzed graphically using LabView 5.0 program, purchased from National Instruments Corporation. Inside the TEOM, there are two temperature-controlled zones. The pre-heat zone controls the inlet gas stream temperature and the other zone controls the temperature of the tapered element and the sample bed. The TEOM performance is quantified in terms of the normalized standard deviation (NSD). The NSD is an indicator of any noise in the test bed and depends upon how well the sample is packed, and whether there is other disturbance. For the equilibrium sorption experiment, a 10 s average time with 12 recording values (approximate gate time of 0.8 s) gives a typical value of NSD below 3 x10^{-6} ppm [24]. More structural details of TEOM can be obtained from the company's website (www.rpco.com).

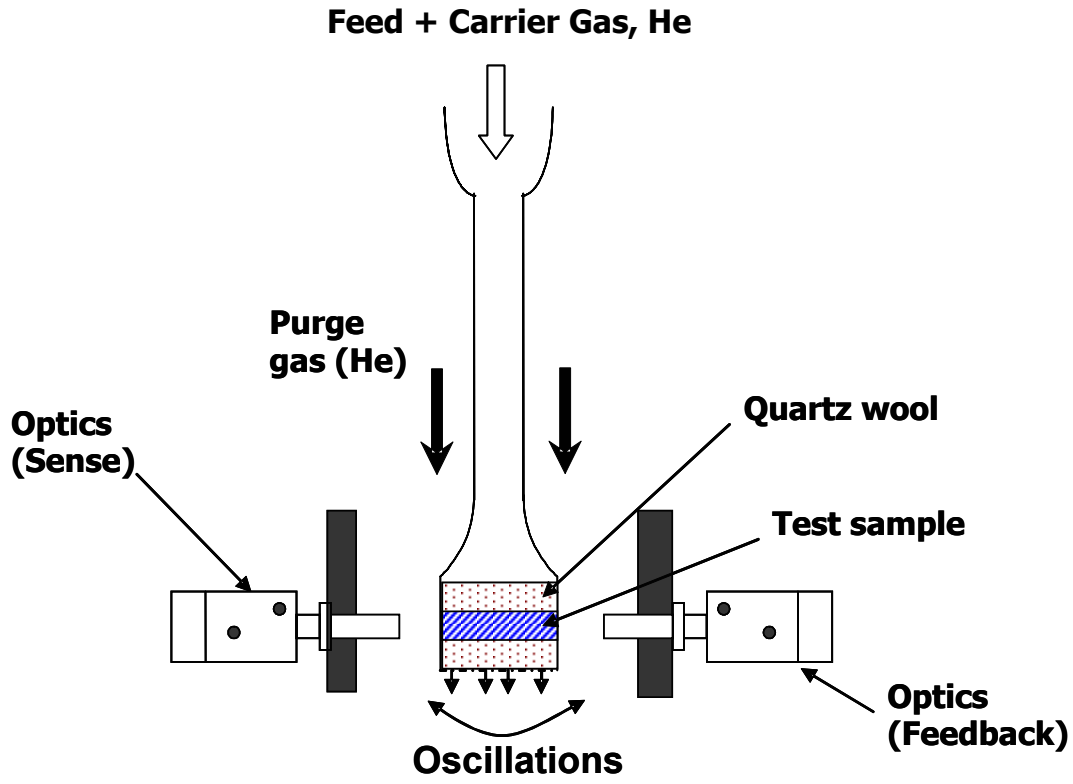

Figure 5.1 Simplified flow diagram of the TEOM test bed and optics. The flow of inlet gas is shown by large arrows.

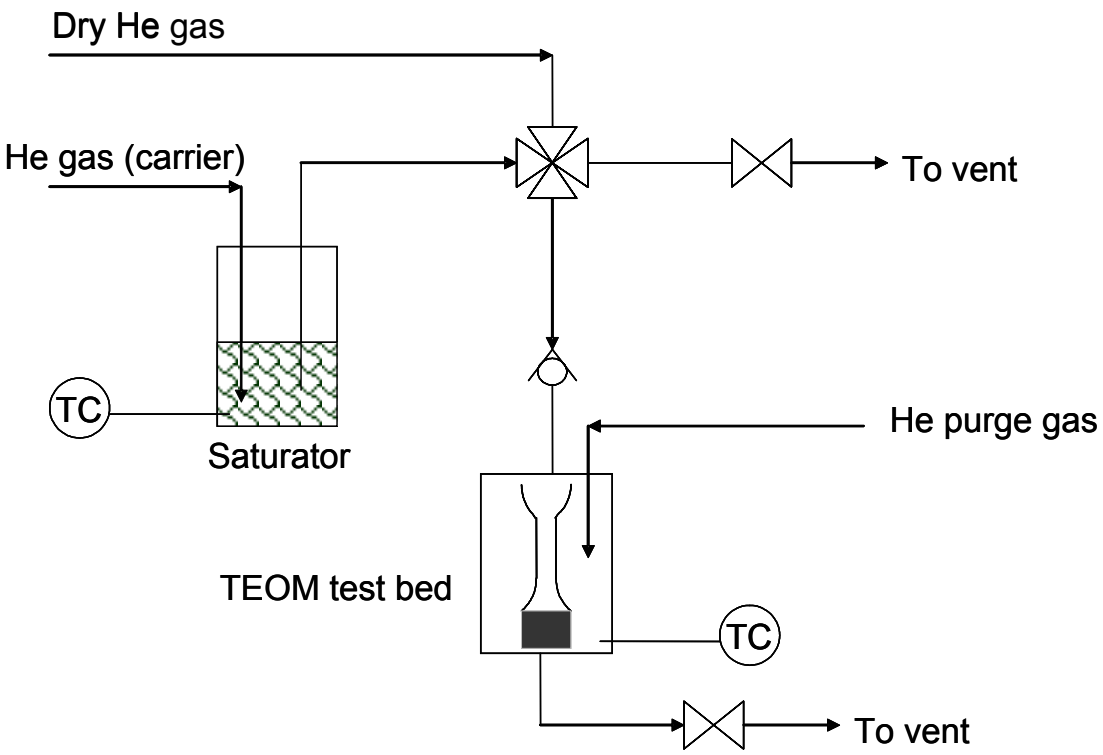

Figure 5.2 Experimental setup for sorption-desorption isotherms.

Since the real-time mass change of the sample can be monitored, TEOM can be utilized for studying both dynamic and equilibrium sorption. Although the present study is focused on equilibrium sorption-desorption process, the diffusion coefficients may also be determined from dynamic sorption and desorption.

5.3.2 Membrane preparation

The Nafion 112 membrane was purchased from Aldrich and then subjected to a pretreatment procedure as described in the literature [27-28]. It was boiled in 3 % H_2O_2 for half an hour. Then it was heated at 60 ^oC in 0.5 M sulphuric acid solution for half an hour. Finally it was heated at 60 ^oC in deionized water for 1 hour. After boiling the membrane, it was washed thoroughly with DI water to remove any acid residues. It was finally dried at room temperature by leaving the membrane untouched. To study the effect of pretreatments on water sorption behavior for Nafion, the membrane synthesized was then subjected to different treatments, as explained later on.

5.3.3 Sorption - Desorption Measurements

A known dry mass of vacuum heated membrane sample was cut into small pieces (1.5 mm x 1.5 mm) using a doctor blade and loaded carefully in the test bed. Quartz wool, purchased from Rupprecht & Patashnick Co., Inc., was used as filler material to keep the sample firmly packed, which is necessary so that the sample does not rattle around affecting the oscillations of the bed. The best way to ensure this is to check the NSD. If it is below $3x\ 10^{-6}$ ppm then, it implies that the sample was properly loaded. Typically, about 20 mg of membrane sample was packed in the test bed to get best reproducibility.

The sorption – desorption data were obtained by a stepwise increase or decrease of the flow rate of humidified inlet gas stream, which changes the RH or activity of the feed gas at fixed temperatures. During the experiments, the He purge gas was kept at around 120-150 sccm, while the carrier gas through saturator was maintained at 10-15 sccm, with the dry He gas varying from 0 to 100 sccm depending on RH required in the test bed. The RH was calculated from the gas flow rates and the saturator temperature. To further confirm this calculation, the inlet stream of gas entering the sample test bed was connected to a humidity probe purchased from Vaishala Inc. For various temperatures of saturator and

flow of helium gas, the RH was measured. The experimental observations were in good agreement with the calculations. After loading the sample, the inlet flow was set to the desired value and sufficient time was allowed for the sample to reach steady state, typically 10 - 30 min. After waiting for sufficient period, if the mass of the test bed did not change for more than 1%, then the equilibrium was assumed. This was good enough for such vapor phase experiments. Thus, the change in sample mass for the set condition was recorded and then the inlet flow was adjusted to get next desired RH. The real-time sample mass variation in TEOM is shown in Figure 5.3 for step changes to 10, 20 and 30 % RH conditions. The total mass of sample increases as it adsorbs solvent. The mass change corresponds to the amount of solvent adsorbed. The increase in mass represents the dynamic changes of the test bed, and hence this data can be utilized to study the kinetic parameters for sorption and desorption process. In the present set up, both sorption and desorption experiments were done in a similar fashion by stepping the RH up and down, respectively. The vapor phase equilibrium sorption data is reported here as λ, defined as the ratio of moles of absorbed solvent per mole of sulfonic acid groups within Nafion. Alternatively, the data can be presented as ratio of mass of absorbed solvent to mass of dry polymer. Both these representations are useful depending on the objective of study.

5.4 Results and Discussion

5.4.1 Water Sorption

The equilibrium water sorption isotherm for 1100 EW Nafion membrane at 30 ^{o}C is shown in Figure 5.4 along with data available in the literature [10,13,30,34] for similar EW membrane. The sorption curve is typical of the swelling membrane, with an extended region of gradually increasing slope that turns sharply higher above water activity of 0.7. At the origin, the isotherm had a sharp initial slope, rapidly leveling off at activity of 0.2, corresponding to the weight uptake of 0.04 g /g and about 2 water molecules. Our data obtained with TEOM are in good agreement with published results from different laboratories, thus validating the accuracy of the technique. The room temperature water sorption isotherm was reproduced and the error bar for each RH condition is shown, confirming that the data are reproducible. The added advantage of the TEOM is that the

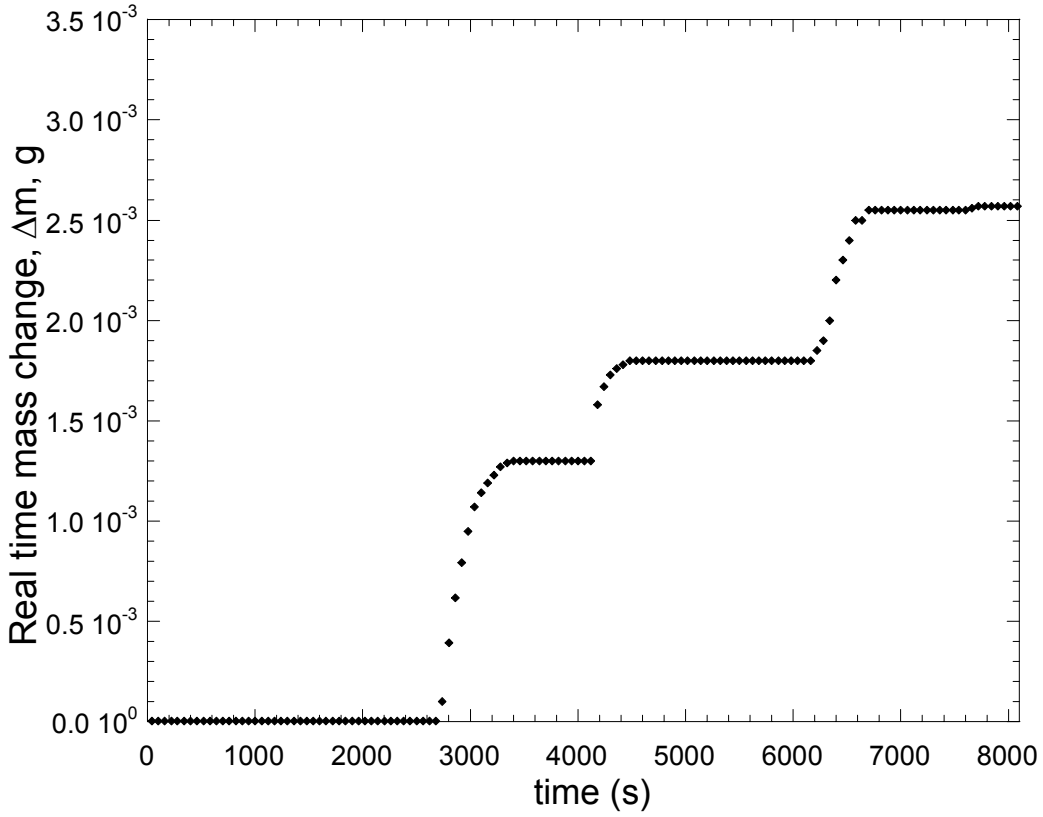

Figure 5.3 Real-time mass change data obtained from TEOM. The plateau represents equilibrium for given vapor activity conditions.

data are obtained rapidly as compared to other gravimetric techniques and are highly reproducible. This is important because of the efforts in laboratory on developing high temperature proton conducting membranes that require accurate measurements of water sorption. The sorption data also agrees with our water sorption model developed recently based on a physicochemical understanding of how the water molecules interact with the PEM [31-32].

The data were also obtained at different temperatures ranging from 30 ^{o}C to 90 ^{o}C. Figure 5.5, thus, shows the effect of temperature on water sorption isotherm for Nafion membrane. The amount sorbed increases gradually with temperature, especially with high water activity. Kawano *et al* have studied the stress-strain characteristics of Nafion membrane at different temperatures and found that the initial slope of the curves *i.e*., the Young's modulus (*E)* decreases with increasing temperature, thus softening the membrane and allowing higher water uptake [14]. A lower *E* reduces the swelling pressure on the imbibed liquid thus equilibrating at higher sorbed amount. We have also recently investigated the effect of water activity and temperature on *E* for Nafion membrane, using the technique of Optoelectronic holography (OEH) [31]. Figure 5.6 shows the variation in *E* versus water activity at two different temperatures. Thus *E* decreases both with water activity and temperature. A thorough investigation of the effects of temperature on physicochemical behavior of polymer is important, since water management and performance of PEMFC depend on operating temperature. Also, the durability of the membrane depends upon the thermomechanical properties.

5.4.2 Methanol Sorption

The methanol sorption isotherm is shown in Figure 5.7 together with water sorption isotherm for comparison. These data are of interest in connection with DMFC [17]. The experimental procedure to measure methanol sorption was similar to that of water sorption. Methanol was filled in saturator and methanol activity in the TEOM test bed was measured. The sorption isotherm for methanol follows a pattern similar to that of water. Also the initial slopes of both curves are similar. There is an extended region of gradually increasing slope for both solvents, as well as a marked upturn for high activities. The mass uptake of 0.106 g for methanol at an activity of 0.4 corresponds to about three methanol

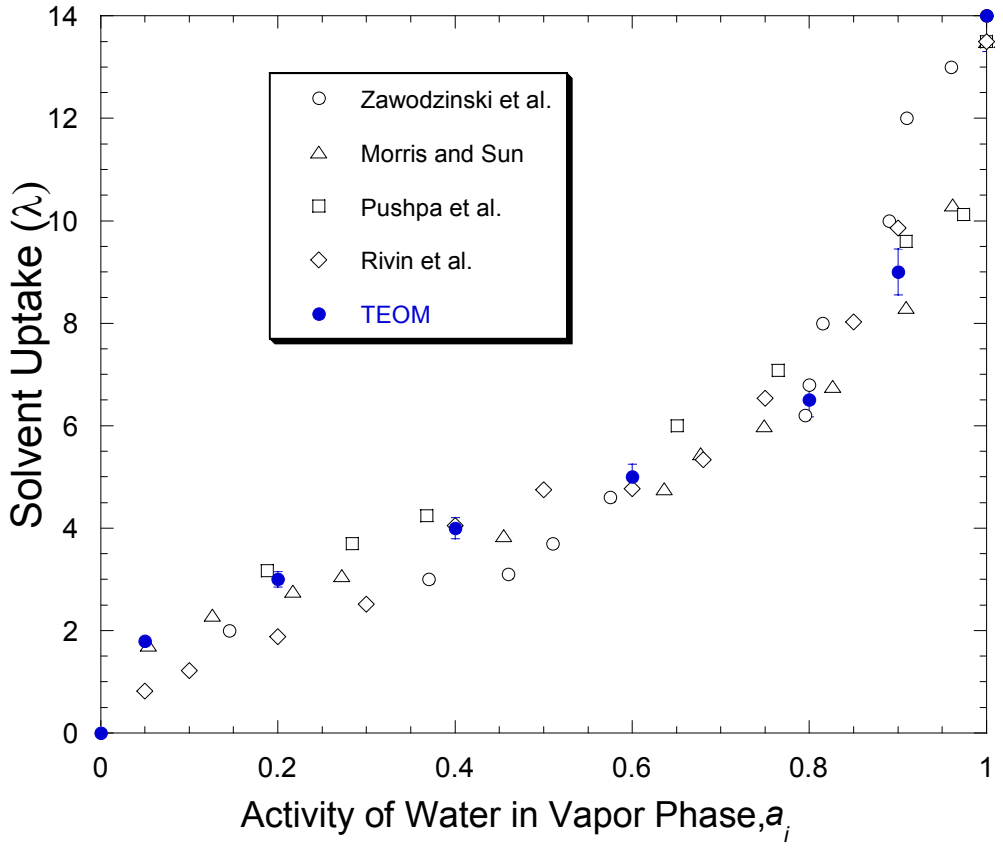

Figure 5.4 Water uptake vs. activity of water vapor for 1100 EW Nafion membrane at 30 ^{o}C (triangle: ref. 10, square: ref. 34, diamond: ref. 30, circle: ref. 13 and dark circle: this work).

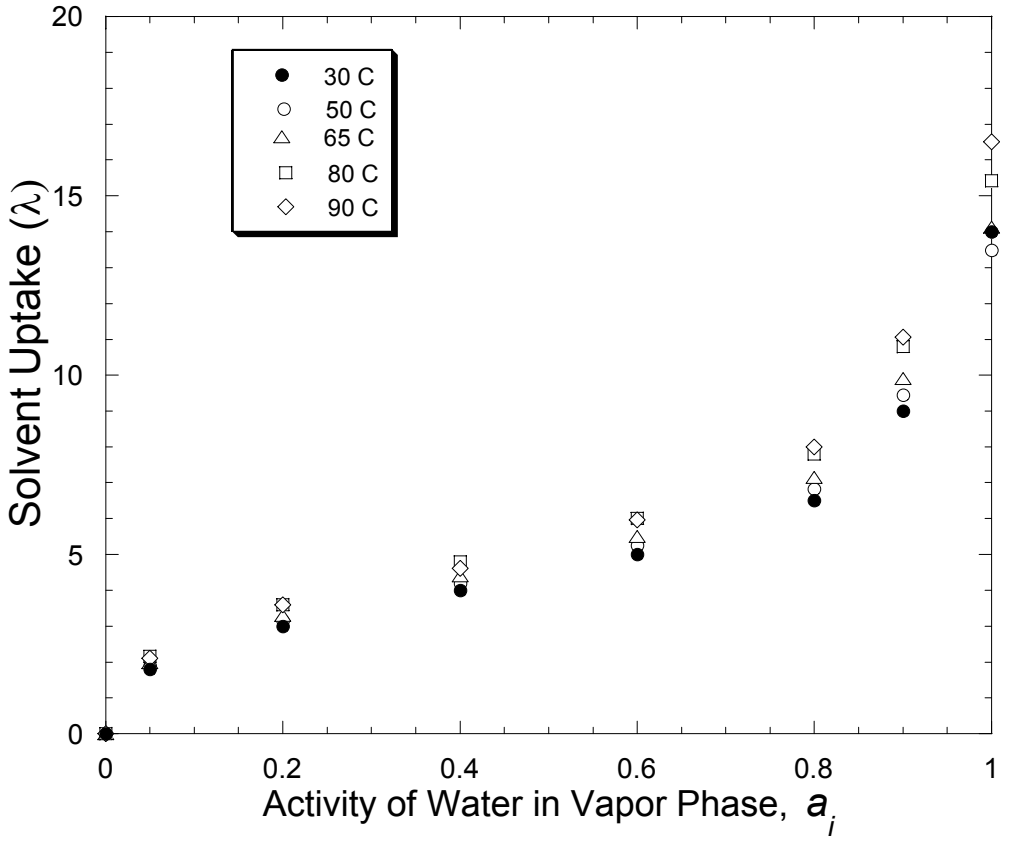

Figure 5.5 Effect of temperature on water uptake vs. activity of water vapor for Nafion membrane.

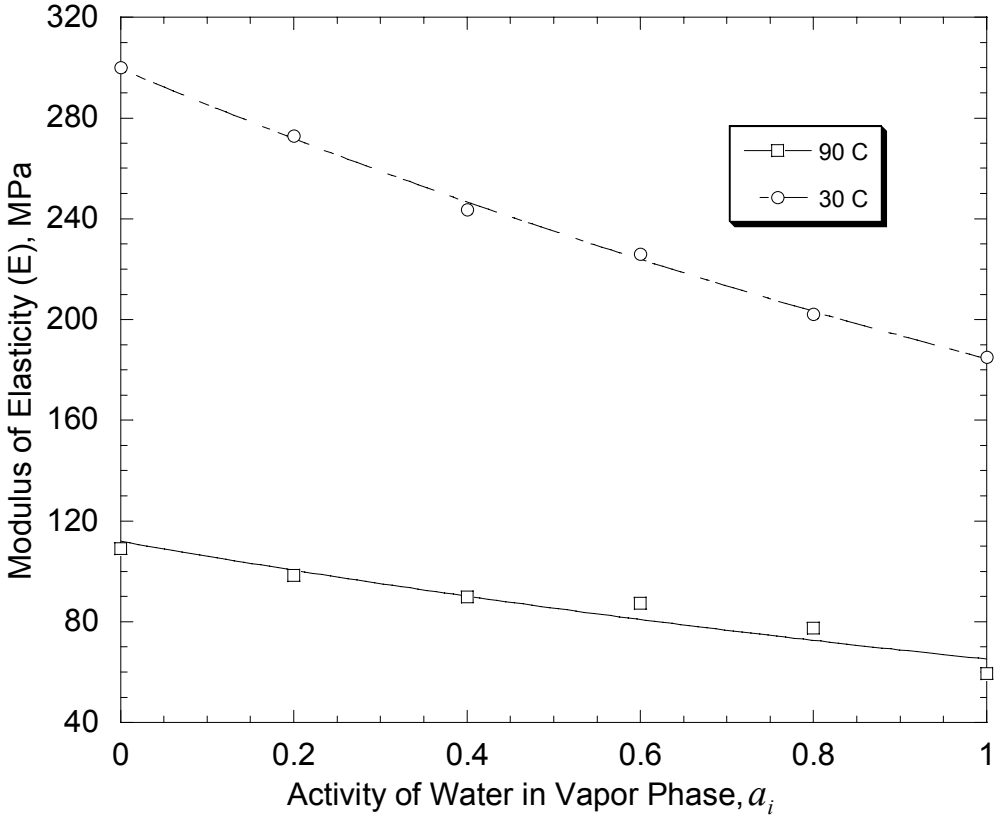

Figure 5.6 The experimental variation of Young's modulus vs. activity of water vapor for Nafion membrane (circle: 30 ^{o}C, square: 90 ^{o}C).

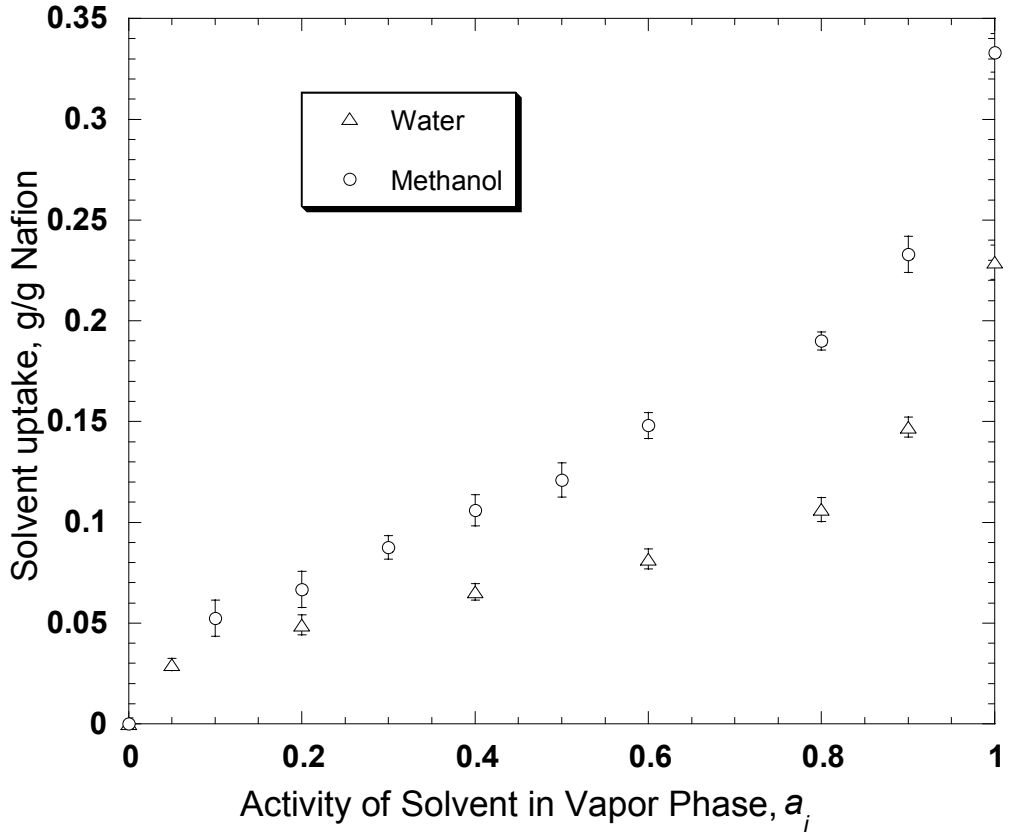

Figure 5.7 Water and Methanol uptake vs. activity of solvent vapor for Nafion membrane at 30 ^{o}C (circle: methanol, triangle: water).

molecules per sulfonic acid site, as compared to five molecules in the case of water sorption. For similar solvent activity, thus, fewer number of methanol molecules are associated with sulfonic acid group as compared to water.

5.4.3 Sorption - Desorption Measurements

Figure 5.8 shows the water and methanol vapor phase sorption and desorption isotherm of a Nafion membrane at 30 ^{o}C. This exhibits a hysteresis for both the solvents. The desorption curve was obtained after the sorption measurements for both the solvents. The sorption experiments were completed for the sample by stepping up the RH, followed by stepping down of RH for desorption. While stepping down, sufficient time was provided to the sample to reach equilibrium. Typically 10- 40 min was required at each RH condition. The desorption exhibits enhanced water and methanol uptake as compared to sorption for activity range of 0.2- 0.9. This might suggest the Nafion membrane underwent swelling during the sorption process that had not fully relaxed during desorption process. According to Rivin *et al*., the hysteresis during the desorption process can be explained by the slow volume relaxation of the hydrophilic clusters in response to the change in vapor activity, resulting in higher swelling of membrane at a given activity [30]. This slow relaxation may be determined by the viscoelastic properties of Nafion. Nguyen *et al* [35] attributes the hysteresis between absorption and desorption to an effect known as “skin effect”. This is due to collapse of pore structure during desorption process, which causes more water to be trapped within the pores of Nafion membrane. Future work includes studying this phenomenon at a more fundamental level and obtain similar curves at different temperatures.

5.4.4 Membrane Pretreatment Effect

Figures 5.9 and 5.10 shows the effect of four different pretreatments on water sorption characteristic of the Nafion membrane at 30 ^{o}C and 90 ^{o}C, respectively. Thus, the equilibrium sorption isotherm was obtained for a) untreated Nafion sample, b) sample heated at 30 ^{o}C and c) 110 ^{o}C for 24 hours in vacuum, and d) sample hot pressed at 170 ^{o}C. The hot press pretreatment is very important especially during MEA preparation for fuel cell testing. Also the vacuum treatment ensures that the membrane is as dry as possible.

The other pretreatment effects were selected as common conditions for synthesizing membranes for high temperature operation. The pretreatment of the Nafion membrane substantially affects the water sorption behavior. For sorption at 30 ^{o}C (Figure 5.9), the sorption amount for both untreated and sample vacuum heated at 30 ^{o}C is rather similar. The hot pressed membrane exhibited the lowest sorption, which is significant in that the procedure for preparing MEA might result in reduced performance. Further, vacuum heating the sample at 110 ^{o}C lowers the amount of water sorbed.

For sorption at 90 ^{o}C, interesting differences were observed (Figure 5.10). The membrane heated at 110 ^{o}C exhibited highest water sorption. Again the sorption for both untreated and sample vacuum heated at 30 ^{o}C was similar. The hot pressed membrane again showed the lowest sorption isotherm. Hence, the water sorption for Nafion membrane depends both on the pretreatment procedure and the sorption temperature. The physical structure of Nafion polymer changes with pretreatment and affects the sorption behavior. Also, for the similar pretreatment procedure, the sorption amount is remarkably different when the sorption temperature is varied. An example of variation of membrane properties at different humidification and temperature is already shown in Figure 5.6, wherein the *E* decreases both with water activity and temperature. Thus, a rigorous study of the effect of pretreatments on the thermomechanical properties of Nafion membrane is called for to further elucidate the observed results.

5.5 Conclusions

From the results obtained, TEOM seems to be a novel technique for investigating sorption-desorption behavior of Nafion membrane for various solvents. Further, the pretreatment study allows determining processing steps to be considered while synthesizing membranes to obtain best fuel cell performance. The results obtained are accurate and reproducible. Future work includes utilizing TEOM to screen various candidates, both polymer and inorganic powders, for higher water uptake to design high temperature proton exchange membrane. Overall, TEOM can be an effective tool in studying both dynamic and equilibrium behavior of Nafion membrane, in particular, for fuel cell applications.

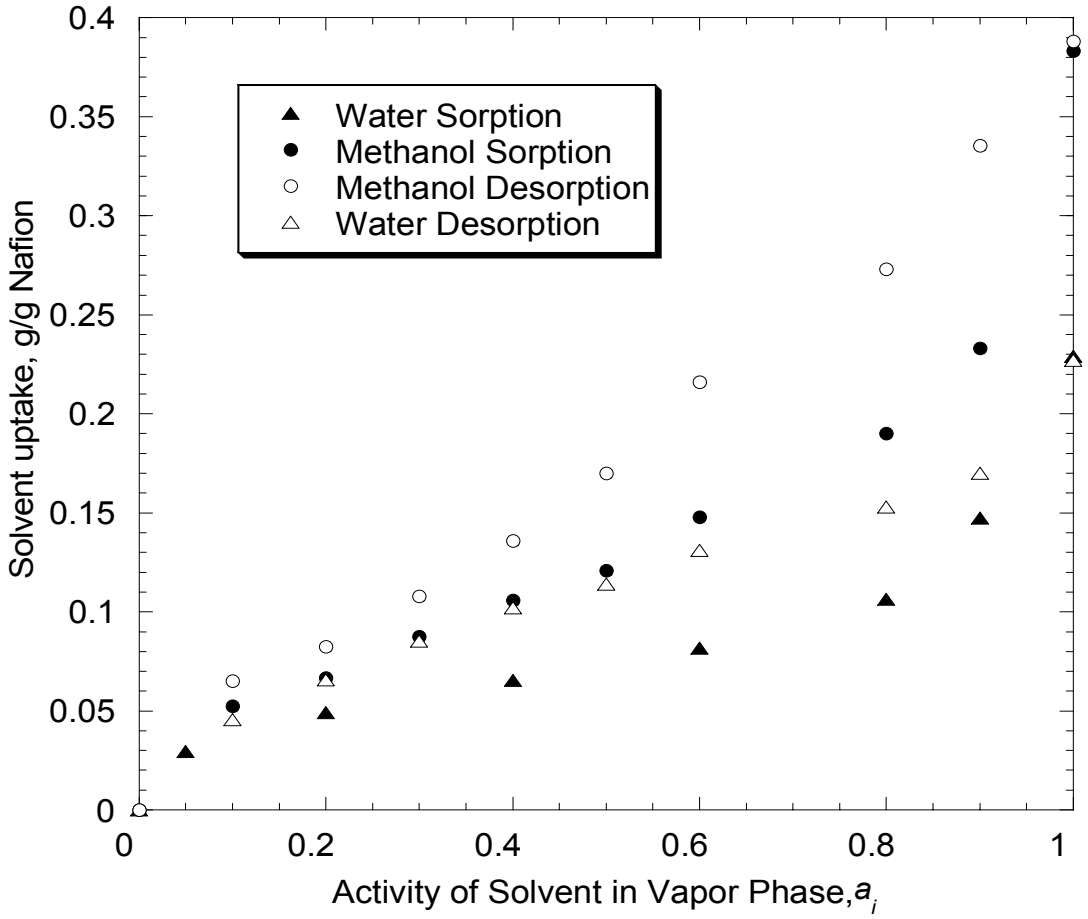

Figure 5.8 Sorption-Desorption characteristic for water and methanol vs. activity of solvent vapor for Nafion membrane at 30 ^{o}C (circle: methanol, triangle: water).

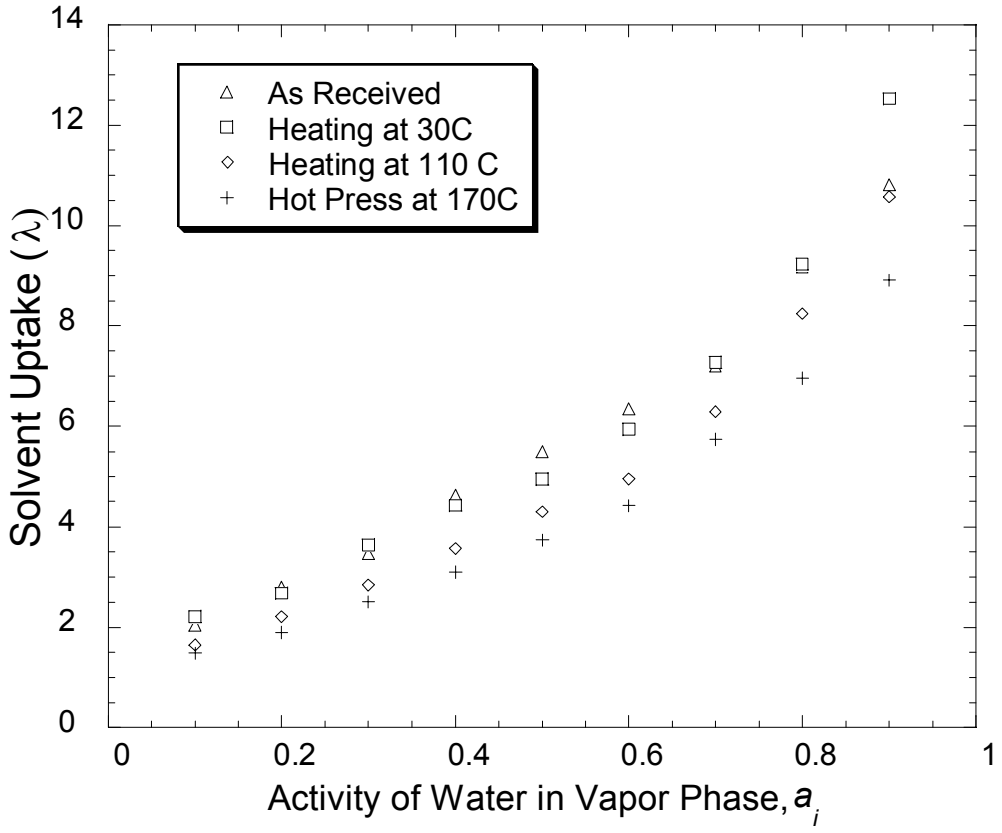

Figure 5.9 Effect of pretreatment procedures on water uptake vs. activity of water vapor for Nafion membrane at 30 ^{o}C

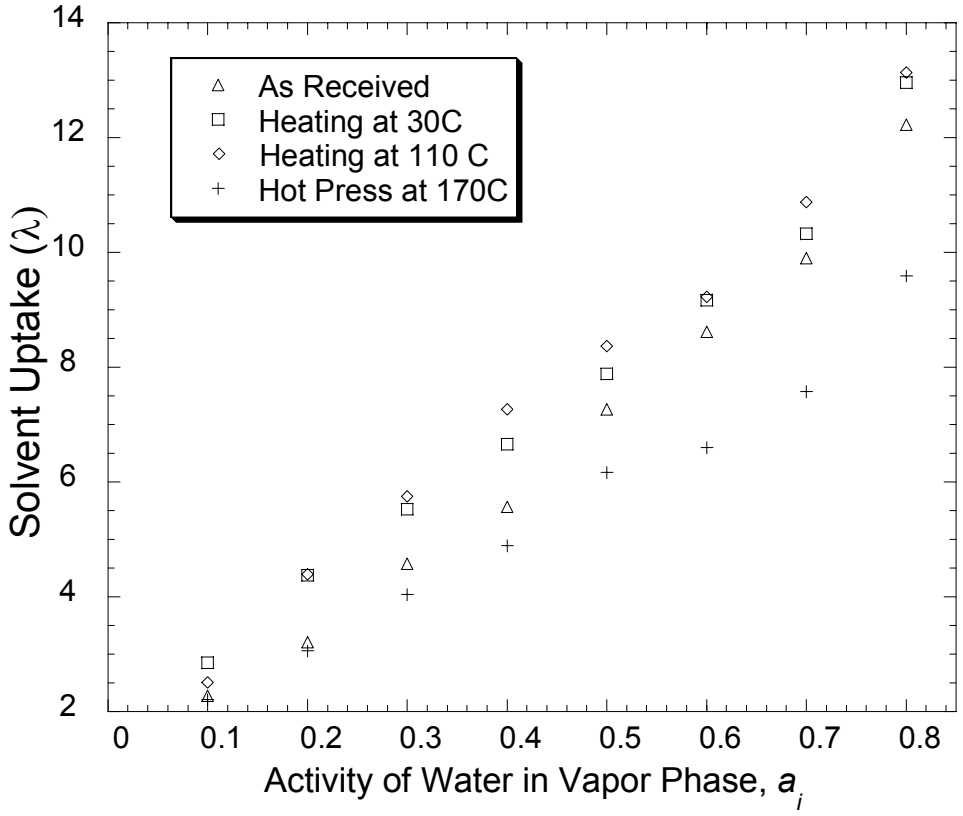

Figure 5.10 Effect of pretreatment procedures on water uptake vs. activity of water vapor for Nafion membrane at 30 ^{o}C

5.6 References

[1] K. D. Kreuer, On the development of proton conducting polymer membranes for hydrogen and methanol fuel cells, J. Membr. Sci., 185 (2001) 29.

[2] A. J. Appleby, and F.R. Foulkes, Fuel Cell Handbook, Van Nostrand Reinhold, New York, 1989.

[3] M. Doyle, M. E. Lewittes, M. G. Roelofs, and S. A. Perusich, Ionic Conductivity of Nonaqueous Solvent-Swollen Ionomer Membranes Based on Fluorosulfonate, Fluorocarboxylate, and Sulfonate Fixed Ion Groups, J. Phys. Chem. B, 105 (2001) 9387.

[4] T. Thampan, S. Malhotra, H. Tang, and R. Datta, Modeling of Conductive Transport in Proton- Exchange Membranes for Fuel Cells, J. Electrochem. Soc., 147(9) (2000) 3242.

[5] T. A. Zawodzinski, J. Davey, J. Valerio, and S. Gottesfeld, The water content dependence of electro-osmotic drag in proton-conducting polymer electrolytes, Electrochim. Acta, 40 (1995) 297.

[6] M. Doyle, L. Wang, Z. Yang, and S. K. Choi, Polymer Electrolytes Based on Ionomer Copolymers of Ethylene with Fluorosulfonate Functionalized Monomers, J. Electrochem. Soc., 150 (11) (2003) D185.

[7] T. E. Springer, T. A. Zawodzinski, and S. Gottesfeld, Water uptake by and transport through Nafion 117 membranes, J. Electrochem. Soc**.,** 140 (1993) 1041.

[8] T. E. Springer, T. A. Zawodzinski, and S. Gottesfeld, A comparative study of water uptake by and transport through ionometric fuel cell membranes, J. Electrochem. Soc., 140 (1993) 1981.

[9] J. T. Hinastu, M. Mizuhata, and H. Takenaka, Water uptake of perfluorosulfonic acid membranes from liquid water and water vapor, J. Electrochem. Soc., 141 (1994)1493.

[10] D. R. Morris, and X. Sun, Water-sorption and Transport Properties of Nafion 117H, J. Applied Poly. Sci., 50 (1993) 1445.

[11] D. Nandan, H. Mohan, and R. M. Iyer, Methanol and water uptake, densities, equivalental volumes and thicknesses of several uni- and divalent ionic

perfluorosulphonate exchange membranes (Nafion 117) and their methanol- water fractionation behavior at 298K, J. Membr. Sci.,71(1992) 69.

[12] P. Choi and R. Datta, Sorption in Proton Exchange Membranes. An explanation of Schroeder's Paradox, J. Electrochem. Soc., 150 (12) (2003) E601.

[13] T. A. Zawodzinski, L. O. Sillerud, and S. Gottesfeld, Determination of water diffusion coefficients in perfluorosulfonate ionometric membranes, J. Phys. Chem., 95 (1991) 6040.

[14] Y. Kawano, Y. Wang, R. A. Palmer, and S. R. Aubuchon, Stress-Strain Curves of Nafion Membranes in Acid and Salt Forms, Polímeros, 12 (2) (2002) 96.

[15] X. Ren, T. E. Springer, and S. Gottesfeld, Water and Methanol Uptakes in Nafion Membranes and Membrane Effects on Direct Methanol Cell Performance, J. Electrochem. Soc., 147(1) (2000) 92.

[16] C. M. Gates, and J. Newman, Equilibrium and Diffusion of Methanol and Water in a Nafion 117 Membrane, AIChE J., 46 (2000) 2076.

[17] X. Ren, P. Zelenay, S. Thomas, J. Davey , and S. Gottesfeld , Recent advances in direct methanol fuel cells at Los Alamos National Laboratory, J. Power Sources, 86 (2000)111.

[18] K. Scott, W. M. Taama, P. Argyropoulos, and K. Sundmacher, The impact of mass transport and methanol crossover on the direct methanol fuel cell, J. Power Sources, 83 (1999) 204.

[19] A. Heinzel, and V. M. Barragán, A review of the state-of-the-art of the methanol crossover in direct methanol fuel cells, J. Power Sources, 84 (1999) 70.

[20] H. R. Zelsmann, and M. Pineri, Water self-diffusion coefficient determination in an ion- exchange membrane by optical measurement, J. Appl. Polym. Sci., 41 (1990) 1673.

[21] S. Malhotra, and R. Datta, Membrane-supported nonvolatile acidic electrolytes allow higher temperature operation of proton-exchange membrane fuel cells, J. Electrochem. Soc., 144 (1997) L23.

[22] T. Thampan, N. H. Jalani, P. Choi, and R. Datta, Systematic Design of Higher Temperature Composite Proton Exchange Membranes, J. Electrochem. Soc., 152(2) (2005) A316.

[23] De Chen, A. Grønvold, H. P. Rebo, K. Moljord, and A. Holmen, Catalyst deactivation studied by conventional and oscillating microbalance reactors, Applied Catalysis A. General, 137(1996) L1.

[24] W. Zhu, J. M. Graaf, L. J. P. Broeke, F. Kapteijn, and J. A. Moulijn, TEOM: A Unique technique for measuring adsorption properties. Light Alkanes in silicalite-1, Ind. Eng. Chem. Res.,37 (1998) 1934.

[25] J. M. Gere, and S. P. Timoshenko, Mechanics of Materials. 4th ed. Boston: PWS Publishing Company (1997).

[26] E. Voltera, and E. C. Zachmanoglou, Dynamics of Vibrations, Columbus, Charles E., Merrill Books, Inc.(1965).

[27] R. B. Moore III, and C. R. Martin, Procedure for preparing solution-cast perfluorosulfonate ionomer films and membranes, Anal. Chem., 58 (1986) 2569.

[28] R. B. Moore III, and C. R. Martin, Chemical and morphological properties of solution- cast perfluorosulfonate ionomers, Macromolecules, 21 (1988) 1334.

[29] K. Arata, Preparation of superacids by metal oxides for reactions of butanes and pentanes, Applied Catalysis A. General, 146 (1996) 3.

[30] D. Rivin, C. E. Kendrick, P. W. Gibson, and N. S. Schneider, Solubility and transport behavior of water and alcohols in Nafion, Polymer, 42 (2001) 623.

[31] P. Choi, N. H. Jalani, and R. Datta, Thermodynamics and Proton Transport in Nafion. Part I. Membrane Swelling, Sorption, and Ion- Exchange Equilibrium., J. Electrochem. Soc., 152(3) (2005) E84.

[32] P. Choi, N. H. Jalani, and R. Datta, Thermodynamics and Proton Transport in Nafion. Part II. Proton Diffusion Mechanisms and Conductivity, J. Electrochem. Soc., 152 (8) (2005) E123.

[33] Yin-Yan Huang, T. J. McCarthy, and Wolfgang M. H. Sachtler, Preparation and catalytic testing of mesoporous sulfated zirconium dioxide with partially tetragonal wall structure, Applied Catalysis A: General, 148 (1) (1996) 135.

[34] K. K Pushpa, D. Nandan, and R. M. Iyer, Thermodynamics of water sorption by perfluorosulfonate (Nafion 117) and polystyrene-divinylbenzene sulphonate (Dowex 50W) ion exchange resins at 298 K, J. Chem. Soc., Faraday Trans. I, 84 (1988) 2047.

[35] T. V. Nguyen and N. Vanderborgh, The rate of isothermal hydration of polyperfluorosulfonic acid membranes, J. Membr. Sci., 142 (1998) 235.

Chapter 6

The effect of Equivalent Weight, Temperature, Cationic Forms, Sorbates, and Nanoinorganic Additives on the Sorption Behavior of Nafion

In this chapter, TEOM (Tapered element oscillating microbalance) is utilized to study the effect of equivalent weights (960 -1200), temperature (30- 90 ^{o}C), various cationic forms (H^+, Li^+, Na^+, K^+ and Cs^+), sorbates (water, methanol, ethanol, and propanol), and inorganic additives on sorption behavior of Nafion membrane. It is observed that water sorption increases with a decrease in EW and an increase in the sorption temperature. This is due to the increase in acid sites for sorption and a decrease in the Young's modulus of the membrane with the increase in temperature. Further, sorption decreases with the increase in size of the counter ion due to a corresponding decrease in ion hydration capacity due to a decrease in the ionization equilibrium constant constant. Also, it is observed that the incorporation of acidic inorganic additives (ZrO_2, TiO_2, and SiO_2) via sol gel methods provides higher water sorption amount at 90 ^{o}C, which is crucial for high temperature operations of fuel cells. This chapter is published in J. Membrane Sci., 264(1-2) 167-175 (2005).

6.1 Introduction

Nafion in protonic form is widely used as the polymer electrolyte in proton exchange membrane (PEM) fuel cells [1-6] as well as in chloro-alkali cells in sodium form. The properties that make the Nafion membrane indispensable are the combination of good water uptake, ion-exchange capacity, proton conductivity, low gas permeability, and excellent electrochemical stability. The amount of water sorbed in the Nafion membrane as a function of relative humidity (RH) is critical as the proton conductivity depends directly on the water content of the membrane which determines the fuel cell performance

[7-8]. The structure of Nafion (Figure 6.1) plays an important role in the sorption of water. Structurally, Nafion consists of a hydrophobic polytetrafluoroethylene (PTFE) backbone with pendant side chains of perfluorinated vinyl ethers terminating with hydrophilic ion-exchange groups. This causes water segregation within Nafion membrane in clusters away from backbone, which results in enhanced conductivity via bulk diffusion. The ion exchange capacity or equivalent weight (*EW*) of Nafion membrane, defined as grams of dry polymer per mole of acid groups, can be modified by changing the ratio of these two components [9-12].

We have recently published our theoretical work on predicting the amount of water sorbed per sulfonic acid site in Nafion membrane based on thermodynamic equilibrium of water in the vapor and sorption phases [13-15]. In the model, the total number of water molecules per acid site in the polymer λ_i is obtained as: *i*) those that are strongly, or chemically, bound to the acid site of the polymer, represented by λ_i^C, and *ii*) those that are free to physically equilibrate between the polymer and the fluid phase, λ_i^F

$$\lambda_i = \lambda_i^C + \lambda_i^F \tag{6.1}$$

For solvent (*i*)-polymer membrane (*M*) systems, the activity of free solvent in the membrane phase $a_{i,M}^F$ is assumed to be given by the Flory-Huggins model derived on the basis of a quasi-crystalline lattice structure [14]. The swelling pressure within the membrane pore may be related to network contractile pressure based on the statistical theory of polymer elasticity. As the membrane imbibes more water, the membrane matrix expands, exerting a swelling pressure on the pore liquid, which in turn affects its chemical potential and limits the equilibrium swelling. The driving force for swelling is the tendency for the water to dilute the polymer network and equalize its chemical potential within polymer and the exterior. The opposing force is due to the swelling pressure within the membrane that depends upon the elastic modulus, *E*, of the membrane, and tends to limit the water ingress. The swelling pressure (Π_M) can be obtained by treating the swelling as a non-affine 'inflation' of the hydrophobic matrix by small aggregates of water molecules, which is in keeping with the structural model of polymer swelling [14], resulting in

$$\Pi_M = \frac{2}{3} G\left(\Phi_M{}^{1/3} - \Phi_M{}^{7/3}\right) \tag{6.2}$$

where Φ_M the volume fraction of polymer and G is the shear modulus of polymer matrix given by the classical theory of polymer elasticity. The shear modulus G is related to Young's modulus E and Poisson's ratio ν by:

$$E = 2(1+\nu)G \tag{6.3}$$

Assuming ν = 0.5 for Nafion®, the shear modulus is, thus, one third of Young's modulus. More details on the model can found elsewhere [13-14].

A curious phenomenon is that Nafion adsorbs around 22 water molecules per acid site from liquid water, while it adsorbs only around 14 water molecules from saturated vapor. This is the so called Schroeder's Paradox [13, 16-17], which is explained within the framework of the model by the additional Kelvin pressure exerted by the curved vapor-liquid interface in a pore.

The factors affecting the extent of the solvent uptake by Nafion are temperature, ion- exchange capacity, pretreatment of membrane, cationic forms of the membrane, and the physical state of absorbing water, i.e., the adsorption is from water in liquid or vapor phase [18]. Many investigators have studied the hydration, swelling, and drying of Nafion under different conditions, based on spectroscopic, gravimetric and other methods [21-42]. It has been found that the adsorption from liquid phase is quicker and more extensive as compared to that from vapor phase. It has also been shown that pretreatments done during membrane synthesis and purifications causes micro structural changes in the membrane, which affect its sorption behavior. Swelling of Nafion has been accomplished using a wide variety of solvents with interesting results, including a swelling of 360 % with tributylphosphate (TBP). Experiments done with the conventional gravimetric methods are, however, rather slow and provided data with considerable scatter, which makes it difficult to systematically investigate effect of changing conditions. Results from these methods are influenced by the flow patterns, bypassing, and incomplete contact of the gas with the sample. Further the gravimetric equipment generally has limited temperature and pressure range. There is also significant reduction in mass resolution at high temperatures. The lack of accurate experimental methodology, thus, limits our knowledge of the subtler aspects of the sorption behavior of Nafion. There is thus, lack of systematic investigation of effect of different sorbents, temperature, equivalent weight, different cationic forms of membrane, and sorbate pretreatments on Nafion. Hence, this provided us with the motivation to

investigate alternate technique which can accurately reproduce, and rapidly provide meaningful sorption data for Nafion systematically under varying conditions.

We, thus recently described the use of a novel and rapid technique, namely the tapered element oscillating microbalance (TEOM) to accurately measure equilibrium solvent sorption-desorption isotherms for PEMs [43]. In continuation of our efforts to develop an understanding of the swelling behavior of Nafion, here we describe results on the systematic investigation of the effect of: i) equivalent weight, 960, 1100 and 1200 ii) temperature, 30-to-90 ^{o}C, on water sorption for 1100 EW membrane, and iii) cationic forms, H^+, Li^+, Na^+, K^+ and Cs^+ on different sorbates, water, methanol, ethanol and propanol on the sorption characteristics of Nafion membranes. Further, we also investigated the water sorption behavior of nanocomposite Nafion/ MO_2 (M = Zr, Ti, Si) at 90 ^{o}C in our efforts to design membranes for operation at higher temperature and low relative humidity conditions of fuel cells [44-45].

6.2 Experimental Section

6.2.1 TEOM Apparatus

The tapered element oscillating microbalance (TEOM) Series 1500 Pulse Mass Analyzer (PMA) purchased from Rupprecht & Patashnick Co., Inc., Albany, NY, was utilized to study the equilibrium solvent sorption behavior for Nafion membranes under various conditions mentioned above earlier. This technique provides dynamic mass change of sample contained in a tapered oscillating fixed-bed while the vapor laden gas passes through the sample. The mass change measurement is based on inertial forces rather than gravity. Additional details of the apparatus can be found elsewhere [43, 46, 47].

The active element in TEOM is the tapered test bed containing the sample which vibrates constantly at its natural frequency of oscillation. A feedback system maintains the oscillation of the tapered bed. The frequency of oscillation is measured optically with a transmitter and receiver located on the opposite sides of the oscillating test bed. The change in mass of system Δm for the corresponding change from initial frequency f_o to final frequency f_f is

$$\Delta m = \kappa_o \left(\frac{1}{f_f^2} - \frac{1}{f_o^2} \right) \qquad [6.4]$$

Thus, the frequency decreases with an increase in the mass, and vice versa [46]. The spring constant κ_o depends weakly on temperature. For instance, change in the spring constant for a temperature range of 30 – 250 ^{o}C corresponds to a mass change of 1×10^{-5} g. Thus, the effect of temperature on the effective spring constant is neglected here [47].

The TEOM experimental set up is shown schematically in Figure 6.2. Helium gas is bubbled through sorbate kept in a bottle (saturator) and is combined with another stream of dry helium gas downstream for obtaining the desired relative humidity. All the gas flows are controlled by means of mass flow controllers. A preheated bath of ethylene glycol – water (50: 50 by volume) is circulated around saturator to maintain the desired temperature, in the range of 25 ^{o}C to 115 ^{o}C. The temperature of sorbate in the saturator is monitored via a thermocouple connected to a digital multimeter. As shown in Figure 5.2, a purge helium stream is used to avoid condensation at the external surface of the test bed and back flow of exiting gas stream from the test bed.

The real-time dynamic mass change of the sample in the TEOM test bed can be analyzed graphically using LabView 5.0 program, obtained from National Instruments Corporation. Inside the TEOM, there are two temperature-controlled zones. The pre-heat zone controls the inlet gas stream temperature and the other zone controls the temperature of the tapered element and the sample bed. The TEOM performance is quantified in terms of the normalized standard deviation (NSD). The NSD is an indicator of "random noise" and depends upon how well the sample is packed in the test bed and whether there is other mechanical or electrical disturbance. For the equilibrium sorption experiment, a 10 s average time with 12 recording values (approximate gate time of 0.8 s) gives a typical value of NSD below 3×10^{-6} ppm.

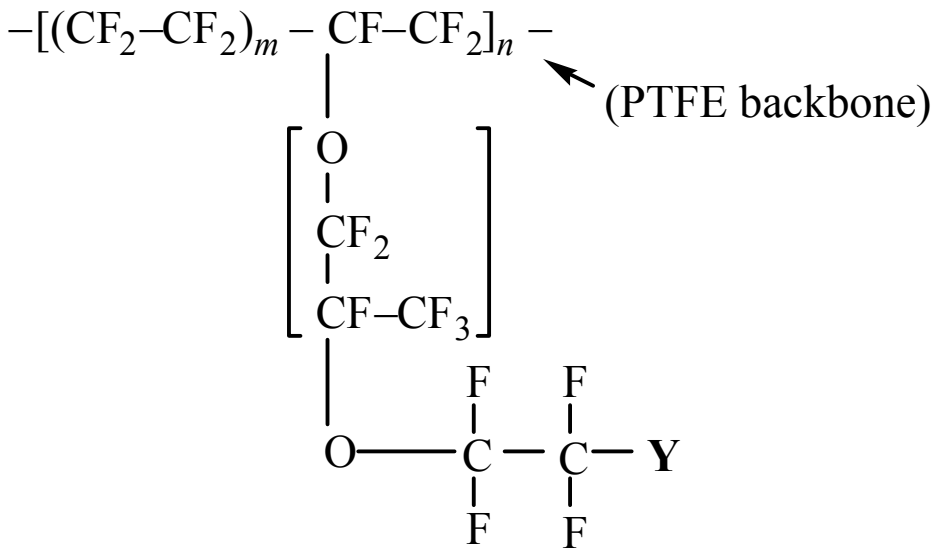

Y= -SO_3M^+ , where $M^+ = H^+, Li^+, Na^+, K^+, Cs^+$

Figure 6.1 Structural details of Nafion membrane.

6.2.2 Membrane preparation

The Nafion membrane was purchased from Aldrich and then subjected to a pretreatment procedure based on the objective of test [48-49]. For studying the effect of EW on water sorption, 5 wt % Nafion solution of different EW were purchased from Aldrich and pliable membranes were cast. The cast membrane was then placed in a convection oven at 100 ^{o}C for 15 minutes, in order to produce a solid membrane. The membrane was then removed from the glass dish with DI water, dried and then annealed in a Teflon sleeve at 170 ^{o}C at 10 tons for 15 minutes in a mechanical press (Carver Model C, Wabash IN). This processing step is necessary to produce pliant, insoluble membranes with mechanical properties similar to those of commercially available Nafion films. The resulting cast membrane had a thickness of around 50 μm. It was then boiled in 3 % H_2O_2 for half an hour to remove any organic impurities. Then it was heated at 60 ^{o}C in 0.5 M sulphuric acid solution for half an hour to convert to H^+ form. Finally, it was heated at 60 ^{o}C in deionized water for 1 hour. After boiling the membrane, it was washed thoroughly with DI water to remove any excess acid residues. It was finally dried at room temperature by leaving the membrane untouched.

In order to convert the H^+ form of membrane to other cationic forms, the membrane was boiled in 1 M solution of LiOH, NaOH, KOH, and $CsCO_3$ for 12 hours to get the corresponding cationic form. The membranes were then washed with water to remove excess electrolyte, and wiped with Kim wipes.

6.2.3 NanoComposite Nafion/ MO_2 Synthesis

The synthesis of a Nafion-MO_2 (M = Zr, Si and Ti) nanocomposite PEM was accomplished via *in situ* sol-gel synthesis wherein the host PEM serves as a template that directs the morphology and particle size of the oxide in the PEM matrix, resulting in nano-sized particles [45,51-52]. As received, Nafion membranes (Sigma-Aldrich Corp., St. Louis MO) were boiled in 3 wt % H_2O_2 for 1 hour and then rinsed in water. They were then immersed in 1 M NaOH solution and heated for 6 hours to convert the membrane to Na^+ form. This ensures mechanical strength of Nafion membrane for withstanding the subsequent processing steps. Then the membranes were rinsed in DI water at 60 ^{o}C for 30 minutes.

The purified and Na^+ form membranes were then placed in a vacuum oven and heat-treated at 110 ^oC for 12 hours. Next, they were immersed in 2:1 ethanol/H_2O solution for an hour. This serves to further swell the pores of the membrane in order to maximize the absorption of the precursor solution. The membranes were removed and immersed in 0.5 M 70 wt % Zirconium (IV) propoxide solution (purchased from Aldrich) for 6 hours and then rinsed in acetone several times in order to clean the membrane surface. The membranes were then removed and heated at 110 ^oC in vacuum for 24 hours to complete the condensation reactions. Then the membranes were converted to H^+ form by boiling in 0.5 M H_2SO_4 for 6 hours. This nanocomposite PEM is denoted here as "Nafion- ZrO_2 sol-gel". Similarly, Titanium (IV) tert-butoxide and Tetraethyl orthosilicate (TEOS) were the precursors utilized to synthesize "Nafion- TiO_2 sol-gel" and "Nafion- SiO_2 sol-gel" membranes, respectively. The membranes synthesized by this method are completely transparent and homogenous.

6.2.4 Sorption Measurements

A known mass of pretreated membrane sample was cut into small pieces (1.5 mm x 1.5 mm) using a doctor blade and loaded carefully in the test bed. Quartz wool, purchased from Rupprecht & Patashnick Co., Inc., was used as filler material to keep the sample firmly packed, which is necessary so that the sample does not rattle around affecting the oscillations of the bed. Typically, about 20 mg of membrane sample was packed in the test bed to get best reproducibility.

The sorbate sorption data were obtained by a stepwise increase of the flow rate of humidified inlet gas stream, which changes the RH or activity of the feed gas at fixed temperatures. During the experiments, the He purge gas was kept at around 120-150 sccm, while the carrier gas through saturator was maintained at 10-15 sccm, with the dry He gas varying from 0 to 80 sccm depending on RH required in the test bed. The RH was calculated from the gas flow rates and the saturator temperature. After loading the sample, the inlet flow was set to the desired value and sufficient time was allowed for the sample to reach steady state, typically 10 - 30 min. After waiting for sufficient period, if the mass of the test bed did not change for more than 1%, then the equilibrium was assumed. The mass change corresponds to the amount of solvent adsorbed. Thus, the change in sample mass

for the set condition was recorded and then the inlet flow was adjusted to get next desired RH. The total mass of sample increases as it adsorbs solvent. This procedure was followed for all the experiments. The equilibrium sorption data is reported here as ratio of mass of absorbed solvent to mass of dry Nafion. It can, of course, equally well be expressed in terms of λ, defined as the ratio of moles of absorbed solvent per mole of sulfonic acid groups within Nafion.

6.3 Results and Discussion

6.3.1 Effect of Equivalent Weight

The equivalent weight (*EW*) of Nafion membrane is related to the number density of acid sites. It is well known that the overall proton conduction in Nafion membrane increases with decrease in EW up to a point, beyond which over swelling causes a reduction in conductivity due to dilution. Hence, it is important to study the effect of water activity on water sorption behavior of the commercially available EWs, 960, 1100 and 1200. Figure 6.2 shows the effect of EW on water sorption behavior of Nafion membrane at 30 ^{o}C. The basic trend of the water sorption isotherm is similar for all three EWs membranes. It is observed, however, that with the decrease in EW, the amount of water sorbed in the membrane increases with greater difference at higher RH. At 0.8 water activity, for example, there was an increase of about 25 % in the amount of water sorbed from 1200 EW to 960 EW. This is because, the lower the EW, the higher is the acid group density and more acidic is the membrane. This increase in acid site density, results in increased water sorption and swelling of the membrane. Due to this, the sorption equilibrium is achieved at higher amount of water. It is important to note however, that the amount of water molecules per sulfonic acid site remains virtually unchanged with λ = 14 at 100 % RH from 1100 to 960 EW membranes (Figure 6.3). As a result, the actual mass of water adsorbed per gram of dry polymer increases. Similar trend for water sorption was observed at 90 ^{o}C, as shown in Figure 6.4.

The trend obtained shows that the membrane swells more at lower EW, there would be an optimum EW to achieve the highest proton conduction while maintaining the physical integrity of polymer matrix. The higher amount of water in the membrane makes

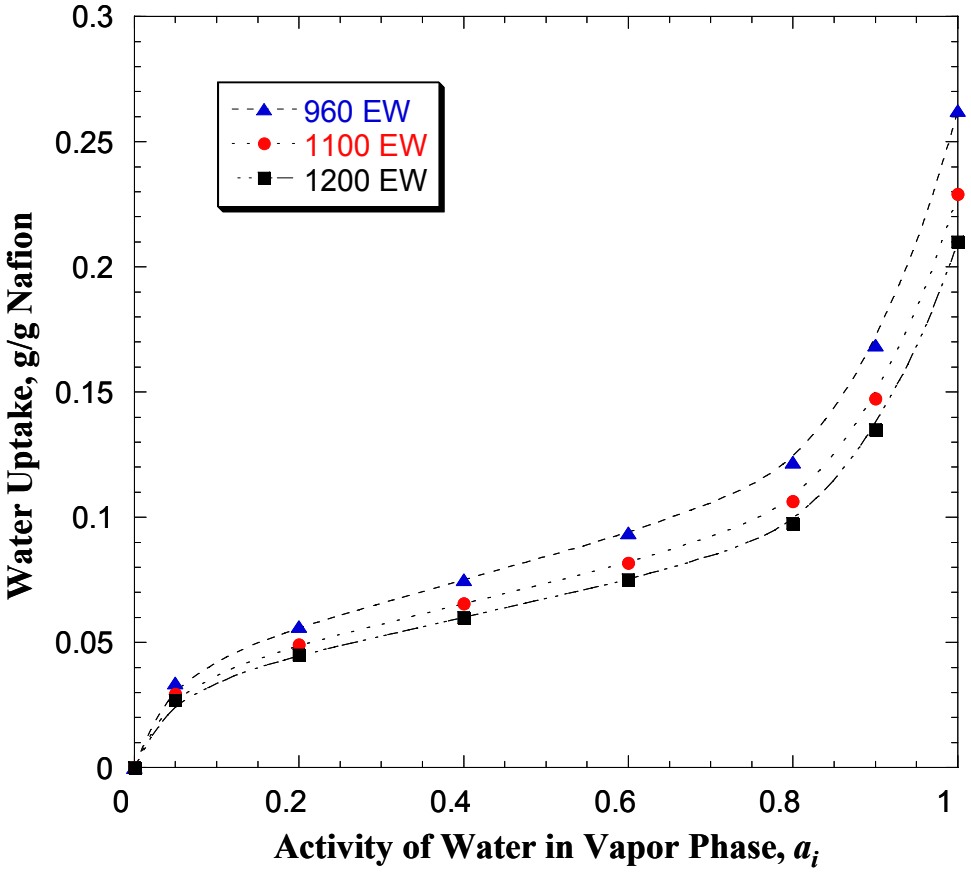

Figure 6.2 Effect of EW on water uptake (g/g Nafion) for different water activity conditions at 30 °C (triangle: EW=960, circle: EW=1100, and square: EW=1200).

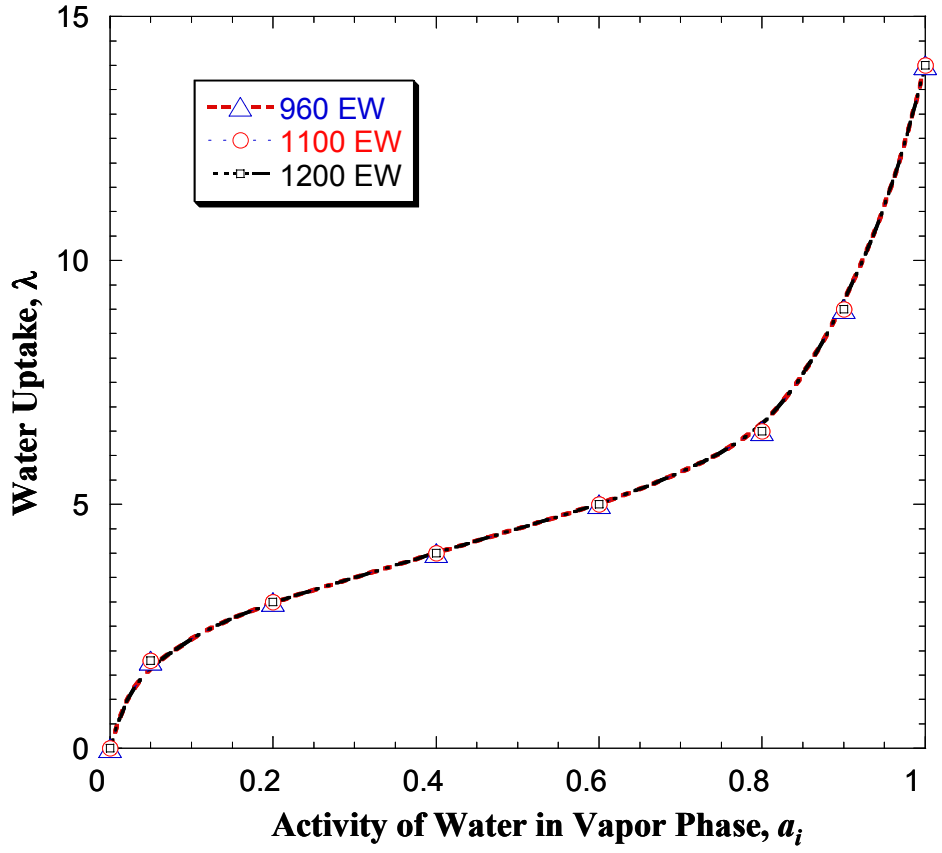

Figure 6.3 Effect of EW on water uptake (λ) for different water activity conditions at 30 °C (triangle: EW=960, circle: EW=1100, and square: EW=1200).

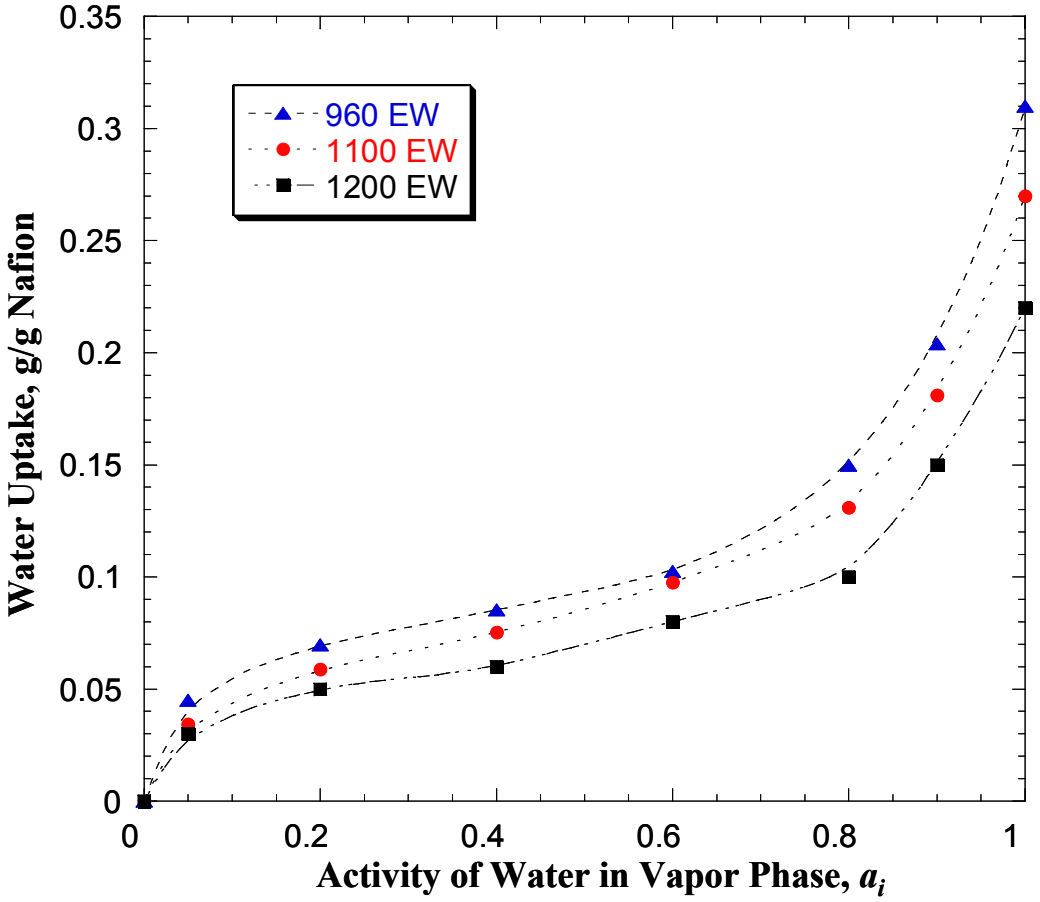

Figure 6.4 Effect of EW on water uptake for different water activity conditions at 90 °C (triangle: EW=960, circle: EW=1100, and square: EW=1200).

the membrane softer, *i.e*., their mechanical properties decrease, which affects the long-term stability of Nafion membrane. We have already published our experimental results [43] for the variation of Young's Modulus (*E*) with water activity and temperature determined by a novel vibrational technique of Optoelectronic Holography (OEH) described by us elsewhere [53]. It was observed that with an increase in the water activity, the membrane becomes softer, *i.e*., the *E* decreases. Similarly with an increase in temperature, the membrane matrix becomes more flexible, which also results in higher water sorption. This is evident when we predict the sorption data at 30 ^{o}C and 90 ^{o}C in the next section discussing the effect of temperature on sorption of Nafion membrane. Hence, it is essential to consider the thermomechanical properties in conjunction with water sorption behavior of membranes in order to design high temperature membranes that would exhibit high proton conduction and desirable performance in fuel cells. Further, although not shown here, *E* decreases with decreasing EW. Thus, although not evident in the range of EW investigated here, water sorption increases sharply at still lower EW, causing dilution of dissociated protons and a reduction in conductivity.

6.3.2 Effect of Temperature

The water sorption data were also obtained at different temperatures ranging from 30 ^{o}C to 90 ^{o}C. Using *E* data for Nafion membrane and theoretical model developed [13]; we can precisely predict water sorption at 30 and 90 ^{o}C as obtained in Figure 6.4. Figure 6.5 shows the effect of temperature on water sorption isotherm for 1100 EW Nafion membrane. The amount of water adsorbed increases gradually with temperature, especially with high water activity. Kawano *et al* have studied the stress-strain characteristics of Nafion membrane at different temperatures and found that the initial slope of the curves *i.e*., the *E* decreases with increasing temperatures, thus softening the membrane and allowing higher water uptake [20]. A lower *E* reduces the swelling pressure on the imbibed liquid thus equilibrating at higher sorbed amount. This is important experimental characterization for Nafion membrane because the durability of the membrane depends upon the thermomechanical properties as mentioned earlier.

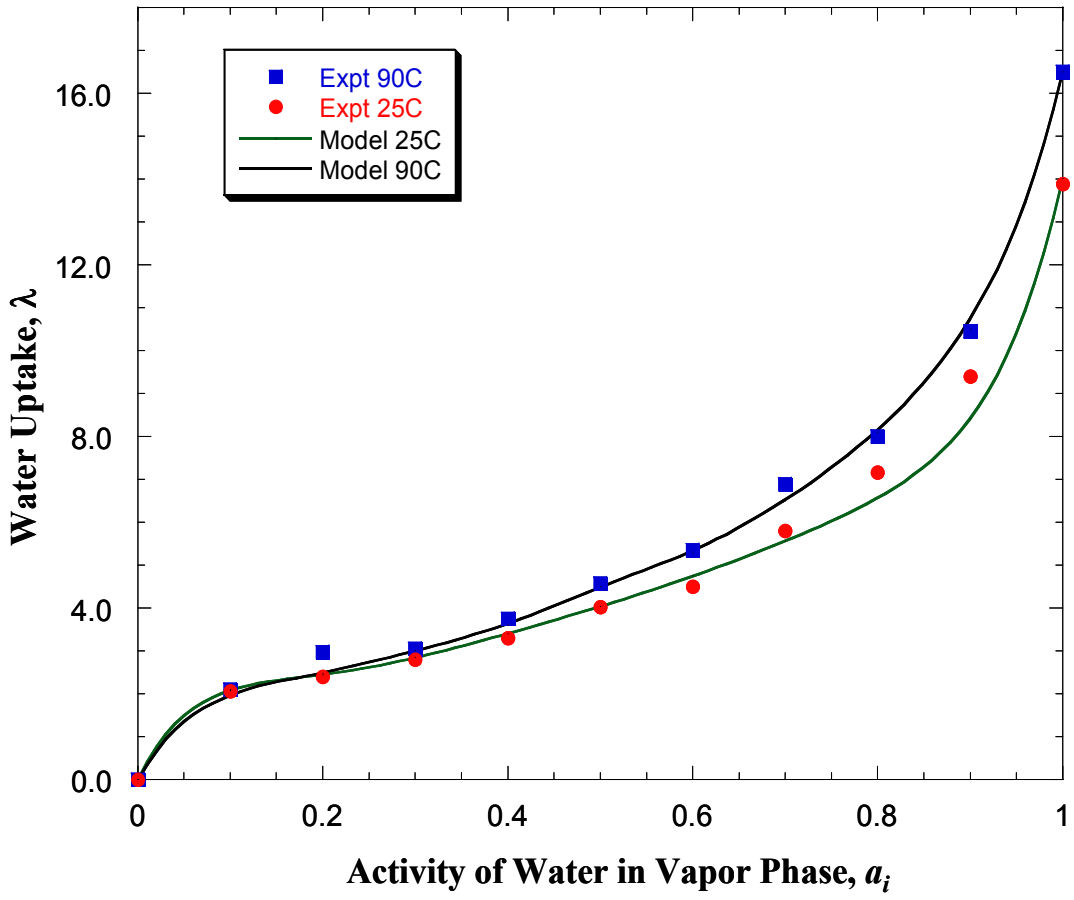

Figure 6.5 Effect of temperature on water uptake vs. activity of water vapor for Nafion membrane.

6.3.3 Effect of Different Cationic Forms

Nafion has wide applications in chloro alkali industry also; hence it is interesting to study the effect of various cationic forms of membrane on the sorbate sorption behavior. Thus, we have selected specific counter cations for systematic variation. Some the cations also have significance in separation processes in chloro alkali industry. Further, these are also of interest for naval applications, where the feed water contains all sorts of cations in the seawater. Figures 6.7-6.10 show the experimental sorption measurements obtained at 30 ^{o}C for different sorbates. In general, for water sorption (Figure 6.6), the following trend was observed: H^{+}> Li^{+}> Na^{+}> K^{+}> Cs^{+} in the order of decreasing water sorption isotherm. The trend is somewhat similar for other sorbates; methanol (Figure 6.7), ethanol(Figure 6.8), and propanol(Figure 6.9), with the exception that for methanol sorption (Figure 6.7), both H^{+} and Li^{+} forms of membrane exhibited similar sorption amount, and for ethanol (Figure 6.8) and propanol (Figure 6.9) sorption both K^{+} and Cs^{+} forms of membrane exhibited similar sorption amount.

The results obtained clearly show that the nature of the counterions dramatically influences the amount of solvent sorbed in dry membrane. From the trends obtained it can be concluded that the amount of water sorbed decreases due to a) reduction in the ionic hydration capacity from H^{+} to Cs^{+} (Table 1), b) increase in size of counter cations from Li^{+} to Cs^{+}, c) decrease in the charge density (charge per unit volume) from H^{+} to Cs^{+}, and d) decrease in swelling from H^{+} to Cs^{+} forms due to increase in Young's Modulus [20], causing similar number of solvent molecules to equilibrate at higher solvent activities.

The smaller the counter cation, i.e. larger the counter cation hydration energy, the higher the amount of solvent sorbed in the membrane. The ion hydration energies, cationic radius and water hydration number for each of cation are summarized in Table 6.1[54]. The size of proton is approximated with that of hydronium ion. It is seen that the hydration energy for H^{+} is twice the value to that of Li^{+}. This means that polar molecules like water and other alcohols are strongly attracted to smaller H^{+} ions.

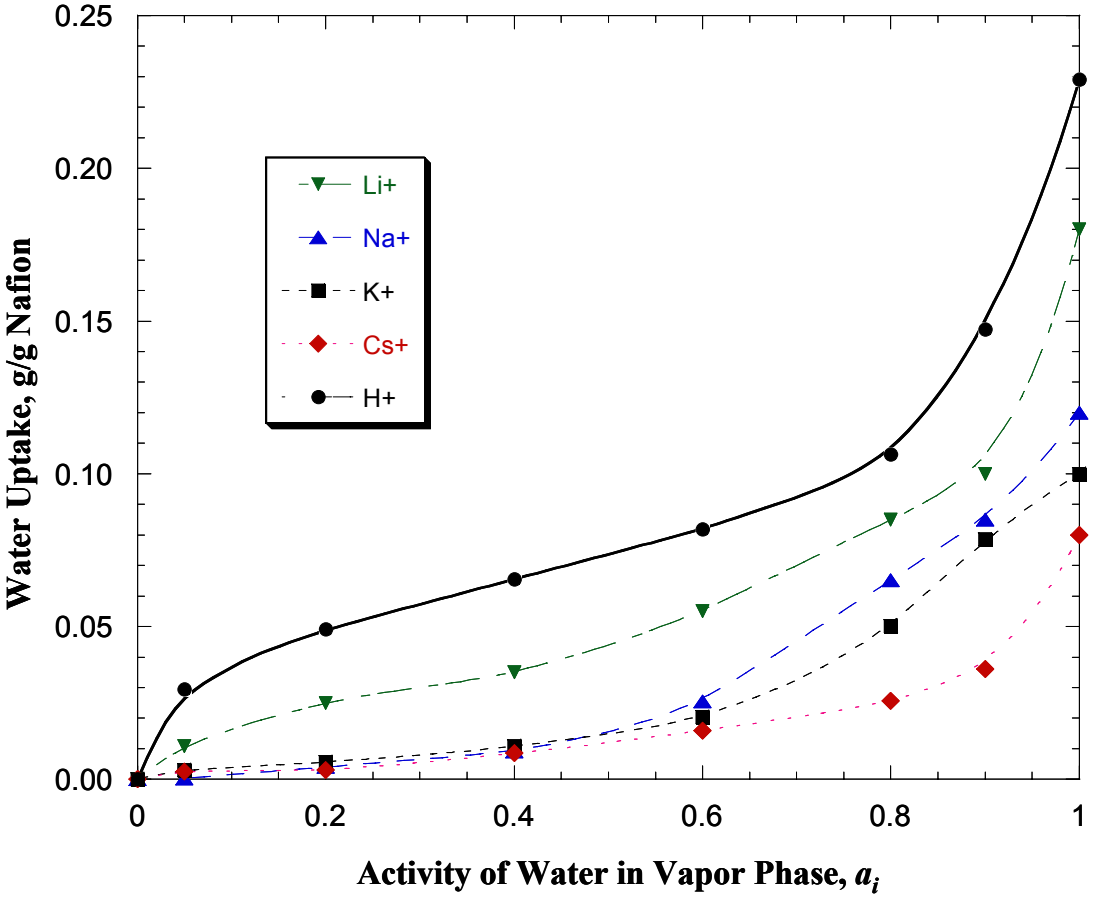

Figure 6.6 Effect of various cationic forms on water uptake vs. activity of water vapor for Nafion membrane at 30 ^{o}C.

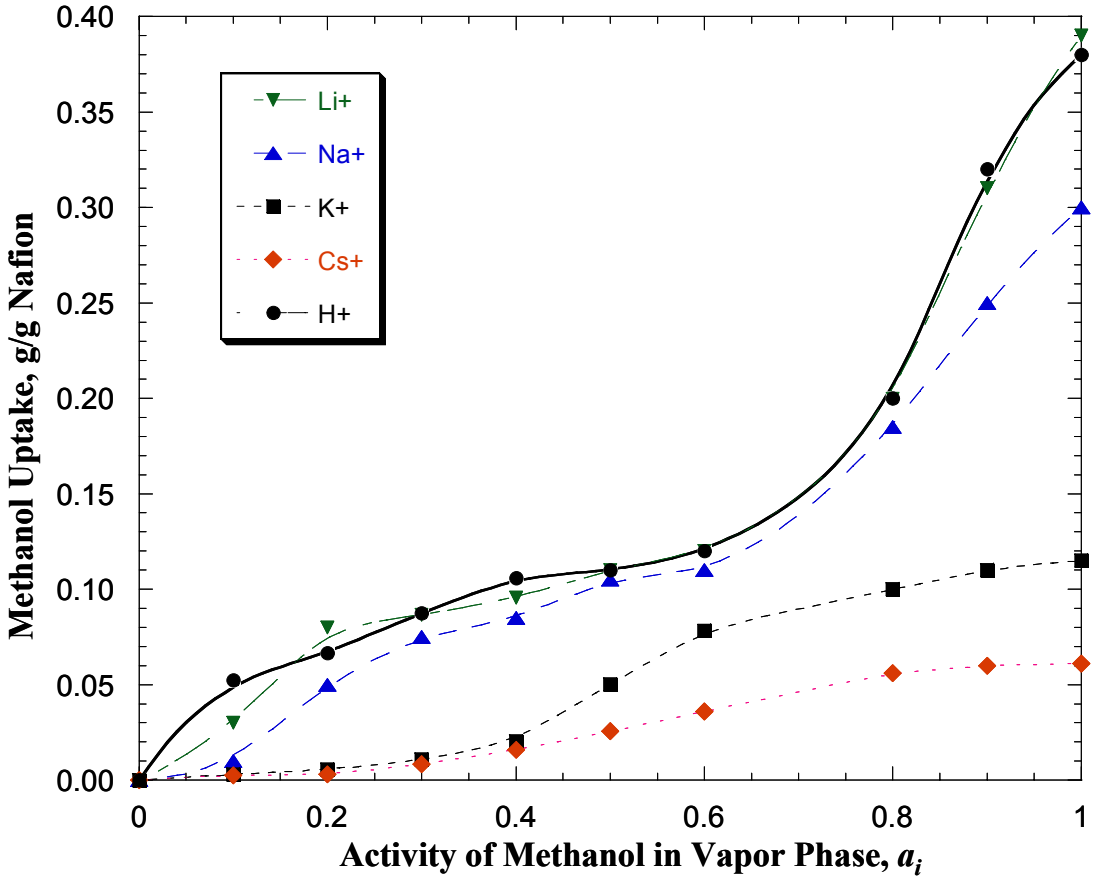

Figure 6.7 Effect of various cationic forms on methanol uptake vs. activity of methanol vapor for Nafion membrane at 30 ^{o}C .

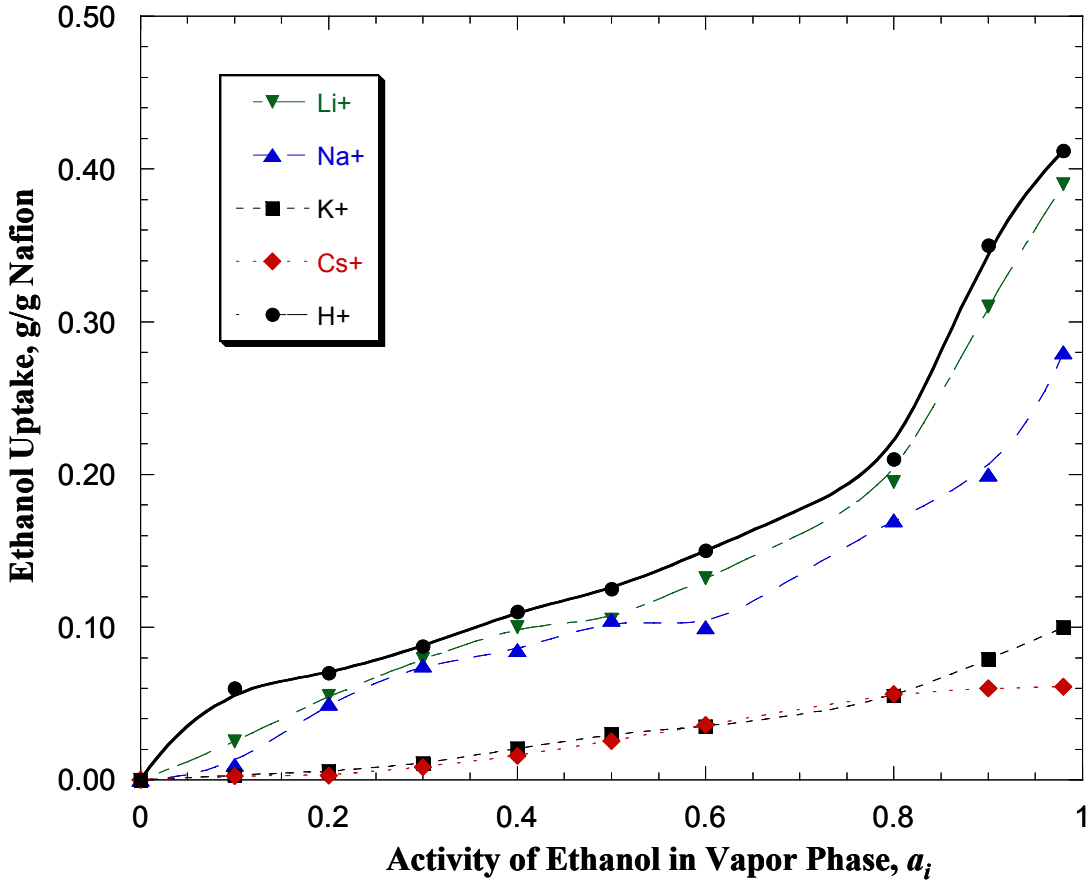

Figure 6.8 Effect of various cationic forms on ethanol uptake vs. activity of ethanol vapor for Nafion membrane at 30 ^{o}C .

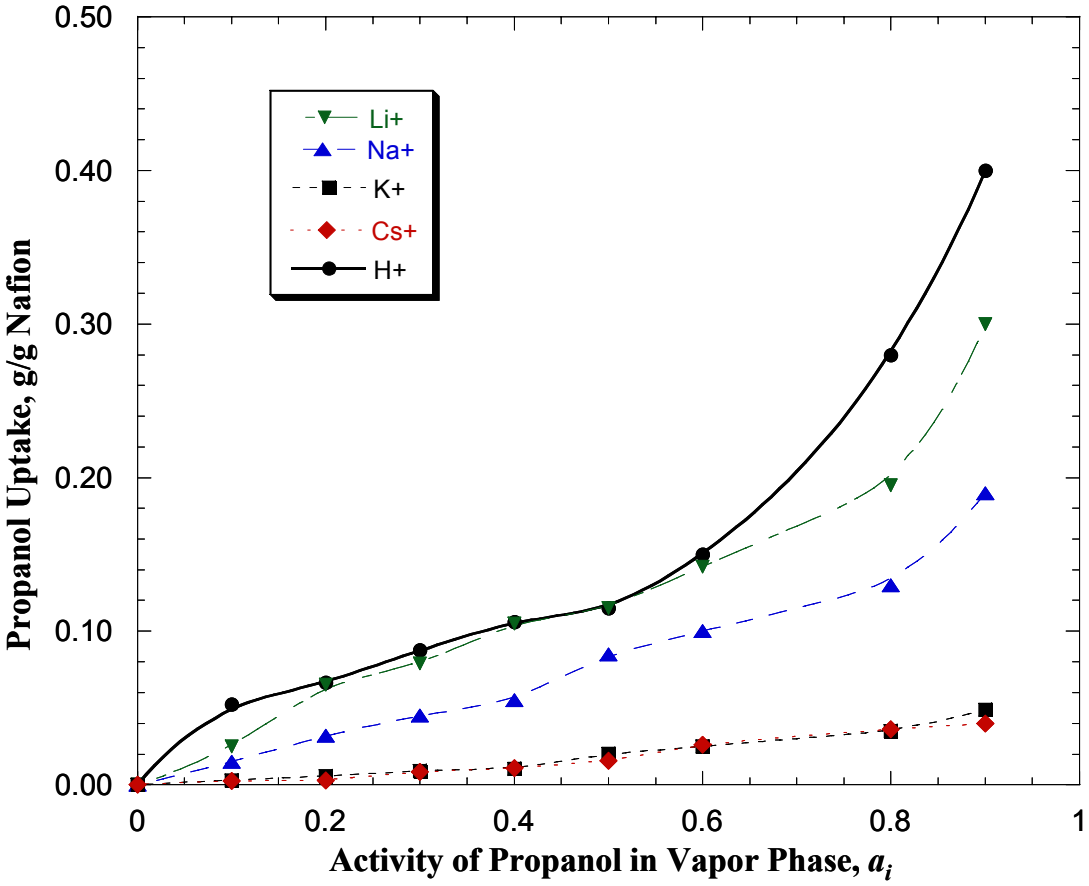

Figure 6.9 Effect of various cationic forms on propanol uptake vs. activity of propanol vapor for Nafion membrane at 30 ^{o}C .

Cationic Type	Water Hydration number	Hydration Energy(KJ/mol)	Cationic radius, nm
H^+	5±1	-1087.84	0.143
Li^+	5±1	-542.67	0.060
Na^+	4±1	-428.02	0.095
K^+	3±2	-348.53	0.133
Cs^+	~0	-298.74	0.169

Table 6.1 Water hydration number, hydration energies, and radius of cations.

The formation of hydration shell may be described by stepwise equilibrium, *i.e.,* the binding of solvent molecules in the solvation shell is assumed to occur by sequential reactions between the polymer acid groups $SO_3^-M^+$ and the polar solvent molecules ROH as evidenced by IR spectroscopic analysis,

$$SO_3^-M^+ + ROH \leftrightarrows SO_3^-M^+(ROH) \qquad K_1 \qquad (6.5)$$

$$SO_3^-M^+(ROH) + ROH \leftrightarrows SO_3^-M^+(ROH)_2 \qquad K_2 \qquad (6.6)$$

$$SO_3^-M^+(ROH)_2 + ROH \leftrightarrows SO_3^-M^+(ROH)_3 \qquad K_3 \qquad (6.7)$$

…..

$$SO_3^-M^+(ROH)_{v\text{-}1} + ROH \leftrightarrows SO_3^-M^+(ROH)_v \qquad K_v \qquad (6.8)$$

where v corresponds to the total number of molecules in the solvation shell, M^+ is the corresponding cation, and R = H, CH_3-, CH_3CH_2- etc and K_i is the equilibrium constant for step *i*.

The first of these, for instance, represents dissociation of the polymer acid group and concomitant protonation of the solvent (*e.g.,* to produce H_3O^+), whereas the second and subsequent steps represent further solvation. The solvent molecules with $K_j \geq 1$ are considered to be strongly bound and the interactions of an acid site with solvent molecules for $K_j < 1$ are considered weak enough to be accounted for by physical equilibration. It was shown in the sorption model developed by Choi and Datta [13] that an adequate expression for λ_i^C (strongly bound sorbate molecules) can be obtained as:

$$\lambda_i^C = \lambda_{i,m} \frac{K_1 a_i}{1-a_i} \left(\frac{1-(v+1)(a_i)^v + v(a_i)^{v+1}}{1+(K_1-1)a_i - K_1(a_i)^{v+1}} \right) \qquad (6.9)$$

In the case of water sorption, the first ionization constant K_1 is used as a fitted parameter. K_1 between water and the side chain of SO_3H^+ was approximated as 10^3 based on the report that *pK* of a Nafion is in the range of -1.0 to -5.1. For example, for H^+ form membrane, there are around 4-5 strongly bound water molecules.

The hydration number decreases with the increase in cationic radius. This means that we have less solvent molecules for each acid site at a given solvent activity with the amount decreasing from H^+ to Cs^+. For Cs^+ strongly bound solvent molecules is almost

approaching zero. Similarly, for other cationic forms, the first ionization constant K_1 between water and the side chain of SO_3Li^+, SO_3Na^+, SO_3K^+ and SO_3Cs^+ is fitted as 10, 2 , 0.8 and 0.1 respectively. This implies that the ionization constant decreases with the increase in cationic size and decrease in hydration energies. Similar arguments also hold for other solvents too.

Kawano *et al*, obtained the stress-strain curves for Nafion membrane substituted by Li^+, Na^+, K^+, Rb^+ and Cs^+ cations [20]. They observed that the initial slope increases in the order Li^+, Na^+, K^+, Cs^+ and Rb^+ cations, with lower degree of elongation as compared to received Nafion membrane. This further supports that solvent sorption would decrease in the order obtained by TEOM.

6.3.4 Sorption in Nanocomposite Nafion / MO_2 membranes

Figure 6.10 shows water uptake measurements of all nanocomposite membranes at 90 ^oC. All the nanocomposite membranes exhibited higher sorption than host Nafion membrane. These membranes have higher water amount at similar water activity, mainly due to the presence of additional Lewis and Bronsted acid sites provided by the inorganic particles [55]. The inorganic oxide particles are in submicron range, and have large surface areas. Zirconia being the most acidic, Nafion- ZrO_2 sol-gel exhibited highest water sorption than other membranes. The sorption trend is similar for all membranes, which shows that the basic mechanism of sorption is unaltered for nanocomposite membranes.

6.4 Conclusions

The TEOM technique is utilized to obtain equilibrium solvent sorption curves for various Nafion and nanocomposite membranes. From the results obtained it can be observed that solvent sorbates behavior in Nafion membrane strongly depend on its acid site density (*EW*), temperature and solvent environment to which it is exposed, and cationic forms of membrane itself. The water sorption increases with an increase in acid group density, albeit at the expense of mechanical strength of membrane. Also, Nafion membrane imbibes more water at higher temperatures. This is due to the fact that the membrane becomes pliable due to decrease in *E*. The sorbates (water, methanol, ethanol, and propanol) sorption decreases with the increase in counter cationic size. The decrease is due

to a decrease in dissociation constant between acid group due to decrease in ionic hydration energies and solvent. Also, with the increase in cation size, the *E* increases which restricts the swelling of membrane resulting in lower solvent sorption. The addition of nanosized inorganic additives via sol gel method, increase the water sorption capacity of membranes. This systematic study on the sorption behavior of Nafion could help in designing pretreatment protocols for developing stable and high performance membrane electrode assemblies for fuel cell applications as well as in understanding their behavior under a variety of conditions.

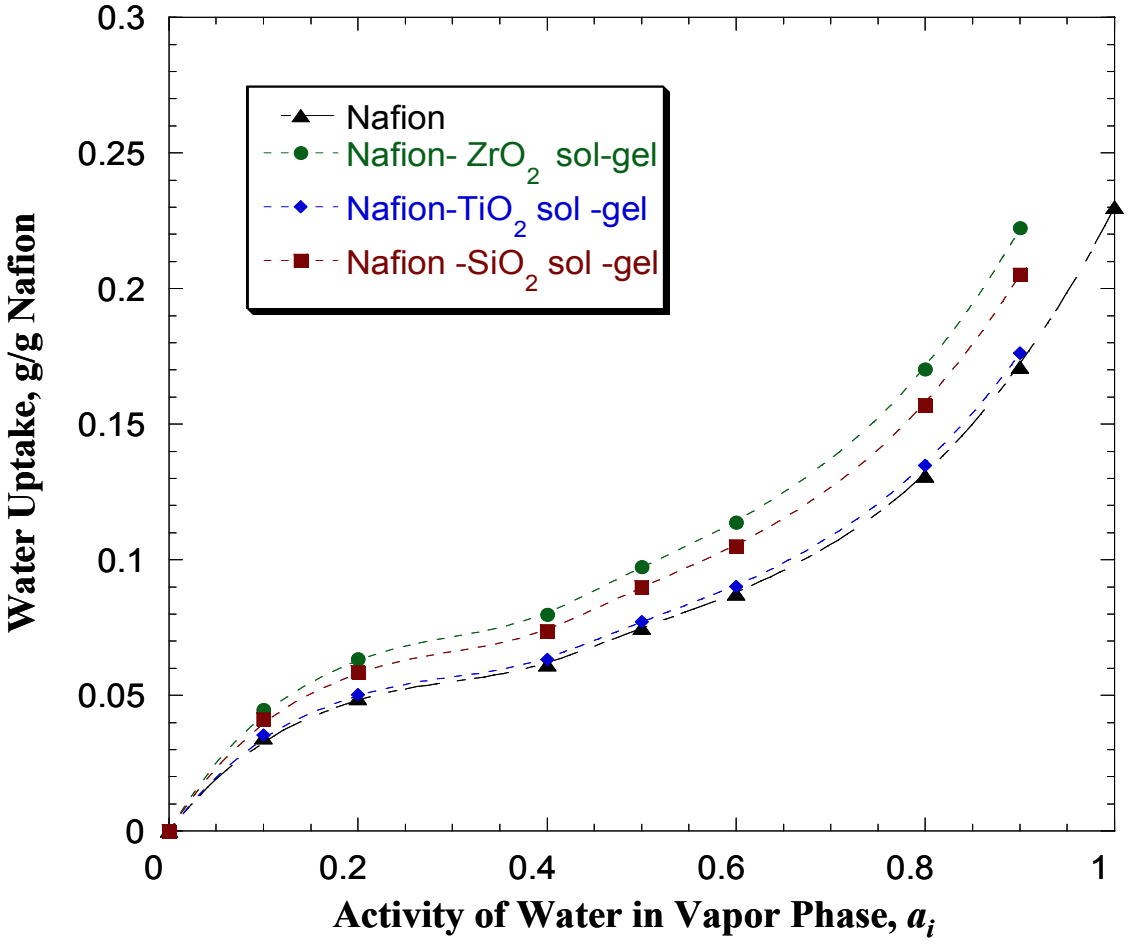

Figure 6.10 Water uptake vs. activity of water vapor for Nanocomposite Nafion/ MO_2 and Nafion membrane at 90 ^{o}C.

6.5 References

[1] K. D. Kreuer, On the development of proton conducting polymer membranes for hydrogen and methanol fuel cells, J. Membr. Sci., 185 (2001) 29.

[2] A. J. Appleby, and F.R. Foulkes, Fuel Cell Handbook, Van Nostrand Reinhold, New York, 1989.

[3] M. Doyle, M. E. Lewittes, M. G. Roelofs, and S. A. Perusich, Ionic Conductivity of Nonaqueous Solvent-Swollen Ionomer Membranes Based on Fluorosulfonate, Fluorocarboxylate, and Sulfonate Fixed Ion Groups, J. Phys. Chem. B, 105 (2001) 9387.

[4] T. Thampan, S. Malhotra, H. Tang, and R. Datta, Modeling of Conductive Transport in Proton- Exchange Membranes for Fuel Cells, J. Electrochem. Soc., 147(9) (2000) 3242.

[5] T. A. Zawodzinski, J. Davey, J. Valerio, and S. Gottesfeld, The water content dependence of electro-osmotic drag in proton-conducting polymer electrolytes, Electrochim. Acta, 40 (1995) 297.

[6] M. Doyle, L. Wang, Z. Yang, and S. K. Choi, Polymer Electrolytes Based on Ionomer Copolymers of Ethylene with Fluorosulfonate Functionalized Monomers, J. Electrochem. Soc., 150 (11) (2003) D185.

[7] T. Thampan, S. Malhotra, J. Zhang, and R. Datta, PEM fuel cell as a membrane reactor, Catalysis Today, 67(2001)15.

[8] T. Thampan, S. Malhotra, H. Tang, and R. Datta, Modeling of Conductive Transport in Proton- Exchange Membranes for Fuel Cells, J. Electrochem. Soc., 147(9) (2000) 3242.

[9] W.G. Grot, Perfluorinated ion exchange polymers and their use in research and industry. *Macromol. Symposia* 82 (1994) 161.

[10] H. L. Yeager, A. A. Gronowski, In: M. T. Tant, K. A. Mauritz, G. L. Wilkes, Editors, Ionomers, synthesis, structure, properties and applications, London: Blackie (Chapman and Hall), 1997.

[11] A. Steck In: O. Savadogo, P.R. Roberge and T.N. Veziroglu, Editors, Proceedings of First International Symposium on New Materials for Fuel Cell Systems,

Membrane Materials in Fuel Cells, Montreal, Canada (1995) 74.

[12] H. L. Yeager, In: A. Eisenberg, H. L. Yeager, Editors, Perfluorinated ionomer membranes, ACS symposium series 180, Washington, DC: American Chemical Society, 1982 (chap. 4).

[13] P. Choi and R. Datta, Sorption in Proton Exchange Membranes. An explanation of Schroeder's Paradox, J. Electrochem. Soc., 150 (12) (2003) E601.

[14] P. Choi, N. H. Jalani, and R. Datta, Thermodynamics and Proton Transport in Nafion. Part I. Membrane Swelling, Sorption, and Ion- Exchange Equilibrium., J. Electrochem. Soc., 152 (**3**) (2005) E84.

[15] N. H. Jalani, P. Choi, and R. Datta, Phenomenological methanol sorption model for Nafion 117, Solid State Ionics, 175(1-4) (2004) 815.

[16] T. E. Springer, T. A. Zawodzinski, and S. Gottesfeld, Water uptake by and transport through Nafion® 117 membranes, J. Electrochem. Soc**.,** 140 (1993) 1041.

[17] T. E. Springer, T. A. Zawodzinski, and S. Gottesfeld, A comparative study of water uptake by and transport through ionometric fuel cell membranes, J. Electrochem. Soc., 140 (1993) 1981.

[18] T. A. Zawodzinski, L. O. Sillerud, and S. Gottesfeld, Determination of water diffusion coefficients in perfluorosulfonate ionometric membranes, J. Phys. Chem., 95 (1991) 6040.

[19] K. K Pushpa, D. Nandan, and R. M. Iyer, Thermodynamics of water sorption by perfluorosulfonate (Nafion 117) and polystyrene-divinylbenzene sulphonate (Dowex 50W) ion exchange resins at 298 K, J. Chem. Soc., Faraday Trans. I, 84 (1988) 2047.

[20] Y. Kawano, Y. Wang, R. A. Palmer, and S. R. Aubuchon, Stress-Strain Curves of Nafion Membranes in Acid and Salt Forms, Polímeros, 12 (2) (2002) 96.

[21] T. V. Nguyen and N. Vanderborgh, The rate of isothermal hydration of polyperfluorosulfonic acid membranes, J. Membr. Sci., 142 (1998) 235.

[22] D. R. Morris, and X. Sun, Water-sorption and Transport Properties of Nafion 117H, J. Applied Poly. Sci., 50 (1993) 1445.

[23] H. R. Zelsmann, and M. Pineri, Water self-diffusion coefficient determination in an

ion- exchange membrane by optical measurement, J. Appl. Polym. Sci., 41 (1990) 1673.

[24] S.C. Yeo and A. Eisenberg, Physical properties and supermolecular structure of perfluorinated ion-containing (Nafion) polymers, J. Appl. Polym. Sci., 21 (1977) 875.

[25] G. Gebel, P. Aldebert and M. Pineri, Swelling study of perfluorosulphonated ionomer membranes, Polymer, 34 (1993) 333.

[26] S. R. Samms, S. Wasmus, and R. F. Savinell, Thermal stability of proton conducting acid doped polybenzimidazole in simulated fuel cell environment, J. Electrochem. Soc., 143 (1996) 1225.

[27] D. A. Siuzdak and K. A. Mauritz, Surlyn [silicon oxide] hybrid materials. 2. Physical properties characterization, J. Polym. Sci. Part B: Polym. Phys., 37 (1999) 143.

[28] J. Kerres, W. Cui, R. Disson and W. Neubrand, Development and characterization of cross-linked ionomer membranes based upon sulfonated and sulfonated PSU. 1. Cross-linked PSU blend membranes by disproportionation of sulfonic acid groups, J. Membr. Sci.,139 (1998) 211.

[29] P. J. James, J. A. Elliot, T. J. McMaster, J. M. Newton, A. M. S. Elliot, S. Hanna, and M. J. Miles, Hydration of Nafion studied by AFM and X-ray scattering, J. Mat. Sci., 35(2000) 5111.

[30] K. Scott, W. M. Taama, P. Argyropoulos, and K. Sundmacher, The impact of mass transport and methanol crossover on the direct methanol fuel cell, J. Power Sources, 83 (1999) 204.

[31] D. K. Yang, W. J. Koros, H. B. Hopfenberg, and V. T. Stannett, Sorption and transport studies of water in Kapton polyimide. I., J. Appl. Polym. Sci., 30 (1985), 1035.

[32] T. D. Gierke, G. E. Munn, and F. C. Wilson, The morphology in Nafion perfluorinated membrane products, as determined by wide- and small-angle X-ray studies, J. Polym. Sci., Polym. Phys., 19 (1981) 1687.

[33] S. Schlick, G. Gebel, M. Pineri, and F. Volino, Fluorine-19 NMR spectroscopy of acid Nafion membranes and solutions, Macromolecules, 24 (1991) 3517.

[34] M. Walker, K.-M. Baumgärtner, M. Kaiser, J. Kerres, A. Ullrich and E. Räuchle, Proton conducting polymers with reduced methanol permeation, J. Appl. Polym. Sci., 74 (1999) 67.

[35] M. Laporta, M. Pegoraro and L. Zanderighi, Perfluorosulfonated membrane (Nafion): FT-IR study of the state of water with increasing humidity, Phys. Chem. Chem. Phys., 1 (1999) 4619.

[36] P. Wang, N. S. Schneider, and N. Sung, Sorption and diffusion of organic vapors in two fluoroelastomers, J. Appl. Polym. Sci., 71 (1999)1525.

[37] D. Rivin, C. E. Kendrick, P. W. Gibson, and N. S. Schneider, Solubility and transport behavior of water and alcohols in Nafion, Polymer, 42 (2001) 623.

[38] J. T. Hinastu, M. Mizuhata, and H. Takenaka, Water uptake of perfluorosulfonic acid membranes from liquid water and water vapor, J. Electrochem. Soc., 141 (1994) 1493.

[39] D. Nandan, H. Mohan, and R. M. Iyer, Methanol and water uptake, densities, equivalental volumes and thicknesses of several uni- and divalent ionic perfluorosulphonate exchange membranes (Nafion 117) and their methanol- water fractionation behavior at 298 K, J. Membr. Sci.,71(1992) 69.

[40] X. Ren, P. Zelenay, S. Thomas, J. Davey , and S. Gottesfeld , Recent advances in direct methanol fuel cells at Los Alamos National Laboratory, J. Power Sources, 86 (2000)111.

[41] C. M. Gates, and J. Newman, Equilibrium and Diffusion of Methanol and Water in Nafion 117 Membrane, AIChE J., 46 (2000) 2076.

[42] X. Ren, T.E. Springer, T. A. Zawodzinski, and S. Gottesfeld, Methanol transport through Nafion membranes electro-osmotic drag effects on potential step measurements, J. Electrochem. Soc., 142(2) (2000) 466.

[43] N. H. Jalani, P. Choi, and R. Datta, TEOM: a novel technique to characterize proton-exchange membranes, J Membr Sci 2004, 252(1-2) (2005) 31.

[44] T. Thampan, N. H. Jalani, P. Choi, and R. Datta, Systematic Design of Higher Temperature Composite Proton Exchange Membranes, J. Electrochem. Soc., 152 (**2**) (2005) A 316.

[45] N. H. Jalani, K. Dunn, P. L. Loyselle, and R. Datta, Synthesis and Characterization

of Nafion - MO_2 (M = Zr, Si, Ti) Nanocomposite Membranes for Higher Temperature PEM Fuel Cells, Electrochimica Acta, 51(3)(2005) 553.

[46] E. Voltera, and E. C. Zachmanoglou, Dynamics of Vibrations, Columbus, Charles E., Merrill Books, Inc. (1965).

[47] D. Chen, A. Grønvold, H. P. Rebo, K. Moljord, and A. Holmen, Catalyst deactivation studied by conventional and oscillating microbalance reactors, Applied Catalysis A. General, 137(1996) L1.

[48] R. B. Moore III, and C. R. Martin, Procedure for preparing solution-cast perfluorosulfonate ionomer films and membranes, Anal. Chem., 58 (1986) 2569.

[49] R. B. Moore III, and C. R. Martin, Chemical and morphological properties of solution- cast perfluorosulfonate ionomers, Macromolecules, 21 (1988) 1334.

[50] K. Arata, Preparation of superacids by metal oxides for reactions of butanes and pentanes, Applied Catalysis A. General, 146 (1996) 3.

[51] N. Miyake, J. S. Wainright, and R. F. Savinell, Evaluation of a Sol-Gel Derived Nafion/Silica Hybrid Membrane for Proton Electrolyte Membrane Fuel Cell Applications: I. Proton Conductivity and Water Content , J. Electrochem. Soc., 148(8)(2001) A898.

[52] S. K. Young, W.L. Jarrett and K. A. Mauritz, Nafion /ORMOSIL nanocomposites via polymer-in situ sol–gel reactions. 1. Probe of ORMOSIL phase nanostructures by Si-solid state NMR spectroscopy, Polymer, 43 (2002) 2311.

[53] N. H. Jalani, S. Mizar, P. Choi, C. Furlong, and R. Datta, Optomechanical characterization of proton-exchange membrane fuel cells, Proc SPIE, 5532 (2004) 316.

[54] Bockris J. O'M. and S. Srinivasan, Fuel Cells: Their Electrochemistry, McGraw Hill, New York (1969).

[55] Yin-Yan Huang, T. J. McCarthy, and Wolfgang M. H. Sachtler, Preparation and catalytic testing of mesoporous sulfated zirconium dioxide with partially tetragonal wall structure, Applied Catalysis A: General, 148 (1) (1996) 135.

Chapter 7

Optomechanical characterization of proton-exchange membrane fuel cells

The properties that make the Nafion membrane indispensable are the combination of good water uptake, ion-exchange capacity, proton conductivity, gas permeability, and excellent electrochemical stability. The amount of water sorbed in the Nafion membrane is critical as the proton conductivity depends directly on the water content of the membrane which determines the fuel cell performance. The factors which affect the extent of the solvent uptake by Nafion are temperature, ion- exchange capacity, pretreatment of membrane, and the physical state of absorbing water, whether it is in liquid or vapor phase. The water sorption in the membrane is explained in terms of thermodynamic equilibrium of water in the vapor and absorption phases. As the membrane imbibes more water, the membrane matrix expands and exerts a pressure on the pore liquid which affects its chemical potential and limits extent of swelling. The extent of matrix expansion of the membranes depends on the elastic modulus, E, of the membrane, which directly affects the sorption. Hence, it is important to understand the variation of E for Nafion membrane with relative humidity (RH) and temperature. In this chapter, the use of Optoelectronic holography (OEH) techniques to perform quantitative, noninvasive, full field of view investigations to determine temperature and water activity dependence of E is explained as a part to investigate the mechanical properties of membranes. The results obtained confirm that with the increase in temperature, E decreases and the membranes imbibes more water. Such results will allow optimization and realization of fuel cells with improved efficiency and performance.

7.1 Introduction

A fuel cell is basically an electrochemical device, which can continuously convert the chemical energy of a fuel and an oxidant to electrical energy [1-3]. One of the major factors that have influenced the development of fuel cells has been the concern from

environmental consequence point of view. Less pollution for the better and safer human life has become a matter of great concern. In this present scenario fuel cells help to reduce our dependence on fossils fuels and diminishes poisonous and toxic emissions in to the atmosphere, since fuel cells have more electrical efficiencies compared to heat engines. The main by-product of fuel cell reaction is water, thus completely eliminating locally all emissions. Fig. 7.1 shows typical schematic of H_2-O_2 fuel cell. Hydrated Nafion, a polymer consisting of a polytetrafluoroethylene (PTFE) backbone with side-chains terminating in $SO_3^-H^+$ groups, is commonly used for PEFC as proton conducting medium. They exhibit excellent chemical, mechanical, and thermal stabilities along with high conductivities when sufficiently hydrated. The amount of water sorbed in the membrane is critical as the proton conductivity depends on the water content of the membrane which affects the fuel cell performance [4] . The factors which affect the extent of the solvent uptake by PEM are mainly temperature, ion exchange capacity, and pretreatment of membrane [5], and also the physical state of absorbing water whether it is in liquid or vapor phase.

We have developed a water sorption model within the membrane in terms of equilibrium of water in the vapor and absorption phases. Until the equilibrium is attained, the membrane imbibes water and the elastic matrix expands. The internal swelling pressure acting on the water in the membrane can be considered as the restoring force of the matrix. The equilibrium of the system is established as a consequence of the balance between the osmotic and mechanical restoring forces. The extent of matrix expansion of the membranes depends on the elastic modulus, *E*, of the membrane, which directly affects the sorption. Hence, it is very essential to determine the thermomechanical behavior of the membrane. Kawano *et al*. studied the stress-strain curves of Nafion membrane for various pretreatments *i.e*. boiling, soaking in other solvents, heating etc [6]. They observed that the slope of stress-strain i.e., Young's Modulus (*E*) of the membrane, decreases for membrane boiled in water, making them more pliable for water uptake. The focus of this paper is to present the use of optoelectro holography (OEH) technique to determine the *E* of Nafion membrane at various operating conditions of fuel cells.

7.2 Water Sorption Model

7.2.1 Model Background

The model developed here assumes that the absorbed water molecules are of two types; *i*) those that are strongly, or chemically, bound to the acid sites, akin to chemisorption, and *ii*) others that are physically equilibrated between the fluid and the membrane phases, akin to physisorption. Then, the total uptake of water molecule by the membrane is the addition of the two types of water molecules as,

$$\lambda_w = \lambda_w^C + \lambda_w^F \tag{7.1}$$

where superscripts C and F are the chemically and physically bound water molecules, respectively.

The thermodynamic condition for the 'chemical' equilibrium that determines λ_i^C, is

$$\sum_{i=1}^{n} v_{\rho i}\mu_i = 0 \qquad (\rho = 1, 2, \ldots, q) \tag{7.2}$$

where $v_{\rho i}$ and μ_i represents the stoichiometric number of species i in reaction ρ and chemical potential of species i in solution, respectively.

For describing phase equilibrium between the membrane and external vapor phases, the thermodynamic condition is

$$\mu_{i,M} = \mu_{i,V} \qquad (i = 1, 2, \ldots, n) \tag{7.3}$$

where subscripts M and V represents the membrane and vapor phase, respectively.

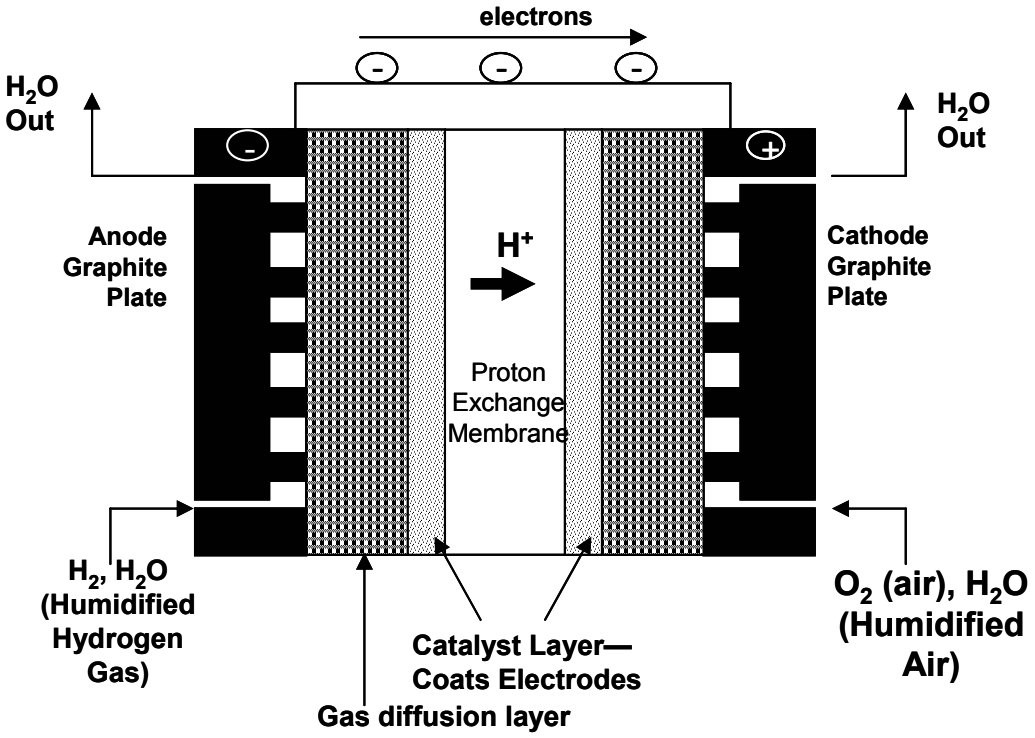

Figure 7.1 Detailed Schematic of hydrogen based proton-exchange membrane fuel cell.

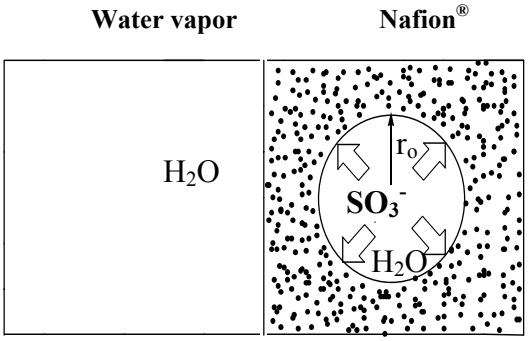

Figure 7.2 Schematic of the internal pore contacting with the elastic membrane.

The general chemical potential for species *i (i = 1,2,. . . , n)* in phase α can be written as a function of temperature, pressure, composition, and other potentials, *e.g.*, $\mu_{i,\alpha} = (T,P, a_{i,\alpha}, \Psi_i)$

$$\mu_{i,\alpha} = \mu_i^{\circ}(T, P^{\circ}) + \int_{P^{\circ}}^{P} \overline{V}_{i,\alpha} dP + RT \ln a_{i,\alpha} + \Psi_{i,\alpha} \tag{7.4}$$

where μ_i° is the standard Gibbs free energy of formation of *i*, *T* is the temperature, P° is the standard pressure, $\overline{V}_{i,\alpha}$ is the partial molar volume of *i* in phase α, $a_{i,\alpha}$ is the activity of *i* in phase α, and Ψ_i represents other types of energy such as electrical energy or surface energy acting on the phase.

7.2.2 Physical Equilibrium between Water Vapor-Water in Membrane

When the membrane equilibrates with water in vapor phase, use of Equations 3 and 4 results in

$$\ln \frac{a_{W,M}^{F}}{a_w} = -\left(\frac{\overline{V}_w}{RT}\right) \Pi_S \tag{7.5}$$

where a_w and $a_{w,M}^{F}$ are activities of water in external vapor phase and within the membrane, $\overline{V}_w$ is the partial molar volume of water, Π_S the swelling pressure, *R* the universal gas constant, and *T* the temperature.

The swelling pressure is taken as a pressure that is needed for a spherical hole in infinite block of elastic materials to stretch from its radius $r_{\circ}$ to r as previously approximated. The pressure can be written by assuming that the membrane follows the simple kinetic theory of rubber elasticity as,

$$\Pi_S = \frac{E}{6}\left(5 - 4\eta^{-1} - \eta^{-4}\right) \tag{7.6}$$

where $\eta = r/r_o$ and E is Young's modulus of elasticity of the membrane. This relation also provides a reasonably good approximation for somewhat more complex elastic behavior. Fig. 7.2 represents the schematic of the internal pore contacting with the elastic membrane.

As the Nafion absorbs water, the density of the membrane decreases progressively. Assuming the volume additivity of the water and dry membrane in the swollen membrane, the density of the water containing membrane can be written as

$$\rho = \frac{\rho_w \rho_o (1 + f_m)}{\rho_w + f_m \rho_o} \tag{7.7}$$

where ρ_o and ρ_w represent the densities of water and dry Nafion, respectively, and f_m is the mass ratio of water amount absorbed to mass of dry Nafion and is evaluated from basic definition as:

$$f_m = \frac{\lambda_w MW_{solvent}}{EW} \tag{7.8}$$

where $MW_{solvent}$ is the molecular weight of the solvent and EW is the equivalent weight of the membrane.

The density of the swollen membrane may also be written as a function of changes in the dimensions of the membrane. Assuming the same geometry of the membrane as the spherical cavity inside of the membrane, the density of water swollen membrane can be written as

$$\rho = \frac{\rho_o (1 + f_m)}{(r_m / r_{m_o})^3} \tag{7.9}$$

where r_{m_o} and r_m denote the radius of the initial and water containing membrane upon sorption, respectively. The volume of the membrane increases as water is absorbed as shown in Nafion film. If the extension ratio of the membrane is approximated as that of the

cavity in the membrane in the context of a simple rubber elasticity shown in Equation 7, then the extension ratio η may be expressed as

$$\eta = \left[\frac{\rho_\circ}{\rho} \left(1 + f_m\right) \right]^{1/3} \tag{7.10}$$

7.3 Chemical Equilibrium

Equations 7.2 and 7.4 when combined yield the usual chemical equilibrium for reaction ρ

$$K_\rho = \exp\left(\frac{-\Delta G_\rho^\circ}{RT} \right) = \prod_{i=1}^{n} a_i^{\nu_{\rho i}} \tag{7.11}$$

where K_ρ is the equilibrium constant for reaction ρ and $\Delta G_\rho^\circ \equiv \sum_{i=1}^{n} \nu_{\rho i} G_i^\circ (T, P)$ is the standard Gibbs energy change of the reaction. The details for the derivation of chemically adsorbed water molecules is provided by Choi and Datta (2003).

The total strongly bound molecules is calculated assuming all K_ρ=1 except K_1 as,

$$\lambda_i^C = \lambda_{i,m} \frac{K_1 a_i}{1 - a_i} \left(\frac{1 - (v+1)(a_i)^v + v(a_i)^{v+1}}{1 + (K_1 - 1)a_i - K_1 (a_i)^{v+1}} \right) \tag{7.12}$$

where $\lambda_{i,m}$ is monolayer coverage to better account for the adsorption.

Combining Equations 7.1, 7.5, 7.6, 7.10 and 7.12 provides an implicit expression of water content in the membrane for vapor phase absorption as,

$$\left(\lambda_w - \lambda^C\right)^{-1} = a^{-1} exp\left\{ \frac{V_i}{RT} \left[\frac{E}{6} \left(5 - 4\eta^{-1} - \eta^{-4}\right) \right] \right\} - 1 \tag{7.13}$$

Equation 7.13 shows that the amount of sorption λ_i can be determined in terms of activity of water (a_i) in vapor phase with the appropriate parameters. It can be observed that E

affects the amount of water sorbed by the membrane. Hence, it is essential to determine E for solving the model and also to study the thermomechanical behavior of membrane at higher temperatures in our concomitant efforts to design high temperature proton exchange membranes.

7.4 Uncertainty Analysis of Sorption Model

It is evident from Equation 7.13 that Young's Modulus strongly affects the properties of Nafion membrane and varies both with temperature and water activity in the fuel cells. An uncertainty analysis for the sorption model will provide the effects of uncertainty in E and other parameters on the amount of water absorbed by the membrane. In addition, this analysis will provide the sorption behavior expected when the parameters are varied in Equation 7.13. The amount of water in the membrane, λ_w can be expressed as:

$$\lambda_w = f(\lambda^C, a_i, T, E, \eta) \tag{7.14}$$

Also, $$\eta = f(\rho_o, \rho, \lambda_w) \tag{7.15}$$

From RSS approach [8] (Square root of the sum of squares of uncertainty) we get following equation,

$$\delta\lambda_w = \left[\left(\frac{\partial\lambda_w}{\partial\lambda_i^C}\delta\lambda_i^C\right)^2 + \left(\frac{\partial\lambda_w}{\partial a_i}\delta a_i\right)^2 + \left(\frac{\partial\lambda_w}{\partial E}\delta E\right)^2 + \left(\frac{\partial\lambda_w}{\partial\eta}\delta\eta\right)^2 + \left(\frac{\partial\lambda_w}{\partial T}\delta T\right)^2\right]^{1/2} \tag{7.16}$$

where δ represents uncertainty in each parameter. Similarly, uncertainty in η is obtained as,

$$\delta\eta = \left[\left(\frac{\partial\eta}{\partial\rho_o}\delta\rho_o\right)^2 + \left(\frac{\partial\eta}{\partial\rho}\delta\rho\right)^2 + \left(\frac{\partial\eta}{\partial\lambda_w}\delta\lambda_w\right)^2\right]^{1/2} \tag{7.17}$$

Now the uncertainty in λ_w is obtained for each contributing factor. Figure 7.3(a) and 7.3(b) shows the plot of all factors contributing to the uncertainty in determination of λ_w *for* saturated conditions at 30 and 90 ^oC respectively.

From Figure 7.3(a), it is observed that at 30 ^oC, the sorption amount is quite sensitive to the extension ratio. The water activity also contributes to the uncertainty but both extensions ratio and activity levels off sooner. The uncertainty due to *E* increases and strongly affects the membrane properties. On the other hand, at 90 ^oC (Fig. 7.3(b)), the total uncertainty in amount of water sorbed by the membrane is more as compared to that at 30 ^oC. The uncertainty due to water activity is high initially and subsequently *E* contributes maximum. From the uncertainty analysis at saturated conditions, it is observed that:

1. *E* has maximum contribution to the uncertainty in amount of water sorbed (λ_w). The uncertainty in *E* increases with temperature, indicating that the physicochemical structure of Nafion membrane changes drastically with *E*.
2. At both temperatures, chemically adsorbed water molecules does not contribute much to the overall uncertainty for the λ_w. This implies that, it is the physically adsorbed water molecules which contribute mainly to the change in the sorption behaviour of the membrane, in turn affecting the *E* of the membrane. Also, at low water activity, where we have only chemically adsorbed water molecules, the membrane behaves quite stably to the changes in the surrounding environment.
3. The uncertainty due to swelling (extension ratio) is more at 90 ^oC. This means that at 90 ^oC even if the membrane absorbs more water, the membrane does not swell much. It has already swelled at that temperature and is just absorbing more water.
4. The uncertainty contribution of water activity is more at 90 ^oC. This implies that membrane properties are sensitive to small changes in water activity at 90 ^oC.

From the uncertainty analysis of the sorption model developed, it can be concluded that to minimize the uncertainty in *E* for the model, we need to accurately determine the membrane density and control water activity in the membrane, especially at 90 ^oC. Hence, OEH is the technique utilized which can accurately determine the *E* for the membrane for various operating conditions.

7.5 Optoelectronic Holography (OEH)

Optoelectronic holography (OEH) methodologies have been successfully applied to different fields of nondestructive testing (NDT) of objects [7-9]. OEH methodologies are noninvasive, remote, and capable of providing full-field-of-view qualitative and quantitative information on shape and deformation of objects subjected to a large variety of boundary conditions and loadings [10]. Implementation of recent technological advances in coherent light sources, computing, imaging, and detector technologies to the OEH methodologies has dramatically increased the versatility of these methodologies. This is the first opportunity to utilize OEH in order to determine Young's Modulus of Nafion membrane in the development of fuel cells. This investigation will give more insights into thermomechanical behavior of Nafion membrane.

7.6 Optoelectronic Holography Microscope Setup

Figure 7.4 shows the OEH experimental setup for the determination of the Young's modulus of Nafion membrane from the measured resonant frequencies. Using this method, the mode shapes corresponding to the first bending frequencies were visualized and the corresponding frequencies were recorded. The samples were excited in a cantilever beam configuration. Care was taken that the base consisted of flat surfaces, to ensure "fixed" boundary conditions. The resonance frequencies were monitored over the temperature range from 25 ºC to 90 ºC, for all of the lengths of the samples. In OEH method the deformation of the object can be obtained by solving for Ω_t defined as

$$\Omega_t = \frac{1}{2}\left\{\left[\frac{1-\cos 2B}{\sin 2B}\right]\frac{I_3 - I_2}{2I_1 - I_2 - I_3}\right\} \tag{7.18}$$

where I represent the laser irradiance field, Ω_t, is the time varying fringe-focus function relating to object displacements, and B is the bias modulations.

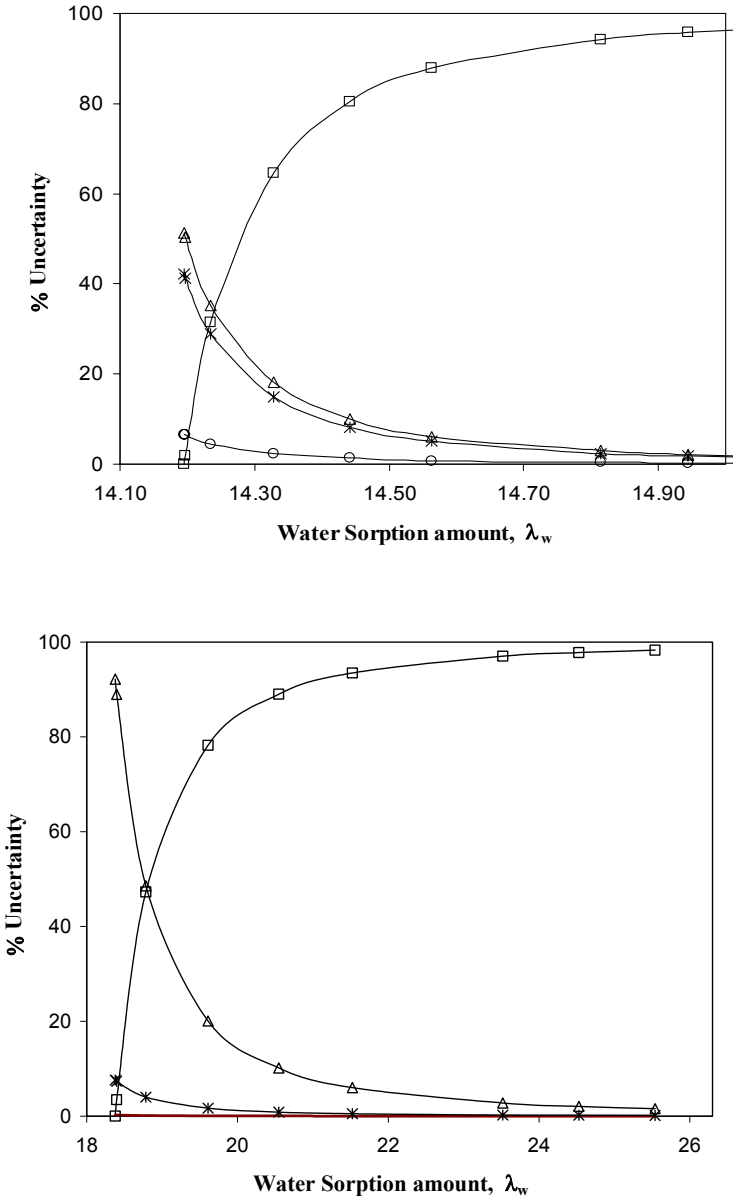

Figure 7.3 Uncertainty due to various parameters at (a) 30 ^{o}C and (b) 90 ^{o}C. The symbol represents % uncertainty for the parameters in Equation. 16 [square: E, triangle: η, star: a_i, circle: λ^C].

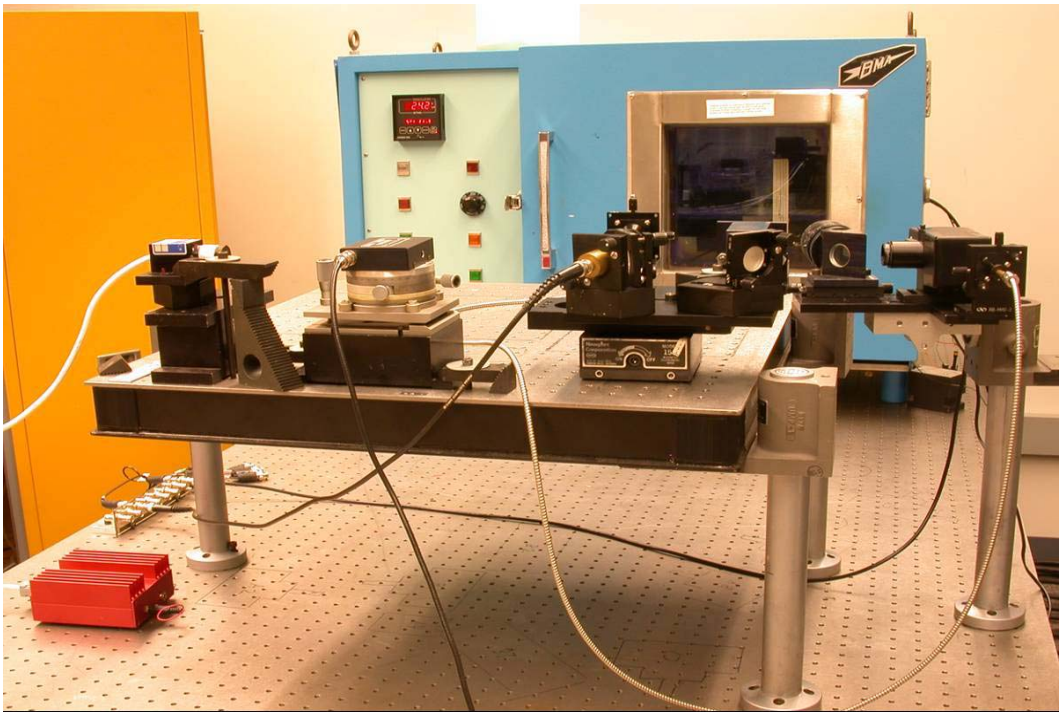

Figure 7.4 OEH setup to determine resonating frequencies of Nafion sample.

7.7 Determination of Young's Modulus

The Young's modulus E depends on the water content in Nafion and changes during the sorption process. The Young's modulus of Nafion is expected to decrease exponentially with the water content. OEH is the experimental method utilized to determine *E* for Nafion membranes. The OEH setup utilized a laser of 532 nm wavelength. Using the equations of motion for the dynamic load of excitation case (free undamped vibrations), the modulus of elasticity, *E*, is obtained as

$$f = \frac{1}{2\pi}\frac{t}{L^2}\sqrt{\frac{E}{\rho}} \tag{7.19}$$

where *f, t, L, E,* ρ are the resonant frequency of the first mode, thickness of sample membrane, length of sample exposed to laser, young's modulus, and density of sample membrane respectively.

Modulus of elasticity of the sample membrane depends strongly on the temperature. Hence, precise knowledge of the temperature of the sample at the instant measurements is necessary. The time constant for these measurements was 60 min, that is, the measurements of parameters used in Equation 7.19 were made 60 min after the temperature change was imposed on the samples within the environmental chamber.

7.8 Experimental Results

Figure 7.5 shows preliminary experimental results obtained for Nafion membrane having thickness of 50 microns and density of 2050 kg/m^3. The length of sample was varied for 3 different lengths to reproduce the results. These values were substituted in Equation 19 with the experimentally determined frequencies. The experiments were accomplished at 30 and 90 ^{o}C. These are the temperatures of interest in case of fuel cell applications. The only reference we had to compare our preliminary results for *E* was from Dupont product information catalog for Nafion. They reported a value of 250 Mpa at 50 % relative humidity at room temperature. From OEH for similar conditions 248 MPa was obtained. This shows that OEH accurately determines the *E* of membrane.

From Figure 7.5 it is observed that the *E* decreases with the increase in water activity and temperature at which sample is placed. This implies that the membrane

becomes flexible with increase in temperature and also when it absorbs water. Also at dry state, the *E* decreases with increase in temperature. The observed trend of decrease in *E* can be visualized as exponential decay with water activity. This is an important result from operation and development of fuel cells point of view. In addition, substitution of *E* into Equation 13 provides complete sorption isotherm for water sorption in Nafion membrane as a function of temperature.

Figure 7.6 shows the experimental results for the change in *E* for Nafion 117 (175 μ thick) as a function of temperature and water activity. The trend observed is similar to previous results. With the increase in temperature and water activity, the *E* decreases exponentially. The effect of membrane thickness is studied in Figure 7.7, where three different Nafion sample thicknesses were tested. The samples were Nafion 112 (50 μ), Nafion 115 (125 μ), and Nafion 117 (175 μ). There was improvement in E with the increase in membrane thickness. Nafion 117 exhibited higher E than Nafion 112 for lower water activity region, whereas the E data converges for all samples at saturated conditions. The results obtained shows that thicker samples may be mechanically attractive at low humidification conditions. Of course, the mechanical advantage will cost fuel cell performance which decreases with membrane thickness due to low proton flux.

Figure 7.8 shows the effect of addition of polytetrafluoroethylene (PTFE), a hydrophobic material which makes up backbone of Nafion membrane. Here I studied the effect of 10 wt % PTFE on Nafion mechanical properties. This new composite membrane exhibits better mechanical properties than unmodified Nafion membrane. But, with higher loading of PTFE decreases the mechanical strength due to high porosity of the membrane due to addition of PTFE (data is not shown in the thesis). A thorough investigation of effect of PTFE content on *E* and porosity will lead us more undertanding on the mechanical nature of the membrane.

Finally, a nanocomposite membrane Nafion-SiO_2 sol gel was tested to study the change in *E* with the addition of inorganic additives. There was about 30-45 Mpa improvement in the mechanical strength of the membrane as compared to Nafion membrane of similar thickness. Figure 7.9 compared the *E* of nanocomposite and PTFE nanocomposite membrane. Nanocomposite exhibited 5-15 Mpa higher *E* than PTFE

membranes. This is very promising because my research objective was to develop better performing membranes than Nafion; by both chemical and mechanical modifications.

7.9 Conclusion and Future Work

(OEH) to study and determine the Young's Modulus of Nafion at different conditions and humidity looks promising and reproducible. The main advantage of this technique is its accuracy and noninvasive nature for the sample. From the sorption model and the *E* obtained it is understood that the membrane adsorbs more water at 90 ^{o}C and can accommodate more water. This is an important phenomenon for operations in fuel cells. OEH can thus be used as a diagnostic technique for characterization of Nafion membrane.
Future work includes reproducing the data obtained so far at other temperatures including 120 ^{o}C, which is the glass transition temperature of the membrane. In addition the behavior of the membrane for heating and cooing cycles will be studied. Since Nafion exhibits hysteresis behavior for sorption and desorption, it is important to investigate the thermomechanical behavior while the sample is heated and cooled. The viscoelastic nature of membrane would be investigated systematically. Also different pretreatments like boiling, vacuum heating, hot press etc, affects the thermomechanical properties of membrane. A thorough investigation for these effects would be considered in our future efforts.

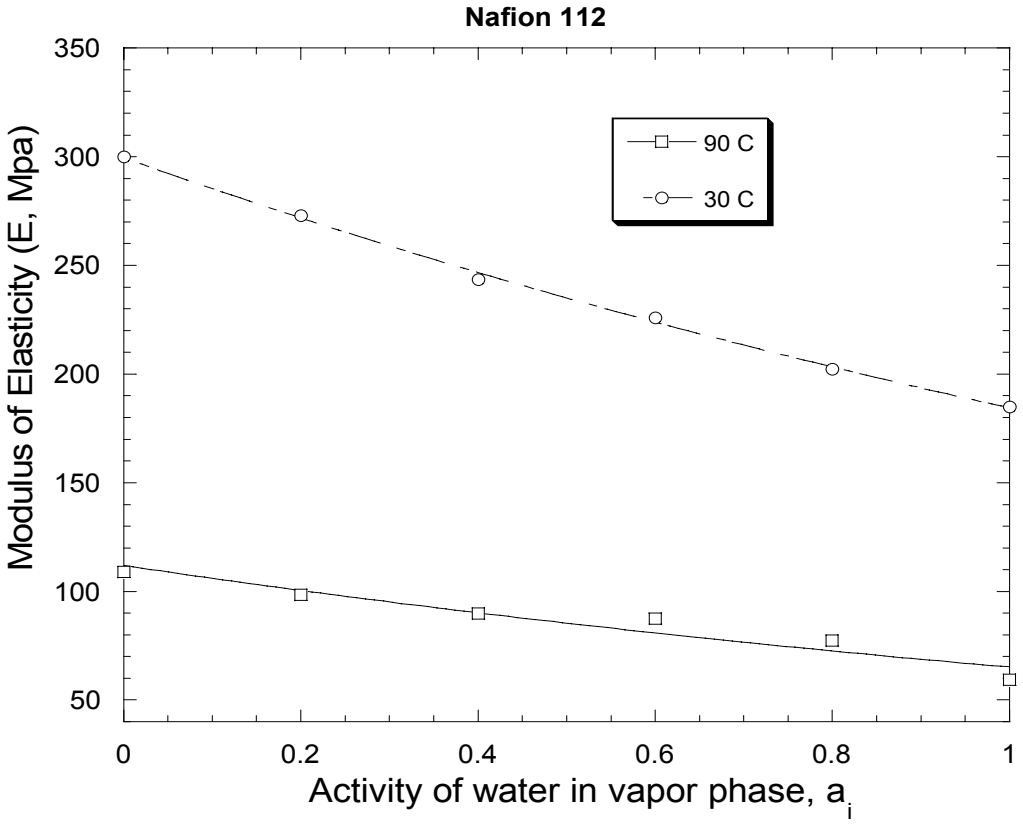

Figure 7.5 Preliminary experimental results for *E* of Nafion 112 membrane [circle: 30 ^{o}C, square: 90 ^{o}C].

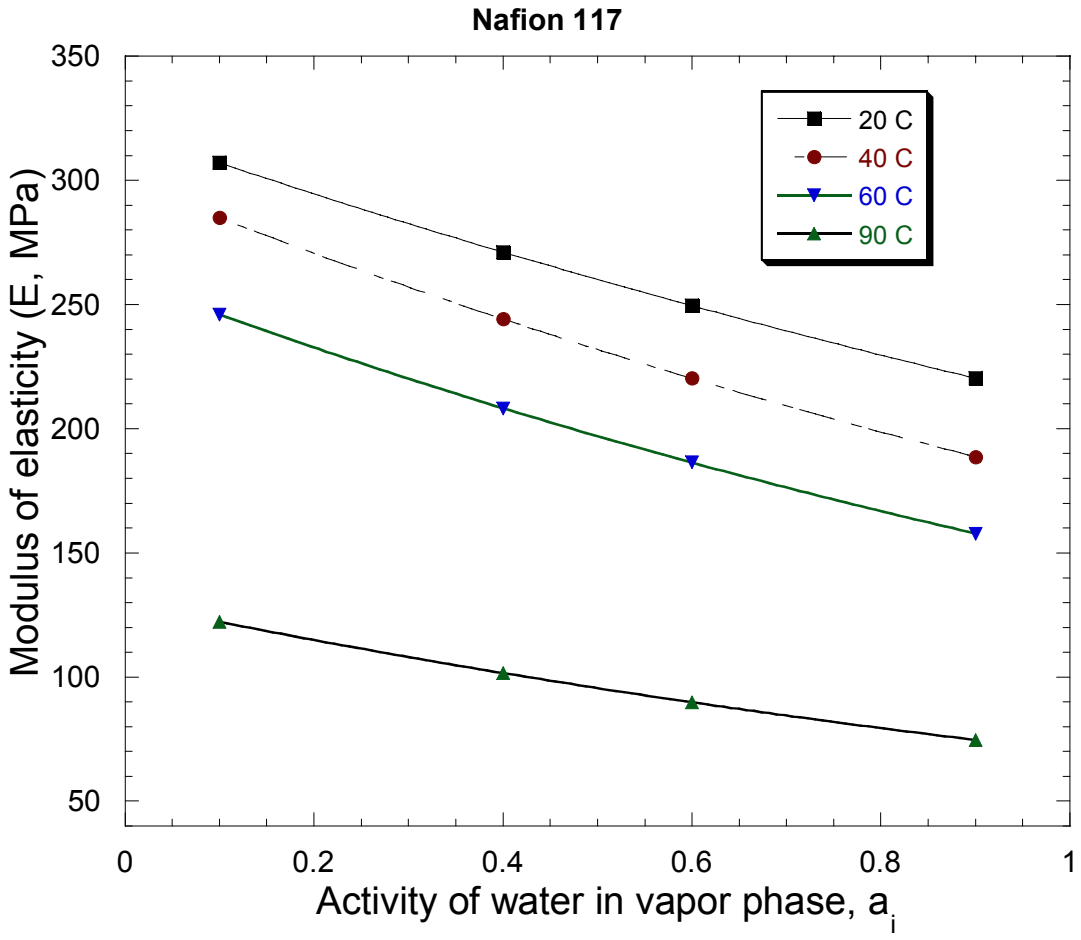

Figure 7.6 Experimental results for *E* of Nafion 117 membrane as a function of temperature and water activity.

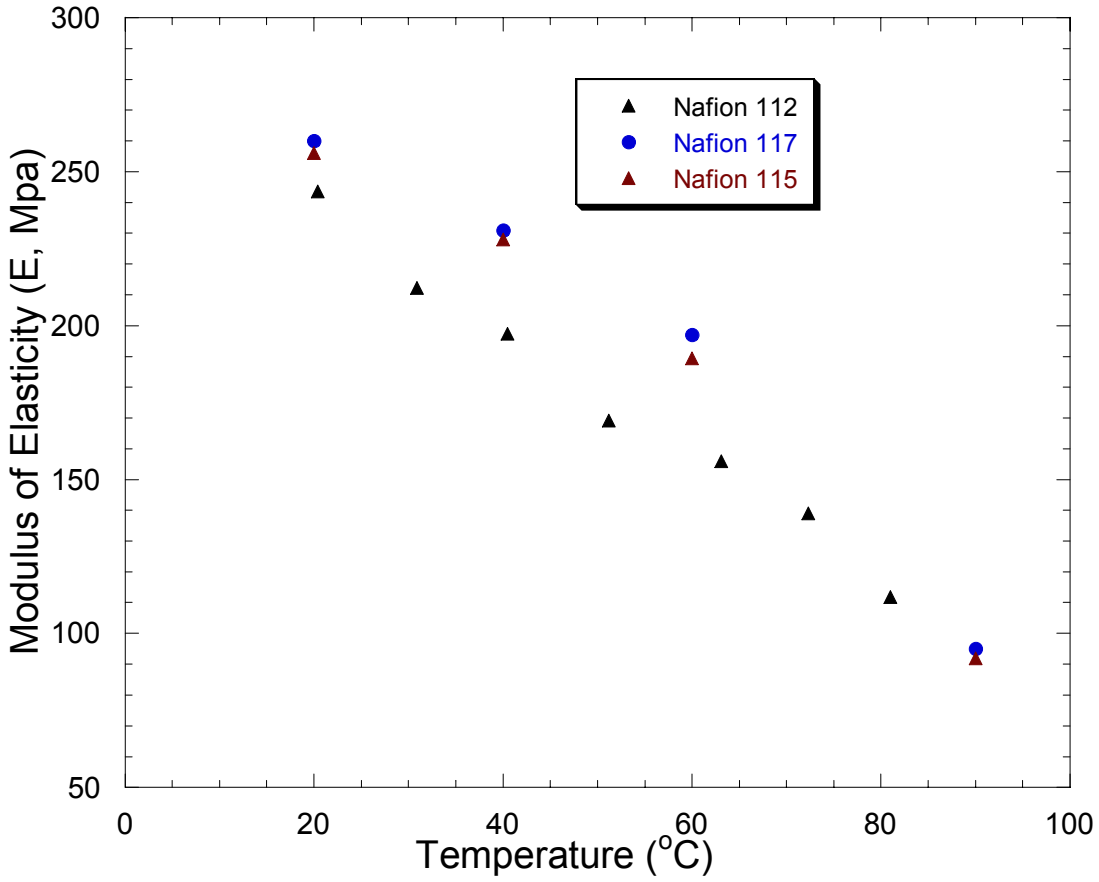

Figure 7.7 Effect of membrane thickness on *E* of Nafion membrane as a function of water activity at 30 °C.

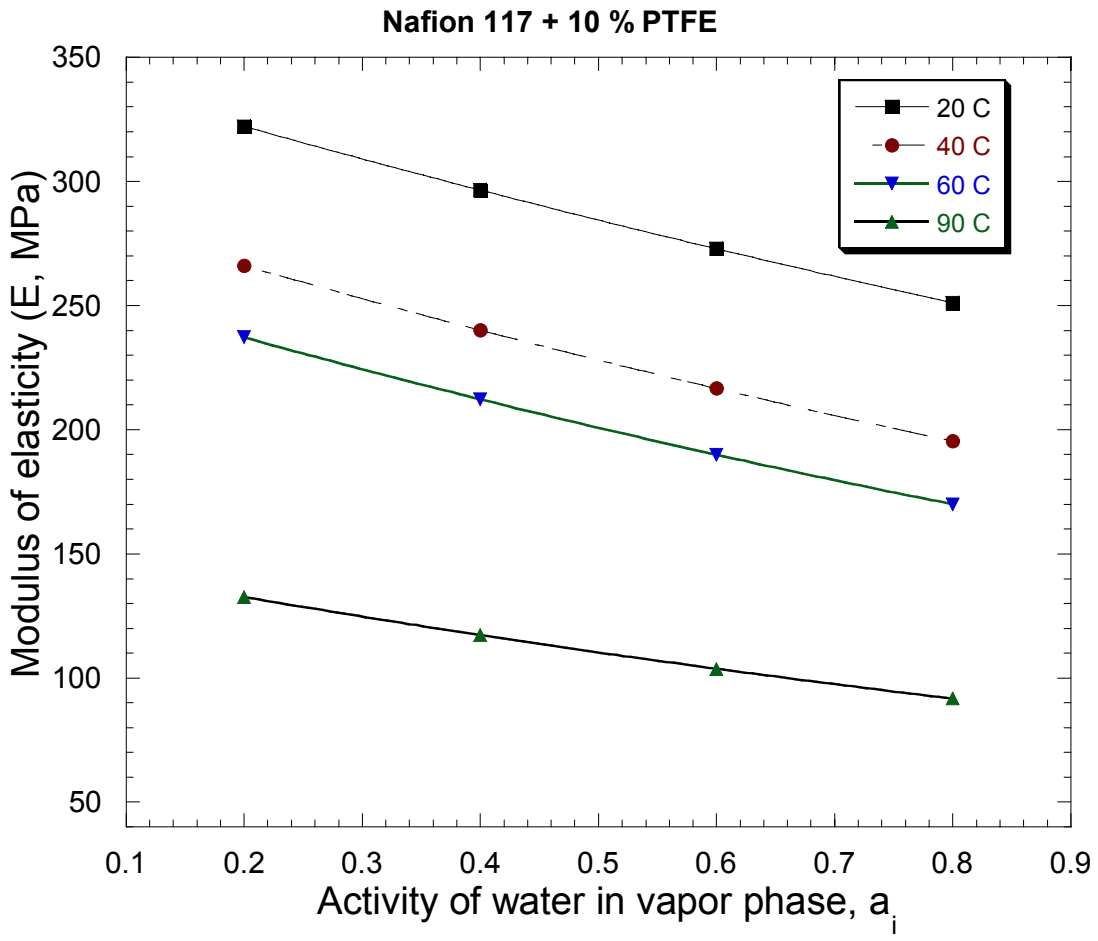

Figure 7.8 Experimental results for *E* of Nafion 117+ 10 % PTFE membrane as a function of temperature and water activity.

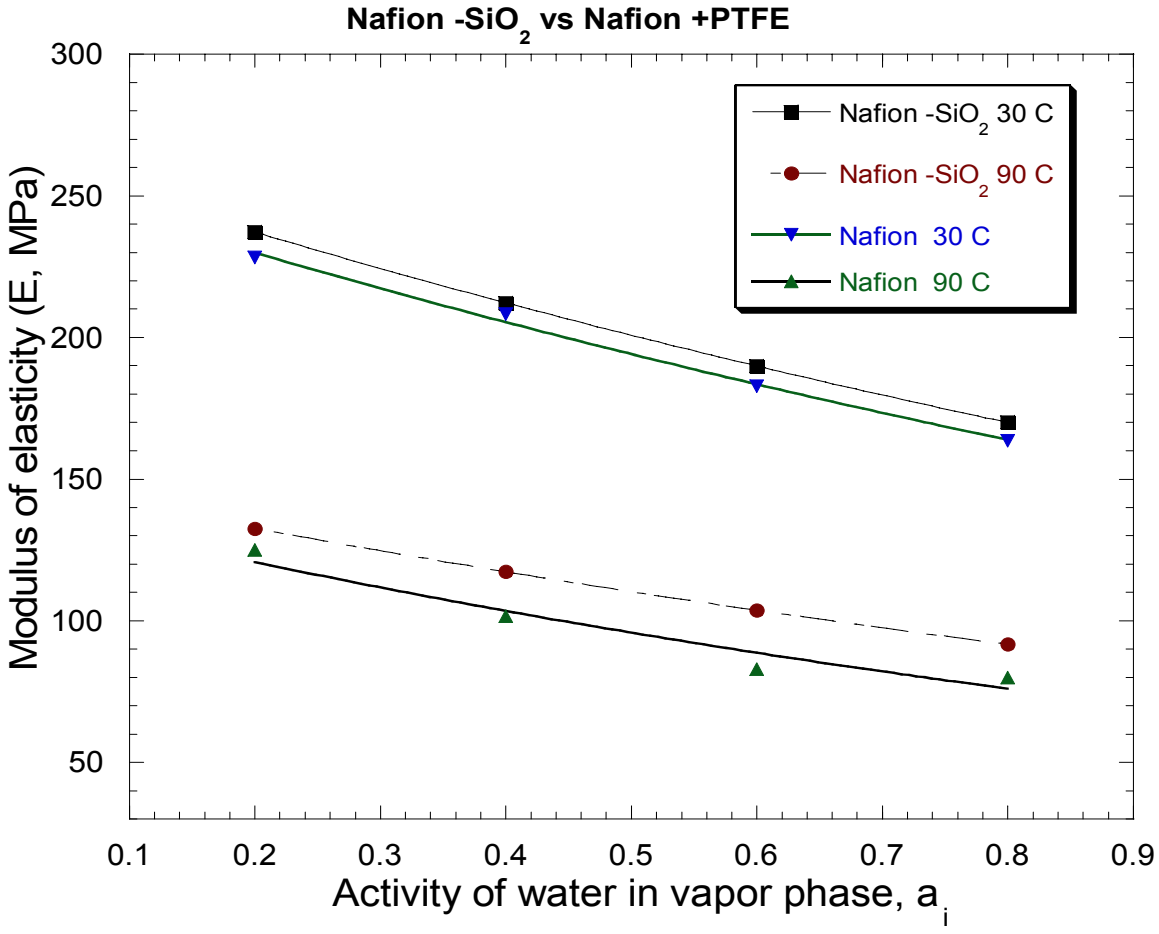

Figure 7.9 Experimental results for *E* of Nafion 117+ 10 % PTFE vs Nafion- SiO_2 membrane as a function of temperature and water activity.

7.10 References

1. K. D. Kreuer, "On the development of proton conducting polymer membranes for hydrogen and methanol fuel cells", *J. Membr. Sci.*, 185:29-39, 2001.
2. A. J. Appleby, and F. R. Foulkes, *Fuel cell handbook*, Van Nostrand Reinhold, New York, 1989.
3. M. Doyle, M. E. Lewittes, M. G. Roelofs, and S. A. Perusich, "Ionic conductivity of nonaqueous solvent-swollen ionomer membranes based on fluorosulfonate, fluorocarboxylate, and sulfonate fixed ion groups", *J. Phys. Chem. B*, 105:9387-9394, 2001.
4. T. Thampan, S. Malhotra, H. Tang, and R. Datta, "Modeling of conductive transport in proton- exchange membranes for fuel cells", *J. Electrochem. Soc*., 147 (9):3242-3250, 2000.
5. P. Choi and R. Datta, "Sorption in proton exchange membranes. An explanation of Schroeder's paradox", *J. Electrochem. Soc*., 150 (12):E601-E607, 2003.
6. Y. Kawano, Y. Wang, R. A. Palmer, and S. R. Aubuchon, "Stress-strain curves of Nafion membranes in acid and salt Forms", *Polímeros*, 12 (2):96-105, 2002.
7. K. A. Stetson and W. R. Brohinsky, "Electro-optic holography system for vibration analysis and nondestructive testing*", Opt. Eng*., 26 (12):1234-1239, 1987.
8. R. J. Pryputniewicz, *Holographic numerical analysis*, Worcester Polytechnic Institute, Worcester, MA, 1992.
9. R. J. Pryputniewicz and K. A. Stetson, "Measurement of vibration patterns using electro-optic holography", *Proc. SPIE*, 1162:456-467, 1989.
10. C. Furlong and R. Pryputniewicz, "Hybrid computational and experimental approach for the study and optimization of mechanical components", *Opt. Eng*., 37 (5):1448-1455, 1998.

Chapter 8

High Temperature Phosphoric Acid-PBI Gel Membrane Fuel Cells: Performance Analysis and Impedance Spectral Signatures

In this chapter, phosphoric acid (H_3PO_4) - Polybenzimidazole (PBI) membrane fuel cells are evaluated in the temperature range of 160-180 ^oC, in an effort to investigate the effect of temperature, anode humidification, various cathode stoichs, and use of oxygen versus air. This is an important system for high temperature operations due to high glass transition temperature of PBI (around 425 ^oC). I*n situ* electrochemical impedance spectroscopy (EIS) was used to obtain various resistances, ohmic, as well as charge transfer, under these conditions. The results obtained show that H_3PO_4 - PBI gel membranes exhibit very good performance in the temperature range of 160-180 ^oC. Mass transfer limitations were quantified by comparing performance polarization curves with air and oxygen, along with EIS. Further EIS was also used to obtain signatures during fuel starvation, and electrical shorting across the cell. This chapter is under review in J. Power Sources.

8.1 Introduction

Nafion-type perfluorosulfonated acid (PFSA) polymers have been widely used as a polymer electrolyte membrane (PEM) and a catalyst-binding material for electrode layers in membrane electrode assemblies (MEAs) [1-3]. However, the conductivity of Nafion is limited by water content in the membrane and hence it cannot be used for fuel cell operations at high temperature (>100 °C) under atmospheric pressure. The dehydration at higher temperatures also results in membrane shrinkage and consequent poor contact between the MEA and the bipolar plates. Hence, the performance benefit arising from higher CO tolerance at higher temperatures is offset by this dehydration. There is, thus a strong incentive to develop alternate polymer electrolytes that can work above 100 ^oC [4].

The development of electrolyte membranes for higher temperature operation is a particularly challenging task. A good polymer electrolyte membrane (PEM) must be thin for low resistance, compliant to make a good contact with electrodes, but rigid enough to provide support to the MEA, thermally and dimensionally stable, impervious to gaseous or liquid fuels as well as electrons, durable, and should be able to provide excellent proton conductivity rivaling liquid electrolytes (~0.1 S/cm) preferably under hot and dry conditions. We have previously published our work on higher temperature membrane synthesis and characterization [4-6].

In the emerging family of higher temperature membranes, phosphoric acid-polybenzimidazole (PBI) membranes have the potential to meet many of the requirements for higher temperature operation. PBI is an amorphous thermoplastic polymer with a glass transition temperature of 425–436 ^{o}C. It has a good chemical resistance and excellent textile fiber properties. As a membrane, PBI has received attention mainly for use in blood dialysis and reverse osmosis at high temperature and in harsh environments. Attempts to graft functional groups onto PBI were first made by Gieselman and Reynolds [7] and there have been persistent efforts ever since [9-22].

Chemically, PBI is a basic polymer and can readily react with acids. Wainright *et al* were the first to suggest the application of acid -doped PBI based membranes for fuel cell applications [8]. Various inorganic acids have since been investigated as dopants such as H_2SO_4, H_3PO_4, $HClO_4$, HNO_3, HBr, HCl, and organic acids like CH_3SO_3H, $C_2H_5SO_3H$ and aromatic phosphoric acids, as well as polymeric acids [9-22]. Among these various doping acids, phosphoric acid and sulphuric acid have been found to provide high conductivity. These acids act both as donors and acceptors in proton transfer and therefore allow for proton migration along the anionic chain. H_3PO_4 is particularly interesting acid due to its high conductivity and thermal stability at temperatures up to 200 ^{o}C. This is, of course, the reason for its use in phosphoric acid fuel cells.

The proton conductivity of phosphoric acid- PBI membranes have been extensively investigated [15-26]. Other properties such as methanol crossover rate, thermal stability, water drag coefficient, mechanical properties, and kinetics of oxygen reduction have also been studied [18-22]. The PBI fuel cells have been operated at temperatures up to 200 ^{o}C without humidification of the reactant gases. At 200 ^{o}C, a PEMFC can tolerate upto 30,000

ppm CO in the reformate stream, thus enabling the elimination of CO conversion stages of the fuel processor. This opens up the possibility for a simpler, compact, and cost effective system [23-26]. This is the reason for our interest in this system.

Song *et al* [27] studied the effect of electrolyte impregnation temperature, alloy catalyst, and single cell structure on electrochemical characteristics of H_3PO_4 - PBI system using EIS. They found that the high frequency resistance of cell does not depend on acid impregnation temperature in the electrodes for fuel cells. However, they observed that the interfacial resistance of the cathode (Pt-electrolyte) increase with the increasing impregnation temperature. They further studied the effect of CO concentration and reactant gas pressure on cell performance.

The goal of this paper is to evaluate the performance of phosphoric acid- PBI gel membranes based fuel cells for higher temperature operations. A comparison with Nafion membrane performance at lower temperature (80 ^{o}C) is done to show that this technology is great potential for fuel cell applications. Hence, we have characterized the performance at Plug Power in the temperature range of 160-180 ^{o}C. Since voltage of a fuel cell at a current or load in a polarization plot lumps together all types of losses, we use AC electrochemical impedance spectroscopy (EIS) for quantifying and discriminating various losses further. Also, it is shown in the present work that *in- situ* EIS provides good estimate for different resistances in fuel cells and are in well agreement with other *ex-situ* measurements. In addition, typical EIS signatures were identified by creating electrical shorts across a cell, during fuel starvation, and post high voltage carbon corrosion stress tests, with the objective of developing diagnostics.

8.2 Experimental

8.2.1 Fuel Cell Assembly and Testing

Commercially available Celtec-P Series 1000 membrane-electrode assemblies (MEAs) from PEMEAS (Frankfurt, Germany) were used in this study. Each MEA consists of a phosphoric acid electrolyte gel membrane is sandwiched between Pt catalyst based gas diffusion electrodes and supported with a polymer sub-gasket. The 44-cm^2 MEAs were compressed to a constant gap between isostatic graphite, serpentine flow-field, and gas

distribution plates. In operation the membrane is approximately 0.002 inch thick. The entire cell assembly is contained within an insulating bag, and the desired cell temperature is maintained using external pad heaters. Inlet gas temperatures were controlled through heated supply lines, and membrane humidifiers were used to control the dew point of the fuel stream. Polarization curves were obtained with hydrogen on the anode side and with air or oxygen on the cathode. Repeatability of polarization curves was confirmed with multiple polarization curves during the course of the test which also sheds light on the stability of these higher temperature fuel cells.

In summary, we studied the effect of 1) temperature, 2) anode humidification (40-80 ^{o}C), 3) cathode flow rate (stoichs), 4) oxidant type (air and oxygen), 5) fuel starvation and 6) induced electrical shorts across the cell. For identifying the voltage losses in the cells, electrochemical impedance spectroscopy (EIS) was employed as a characterization tool to investigate charge-transfer reaction resistance and transport resistances, including charge transport of electronic and ionic charge carriers, and mass transport through gas diffusion layer.

8.2.2 Electrochemical Impedance Spectroscopy (EIS) measurements

Voltage of a fuel cell is an overall response for a current drawn, all the losses being lumped in the response, which are not easy to separate with just direct current (DC) operation. During the operation of a fuel cell, the gases are fed through at specific volumetric flow rate (standard liters per minute or slm) depending upon the current. The gases further diffuse across the gas diffusion layer (GDL) to the electrode at a rate determined by the effective diffusion coefficient of the gases in the GDL at a given temperature [28]. Once the gases reach the catalyst site, a series of reaction steps take place, some of which are chemical while others are electrochemical involving charge transfer. These reactions are also influenced by the transport of protons to or from the site. All of these individual transport and kinetic steps have a characteristic time-constants associated with them. Electrochemical impedance spectroscopy (EIS) helps separate many of these steps when a spectrum with various perturbation frequencies is utilized *in-situ* in an operating fuel cell. The EIS experiment involves the application of a sinusoidal electrochemical perturbation (potential or current) to the sample that covers a wide range of

frequencies. This multi-frequency excitation allows (1) the measurement of several electrochemical reactions that take place at different rates and (2) the measurement of the capacitance of the electrode.

During our measurements, the cell was stable and the perturbation amplitude was chosen making sure the system was close to linear at all current densities (C.D's), especially at low and high current densities. Thus, the EIS measurements were performed with a perturbation current of 4 – 6 % of the DC current in the frequency range 0.01 Hz to 10^6 Hz using a Solartron SI 1260 FRA system, Solartron, Hampshire, U.K). The set-up is schematically illustrated in Figure 8.1(a), showing various cell interfaces with EIS instrumentation.

There has been extensive research done using EIS to characterize working of fuel cells [29-30]. A typical EIS spectrum during frequency sweep is shown in Figure 8.1(b). Both real and imaginary components of the impedance are measured and the real *z*-axis intercept at high frequency (i.e. intercept at the left) is assumed to provide mainly the membrane resistance, and hence, its conductivity. The low frequency intercept (on the right) is used to calculate the kinetic and mass transport resistances. A brief explanation on using the EIS spectra to obtain various losses is discussed below.

In the higher frequency range of the spectrum, typically when the frequency is more than 10 Hz, the high-frequency intercept on the real axis in Figure 8.1(b) corresponds to the ohmic resistance R_M . Now, the overall charge-transfer resistance R_P , i.e. the sum of the anodic and cathodic charge-transfer resistance is obtained distance from the difference of high-frequency real axis intercept to the next lower frequency real axis intercept. It is evident that the overall charge-transfer resistance R_P is mostly dominated by the cathode impedance due to the sluggish oxygen reduction reaction (ORR) kinetics. The lower frequency part of the spectrum, typically when frequency is less than 1 Hz, represents the sum of a capacitive loop in the anode spectrum and an inductive loop in the cathode spectrum, which appear in a similar frequency range.

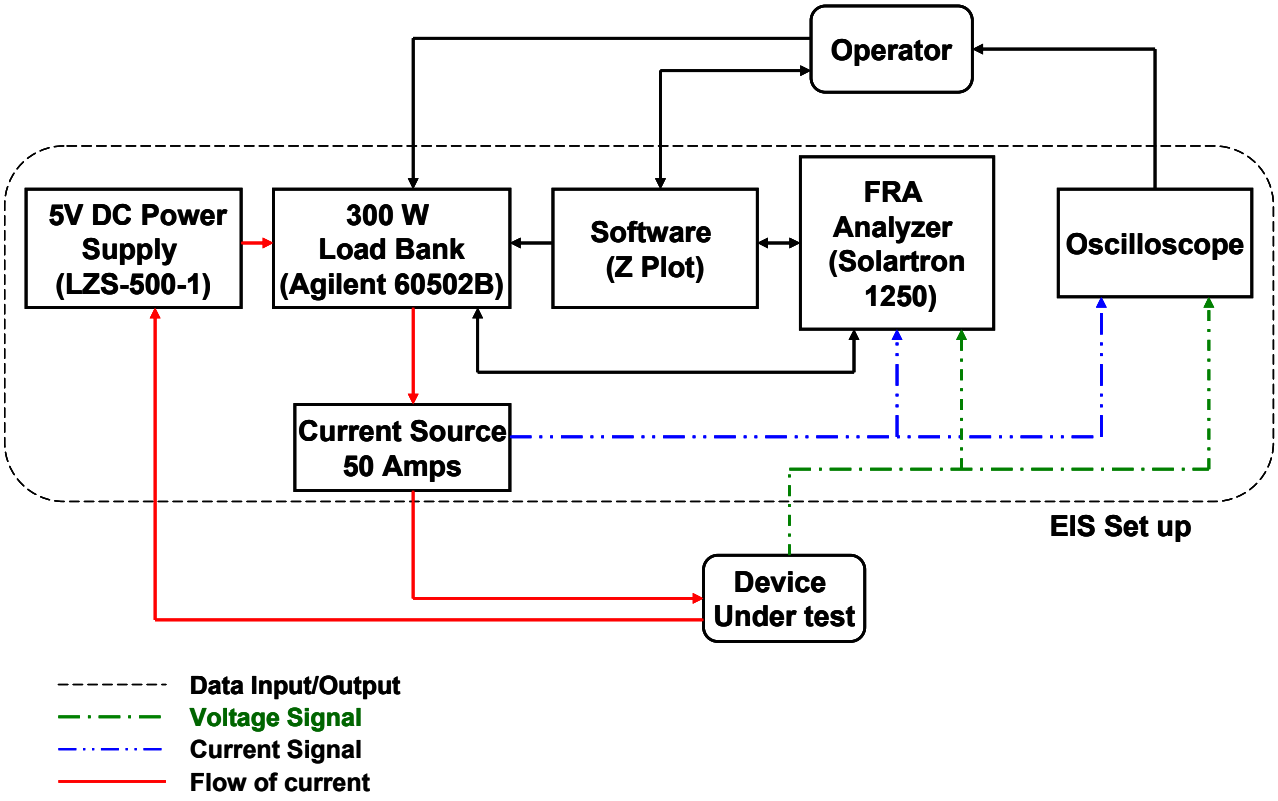

Figure 8.1(a). EIS instrumentation schematic.

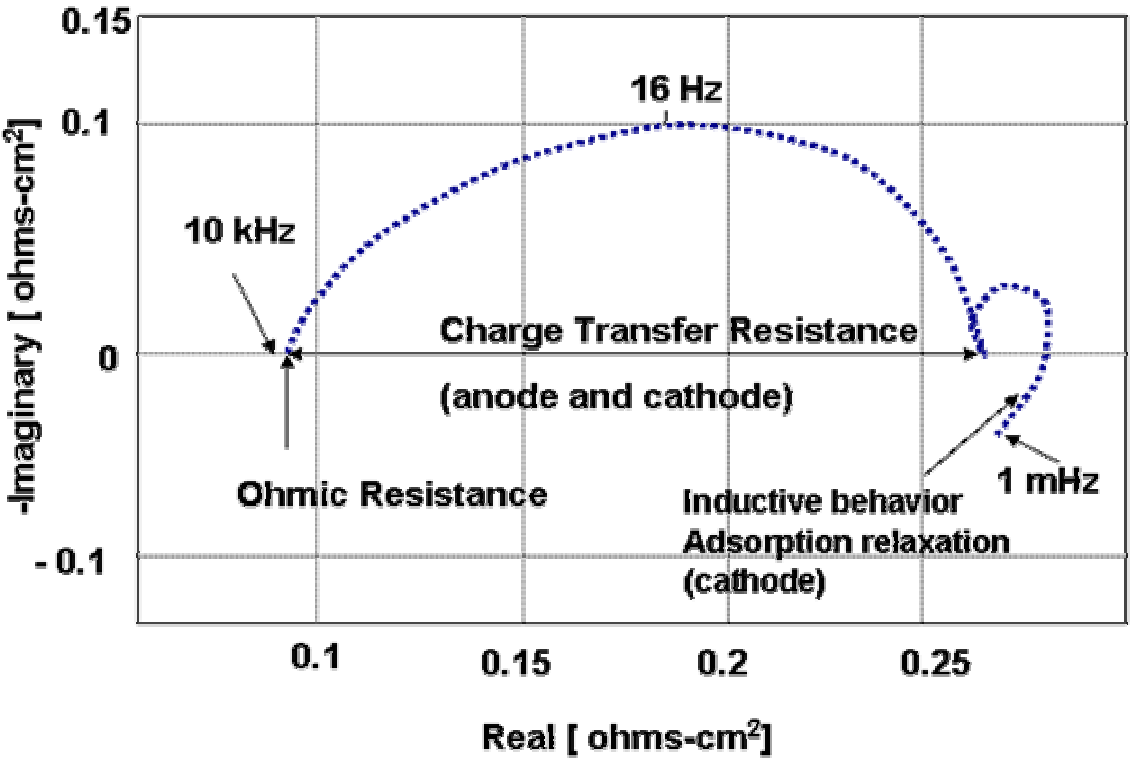

Figure 8.1(b). Correlation between different parts of a EIS spectrum and limiting processes.

The capacitive arc seen in the low frequency range can be attributed to a finite diffusion process. This is due to the mass transport in GDL and electrode layers at anode and cathode. Because the lower frequency part of the impedance spectrum is the sum of a capacitive loop in the anode spectrum and an inductive loop in the cathode spectrum, it is not possible to extract quantitative data from the lower frequency part of the local two-electrode spectra. The anode and cathode contributions to the overall local two-electrode spectrum are unknown. It should be mentioned here that the inductive behavior seen in the high-frequency range of some of the local impedance spectra to be presented later is due to mutual inductance (i.e., cable) effects.

8.3. Results and Discussion

8.3.1. Effect of Temperature

The cell temperature was varied using pad heaters and polarization curves were obtained at three temperatures namely of 160, 170 and 180 ^{o}C with 55 ^{o}C dew point hydrogen on anode side and dry air on cathode side. It is well known that with an increase in temperature, the exchange current density and the conductivity of the membrane increases [28]. The DC performance of the fuel cell increased with temperature as shown in Figure 8.2 (a). Also, the performance obtained is compared with Nafion membrane at 80 ^{o}C under saturated conditions. It can be seen that the performance of PBI system is substantially high at higher current densities indicating that this system has very high diffusion of oxygen in GDL and hence has higher limiting current density. Also, another reason for good performance in PBI is due to the absence of water in GDL which keeps the pores open for effective mass transport of oxidant. The DC performance lumps the ohmic losses, activation losses and mass transport losses. On the other hand, EIS measurements at high frequency clearly separates ohmic resistance. These values were used to correct the polarization curves to obtain cathode over potential at different temperature assuming negligible anode overpotential. The apparent cathode Tafel slope, thus, was extracted to be about 0.105 – 0.11 V/decade as shown in Figure 8.2(b).The intercept values were used to extract exchange current densities at different temperatures.

The high frequency intercepts of the Nyquist plots are compared against typical

ohmic resistance values obtained from the slope of the hydrogen pumping were similar to the values obtained from the high frequency intercept using EIS measurement. As shown in Figure 8.3, a scatter of 0.02 ohm-cm^2 is seen when the EIS is performed at different C.D's at 160 ^oC. All values at frequencies less than 1 kHz also account for additional ohmic resistance from electrolyte present in the catalyst.

The R_P is also plotted in Figure 8.4 against current density at three different temperatures when H_2/O_2 was used. The trend is similar at all temperatures and the values are relatively close to each other except at higher current density of 0.3 A/cm^2, where a decrease in R_P is more evident.

8.3.2 Effect of Anode Dew Point

Experiments described in this study were performed at a constant fuel inlet dew point of 55 ^oC. The water content in the hydrogen stream could conceivably impact the high frequency resistance via a change of the liquid H_3PO_4 electrolyte concentration within the membrane as well as the electrode layer. In order to study this effect, polarization curves were obtained by varying the dew point of the inlet fuel from 40 – 80 ^oC at a constant cell temperature of 160 ^oC, as shown in Figure 8.5. It can be seen that the cell performance declines somewhat with increasing anode dew point, although below 50 ^oC, there was no discernible difference in the polarization curves. This effect may possibly be explained by either a change in the hydrogen partial pressure as dew point increases, or due to the fact that the liquid electrolyte content in the membrane/electrode interface changes. Further experiments are planned to understand this effect using EIS.

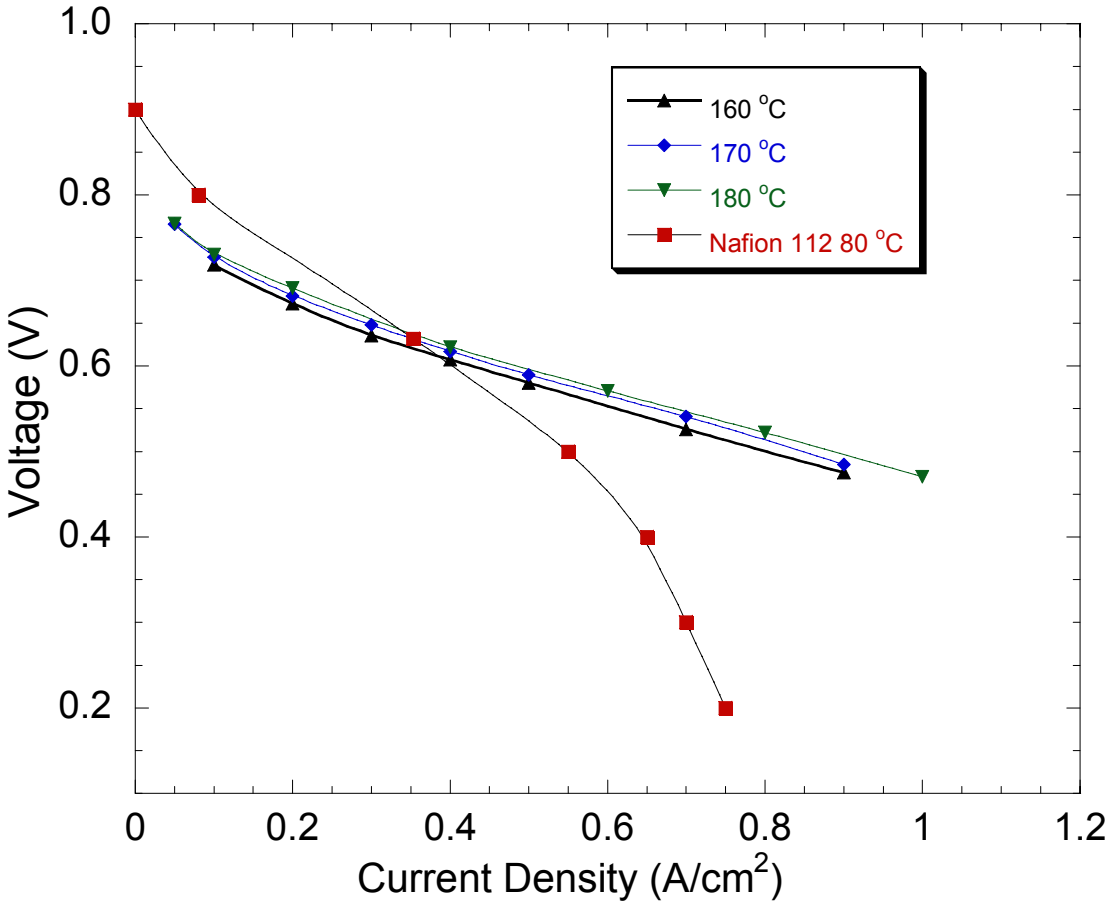

Figure 8.2(a) Polarization curves at different temperatures with air as oxidant (160-180 °C) compared with Nafion.

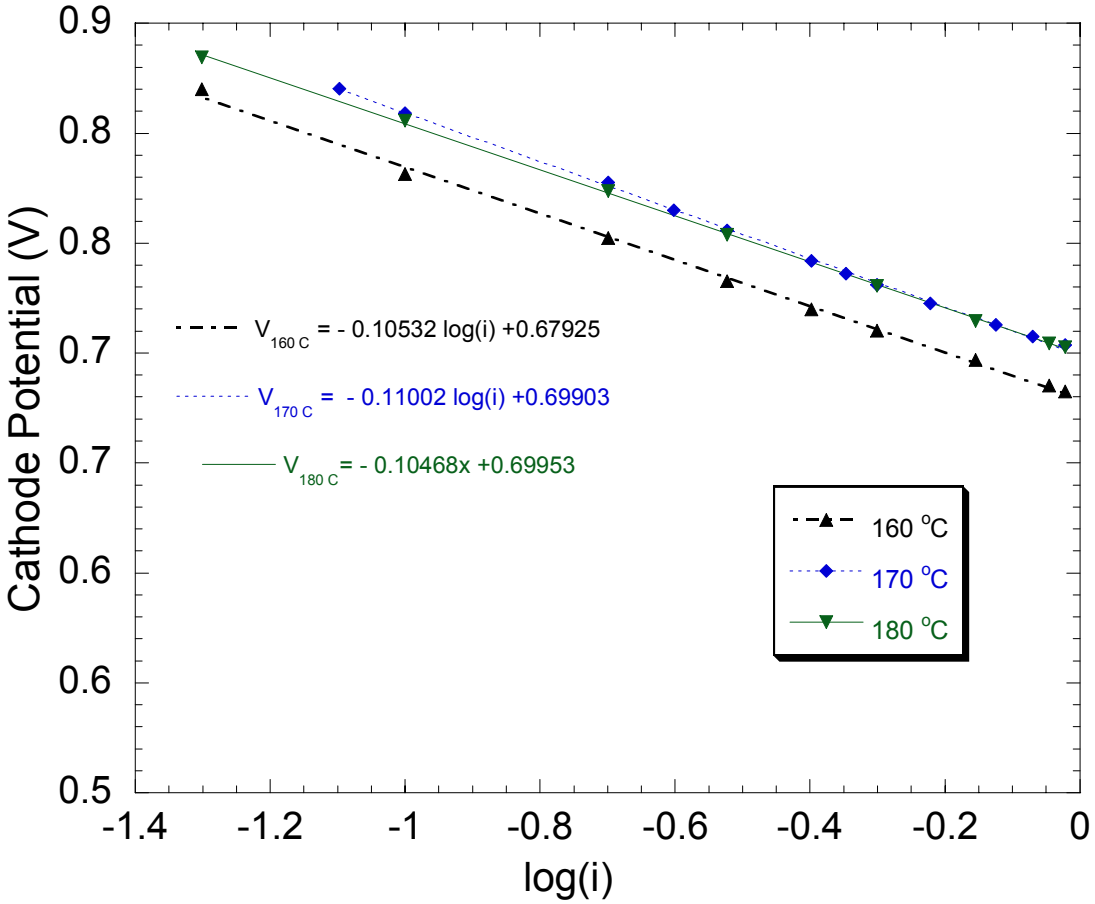

Figure 8.2(b). IR corrected polarization curves at different temperatures using air (160-180 °C).

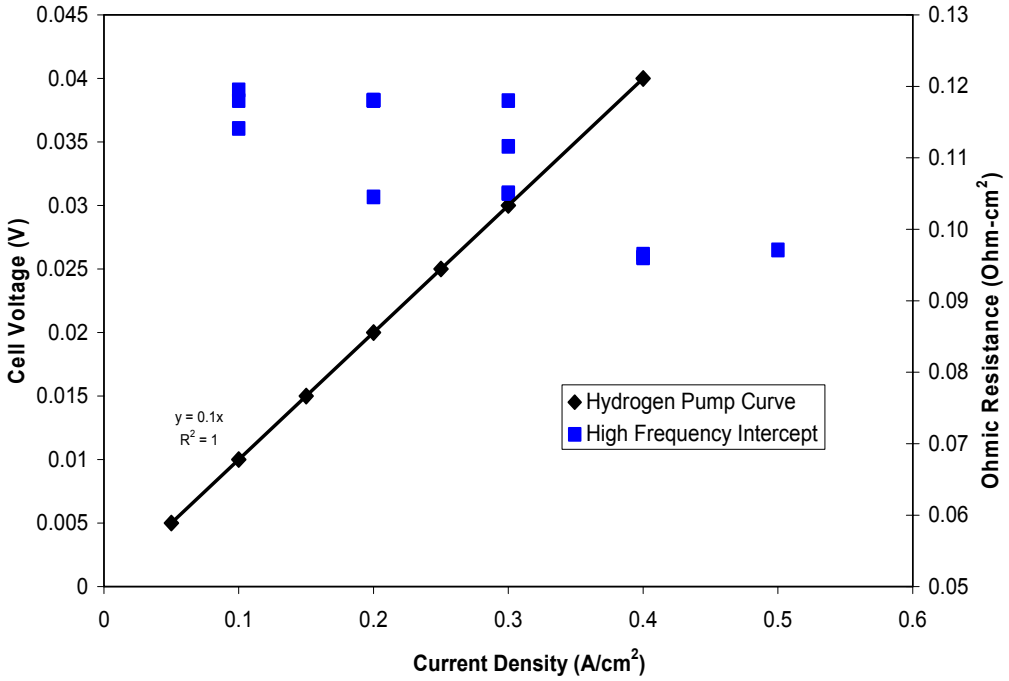

Figure 8.3 Hydrogen pumping in comparison with high frequency intercepts at 160 ^{o}C

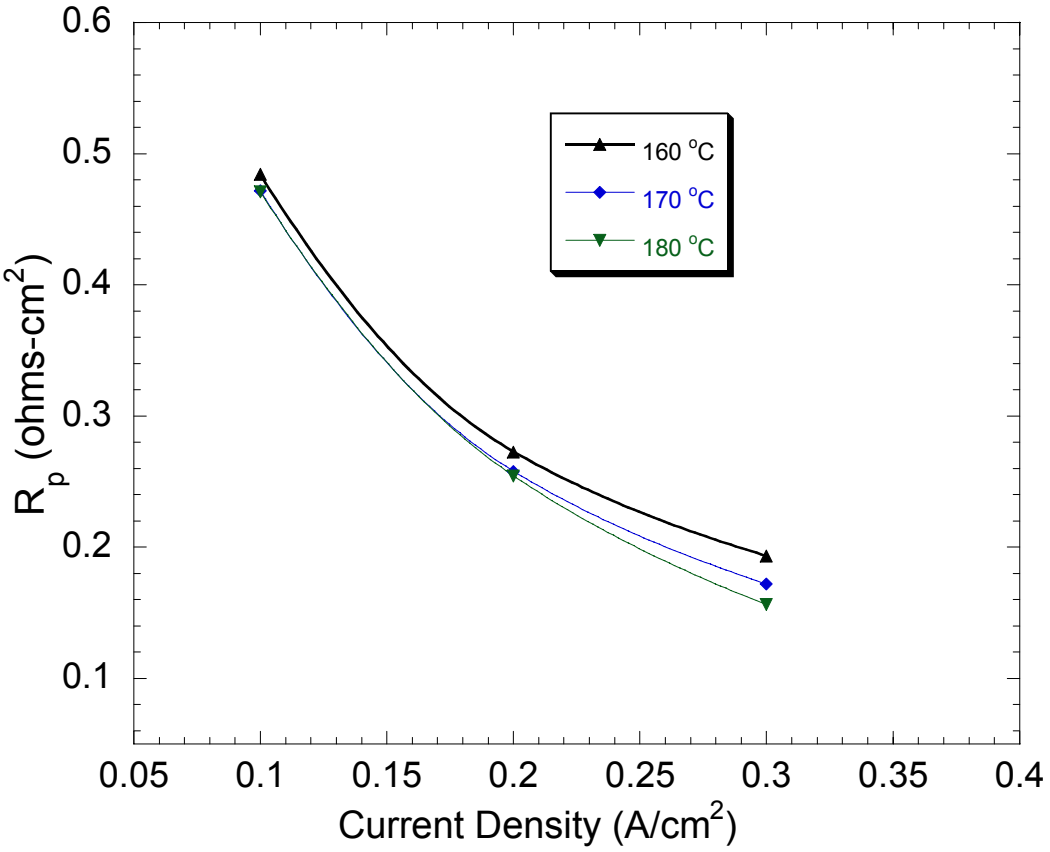

Figure 8.4 Low frequency intercept as a function of current at different temperatures using oxygen as an oxidant.

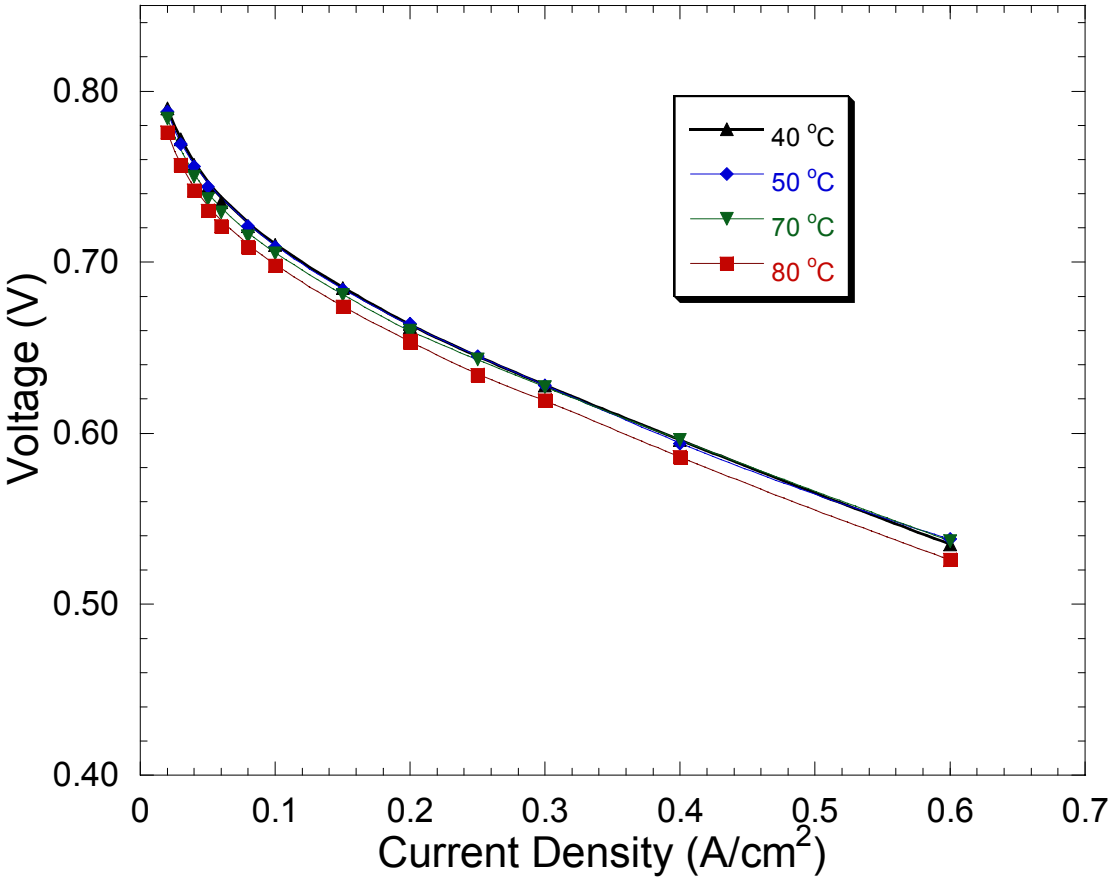

Figure 8.5 Effect of fuel inlet dew point temperatures on the performance curves at 160 ^{o}C.

8.3.3 Effect of Cathode Stoichs:

Figure 8.6 shows the effect of cathode stoich on the polarization curves at 160 ^{o}C. Substantial improvement in performance is seen with an increase in the cathode stoichs from 1.4 to 6. These measurements indicate the onset of GDL/electrode interface mass transport resistance at current densities greater than 0.2 A/cm^2. EIS was also performed at multiple cathode stoichs and the results are summarized in Figure 8.7 for a current density of 0.2 A/cm^2 at two different temperatures. Cathode stoichs had a significant impact on the *Rp* values indicating flow channel /GDL interface mass transport resistance. With an increase in cathode stoichs, the high frequency resistance remained unaffected, but the *Rp* (which includes charge transfer and diffusive losses) decreased significantly as shown in Figure 8.7 which shows the trend of R_P at different current densities as a function of cathode moles/min (converted from flow rate). In Figure 8.7, a theoretical charge transfer resistance obtained from tafel kinetics slope is also plotted to show the deviation from theoretical even when pure oxygen is used at lower current densities. This hints at solubility of oxygen being a significant contributing factor and further understanding with varying concentration of oxygen content is required. Further, while the backpressure of the cathode chamber also increases as the air flow rate is increased; it does not contribute to substantial increase in oxygen partial pressure. It is hypothesized, however, that with an increase in the cathode stoichs, the current generated is more uniform across the MEA, since the log-mean or average concentration from inlet to outlet varies less significantly. Similar behavior was also observed for a current density of 0.1 A/cm^2. Above 0.021 moles/min, not much change in R_p was observed for 0.2 A/cm^2, while for 0.1 A/cm^2, the threshold was closer to 0.01moles/min.

8.3.4 Oxygen versus Air

Polarization curves and EIS parameters were measured with both air and oxygen. This study further explicates the diffusion effects across GDL. Figure 8.8 shows the polarization curves with oxygen at 160 – 180 ^{o}C compared with Nafion membrane at fuel cell temperature of 80 ^{o}C under saturated conditions. They are about similar which again shows that the PBI system produces decent power at higher temperatures. The performance obtained in Figure 8.9 is difference in the polarization curves obtained with

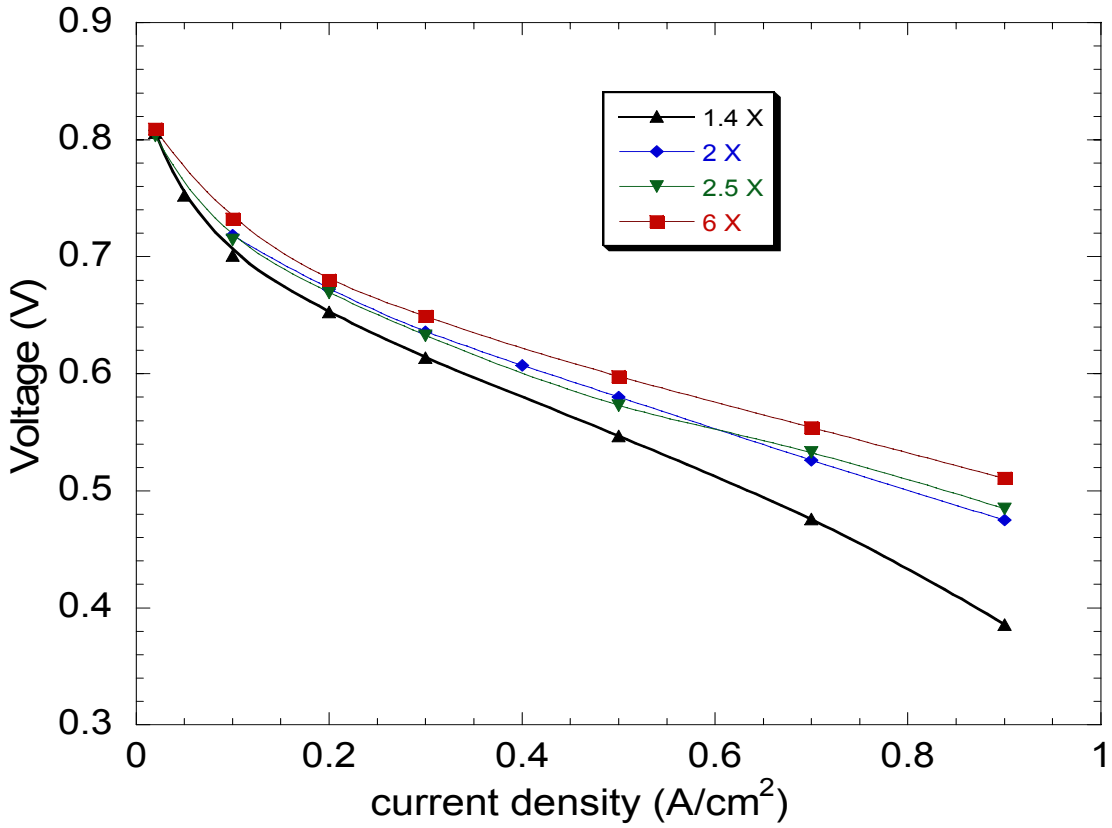

Figure 8.6 Effect of cathode stoichs on the performance curves at 160 ^{o}C.

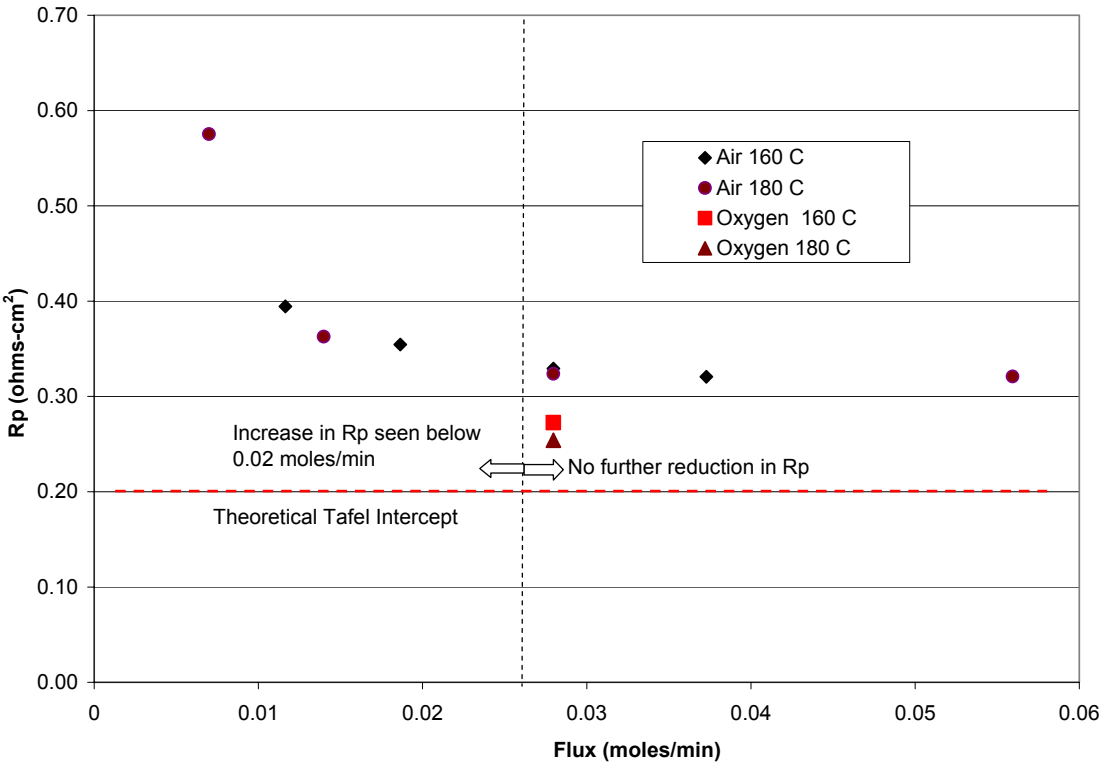

Figure 8.7 Low frequency intercept as a function of current density at 160 and 180 ^{o}C.

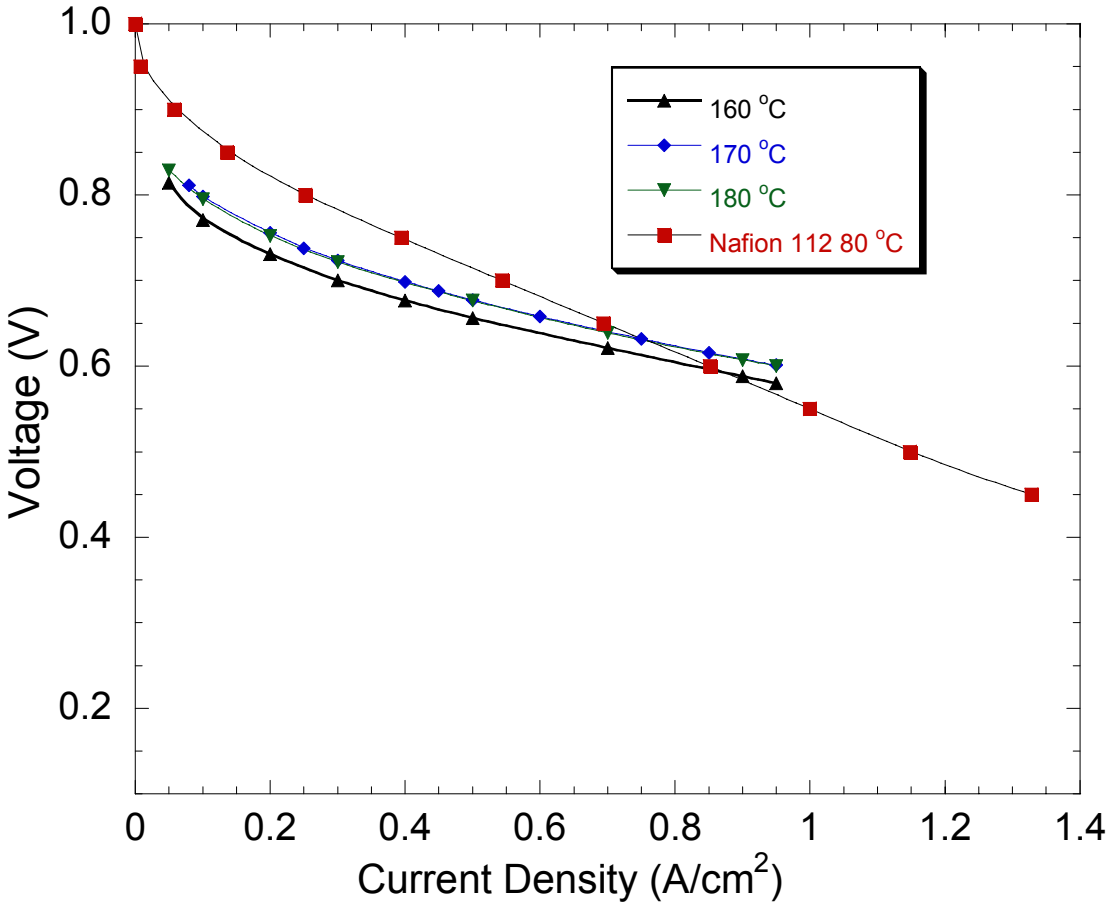

Figure 8.8 Polarization curves at different temperatures with oxygen as oxidant (160-180 °C) compared with Nafion.

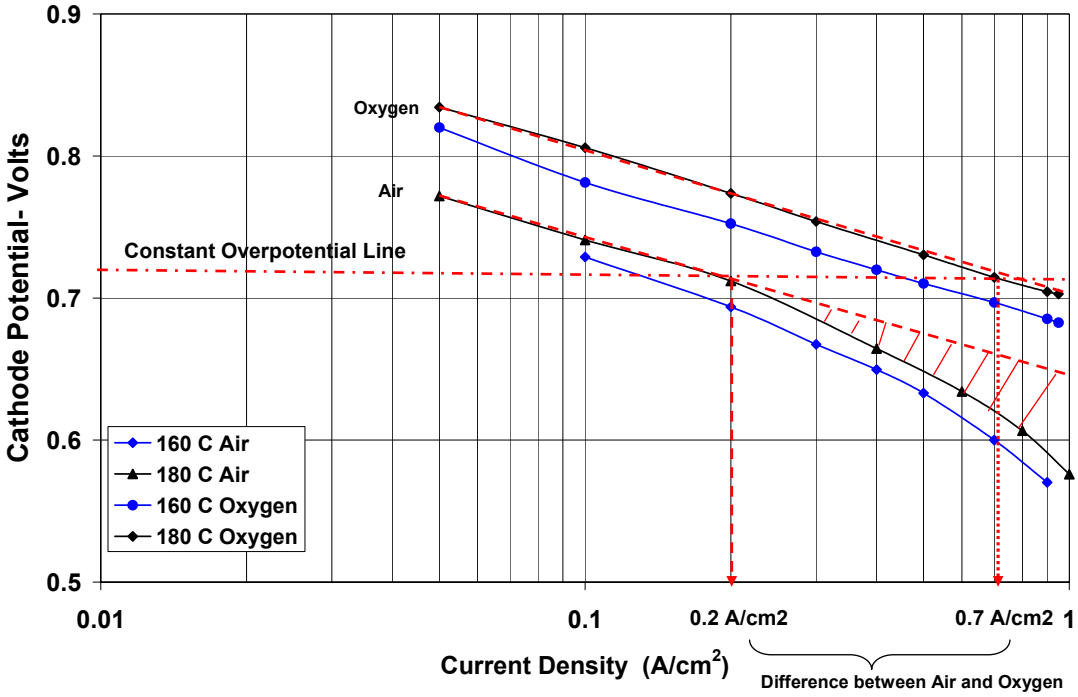

Figure 8.9 Effect of oxygen concentration on polarization curves at 160 ^{o}C and 180 ^{o}C.

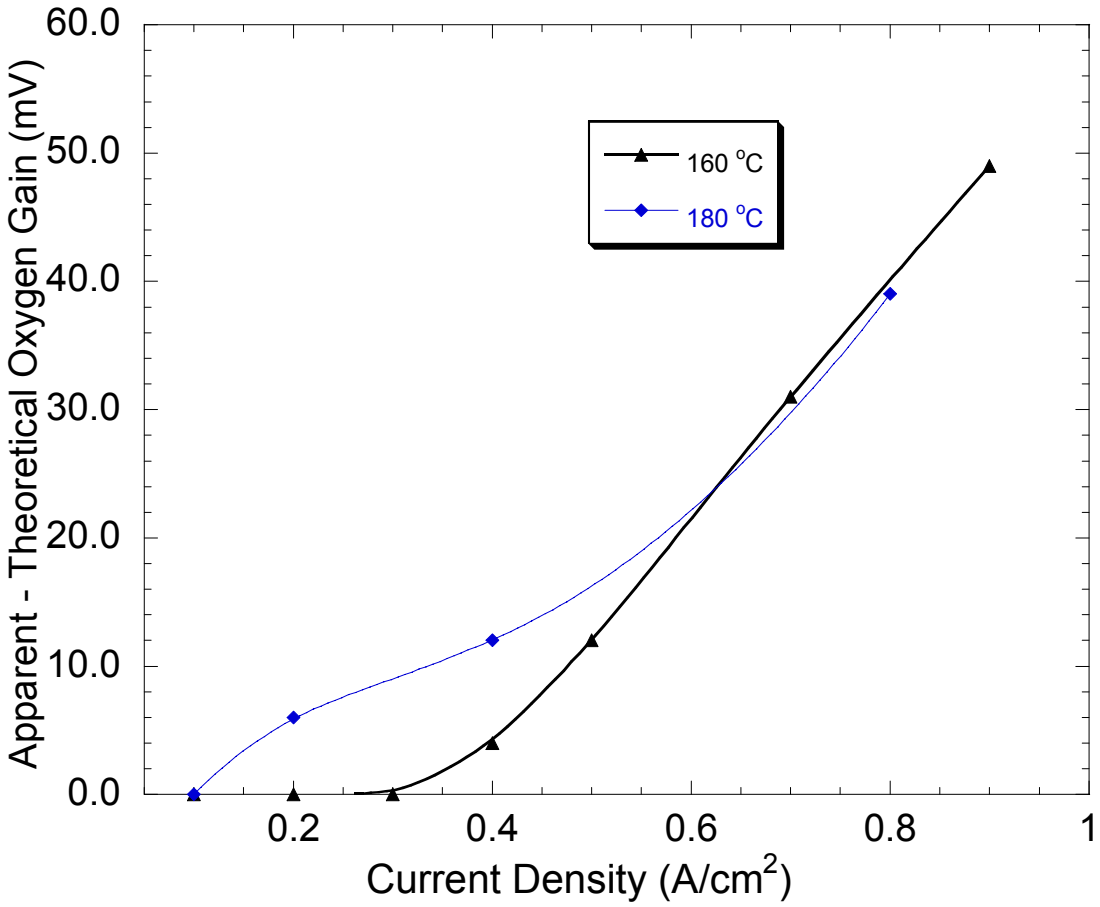

Figure 8.10 Oxygen gain measurements at 160 °C and 180 °C.

oxygen and air. A Tafel slope of 0.1 V/decade was obtained for oxygen curves at both 160 C and 180 ^{o}C, i.e., Tafel slope was independent of temperature in this range. However, with air, even after correcting for the ohmic contribution, the resulting E vs. log (i) plot showed non linearity above 0.2 A/cm^2 due to diffusion limitations. Such behavior in general is seen in two different cases: (1) – distributed ohmic resistance across the electrode, (2) – mass transport limitations across the GDL. Theoretical oxygen gain was calculated to be approximately 66 mV. This provided the maximum gain one could obtain if there were no diffusion limitations across the MEA.

Figure 8.10 plots the deviation from this ideal gain at 160 ^{o}C and 180 ^{o}C as a function of current density. This clearly indicates that the mass transport across the GDL becomes significant after 0.2 A/cm^2 at 180 ^{o}C and at 0.4 A/cm^2 at 160 ^{o}C. At a constant overpotential in IR corrected polarization curves as shown in Figure 8.9, the ratio of currents obtained using oxygen and air may be expected to be assumed 4 or 5, i.e., equal to the ratio of oxygen partial pressures. This is true only if the polarization curve is activation controlled and the kinetics of oxygen in oxygen is first- order. With the polarization curve corrected for ohmic losses obtained from the 1 kHz intercept via EIS, we conclude that resulting ratio of 3.5 for currents indicates less than the theoretical. This observation begs further investigation to gain insights on the precise concentration at the electrode surface rather than the bulk feed concentration.

The R_P values were collected from EIS curves for both air and oxygen at various current densities. This enabled a comparison against theoretical R_P values obtained from known Tafel curve for oxygen which is approximately 0.1 V/decade. The difference between measured R_P when using oxygen and air was found to be approximately 0.055 ohm-cm^2 to 0.059 ohm-cm^2. The difference between the theoretical charge transfer resistance from known Tafel slope and R_P using oxygen was approximately 0.059 ohm-cm^2. The IR corrected performance or the cathode potential can be expressed either as a function of current density or as a function of R_P.

Cireunnu *et al*. [31] and Raistrick *et al*. [32] explained the significance of using such a plot to separate charge transfer, agglomeration of catalyst particles and thin film contribution. The cathode potential was plotted as a function of log (R_P^{-1}). This provided a simple relationship where we estimated the cathode potential assuming that the anode

contribution to R_P is small. Figure 8.11 explains the relationship for both air and oxygen. This can be further used to understand the exchange current densities using air and oxygen. This shows that there might be some charge transfer and agglomeration contribution when using air at higher stoichs whereas at lower stoichs equal to 2.5, thin film or channel /GDL contribution dominates.

8.3.5 Effect of Fuel Stoich and Short Circuiting:

The fuel stoich was reduced by increasing the anode utilization from 70 % to just over 100 %. The cell was operated at 160 ^{o}C at 0.3 A/cm^2 and a 3.6 cathode stoichs during the course of the test. The cell was kept running at 1.3 stoich for 5 minutes and then reduced, while logging low frequency intercept at 0.1 Hz continuously every 5 seconds. As seen in Figure 8.12, multiple low frequency spectrum (1 kHz – 0.1 Hz) measurements were also conducted at discrete stoichs to show the onset of 45 ^{o} line, which is also a characteristic of electrical short, when stoich are close to 1.0 and less. The fuel stoichs show insignificant signatures in impedance until 1.0 stoich, below which the infinite diffusion trend takes over characterized by the 45 ^{o} line. At this point, the cell becomes fuel limited and the performance starts to decline at an alarming rate. In fact, the cell needs to be protected against such incidents in general since the anode potential during fuel starvation can exceed 1 V if a cell is connected to a power supply during such transients. This can irreversibly damage the anode and cathode electrode of a fuel cell limiting its life. The impedance signatures can show the trend before cell performance starts to decline and can be used to control then fuel cells more pro-actively.

A cell was also electrically shorted with a 40 milli-ohm resistor, while operating at 180 ^{o}C at 0.219 A/cm^2 with 1.5 fuel stoich and 2 air stoich. During this measurement, the cell experienced increased net current due to two parallel current demands – one from the load bank and the other through the shorted electrical resistor. At this point, as seen in Figure 8.13, the 45 ^{o} line starts to take over at 25 Hz with the short applied across the cell. This signature is similar to the fuel starvation signature, however in this case; one or both electrodes may be starved of reactants. Increasing both the fuel and air stoichs resulted in normal behavior after the increased current demand was met by the increased fuel and air

flow rates. However the 3 – 20 Hz lobe is reduced post shorting since additional current is being drawn.

8.4 Conclusions

It has been demonstrated that the PEMEAS phosphoric acid –PBI based MEAs provide good performance in the operating temperature range of 160 – 180 ^{o}C. The high frequency intercept in EIS experiments indicate an ohmic contribution of about 0.1 ohm-cm^2 which is similar to that for Nafion based membrane systems. Performance was investigated at various fuel inlet dew points and it was found that an increase in dew point somewhat effects the performance of the PBI system. By varying cathode stoichs the observed change in performance and impedance behavior indicates that current generation from inlet to outlet of a fuel cell have a profound effect on measured global responses in voltage and impedance. Comparing polarization curves with air and oxygen, it is apparent that the diffusive losses exist across the GDL. Diffusion losses quantified at two different temperatures indicate that there are significant diffusion losses at current densities greater than 0.4 A/cm^2. A simple expression for cathode potential obtained as a function of R_P at 160 ^{o}C shows charge transfer contribution as the dominant resistance in the current density range selected with oxygen. Two extreme cases of reactant starvation were studied using fuel starvation and electrically shorting the cell. Impedance signatures developed during fuel starvation shows a 45^{o} degree line and this signature is similar when a cell is electrically shorted with a 40 milli-ohm resistor.

Acknowledgements

The authors thank the National Institute for Standards and Technology (NIST) for funding this research. We particularly thank Gerald Caesar, Program Manager at ATP, and John Nail, Business Manager, for their support.

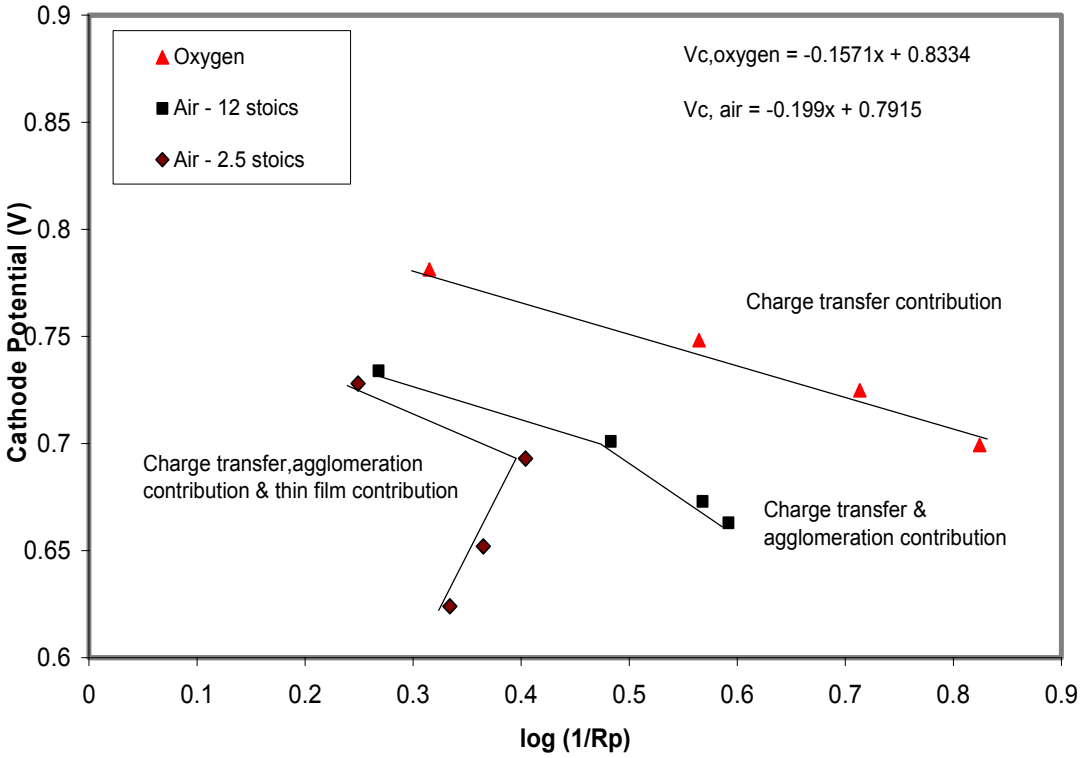

Figure 8.11 Cathode potential at two concentrations of oxygen as a function of low Frequency intercept at 160 ^{o}C.

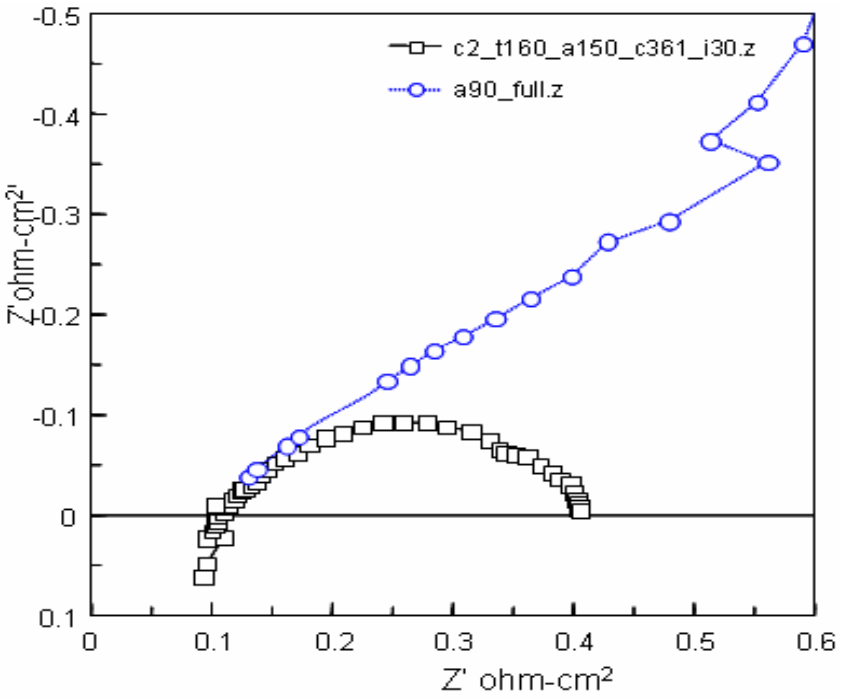

.

Figure 8.12 EIS spectrum when fuel stoichs are lowered to close to 100 % utilization at 0.3 A/cm^2 .

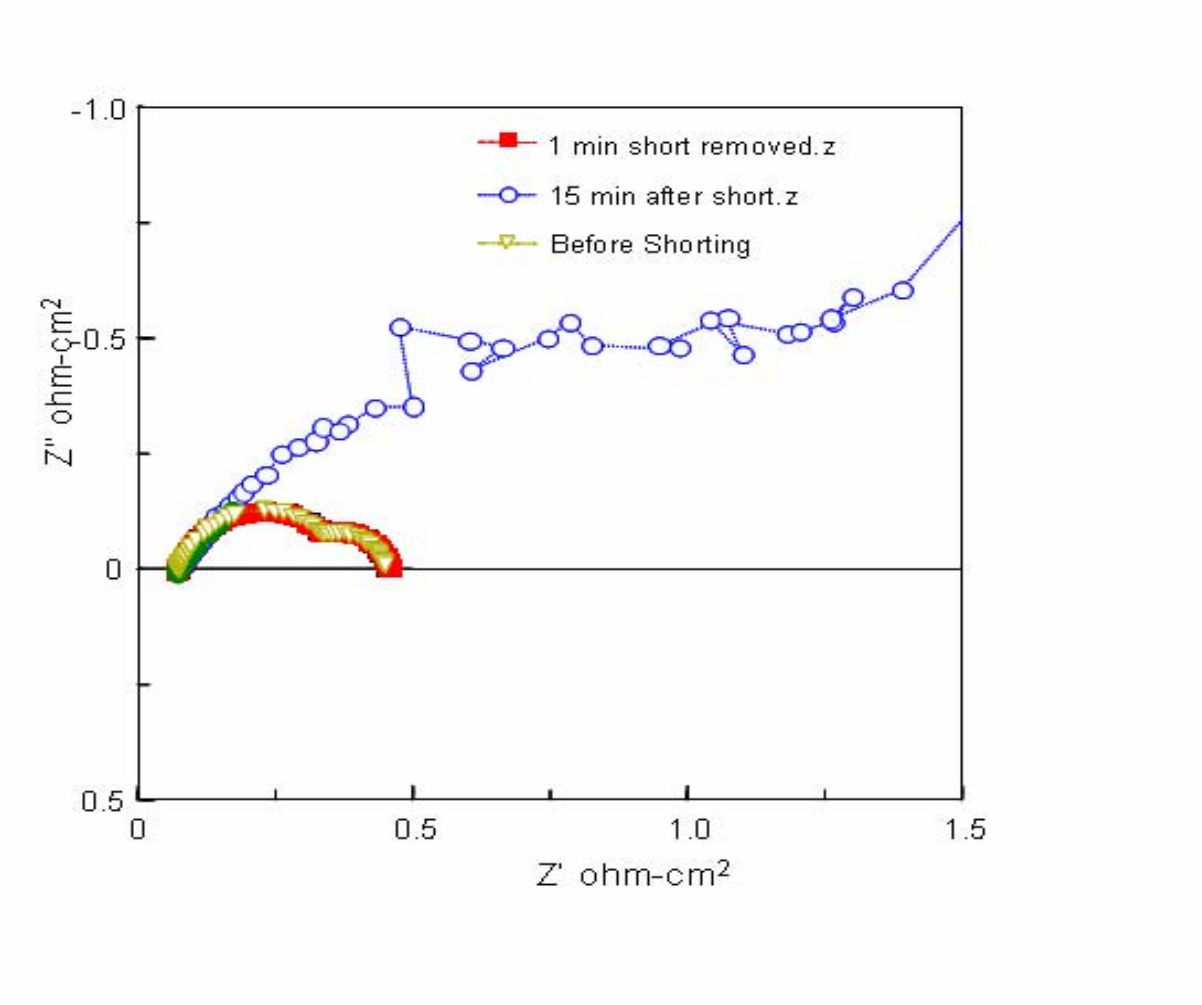

Figure 8.13 EIS spectrum as cell is electrically shorted with 40 milli-ohm resistor.

8.5 References

[1] K. D. Kreuer, J. Membr. Sci., 185 (2001) 29.

[2] A. J. Appleby, and F.R. Foulkes, Fuel Cell Handbook, Van Nostrand Reinhold, New York, 1989.

[3] M. Doyle, M. E. Lewittes, M. G. Roelofs, and S. A. Perusich, J. Phys. Chem. B, 105 (2001) 9387.

[4] N. H. Jalani, K. Dunn, R. Datta, Electrochimica Acta, 51 (3) (2005) 553.

[5] N. H. Jalani and R. Datta, J. Membr. Sci., 264 (1-2) (2005)167.

[6] N. H. Jalani; P. Choi, and R. Datta, J. Membr. Sci., 254 (1-2) (2005) 31.

[7] M.B. Gieselman, J.R. Reynolds, Macromolecules, 26 (1993) 5633.

[8] P. Staiti, F. Lufrano, A.S. Arico`, E. Passalacqua, V. Antonucci, J. Membr. Sci., 188 (2001) 71.

[9] J.S. Wainright, J.-T. Wang, D. Weng, R.F. Savinell, M. Litt, J. Electrochem. Soc.,142 (1995) L121.

[10] G. Xiao, Q. Li, H.A. Hjuler, R.W. Berg, N.J. Bjerrum, J. Electrochem. Soc., 142 (1995) 2890.

[9] Q. Li, R. He, J.O. Jensen, N.J. Bjerrum, Chem. Mater., 15 (2003) 4896.

[10] J.S. Wainright, T. Wang, D. Weng, R.F. Savinell, M. Litt, J. Electrochem. Soc., 142 (1995) L121.

[11] J.S. Wainright, M.H. Litt, R.F. Savinell, in: W. Vielstichm, A. Lamm, H.A Gasteiger (Eds.), Handbook of Fuel Cells, vol. 3, John Wiley & Sons Ltd., 2003, p. 436.

[12] Q. Li, R. He, J.O. Jensen, N.J. Bjerrum, Fuel Cells Fundam. Syst., 4 (2004) 147.

[13] X. Glipa, M.E. Hadda, D.J. Jones, J. Roziere, Solid State Ionics, 145 (1997) 61.

[14] R. Bouchet, E. Siebert, Solid State Ionics, 118 (1999) 287.

[15] X. Glipa, B. Bonnet, B. Mula, D.J. Jones, J. Roziere, J. Mater. Chem, 9 (1999) 3045.

[16] B. Xing, O. Savadogo, J. New Mater. Electrochem. Syst., 2 (1999) 95.

[17] M. Kawahara, J. Morita, M. Rikukawa, K. Sanui, N. Ogata, Electrochim. Acta, 45 (2000) 1395.

[18] Q. Li, H.A. Hjuler, N.J. Bjerrum, J. Appl. Electrochem., 31 (2001) 773.

[19] J. J. Fontanella, M.C. Wintersgill, J.S. Wainright, R.F. Savinell, M. Litt, Electrochim.Acta, 43 (1998) 1289.

[20] H. Pu, W.H. Meyer, G. Wegner, J. Polym. Sci., Part B, Polym. Phys., 40 (2002) 663.

[21] H. Akita, M. Ichikawa, K. Nosaki, H. Oyanagi, M. Iguchi, U.S. Patent 6 124 060 (2000).

[22] J.A. Kerres, J. Membr. Sci., 185 (2001) 3.

[23] Q. Li, R. He, J. Gao, J.O. Jensen, N.J. Bjerrum, J. Electrochem. Soc., 150 (2003) A1599.

[24] R. He, Q. Li, G. Xiao, N.J. Bjerrum, J. Membr. Sci., 226 (2003) 169.

[25] Q. Li, R. He, J. Gao, J.O. Jensen, N.J. Bjerrum, J. Electrochem. Soc., 150 (2003) A1599.

[26] Q. Li, H.A. Hjuler, C. Hasiotis, C.G. Kontoyannis, N.J. Bjerrum, Electrochem. Solid State Lett., 5 (2002) 125.

[27] R. H. Song, D. J. Kim, C. S. Kim, D. R. Shin ,J. New Mat. For Electrochem. Syst., 4 (2001) 47.

[28] T. Thampan, N. H. Jalani, P. Choi, and R. Datta, J. Electrochem. Soc, 152(2) 2005 A 316.

[29] I. A. Schneider, H. Kuhn, A. Wokaun, and G. G. Scherer, J. Electrochem. Soc., 152 (2005) A2092.

[30] O. Antoine, Y. Bultel, and R. Durand, J. Electroanal. Chem., 499 (2001) 85.

[31] M. Ciureanu, J. Phys. Chem, B, 105 (2001) 3531.

[32] I. D. Raistrick, Electrochimica Acta, 35 (1990) 1579.

Chapter 9
Conclusions and Recommendations for Future Work

9.1 Conclusions

In this research, higher temperature nanocomposite proton-exchange membranes (NCPEMs) with adequate performance under low relative humidity (RH) were developed based on theoretical and experimental considerations. The approach was based on enhancing the acidity and water sorption of a conventional polymer electrolyte membrane by incorporating in it a solid acidic nano sized inorganic material. A systematic investigation of the nanocomposite Nafion/inorganic additive PEMs based on various characterization techniques was done in order to accomplish the goals of this research. The effects of particle size, chemical treatment, additive loading and alternate processing methodologies was thoroughly investigated. The NCPEMs developed through modification with inorganic nano additives (ZrO_2, SiO_2 and TiO_2) demonstrated good thermomechanical and chemical properties for PEM fuel cell technology in the temperature range of 100–130 ^oC.

A phenomenological thermodynamic model was utilized to study the sorption in PEMs, which is based on a plausible picture involving strongly bound and free water molecules, wherein the chemical potential and activity (described by Flory-Huggins theory) of the free water molecules was affected by the osmotic pressure increase within the pores of the membrane as more water is imbibed, eventually reaching equilibrium with external water. Additional pressure terms were used to account for the vapor-liquid interface at the pore mouth for the case of adsorption from vapor. The difference hence accounted for the so-called Schroeder's paradox. When combined with a model for the strongly bound water molecules, the theory provided a very good fit of experimental data with a single fitted parameter, namely the Flory-Huggins interaction parameter.

In addition, a comprehensive proton transport framework was also developed for NCPEMs incorporating the various transport mechanisms, namely, surface hopping, Grotthuss diffusion, and *en masse* diffusion. The resulting model provided an excellent prediction of proton conductivity in Nafion as a function of relative humidity without the use of any additional fitted parameters. The prediction showed higher water sorption and conductivity at 90 ^oC for complete range of water activity.

From the theoretical model, it was concluded that the formation of a high fraction of pore bulk water in PEMs is desirable for high conductivity because of the dominance of Grotthuss diffusion mechanism in conductivity, which occurs in bulk water rather than at the surface water. This is the key reason for the success of Nafion, where strong backbone hydrophobicity helps water cluster formation away from surface. Most of the design variables of the proton conductivity model are related directly or indirectly to the amount of water uptake in PEMs, which, thus, is the key variable in designing of new NCPEMs. The transport model provided a theoretical framework for understanding the proton transfer in NCPEMs and was taken as guideline for systematically developing alternate high proton-conducting PEMs for fuel cell applications.

Nafion-MO_2 (M = Zr, Si, Ti) nanocomposite membranes were synthesized with the goal of increasing its the proton conductivity and water retention at higher temperatures and lower relative humidities (120 ^{o}C, 40 % RHs) as well as to improve the thermo-mechanical properties. The sol gel approach was utilized to incorporate inorganic oxide nanoparticles within the pores of Nafion membrane. The membranes synthesized by this approach were completely transparent and homogenous as compared to membranes prepared by alternate casting methods which were cloudy due to the larger particle size.

Various experimental techniques, namely, TEOM (Tapered Element Oscillating Microbalance), Impedance Spectroscopy, MEA (membrane electrode assembly) testing, Ion Exchange Capacity, Scanning Electron Microscope (SEM), Optical Electronic Holography (OEH), Thermal Gravimetric Analysis (TGA), and Dynamic Mechanical Analysis (DMA) were employed to characterize the NCPEMs.

At 90 ^{o}C and 120 ^{o}C, all Nafion-MO_2 sol-gel nanocomposites exhibited higher water sorption than Nafion membrane. However, at 90 ^{o}C and 120 ^{o}C, the conductivity was enhanced in only Nafion-ZrO_2 sol-gel nanocomposite with a roughly 10 % enhancement at 40 % RH over Nafion. This can be attributed to the increase in acidity of zirconia based sol gel membranes shown by a decrease in equivalent weight in comparison to other nanocomposites based on Ti and Si. In addition, the TGA and DMA analyses showed improvement in degradation and glass transition temperature, T_g, for nanocomposite membranes over Nafion. The T_g for Nafion-ZrO_2 sol-gel composite increased by about 30 ^{o}C as compared to Nafion. This opened the door for operating the PEM fuel cell at even

130-135 ^{o}C under low humidification. At 135 ^{o}C, relatively good performance was obtained for Nafion- ZrO_2 sol-gel nanocomposite membranes where Nafion membranes fail to perform at this temperature. These results suggest that there is a substantial potential for improvement in fuel cell performance using sol gel nanocomposites. However these are ultimately limited by the glass transition temperatures of the host polymer. To pass through the 140 ^{o}C barrier will require the development of new novel polymers. Although the membranes developed in the present work demonstrated glass transition temperature above 140 ^{o}C, long term testing (more than 2000 hours) is necessary to confirm the stability of these membranes for higher temperature PEM fuel cells.

An important outcome of this research was the development of TEOM and OEH, two novel optical characterization techniques, to study the relation of swelling behavior within the framework of mechanical properties of the polymeric. This is a key to membrane developing strategies. TEOM was used to study the effect of equivalent weights (960 -1200), temperature (30- 90 ^{o}C), various cationic forms (H^+, Li^+, Na^+, K^+ and Cs^+), sorbates (water, methanol, ethanol, and propanol), and inorganic additives on the sorption behavior of Nafion membrane. The results provided insights into the swelling behavior of ion-exchange membranes, and, thus, were useful in evaluating and designing alternate PEMs for fuel cell applications. Similarly, optoelectronic holography (OEH) was developed and applied for the first time to determine modulus of elasticity (E) of membranes as a function of RH and temperature. These two novel experimental characterization techniques developed in this study provide the foundation for developing higher temperature fuel cell membranes and electrodes, since they provide understanding of the effect of the rendered modifications on its thermomechanical properties.

Finally, the performance of commercially available high temperature PBI (polybenzimidazole)-H_3PO_4 (phosphoric acid) gel membrane fuel cell was investigated in the temperature range of 160-180 ^{o}C. This system exhibited very good and stable performance in this temperature range. PBI exhibited very high current densities at 180 ^{o}C (0.9 A/cm^2 at 600 mV). The conductivity of PBI-H_3PO_4 was about 0.08 S/cm under no external humidification, which is very important for higher temperature PEM development. The durability and stability of H_3PO_4 within the catalyst layer and PBI matrix is yet to be studied, and may be a key factor in determining the practicability of this technology.

It is, thus, apparent based on this research that the polymer-inorganic nanocomposite membranes can provide additional water within the membrane for a given water activity. This additional water does translate into somewhat higher conductivities. Another key advantage of polymer-inorganic nanocomposite membranes is their better thermomechanical properties. The following factors are thus important while selecting an appropriate functional additive: 1) The hydrophilicity of the inorganic; 2) The acid-site density and strength on the inorganic nanoparticle surface; 3) the particle size or the specific surface area of the inorganic particles; and 4) the amount of inorganic loading. The strategy should increase the water content of the membrane under hot and dry conditions, such that the majority of the water is not strongly tied to the particle surface, and at a loading that does not inordinately increase the frictional resistance to proton transport.

9.2 Recommendations for Future Work

A key current goal for commercialization of the PEM technology can be summarized as identification of suitable membrane material, keeping in view the desired membrane properties, developing accelerated durability methodologies to characterize the membrane within a short span of time, and developing newer synthetic methods to develop Nafion like polymer systems.

9.3 Strategies for Alternate PEMs

Various solid polymer electrolytes membranes have been studied and tested for fuel cell applications. A comprehensive review was provided in Chapter 1. The review reveals that Nafion is a more “mature” membrane. Much research has been conducted on the details of the transport of protons through the polymer matrix and on novel methods of improving its properties but development of a sturdy inexpensive substitute to Nafion is not in sight. From the work carried out so far world wide, fuel cell membranes could be divided into four main categories namely, perfluorinated ionomers, non-fluorinated hydrocarbons, sulfonated polyarylenes and acid–base complexes. From the review, it is apparent that Nafion is the prominent polymer in the first category; SPEEK appears promising in third category [1-4]; while phosphoric acid doped PBI membranes appear

most promising in the fourth category [5-9]. In my view, the next step would be to prepare blends of these different polymeric systems to meet the targets.

Table 9.1 shows two such probable cases where the properties of SPEEK and PBI can be combined to get higher conductivity (Fig 1.10) and under no humidifications [1-10]. These polymers meet the requirements of fuel cell membranes such as ionic conductivity, chemical and thermal stability besides low fuel permeability. Though, as seen in the review in Chapter 1, the progress in the third (sulfonated polyarylenes) and fourth (acid–base blends) categories has been steady, in each case work is still focused on investigating the mode of proton transport and on the practical applications of these membranes in a PEM fuel cell. However, with further detailed investigations and research, the class of membranes based on acid–base complexes could become competitive to Nafion, especially in ease of synthesis and cost-effectiveness. Suitable blending procedure and newer synthesis routes might render these complexes a promising alternative, along with the long-term endurance.

Composites/Blends	Attributes	Remarks	Goals
• SPEEK/PBI • PEEK/PBI • SPEEK/PBI-H_3PO_4 • Sol-gel SPEEK/ ZrO_2	High temperature tolerance to 350 °C; thermally stable; good miscibility	Short-term tests (300 h) yield comparable performance to Nafion 112[1-4]	High Performance expected: 600 mV at 1000 mA/cm^2 already obtained with PBI- H_3PO_4 in this work. So by blending SPEEK, the durability may improve to a greater extent. Improved T_g.
• PBI/H_2SO_4, • PBI/H_3PO_4, • Nafion/PBI/H_3PO_4, • Sol-gel PBI/H_2SO_4/ MO_2	Good mechanical strength; thermally stable	Doped PBI shows greater potential for fuel cell temperatures 100-180 ^oC [5-9]	Conductivity of 8×10^{-2} S/cm found in present research work. Improved T_g.

Table 9.1 Potential high temperature PEMs

Replacement of sulphonic group with other acidic groups like phosphonic or sulfonimide groups also provide membranes with interesting properties.

Based on these guidelines the following polymer systems may be of interest:

1. Polysulfone
2. Polyimide
3. Poly arylene ether

Their corresponding sulfonated structures are,

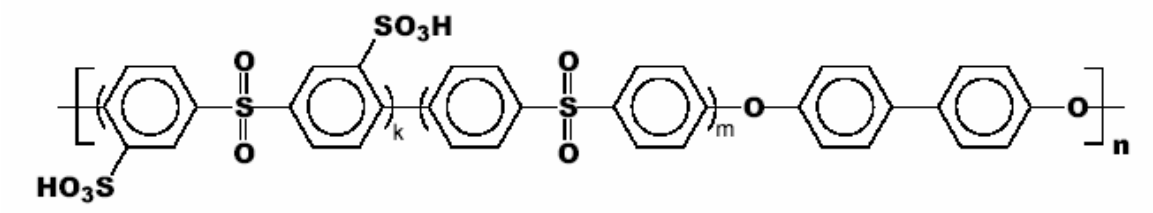

Sulfonated Poly (sulfone)

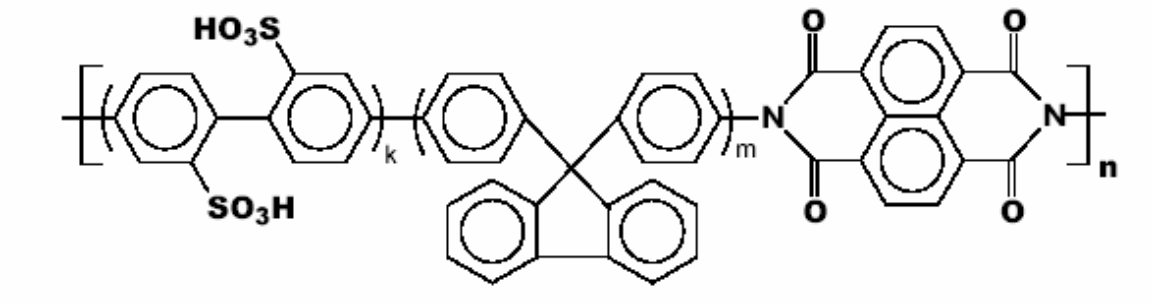

Sulfonated Polyimide

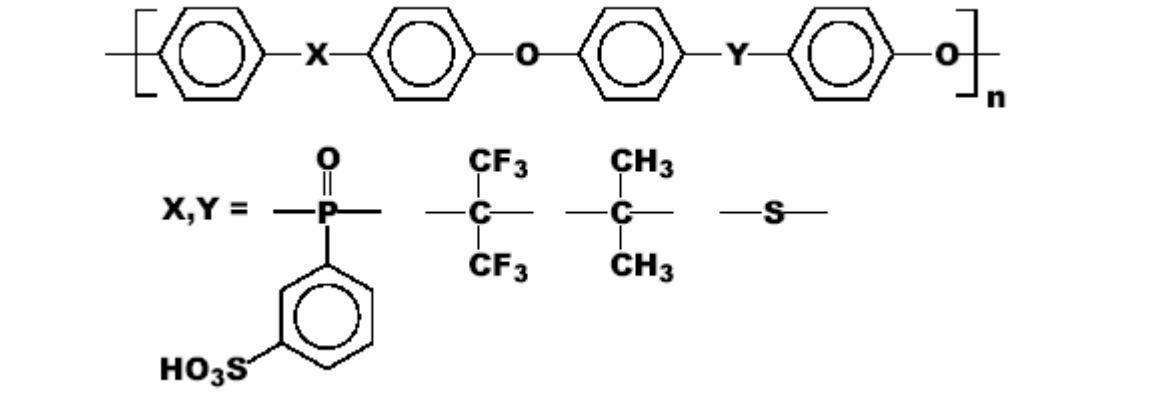

Sulfonated Poly arylene ether

These polymer systems are good candidate for polymeric membranes working at temperatures more than 120 ^{o}C. However, their stability may not be as good as Nafion. These membranes can be modified by adding inorganic additives, as discussed above for Nafion.

9.4 Nanocomposite Nafion

One possibility with great promise is continuation of the present work for developing sol–gel porous metal oxides. Different types of stronger acid, e.g., heteropolyacids etc could be supported on these sol-gel oxides to provide a high proton conducting matrix. Other composite membranes may incorporate the conductive properties of organic species such as fullerene because of their stability in higher temperatures.

Another approach would be to develop thin film sol gel incorporated catalyst for fuel cells which would introduce long term stability for MEA. Also, this would reduce the polymer degradation of the catalyst layer, and also the humidification requirements. While these modifications to the design of the membrane and electrodes have the potential to increase the conductivity significantly, constructing an efficient MEA may require small design changes. For example, it is important to ensure that the tri-phase electrode/catalyst/membrane interphase contact is optimized. In addition to being highly suited for use in high temperature PEMFCs, solid acid membranes also have potential applications for use as direct alcohol fuel cells. High fuel crossover is a significant problem in polymer membranes which leads to large efficiency losses (30 %). Solid acid membranes do not have this problem because of their different structure and transport mechanisms.

9.4.1 Thinner Supported Membranes

Preparing thinner supported Nafion membranes and studying the water uptake characteristics, performance and conductivity of these membranes. The current thickness of the Nafion is dictated largely by mechanical strength required. By supporting Nafion on porous PTFE sheets, which is about 25 microns thick, the mechanical strength can be improved a lot. This, of course is the basis of the W. L. Gore membranes. Nanoinorganic can also be incorporated in these membranes. Thinner membranes can effect the water

management in fuel cells. Effect of this on fuel cell performance will be studied. It is possible that due to effective water management, the membrane does not dry out as easily at higher temperatures and the performance remains high.

9.4.2 Bilayered Membranes

Bilayered membranes involving membranes with different equivalent weights can be synthesized. If two membranes of different equivalent weights are hot pressed or otherwise fabricated, it may induce concentration gradient for protons within the membrane. This could further facilitate the proton transport rate and hence the performance of fuel cells. It should be noted that the membrane with lower equivalent weight would be on cathode side. This strategy could be applied even for two membranes with different acid groups. For example, the Aciplex membrane with carboxylic acid group could be bilayered with Nafion having sulfonic acid groups. These membranes can also be prepared in a straight forward manner via casting.

9.4.2 Water Retention

Depositing a hydrophobic layer on the membrane electrode assembly (MEA). This hydrophobic layer would not allow the water which is inside the membrane to dry out easily. This might keep the membrane humidified at temperatures above 100^{o}C and low RHs. A porous Teflon layer could possibly be deposited uniformly over the MEA to test this strategy.

9.4.2 Alternate Ionomer in Catalyst Layer

The significance of maintaining high conductivity within the catalyst layer under dry conditions has been largely overlooked so far in efforts to develop higher temperature PEMs. This could very well be the bottleneck in developing high performing fuel cells. It would be interesting to test different ionomers, both polymeric and inorganic within the catalyst layers. The performance on the cathode is greatly affected by the acidic conditions.

9.5 Membrane Stability and Longevity

It is essential to develop protocols to study membrane durability and chemical stability. In both the strategies mentioned above, the PEM system needs to be tested for long term endurance and stability. Similarly standardized accelerated durability protocols needs to be developed to study the performance of new PEMs.

9.5.1 Fenton's Reagent

Fenton's reagent can be used to study the chemical stability of the membranes. This reagent is based on the principle developed by H.J. H. Fenton in 1894. Iron catalyst ($FeSO_4$ solution) is added to the system followed by H_2O_2 solution. The reaction forms highly reactive species ·OH. This method is very common for waste water treatment. It would allow us to study membrane degradation by hastening the process via a mechanism similar to that suspected at the cathode.

The reaction taking place is:

$$Fe^{2+} + H_2O_2 \rightarrow Fe^{3+} + OH^- + {}^{\bullet}OH$$

$$Fe^{3+} + H_2O_2 \rightarrow Fe^{2+} + {}^{\bullet}OOH + H^+$$

Reaction rates with Fenton's Reagent are generally limited by the rate of. OH generation (i.e., concentration of iron catalyst).

The goal would be first implement this for Nafion and then compare the results with composite membranes synthesized or blends. The parameter to be studied would be the 'level of degradation of membrane with time' which would translate into degradation of MEA performance with failure via pinhole formation. The factors contributing to a decrease in degradation membranes will be of interest. This will include the testing the effect of inorganic material type and loading, type of polymer and bilayered membrane on the degradation characteristics of higher temperature membranes.

9.5.2 Accelerated Durability Testing

The goal here is to combine chemical and mechanical degradation mechanisms in a single accelerated test. The humidity cycling under a certain load should provide us good information of the durability.

One such proposed protocol is as follows:

The following two cycle modes should be interchanged every 24 hrs:

Humidity cycle:

N_2 / N_2, 80 ^oC

Cycle Relative Humidity (RH) of inlet gases between 0 and 100 % RH every 10 minutes

Load cycle:

H_2 / O_2; 50 %RH, 80 ^oC

Load cycled between 10 and 800 mA/cm^2 (10min / 5 min)

Target

Monitor crossover current density (by Linear Sweep Voltametry) as a function of time

Stop test when > 15 mA/cm^2

Another important property that can be tested is OCV (open circuit potential), i.e, under no load conditions. OCV degradation is an indicator of fluoride release rate.

Proposed protocol:

Conditions accelerating decay

Higher operating temperature

Use of pure oxygen and very low relative humidity

Operation at OCV

Test conditions

Operate fuel cell at 80 ^oC, H_2/O_2, 30 % RH, OCV, 48 hours.

Targets

Fluoride emission rate and OCV degradation rate:

Now, along with these protocols, it is beneficial if following are incorporated:

⇒ *In situ* characterization of MEAs by polarization curves, electrocatalyst surface area measurements (ECSA), high-frequency resistance to determine membrane resistance.

⇒ Post-characterization of tested MEAs by XRF, XRD, SEM/EDS, TEM.

This includes:

1. Examination of some Pt alloys for particle size growth with *in situ* XRD.
2. Analyze particle size in real time during simulated fuel cell operation.
3. Model platinum particle growth.
4. Examine carbon corrosion during simulated shut-down and start-up process.

9.6 References

1. J. Kerres, A. Ullrich, F. Meier and T. Haring, Synthesis and characterization of novel acid–base polymer blends for application in membrane fuel cells, *Solid State Ionics* **125** (1999), 243–249.
2. J. Kerres, W. Zhang and W. Cui, New sulfonated engineering polymers via the metalation route.2. Sulfonated-sulfonated poly(ethersulfone) PSU Udel® and its crosslinking, *J. Polym. Sci. A: Polym. Chem.* **36** (1998),1441–1448.
3. J.M. Bae, I. Honma, M. Murata, T. Yamamoto, M. Rikukawa and N. Ogata, Properties of selected sulfonated polymers as proton-conducting electrolytes for polymer electrolyte fuel cells, *Solid State Ionics* **147** (2002),189–194.
4. J. Kerres, A. Ullrich, T. Haring, W. Priedel, M. Baldauf and Prepaartio, Characterization and fuel cell application of new acid–base blend membranes, *J. New Mater. Electrochem. Syst.* **3** (2000), 229–239.
5. S.R. Samms, S. Wasmus and R.F. Savinell, Thermal stability of protons conducting acid doped PBI in simulated fuel cell environments, *J. Electrochem. Soc.* **143** (1996),1225.
6. A. Bozkurt and W.H. Meyer, Proton conducting blends of poly(4-vinylimidazole) with phosphoric acid, *Solid State Ionics* **138** (2001), 259–265.
7. J.C. Lassegues, J. Grondin, M. Hernandez and B. Maree, Proton conducting polymer blends and hybrid organic inorganic materials, *Solid State Ionics* **145** (2001), 37–45.
8. A. Bozkurt and W.H. Meyer, Proton-conducting poly(vinylpyrrolidone)-phosphoric acid blends, *J. Polym. Sci., Polym. Phys.* **39** (2001),1987–1994.
9. C. Hasiotis, V. Deimede and C. Kontoyannis, New polymer electrolytes based on blends of sulfonated polysulfones with polybenzimidazole, *Electrochim. Acta* **46** (2001), 2401–2406.

Appendix A

Methods of Preparation of Nafion and other nanocomposite membranes.

1. Cast Nafion

a. Addition of 23 wt. % Nafion/Ethanol solution to glass dish utilizing doctor blade.
b. Cast membrane at 100 ^{o}C for 15 mins.
c. Remove membrane with DI water.
d. Anneal membrane at 170 ^{o}C at 10 Tons for 15 mins.

2. 5 % Calcined ZrO_2/Nafion

a. Stir ZrOH (MEI) in 0.5 M H_2SO_4 for 15 mins.
b. Decant acid and dry powder at 100 ^{o}C for 2 hours.
c. Calcined in air at 600 ^{o}C for 2 hours and crush resulting particles (with mortar and pestle).

Incorporation in Membrane

d. Measure required mass loading of particles.
e. Add required amount of 23 wt. % Nafion/Ethanol solution to particles and mix for 8 hours utilizing magnetic stir bar.
f. Pour in Teflon Dish.
g. Cast membrane at 80 ^{o}C for 8 hours.
h. Anneal membrane at 170 ^{o}C at 60 mins.
i. Boil membrane in 0.5 M H_2SO_4.

3. 5 % Calcined ZrO_2/Nafion

a. Same steps as 2 from (a) through (c).

Incorporation in Membrane

b. Measure required mass loading of particles.
c. Add required amount of 23 wt. % Nafion/Ethanol solution to particles and mix for 8 hours utilizing magnetic stir bar.

d. Apply with syringe (as soon as done stirring) to glass dish, membrane drawn utilizing doctor blade.
e. Cast membrane at 100 ^{o}C for 15 mins.
f. Removal of membrane with DI water.
g. Anneal membrane at 170 ^{o}C at 10 Tons for 15 mins.

4. 5 %, 10 % and 20 % Nanoprecipitated ZrO_2 in Nafion

a. Heat a colloidal solution of 20 wt. % ZrO_2 /Acetic Acid (Nyacol Nano. Technologies) to remove solvent.
b. Precipitate boiled in 6 M H_2SO_4, decant acid and dry at 120 ^{o}C for 2 hours.
c. Calcined in air at 600 ^{o}C for hrs and crush resulting particles (mortar and pestle).

Incorporation in Membrane

d. Same steps as 3 from (b) through (g).

5. 15 %, 20 % PTA/Nafion

a. Add a measured amount of PTA to measured amount of 23 % Nafion®/Ethanol solution to obtain required loading.
b. Same steps as 3 from (c) through (g).

6. Sol gel ZrH_3PO_4 – Nafion 112

a. Soak membrane in 30 wt. % $ZrOCl_2$ / HCl @ 80 ^{o}C for 20 hours
b. Rinse membrane in DI H_2O.
c. Soak membrane in 43 wt. % H_3PO_4 @ 80 ^{o}C for 20 hours.
d. Rinse membrane in DI H_2O, and boil membrane in DI H_2O for 1hour.
e. Anneal membrane at 170 ^{o}C, 15 Tons for 3 or 15 min.

7. 5 %,10 % and 20 % Nanoprecipitated & Pulverized ZrO_2 in Nafion -Mix A

a. Heat a colloidal solution of 20 wt. % ZrO2 /Acetic Acid (Nyacol Nano. Technologies) to remove solvent.

b. Precipitate boiled in 6 M H_2SO_4, decant acid and dry at 120 ^oC for 2 hours.
c. Calcine in air at 600 ^oC for 2 hours and crush resulting particles (mortar and pestle).
d. Crush in Glen Mills Air jet.

Incorporation in Membrane

e. Same as 3 from (b) through (e).

- Mix B-Same as 10 but slowly add particles to stirring solution of 23 wt. % Nafion/Ethanol solution.

- Mix C-Same as 10 but slowly add particles to stirring solution of concentrated solution of 35 wt. % Nafion/Ethanol solution, and then after 8 hours add rest of Nafion/Ethanol to obtain final loading.

- Mix C-Same as 10 but slowly add particles to stirring solution of concentrated solution of 35 % wt. Nafion/Ethanol solution, and then sonicate. After 4 hours add rest of Nafion®/Ethanol to obtain final loading, continue sonnication.

8. Sol Gel ZrO_2 Procedure

a. Membrane initially boiled in 3 wt. % H_2O_2 for 1 hour., rinsed in water, heated in 50 % vol. HNO_3/H_2O for 6 hours, rinsed in water, and then heated in 50 % vol. H_2SO_4/H_2O for 6 hours and then rinsed in water (to remove and acid) and boiled in water for 1 hour.
b. Purified membrane placed in vacuum oven and heat treated at 100 ^oC for 24 hours. After membrane cooled, mass measured.
c. Membrane boiled in H_2O for 1 hour and then dried at 50 ^oC for 4 hours.
d. Membrane immersed in 10:1 Ethanol/ H_2O solution for 1 hour.
e. Membrane removed and immersed into 40:1 Ethanol: Zirconium tert butoxide for prescribed time, and rinsed in ethanol to remove surface ZrO_2.
f. Membrane then removed and heated at 100 ^oC in vacuum, after cooling, mass measured again to determine uptake.
g. Boiled in 0.5 M H_2SO_4 for 1 hour and H_2O for 1 hour.

9. Sol Gel SiO_2 Procedure

a. Membrane initially boiled in 3 wt. % H_2O_2 for 1 hr., rinsed in water, heated in 50 % vol. HNO_3/H_2O for 6 hours, rinsed in water, and then heated in 50 % vol. H_2SO_4/H_2O for 6 hours and then rinsed in water (to remove and acid) and boiled in water for 1 hour.

b. Purified membrane placed in vacuum oven and heat treated at 110 ^oC for 24 hours. After membrane cooled, mass measured.

c. Membrane boiled in H_2O for 1 hour and then dried at 50 ^oC for 4 hours.

d. Membrane immersed in 2:1 methanol/ H_2O solution for 5 min.

e. Membrane removed and immersed into 3:2 Tetraethyl-orthosilicate: methanol for prescribed time.

f. Membrane then removed and heated at 100 ^oC in vacuum, after cooling, mass measured to determine SiO_2 uptake.

g. Boiled in 0.5 M H_2SO_4 for 1 hour and H_2O for 1 hour.

10. **Alternate Sol gel ZrO_2 procedure**

Pretreatment of Membranes

a. Nafion 112 is immersed in conc. HNO_3 at 60 ^oC for 24 hours

b. Acid is decanted

c. Films are placed sequentially in aqueous solutions of 60 %, 40 %, and 20 % nitric acid each for 1 hour.

d. Wash with Deionized water and vacuum dry at 110 ^oC for 6 hours.

Formation of ZrO_2

A: Preparation of required solution

a. Prepare 0.5 M $Zr(OC_4H_9)_4$ solution in Isopropanol.

b. Soak the pretreated membranes in the above solution for 48 hours.

B: Post Treatment of Membranes

a. Wash the membranes with Isopropanol to clean the film surface.

b. Rinse with acetone several times.

c. Boil the membranes in water to complete the hydrolysis.

d. Vacuum dry the membrane at 110 ^oC for 6 hours.

11. Preparation of Highly dispersed ZrO_2 particles

1. Purification of as received Nafion 112. (much simpler than previous procedures).
    a. Washed /heated in DI water at 60 ^oC for 10 minutes.
    b. Heated in 3 wt. % H_2O_2 at 60 ^oC for 30minutes
    c. Heated in DI water at 60 ^oC for 30 minutes.
2. Conversion to Na^+ form.
    a. Heated in 1 M NaOH at 60 ^oC for 30 minutes.
    b. Washed /heated in DI water at 60 ^oC for 30 minutes.
3. Dried under vacuum at 80 ^oC for 4 hours.
4. Impregnation With TiO_2
    a. The Na^+ exchanged PEM is soaked in Zr $[OCH(CH_3)_2]_4$ ZIP / 1 propanol soln at **25°C**, (the effect of this parameter not investigated fully?) in stoppered soaking vessel. Concentration ranged from 260 ppm to **9600** ppm ZrO_2, with resulting loading 1 to 6 wt. %. The saturation value of 6 wt. % was reached with >2000 ppm ZrO_2. (Concentration we may use 500 ppm ~ 1wt. % loading and 5000 ppm ~ 5 wt. % loading)
    b. At various time intervals (25 mins to 240 mins) the PEMs was removed and hydrolyzed. Time from 25 mins to 240 mins, time set as **240** mins.
5. Hydrolysis / Condensation Reactions
    a. PEM removed from container, rapidly blotted dry and subjected to following treatment.
    b. PEM placed in 2-propanol / H_2O solution for 2 hours (time not fully investigated) at 80 ^oC (probably maximum temp. for soln).
    c. PEM removed and vacuum dried thoroughly at 25 ^oC for 24 hours and then at 130 ^oC for 2 hours.
6. Post treatment
    a. Heating in 3 wt. % H_2O_2 at 60 ^oC for 30 mins.
    b. Heating in 1 M HNO_3 at 60 ^oC for 30 mins.
    c. Rinsed in water and allowed to air dry.

Appendix B
Experiment Procedures

12. Ion Exchange Capacity Measurements [1]

A 0.2 g sample of the PEM was taken and exchanged with NH_4^+ by immersing the sample in 1M ammonium acetate for 24 hrs and then in Ammonium chloride fro an additional hour. The PEM was then washed with DI water to remove any excess NH_4^+ ions. Utilizing a 1M silver Nitrate, a visual test was utilized to ensure that no excess NH_4^+ remained. The PEMs was then stored in 50ml DI water and stirred with a magnetic stirrer.

Adding a 2ml of 5M NaOH solution to the sample, forced the exchange of NH_4^+ into the solution where exits as dissolved NH_3. Utilizing a calibrated ammonia electrode (Model 95-12 ORION, Boston MA 02129), the amount of NH_3 can be accurately quantified thus a measurement of the ion exchange capacity can be made based on the amount of NH_4^+ measured.

13. Conductivity Measurements [2]

The sample was clamped in a conductivity cell and then placed in a humidity controlled chamber. The humidity of the chamber is monitored utilizing a dew point / temperature probe (HMP 238, Vaishala, Woburn, MA). An air stream is saturated with water by bubbling the dry gas through a humidifier, this wet stream is heat traced to the chamber, prior to which it contacts a dry air stream. The chamber and the humidifier are both heated to 90°C / 120°C and 90°C respectively to obtain the necessary partial pressures of water. By metering the flows of the wet and dry stream in to the chamber, the RH is controlled.

Protocol for Measuring Conductivity

1. Cut a piece of Nafion (2'' X 1.5'').
2. Pretreatment Procedure
    - Boil in DI water at 60^0C for 10 min.
    - Heated in 3 wt% H_2O_2 at 60^0C for 30 min.
    - Rinse in water at least 3x.

- Heated in 1M HNO_3 at 60^0C for 30 min.
- Rinse in water at least 3x
- Washed in DI water at 60^0C for 30 min.
- Rinse in water at least 3x

3. Dry the membrane in room temperature and wipe the surface, store in small plastic bag.
4. Set up the Conductivity cell for measurements. Set the cell in a horizontal position, thus the PEM is raised up by the legs of the cell.
5. After completely closing the apparatus, follow the steps:
    - Increase the reactor temperature to 120C. At this point, only dry gas is flowing and no flow through saturator.
    - Once the temperature reaches 120C, maintain it for at least an1 hour with dry gas flowing through the system.
    - Increase saturator temp to 90C.
    - Once saturator is at 90C, increase flow through saturator using Control Box to get required RH.
    - Start from low RH to higher RH.

At 120C, **Do not cross 40%RH.**

6. After the reading set at 120C, lower the saturator temperature to 85C.
7. Stop flow through saturator. Increase dry flow.
8. Lower the reactor temp to 90C.
9. Start reading from lower RH to higher RH.
10. At 90C, **Do not cross 80% RH for safety of probe.**

Precautions:

1. Do not cross limits of RH specified, at 90C the limit is 90% RH, while at 120C it is 40%.
2. Check level of water in saturator. Should be at least more than half filled.
3. Check line heater setting. Do not cross 35%.
4. When the taking the reading it is important to ensure a constant conductivity reading is obtained by check that the conductivity intercept is not changing and this usually means a minimum time of 10 mins.

14. MEA Testing

The electrodes utilized are commercially available from E-TEK (Somerset, NJ). The type selected was the single -sided ELAT® gas-diffusion electrode (20% Pt-on-C, 0.35~0.4 mg Pt/cm^2). The active layer of electrode was brushed with 5% Nafion® solution (0.6 ~0.8mg/cm^2 MEA). This electrode was placed on either side of the PEM and the resulting membrane-electrode assembly (MEA) placed in a hot press. The temperature of the hot press was then raised to 130°C and a pressure of 272 atm applied for 120s. The MEA thus prepared was mounted in a 5 cm^2 fuel cell test fixture, obtained from Fuel Cell Technologies (Los Alamos, NM). The cell was fed with humidified H_2 and O_2 or air supplied at pressure 1 ~3 atm utilizing electronic mass flow controllers (MKS Model No. 1179A22CS1BV-S, Andover, MA) and as controlled by the electronic load (Series 890B Fuel Cell Test System, Scribner Associates Inc. Southern Pines, NC). Utilizing software (Fuel Cell Test Software Version 2.0, Scribner Associates, Inc.) the mass flow rate of the feed gas was programmed to stoichiometry dependent flow rates. The load has an inbuilt feature of measuring *in situ* MEA ohmic resistance utilizing a current interruption method.

The pressure of the reactant gases was monitored using pressure gages (Matheson, Model No. 63-5612). Back pressure regulators (Tescom Model No. 44-2300) were used at the outlet of both the anode and the cathode to control the gas pressure. Humidification of the cell was accomplished by bubbling the feeds through stainless steel cylinders containing DI water and equipped with a sight glass. Heating tape was wrapped around the feed lines to prevent any condensation in the lines, and water traps were added to facilitate removal of water. The temperature of the humidifiers as well as that of the fuel cell was controlled using individual temperature controllers (Omega CN9100A).

The following MEA test protocol was utilized [3]. The start up procedure involved bringing the humidifier temperature up to a set value of 80°C, then increasing the test fixture to 70°C and operating the fixture on 1 atm H_2 and Air at current controlled mass flow rates, being 1.3x(anode stoichiometric flow) for H_2 and 2.0x(cathode stoichiometric flow) for air. The load was cycled for additional 6 hours and then a constant voltage polarization curve was taken. Thereupon, another 12 hours of break-in period was utilized and then a final polarization curve was obtained as follows. 0.6V set for 10 min then data is taken every 6 seconds for 3 minutes. The measurement is initially held for 3 minute, before

the first data point is collected, and then data is collected every 6 seconds for 3 minutes for each voltage set-point. This continues in the following voltage sequence, 0.55V, 0.5V, 0.45V, 0.4V, 0.6V, 1(for 1 minute), 0.65V, 0.7V, 0.75V, 0.8V, 0.85V and 0.6V. The electrochemical surface area (ECA) and the crossover were then measured utilizing the potentiostat.

Potentiostat often allow the choice of 2, 3, or 4 terminal connections to the cell depending on the particular application to measure the ECA and cross-over current. The two terminal connections are usually used when it is difficult to position the reference electrodes inside the cell itself. Although there is a reference electrode machined in the test fixture, it is assumed that the H_2 anode behaves as a reference electrode. The ECA or H_2 electrochemical stripping is a measure of the amount of Pt that takes part in the reaction. The crossover measurement is a measure of the H_2 that diffuses through the PEM and is oxidized at the cathode. The ECA and the cross over current were measured in the following manner:

27. The cathode is purged with N_2 and the anode with H_2, both set at 50 sccm and 1 atm.
28. After the OCV is < 0.14V, the ECA is measured by utilizing the 1287 potentiostat (Solartron, Hampshire, U.K.). The counter electrode (CE) and reference electrode 1 (RE 1) are connected to the anode, while the working electrode (WE) and the reference electrode 2 (RE2) are connected to the cathode.
29. To measure the ECA of the MEA, the potential is swept from 0.0V to 0.6V for 4 cycles at 100 mV/s, while the cross- over is measured at 0.0 V to 1.0 V at 2 mV/s for 3 cycles.
30. The total charge between 0.0V and 0.6V is integrated and after correcting for the double layer (assuming it is the baseline), the total charge produced by the reaction is calculated. The ECA can be calculated by assuming a stoichiometry of

    1 e^- / Pt. Site [4]. The crossover is simply the plateau in current observed.

The pressure of the cell was increased to 1.5 atm for both the H_2 and air feeds, and a polarization curve was obtained. The temperatures of the fuel cell and the humidifers were then increased to 90°C. After utilizing the break in protocol for 1~2 hrs, to ensure steady-state performance has been reached, a polarization curve was obtained. Finally the ECA and crossover current were measured again.

In a similar fashion, the polarization curves, ECA and crossover current were measured at increasing temperatures. The temperatures of the humidifiers were maintained at 90°C and the cell temperature was returned to 70°C at the end of the experiment. Thus the temperature test protocol was: (a) Cell = 70°C, Hum. = 80°C, Beginning of Life (BOL), (b) Cell = 90°C, Hum. = 90°C, (c) Cell = 100°C, Hum. = 90°C, (d) Cell = 110°C, Hum. = 90°C, (e) Cell = 120°C, Hum. = 90°C (f) Cell = 130°C, Hum = 130°C and P = 3 atm O_2 and (g) Cell = 70°C, Hum. = 80°C, End of Life (EOL).

References:

1. E. Busenberg and C.V. Clemency, *Clays and Clay Materials,* **21** (1973) 213
2. Y. Sone, P. Ekdunge and D. Simonsson, *J. Electrochem. Soc.*, **143** (1996) 1254.
3. B. Bahar, C. Cavalca, S. Cleghorn, J. Kolde, D. Lane, M. Murthy, G. Rusch, *J. New Mater. Electrochem. Syst.*, **2(3)**, 179 (1999).
4. T.J. Schmidt, H.A. Gasteiger, G.D. Stäb, P.M. Urban, D.M. Kolb and R.J. Behm, *J. Electrochem. Soc.*, **145**(7), 2534 (1998).

Appendix C

Journal Publications of Author

1. N. H. Jalani, R. Manikandan, S. Buelte, G. Pacifico, R. Pollard, R. Staudt, and R. Datta, "Electrochemical Impedance Modeling for higher temperature fuel cells (160-180 ^{o}C)", in review, J. Power Sources (2005).

2. N. H. Jalani; K. Dunn, and R. Datta, "Synthesis and Characterization of Nanocomposite Nafion- MO_2 (M = Zr, Ti, Si) for higher temperature fuel cell applications", Electrochimica Acta, 51(3), 553-560 (2005).

3. N. H. Jalani and R. Datta, "The effect of Equivalent Weight, Temperature, Cationic Forms, Sorbates, and Nanoinorganic additives on solvent sorption of Nafion membrane", J. Membr. Sci., 264 (1-2), 167-175 (2005).

4. N. H. Jalani; P. Choi, and R. Datta, "TEOM: A Novel Technique for Investigating Sorption in Proton Exchange Membranes", J. Membr. Sci., 254 (1-2), 31-38 (2005).

5. P. Choi, N. H. Jalani and R. Datta, "Thermodynamics and Proton Transport in Nafion III. Proton Transport in Nafion/ Sulfated ZrO_2 Nano-composite Membranes", J. Electrochem. Soc., 152(8), A1548-1554 (2005).

6. P. Choi, N. H. Jalani and R. Datta, "Thermodynamics and Proton Transport in Nafion II. Proton diffusion Mechanisms and Conductivity", J. Electrochem. Soc., 152(3), E123-130 (2005).

7. P. Choi, N. H. Jalani and R. Datta, "Thermodynamics and Proton Transport in Nafion I. Membrane Swelling, Sorption, and Ion-Exchange Equilibrium", J. Electrochem. Soc., 152(3), E84-89 (2005).

8. T. Thampan, N. H. Jalani, P. Choi and R. Datta, "Systematic Approach to Design Composite Higher Temperature Proton Exchange Membranes", J. Electrochem. Soc., 152 (2), A316-325 (2005).

9. N. H. Jalani, P. Choi, and R. Datta, "Phenomenological Methanol Sorption Model for Nafion 117", Solid State Ionics, 175, 815-817 (2004).

10. N. H. Jalani; S. Mizar, P. Choi, C. Furlong, and R. Datta, "Optomechanical characterization of proton exchange membrane fuel cells", Proc. SPIE, Vol 5532, 316-325 (2004).

Conference Presentations of Author

1. N. H. Jalani and R. Datta, "Development of Composite Membrane Electrode Assemblies (CMEAs) for higher temperature proton exchange membrane fuel cells", poster presented in "*Meet the Faculty Session*" at 2005 AIChE annual meeting, Cincinnati, OH. (October 30- November 4, 2005)

2. N. H. Jalani and R. Datta, "Application of Electrochemical Impedance Spectroscopy (EIS) in PEM Fuel Cell", presented at 2005 AIChE annual meeting, Cincinnati, OH. (October 30- November 4, 2005)

3. N. H. Jalani and R. Datta, "Nafion-MO_2 (M= Zr, Si, Ti) nanocomposite membranes for higher temperature operation of PEM fuel cells", presented at 2005 AIChE annual meeting, Cincinnati, OH. (October 30- November 4, 2005)

4. N. H. Jalani and R. Datta, "TEOM: A Novel Technique to Study Sorption in Nafion Membranes", poster presented at 2005 AIChE annual meeting, Cincinnati, OH. (October 30- November 4, 2005)

5. N. H. Jalani and R. Datta, "Studying effect of sorbates (water, methanol, ethanol, and propanol) sorption on different cationic forms of Nafion membrane", presented at 208th ECS Meeting, Los Angeles, CA. (October 16-21, 2005)

6. N. H. Jalani and R. Datta, "Effect of Inorganic Additives on the properties of Nafion membranes", presented at 208th ECS Meeting, Los Angeles, CA. (October 16-21, 2005)

7. N. H. Jalani and R. Datta, "Nanocomposite Proton-Exchange Membranes for Higher Temperature PEM Fuel Cell", poster presented at 208th ECS Meeting, Los Angeles, CA. (October 16-21, 2005)

8. N. H. Jalani and R. Datta, "Application of Optoelectronic Holography (OEH) methodology to characterize thermo-mechanical properties of Nafion membrane for PEM fuel cells" presented at NAMS 2005 meeting, Providence, RI. (June 11-15, 2005)

9. N. H. Jalani and R. Datta, "A novel microbalance technique to study solvent sorption behavior of Nafion membrane for fuel cell applications" presented at NAMS 2005 meeting, Providence, RI. (June 11-15, 2005)

10. N. H. Jalani; P. Choi, and R. Datta, "TEOM: A Novel Technique for Investigating Sorption in Proton Exchange Membranes", presented at 2004 AIChE annual meeting, Austin, TX. (November 7-12, 2004)

11. N. H. Jalani, T. Thampan, P. Choi, and R. Datta, "Systematic Design of Composite Higher Temperature Proton Exchange Membranes", Poster presented at 2004 AIChE annual meeting, Austin, TX. (November 7-12, 2004)

12. N. H. Jalani, S. Mizar, P. Choi, C. Furlong , R. J. Pryputniewicz and R. Datta "Optomechanical study of Nafion membrane for micro fuel cell applications", Poster presented at 15th International Invitational UACEM Symposium for SEM, Springfield, MA. (October 27-29, 2004)

13. N. H. Jalani, S. Mizar, P. Choi, R. Datta, and C. Furlong "Optomechanical characterization of proton exchange membrane fuel cells", presented at 49th SPIE Annual Meeting, Denver, CO. (August 2-6, 2004)

14. N. H. Jalani, P. Choi, and R. Datta, "Modeling Temperature Effect on Water Sorption in Proton Exchange Membranes", presented at 205th ECS Meeting, San Antonio, TX. (May 9-13, 2004)

15. P. Choi, N. H. Jalani, and R. Datta, "Proton Transport in Proton Exchange Membranes: Implications in Design", presented at 205th ECS Meeting, San Antonio, TX. (May 9-13, 2004)

16. P. Choi, N. H. Jalani, and R. Datta, "Swelling in Nafion membrane: Effect of Equivalent weight (EW) and Polymer Elasticity", presented at 205th ECS Meeting, San Antonio, TX. (May 9-13, 2004)

17. N. H. Jalani, P. Choi, and R. Datta, "Design of High Temperature Membranes for PEMFC", Poster presented at 205th ECS Meeting, San Antonio, TX. (May 9-13, 2004)

18. N. H. Jalani, T. Thampan, P. Choi and R. Datta, "Rational Design of Higher Temperature Composite Proton Exchange Membranes"; presented at 2003 AIChE annual meeting, San Francisco, CA. (November 17-21, 2003)

19. N. H. Jalani, P. Choi, and R. Datta, "Thermodynamics of methanol sorption in Nafion 117", presented at 226th ACS National Meeting, New York, NY. (September 7-11, 2003)

20. P. Choi, N. H. Jalani, and R. Datta, "Phase Equilibrium in Proton Exchange Membranes for Vapor Sorption", presented at 226th ACS National Meeting, New York, NY. (September 7-11, 2003)

21. N. H. Jalani, P. Choi, and R. Datta, "Phenomenological Methanol Sorption Model for Nafion 117", Poster presented at 14th International Conference on Solid State Ionics, Monterey, CA. (June 22-27,2003)

22. P. Choi, N. H. Jalani, T. Thampan, and R. Datta, "Membrane Swelling and Proton Transport in Nafion"; presented at Computational Fuel Cell Dynamics session in Banff International Research Meeting, Alberta, Canada (April 1-25, 2003)

23. T. Thampan, N. H. Jalani and R. Datta, "Development and Characterization of Modified PEMs Designed for Higher Temperature Operation"; presented at 2002 AIChE annual meeting, Indianapolis, IN. (November 2002)